2008-01-01

Swelling Effects in Dynamic Equi-Biaxial Testing of EPDM Elastomers by the Bubble Inflation Method

John Hanley
Technological University Dublin

Recommended Citation

Hanley, J. (2008) *Swelling effects in dynamic equi-biaxial testing of EPDM elastomers by the bubble inflation method.* Doctoral Thesis, Technological University Dublin. doi:10.21427/D7XG8F

Swelling Effects in Dynamic Equi-Biaxial Testing of EPDM Elastomers by the Bubble Inflation Method

John Hanley

Ph.D

Dublin Institute of Technology

Supervisors: Dr. Steve Jerrams

Dr. Georg Clauss

School of Manufacturing and Design Engineering

February 2008

Abstract

The thesis describes the effect of oil swelling on the fatigue life of EPDM under conditions of multi-axial fatigue using bubble inflation. The motivation for the research is outlined, along with a review of previous research conducted on the topic. Initial test results are presented and the evolution of the procedure for the final set of tests is described. One principal requirement identified when carrying out the fatigue tests was the need for constant stress control. Following development of the final test procedure, specimens were subjected to varying degrees of swelling in reference oils and cycled at constant engineering stress amplitudes at a frequency of 1Hz. The degree of rubber swell was controlled by using reference oils for the swelling tests. Sample swelling during cycling was minimised by using silicone based oil as the inflation fluid. Three specimen sets were used in the fatigue tests, one dry set and two other sets with different degrees of oil swelling. S-N (alternating stress versus cycles to failure) curves were generated for the dry and swollen specimens, with the fatigue life of the EPDM reduced in proportion to the amount of swelling. The changes in complex elastic modulus E* and dynamic stored energy were analysed and a relationship between the stored energy and the cycles to failure for the dry EPDM was observed. However, the stored energy at failure is reduced as the degree of swelling increases. Moreover, it was found that if the residual, or specific moduli for the swollen test-pieces were considered against a datum of the initial conditioned modulus of the dry rubber at a similar stress amplitude, a limiting range of E*residual, was established for both the dry and swollen specimens. E* for different levels of swelling was also calculated using models generated from the experimental data. Additionally, the differences in the fracture surfaces of the

specimens due to swelling were analysed using scanning electron microscopy showing that the morphology of the failure surfaces are greatly influenced by the degree of oil swelling.

I certify that this thesis which I now submit for examination for the award of Ph.D, is entirely my own work and has not been taken from the work of others save and to the extent that such work has been cited and acknowledged within the text of my work.

This thesis was prepared according to the regulations for postgraduate study by research of the Dublin Institute of Technology and has not been submitted in whole or in part for an award in any other Institute or University.

The Institute has permission to keep, to lend or to copy this thesis in whole or in part, on condition that any such use of the material of the thesis be duly acknowledged.

Signature John Hanley Date 01/08/08

Candidate

Acknowledgements

I would like to thank the School of Manufacturing and Design Engineering and the Directorate of Research and Enterprise in the Dublin Institute of Technology (D.I.T) for supporting this work.

I would especially like to thank Dr. Steve Jerrams for his support and advice in all aspects of this work and in his supervision of this PhD and Mr. Niall Murphy for his expertise in test system design, interpretation of results and assistance in co-authoring several papers as part of this research.

I would like to thank Pauline for her personal support for the duration of this PhD.

The author would also like to thank Dr. Hassan Ali for his guidance in analysis of results and advice on the polymer chemistry aspects of the thesis.

Abbreviations

NR	Natural Rubber
EPDM	Ethylene-Propylene-Diene Polymer
FEA	Finite Element Analysis
LVDT	Linear Variable Differential Transducer
SBR	Styrene-Butadiene Rubber
SEM	Scanning Electron Microscope
SME	Small-Medium Enterprise
A	Helmholtz Free Energy (Swelling)
a	Major Bubble Radius (Bubble Inflation), mm
b	Minor Bubble Radius (Bubble Inflation), mm
e	Cohesive Energy (Swelling)
E*	Complex Elastic Modulus, MPa
G'	Rigidity Storage Modulus, MPa
G''	Rigidity Loss Modulus, MPa
$E^*_{conditioning}$	E* after conditioning, MPa
$E^*_{residual}$	Percentage of Original Elastic Modulus, %
G	Gibbs Free Energy (Swelling), Joules
L	Latent Heat, Joules/unit mass
I	Strain Invariant
k	Boltzmann's constant
M_c	Mean Chain Molecular Weight
M	(1 - % Increase in mass due to swelling)
n	Number of chains per unit area
N	Number of chains per unit volume (Moles of Crosslinks)

N	Number of cycles
P/p	Pressure, Bar
pphr	Parts per hundred rubber
Q	Swelling Ratio/Degree of Swelling (Swelling)
R	Gas Constant
R	Stress Ratio (Fatigue)
R	Bubble Radius (Bubble Inflation)
S	Entropy, J/K
T	Absolute Temperature, K
T	Tearing Energy
T_g	Glass Transition Temperature
t	Specimen Thickness, mm
t	True Stress, MPa
tan δ	Loss Factor/Tangent
U	Internal Energy, Joules
U/W	Strain Energy, Joules
V	Molar Volume (Swelling)
x	Displacement, mm
Z	Loading Factor
α	Alpha Term (Stretch Ratio in Swollen State)
γ	Shear Strain
δ	Solubility Parameter (Swelling)
ε	Elastic Strain
λ	Stretch Ratio
ρ	Density, kg/m^3

σ_a	Stress Amplitude
σ_e	Engineering Stress, MPa
σ_{max}	Maximum Stress, MPa
σ_{min}	Minimum Stress, MPa
σ_m	Mean Stress, MPa
σ_t	True Stress, MPa
τ	Shear Stress, MPa
f/τ	Equilibrium Retractive Force of Swollen Rubber (Swelling), N
υ	Volume Fraction (Swelling)
υ_e	Average Crosslink Density (Swelling)
χ	Flory-Rehner Interaction Parameter (Swelling)

Table of Contents

Abstract i

Abbreviations v

Table of Contents viii

Table of Figures xiii

List of Tables xvi

Chapter 1 Introduction 1

1.1 The motivation for the research programme 1

1.2 Aims and Objectives 3

1.3 An overview of the research 6

Chapter 2 Literature Review 8

2.1 Properties of Rubber 8

2.1.1 Definition of general polymer properties *8*

2.2 Thermodynamical analysis of a rubber network and development of statistical theory 10

2.2.2 Extension of theories to swollen rubber *13*

2.2.3 The dependence of swelling on strain *17*

2.2.4 Swelling and Extension Ratios – Alpha Terms *24*

2.3 The influence of swelling on rubber-like materials 28

2.3.1 Introduction 28

2.3.2 Early Research into swelling phenomenon 29

2.3.3 Further Research of Swelling Phenomenon - Development of the thermodynamics of swelling 30

2.3.4 Determination of Crosslinking in Rubbers 32

2.3.5 Swelling of Rubber - Oil Resistance 33

2.3.6 Swelling and determination of rubber mechanical properties 36

2.3.7 Carbon Black and Dynamic Testing of Swollen Rubber 43

2.4 Fatigue of Materials **48**

2.4.1 Fracture Mechanics and Crack Propagation 50

2.4.2 Crack Propagation and its application to elastomers 51

2.4.3 Fatigue Crack Growth 52

2.4.4 Fatigue of Non-Strain Crystallising Elastomers – Non Relaxing Tests 54

2.4.5 Fatigue Live Determination – Recent Investigations 55

2.4.6 Fatigue of Swollen Rubber – Previous Research 57

2.5. Summary of Literature Review **63**

Chapter 3 An Equi-biaxial Fatigue Rig **65**

3.1 Evolution of the rig **65**

3.1.1 Bubble Inflation Method 66

3.1.2 Bubble Inflation Theory 66

3.1.3 Development of the bubble inflation fatigue rig 70

3.2 Swelling phenomenon in equi-biaxial fatigue **74**

3.2.1 Selection of appropriate swelling media for EPDM *75*

3.2.2 Variation of dynamic strain energy in swollen rubber subjected to fatigue *78*

Chapter 4 Methodology and Test Procedure Evolution 80

4.1 Preliminary Testing 80

4.2 Initial equi-biaxial fatigue testing– Pre-Pressurisation Tests 81

4.3 Initial equi-biaxial fatigue testing – Stress-Strain Analysis 84

4.4 Fatigue and Swelling Tests using Toluene 87

4.5 Fatigue and Swelling with Reference Oils 93

4.5.1 Oil Swelling Test Procedure *94*

4.5.2 Oil Fatigue and Swelling Test Results *94*

4.6 Development of Constant Stress Controlled Tests 97

Chapter 5 Equi-biaxial fatigue and Swelling – Results 100

5.1 Test Schedule 100

5.2 Test Preparation – Swelling Tests 100

5.3 Equi-biaxial Fatigue Tests – S-N Curves, Stress Control 101

5.4 Analysis of Results – Elastic Modulus 102

5.4.1 Modelling of Decreases in Modulus *107*

5.5 Analysis of Results – Dynamic Stored Energy 110

5.6 Analysis of Results - Microscopy of Failure Surfaces 112

Chapter 6 Conclusions 118

Chapter 7 Outlook 123

Glossary 126

References 142

Appendix 158

Appendix 1 – Published Papers Relevant to the Research A1-1

Appendix 2 – Control Program Process Description A2-1

Appendix 2.1 System Hardware A2-1

Appendix 2.2 Labview Program Overview A2-5

Appendix 2.2.1 Fatigue Program *A2-6*

Appendix 2.2.2 Vision Program *A2-14*

Appendix 2.2.3 Stress and Valve Rate Sub-Programs *A2-26*

Appendix 3 – Vision System Details and Stress-Strain Calculations A3-1

Appendix 3.1 CCD Camera Specifications A3-2

Appendix 3.2 Camera Calibration Spreadsheets A3-4

Appendix 3.3. Conversion of Camera Measurements from Pixels to Millimetres A3-6

Appendix 3.4. Method of calculating the radius of the ellipse A3-7

Appendix 3.5. Stress and Stretch Ratio Calculations A3-11

Appendix 4 – Supplemental Literature Review A4-1

Appendix 4.1. Hyperelastic and Viscoelastic Properties of Rubber A4-2

Appendix 4.2. Development of Phenomenological Theories A4-8

Appendix 4.3. Thermodynamics of Swelling and Cohesive Energy Densities A4-23

Appendix 4.4. Fatigue of Elastomers A4-31

Appendix 5 – Plots of E* Models A5-1

Appendix 6 – Test Materials Specifications A6-1

Table of Figures

Figure 1.1. Overview of testing and analysis carried out to achieve the research objectives. 6
Figure 2.1. Equilibrium of swollen rubber under stress 18
Figure 2.2. Unit cube of rubber (a) and (b), the same cube subject to a homogeneous deformation (tensile). 26
Figure 2.3. Unit cube of rubber at a volume V_u (a) and (b), the same cube subject to deformation due to swelling, occupying a volume V. 27
Figure 2.4. Heat and oil resistance of commercial elastomers [25]. 36
Figure 2.5. Qualitative interpretation of strain amplitude dependence of G' [40]. 46
Figure 2.6. Parameters used in the description of constant-amplitude mechanical loading history [46]. 49
Figure 2.7. Typical S/N curve for a material, in this case EPDM Shore A70 E9566 EPDM rubber. 50
Figure 2.8. Lindley's [53] fatigue crack growth results for unfilled natural rubber, showing typical regimes of behaviour, and the effects of $R > 0$ loading. 53
Figure 2.9. Fatigue properties of filled EPDM (maximum stress dependency) [3]. 56
Figure 2.10. Fatigue properties of filled EPDM (energy dependency) [3]. 57
Figure 2.11. Relation of fatigue resistance, y to the degree of swelling of vulcanised natural rubber in paraffin oil [59]. 58
Figure 2.12. Change in relative fatigue resistance with increase in % volume swell for natural rubber swollen in four different solvents [57]. 60
Figure 2.13. Scanning electron micrographs of torn surface for SBR-H vulcanisates, (a) in dry condition, (b) in swollen condition [59]. 62
Figure 3.1 Free bubble inflation. 66
Figure 3.2 Bubble inflated shell element [61]. 67
Figure 3.3 Bubble Inflation Rig Process Overview. 71
Figure 3.4 Bubble inflation rig, showing camera set-up and subsequent co-ordinate extraction. 73
Figure 3.5. Aniline Point versus Solubility Parameter [24]. 77
Figure 4.1. Testing matrix for equi-biaxial bubble inflation fatigue tests. 81
Figure 4.2. Plot of Pressure versus log of cycles for fatigued 2mm C-14 EPDM with zero and non-zero minimum cycling pressure. 82
Figure 4.3. Plot of increasing pressure and stress for 2mm C-14 EPDM showing relationship in terms of true stress and engineering stress. 83
Figure 4.4. Typical specimen failures modes which occurred during equi-biaxial tests. 84
Figure 4.5. Low fatigue life behaviour at constant pressure, 2mm E9566 EPDM specimen. 85
Figure 4.6. Medium fatigue life behaviour at constant pressure, 2mm E9566 EPDM specimen. 86
Figure 4.7. Gas spectrum from vacuum rig showing toluene content in mbar. X-axis shows atomic weight and y-axis partial pressure in mbar. 89
Figure 4.8. Fatigue results for equi-biaxial tests on the two EPDM types (E-1M and C-14), with a minimum cycling pressure of zero bar (2mm original specimen thickness). 90

Figure 4.9. Comparison of fatigue lives of swollen and unswollen C-14 EPDM 2mm specimens, for a 0-2 bar test. 92
Figure 4.10. Pressure-Engineering Stress relationship for swollen 2mm E9566 rubber (0-0.6 MPa). 95
Figure 4.11. Stress amplitude versus cycles to failure, swollen/unswollen 2mm E9566 EPDM. 96
Figure 4.12. Stress-strain curves, swollen and unswollen 2mm E9566 EPDM, 0.6 MPa upper engineering stress, cycles 10 and 1000. 96
Figure 4.13. Relationship between bubble radius and applied volume, in this case for unswollen 2mm E9566 EPDM. 98
Figure 4.14. Stress-strain behaviour of 2mm E9566 EPDM for a stress controlled fatigue test for selected cycles, 1-9068. 99
Figure 5.1 – Plot of stress amplitude versus cycles to failure for the dry and swollen 2mm E9566 EPDM specimens. 102
Figure 5.2. Percentage drop in Specific Modulus for Dry 2mm E9566 EPDM during fatigue testing. 103
Figure 5.3. Comparison of E* versus cycles for the three specimen sets at σ_a = 1MPa. 104
Figure 5.4. Percentage drop in $E^*_{residual}$ versus cycles for 4.2% Swollen 2mm E9566 EPDM during fatigue testing. 105
Figure 5.5. Percentage drop in $E^*_{residual}$ versus cycles for 10% Swollen 2mm E9566 EPDM during fatigue testing. 105
Figure 5.6. Percentage drop in Specific Modulus versus cycles for the dry and 4.2% swollen specimens sets at four different stress amplitudes, where $E^*_{conditioning}$ is based on that of the dry 2mm E9566 EPDM. 106
Figure 5.7. Percentage drop in $E^*_{residual}$ versus cycles for the 3 specimens sets at σ_a = 1MPa, where $E^*_{conditioning}$ is based on that of the dry 2mm E9566 EPDM. 107
Figure 5.8. Experimental and modelled E* plots for three specimen sets at a stress amplitude of 1MPa. 108
Figure 5.9. Plot of loading factor Z versus applied stress for the three specimen sets. 109
Figure 5.10. Basis of Calculation of Dynamic Stored Energy from Stress-Strain Data. 110
Figure 5.11. Plot of Dynamic Stored Energy at Failure for dry 2mm E9566 EPDM. 111
Figure 5.12. Trends of Dynamic Stored Energy at Failure for all three 2mm E9566 EPDM specimen sets. 112
Figure 5.13 – Fracture surface of dry and swollen E9566 2mm EPDM specimens, magnification factor X200. 113
Figure 5.14 – SEM Imaging of fracture surface of dry, 4.2% and 10% swollen 2mm E9566 EPDM specimens, magnification factor X140. 114
Figure 5.15 – SEM Imaging of fracture surface of dry and 10% swollen 2mm E9566 EPDM specimens, magnification factor X190. 115
Figure 5.16 – SEM Imaging of fracture surface of dry and swollen 2mm E9566 EPDM specimens, magnification factor X400. 116
Figure Appendix 2.1 Main User Screen. A2-5
Figure Appendix 2.2 Interlocks and Zero LVDT Setting A2-6
Figure Appendix 2.3 Fatigue Program User Interface. A2-7

Figure Appendix 2.4 Fatigue Program Step 1. A2-8
Figure Appendix 2.5 Fatigue Program Step 2, Subroutine Step 1. A2-9
Figure Appendix 2.6 Fatigue Program Step 2, Subroutine Step 2a. A2-10
Figure Appendix 2.7 Fatigue Program Step 2, Subroutine Step 2b. A2-10
Figure Appendix 2.8 Fatigue Program Step 2, Subroutine Step 3a. A2-11
Figure Appendix 2.9 Fatigue Program Step 2, Subroutine Step 3b. A2-11
Figure Appendix 2.10 Fatigue Program Step 3. A2-12
Figure Appendix 2.11 Fatigue Program Step 4. A2-13
Figure Appendix 2.12 Vision Program User Interface. A2-14
Figure Appendix 2.13 Vision Program Step 1. A2-15
Figure Appendix 2.14 Vision Program Step 2. A2-16
Figure Appendix 2.15 Vision Program Step 3. A2-17
Figure Appendix 2.16 Vision Program Step 4. A2-18
Figure Appendix 2.17 Vision Program Step 5, Substep 1. A2-19
Figure Appendix 2.18 Vision Program Step 5, Substep 2a. A2-20
Figure Appendix 2.19 Vision Program Step 5, Substep 2b. A2-20
Figure Appendix 2.20 Vision Program Step 5, Substep 2c. A2-21
Figure Appendix 2.21 Vision Program Step 6, Substep 1. A2-22
Figure Appendix 2.22 Vision Program Step 6, Substep 2a. A2-23
Figure Appendix 2.23 Vision Program Step 6, Substep 2b. A2-23
Figure Appendix 2.24 Vision Program Step 6, Substep 2c. A2-24
Figure Appendix 2.25 Vision Program Step 7. A2-25
Figure Appendix 2.26 Get Stress Sub Program User Interface. A2-26
Figure Appendix 2.27 Get Stress Sub Program Step 1. A2-26
Figure Appendix 2.28 Get Stress Sub Program Step 2. A2-27
Figure Appendix 2.29 Get Stress Sub Program Step 3. A2-27
Figure Appendix 2.30 Get Stress Sub Program Step 4. A2-28
Figure Appendix 2.31 Valve Rate Sub Program. A2-28
Figure Appendix 3.1 Rotation Calibration Procedure A3-4
Figure Appendix 3.2 Translation and Scaling Calibration Procedure A3-5
Figure Appendix 3.3 Calculations for converting pixels to millimetres. A3-6
Figure Appendix 3.4. Ellipse parameters and evolute curve. A3-8
Figure Appendix 3.5 Calculations of σ_t, σ_e and $\lambda_{1,2}$ (stretch ratio). A3-11
Figure Appendix 4.1. A typical uniaxial stress/strain curve for a filled rubber A4-2
Figure Appendix 4.2. Rubber in the strained and unstrained state A4-3
Figure Appendix 4.3 Tri-axial stress system applied to a cuboid of elastomeric material A4-9
Figure Appendix 4.4. Unit cuboid in simple shear A4-13
Figure Appendix 4.5. Typical Mooney plots A4-16
Figure Appendix 4.6. Thermodynamic representation of a rubber benzene system. A4-25
Figure Appendix 4.7. $\frac{T\Delta S_0}{C_2}$ against degree of swelling Q. A4-26
Figure Appendix 4.8. Plot of Q against $\sqrt{\frac{L_0}{V_0}}$ A4-29

Figure Appendix 4.9. Q as a function of $\sqrt{V_0}\left(\sqrt{\frac{L_0}{V_0}} - \sqrt{\frac{L_r}{V_r}}\right)$. A4-30
Figure Appendix 4.10. (a) Cracked body under tensile load and (b) associated force displacement curves for changes in crack length a, due to constant displacement and load. A4-32
Figure Appendix 4.11. Physical model for Griffith's analysis. A4-33
Figure Appendix 4.12. Typical specimen types used in crack propagation tests on elastomers, (a) Tensile strip, (b) Trousers test-piece, (c), Specimen with central crack, (d), Pure shear specimen [49]. A4-35
Figure Appendix 5.1 E* Measured versus E* modelled, σ_a = 1.2MPa A5-1
Figure Appendix 5.2 E* Measured versus E* modelled, σ_a = 1.1MPa A5-1
Figure Appendix 5.3 E* Measured versus E* modelled, σ_a = 1.05MPa A5-2
Figure Appendix 5.4 E* Measured versus E* modelled, σ_a = 0.95MPa A5-2
Figure Appendix 5.5 E* Measured versus E* modelled, σ_a = 0.8MPa A5-3

List of Tables

Table 3.1 Reference oil properties. 78
Table 4.1 Crosslink densities of EPDM specimens. 88
Table 5.1 Table of constants to describe form of loading factor Z. 109

Chapter 1 Introduction

1.1 The motivation for the research programme

The importance of elastomers as engineering materials cannot be underestimated. Elastomeric components can be found in the automotive, aeronautical and biomedical sectors in diverse applications such as automobile tyres, conveyor belts, gaskets in supersonic jet planes and in heart valves.

The profitability of rubber component manufacturers is dependant on a number of factors, the most significant of which is the unit cost of component manufacture. The prices of many raw materials reached record levels in the first half of 2006. Instability in the Middle East, strong demand from China and market speculation were all contributory factors that resulted in the raw materials markets adding pronounced pressure to leading vehicle and rubber component manufacturers. In turn, this pressure permeated and adversely affected the profitability and viability of European SME's. Though in a global economy, increases in the costs of raw materials apply to all, a competitive advantage can be gained by producing better components through improved functionality of materials. With raw materials costs continually increasing, the requirement for improvements in manufacturing processes and component design is paramount. Companies which are capable of maintaining high product quality will have the advantage over others in terms of customer satisfaction and brand recognition. While developing countries in Asia, including China, are responsible for an ever increasing market share in the supply of rubber components worldwide, improvements in design standards of elastomeric components tend to be dictated by Japan, Europe and the United States. This advantage possessed by the more

developed countries offsets some of the disadvantages these countries have to contend with; most notably manufacturing overheads.

With environmental concerns dictating governmental policy worldwide, automobile design standards are becoming more and more rigorous. The increased need for fatigue life data for elastomeric materials, prompted by Japanese automotive standards [1] and higher expectations for automotive component reliability worldwide [2] require consideration of appropriate criteria for assessing rubber component life.

Previous research [3-6] has shown that fatigue resistance and crack propagation are dependant on a range of factors and the test parameters applied. For Ethylene-Propylene-Diene Polymer (EPDM) and Styrene-Butadiene Rubber (SBR) test-pieces subjected to uniaxial constant strain amplitude cycles, the levels of minimum and consequently mean stress were found to significantly influence fatigue life and in general for these materials the number of cycles to failure of specimens were increased by pre-stressing.

The results of most fatigue tests are produced using testing equipment which loads the specimens in uniaxial tension, combined tension and torsion or in shear. While these methods provide much useful insight into the fatigue behaviour of elastomers, they do not describe the full spectrum of elastomeric material behaviour under cyclic loading. Few engineering components are merely loaded uniaxially in service and rubbers are quite different materials when loaded multi-axially, due to the orientation of long chain molecules. Dynamic bubble inflation, which is capable of loading test-pieces in equi-biaxial tension for multiple cycles, allows specimens to be fatigued to failure equi-biaxially and facilitates completion of the characterisation of fatigue life for all loading cases

for a particular elastomer. The static rig developed in Robert Bosch by Johannknecht [7] for tests to determine hyperelastic properties, led to the consideration of developing an equivalent dynamic test apparatus. Johannknecht used both hydraulic and pneumatic inflation methods. However, for fatigue testing of elastomers, pneumatic inflation and deflation is not feasible due to the compressibility of air, which unavoidably introduces lag during cycling. Therefore, a hydraulic fluid is required as the inflation medium to cycle test specimens. A beneficial and important consequence of using hydraulic media for bubble inflation is that the swelling effects of specific liquids on a range of dynamically loaded rubber compounds can be investigated. The investigation can be extended to determine the effect of swelling on the equi-biaxial properties of initially dry elastomers.

1.2 Aims and Objectives

The primary aims of this research are:

- To develop a novel control methodology for dynamic bubble inflation which is capable of maintaining the values of maximum and minimum engineering stress between acceptable limits during cycling of the test-piece for dry and swollen EPDM test-pieces.
- To answer a fundamental question: Does altering the rubber-filler matrix by the introduction of a swelling agent affect the fatigue behaviour of the rubber, where it is subjected to prior treatment and subsequent loading?

It was anticipated that the outcomes of the tests proposed would determine the resultant damage caused by swelling and the consequent influence that swelling has on fatigue resistance. To investigate the influence of swelling in equi-biaxial

fatigue and in order to fully evaluate the problems presented, a programme of parallel investigations was required.

Equi-biaxial fatigue tests were carried out on non-strain crystallising elastomers at room temperature (15-20 °C), using inflation media that would give rise to minimal swelling with equal pressure and stress amplitudes. The swollen samples were pre-treated with liquids having varying solubility parameters, e.g. one liquid swelled the sample readily during the test, while the other liquid had minimal effect on the volume of the rubber-filler matrix.

The fatigue failure surfaces were studied using light imaging microscopy and scanning electron microscopy (SEM) to determine the effects on fracture surface due to swelling in the samples.

Consequently, the objectives of the research were:

- To develop a methodology for oil swelling tests to prepare swollen EPDM samples for use in fatigue tests, initially from experiments using toluene, followed by ASTM reference oils.
- To determine if fatigue strength reductions due to swelling in EPDM rubber specimens loaded equi-biaxially were consistent with strength reductions in samples subjected to uniaxial tests to failure [3-6].
- To establish equi-biaxial Wöhler (S/N) curves for a range of EPDM rubbers swollen in different media in tests conducted at constant pressure and stress amplitudes.
- To develop a method of controlling engineering stress limits during fatigue testing of EPDM specimens.

- To establish relationships between cycles to failure and dynamic modulus and stored energy for the EPDM rubber tested.
- To offer predictors of fatigue life for swollen/unswollen EPDM specimens subjected to equi-biaxial fatigue.
- To determine if a fatigue life predictor similar to that advanced by Abraham *et al* [3-6] of dynamic stored energy is applicable when determining the service life of EPDM compounds subjected to the following conditions:
  - Dry EPDM rubbers loaded equi-biaxially between constant pressure limits, with a zero pressure as the lower pressure limit.
  - Swollen EPDM rubbers loaded equi-biaxially between constant pressure limits, with a zero pressure as the lower pressure limit.
  - Dry EPDM rubbers loaded equi-biaxially between constant stress limits, with a zero minimum stress as the lower stress limit.
  - Swollen EPDM rubbers loaded equi-biaxially between constant stress limits, with a zero minimum stress as the lower stress limit.

Figure 1.1 shows the structure of the testing and analysis carried out to achieve the research objectives.

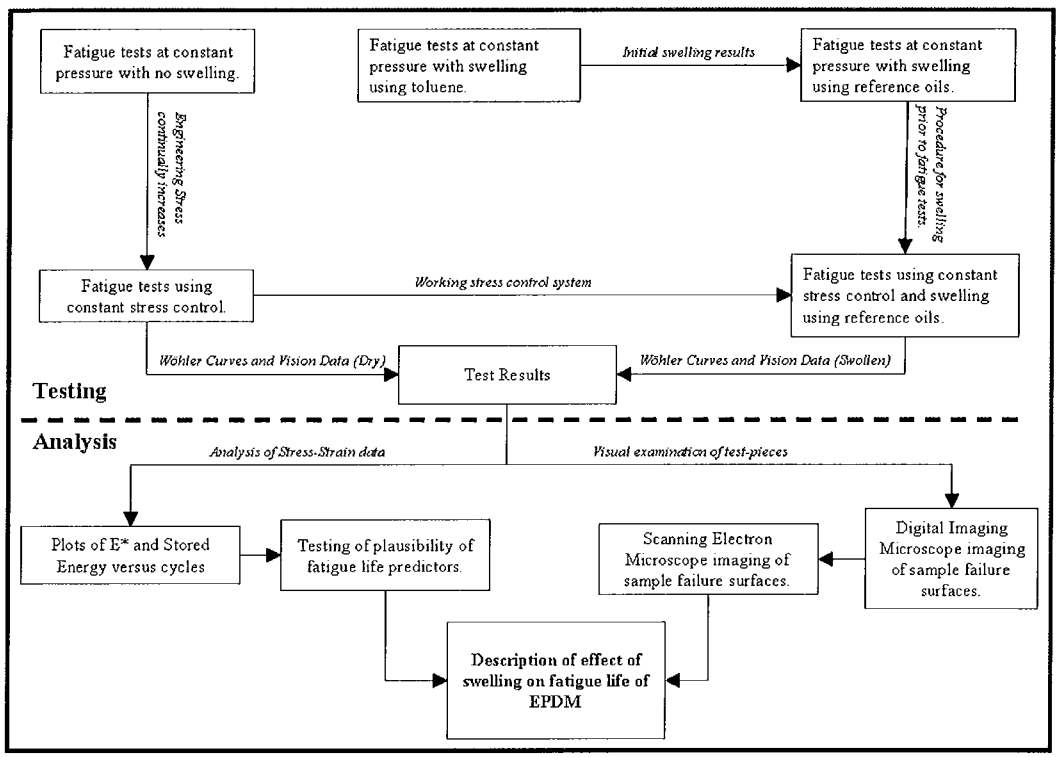

Figure 1.1. Overview of testing and analysis carried out to achieve the research objectives.

1.3 An overview of the research

This text outlines the different activities carried out to achieve the objectives of the research. These activities are listed below, but are described fully in the chapters and sub-sections of the dissertation. The research adopted the following methodology:

- Conducting a literature review of elastomeric theory, including typical properties of rubbers, the influence of swelling on rubberlike materials and a discussion of the fatigue and dynamic behaviour of elastomers (Chapter 2).

- Developing an equi-biaxial fatigue test system, including the evolution of rig design and a consideration of investigating swelling phenomenon in equi-biaxial fatigue using the facility (Chapter 3).
- Determining a methodology and test procedure, describing preliminary testing using constant pressure, the consequent methods used to achieve constant stress cycling and initial tests which incorporated swelling (Chapter 4).
- Testing of EPDM rubbers in equi-biaxial fatigue incorporating swelling, with results depicted using Wöhler curves and including discussion on failure modes, the influence of test parameters on fatigue life, comparison of hysteresis curves, energy and fatigue life. A discussion on the effect of oil swelling on the fatigue life of EPDM is also provided (Chapter 5).
- Presenting discussion of the results of the final testing and conclusions for the research (Chapter 6).
- Providing an outlook for the research programme and recommendations for future work (Chapter 7).

Chapter 2 Literature Review

2.1 Properties of Rubber

All non-linear materials have unique properties associated with them, but in particular, rubber has phenomenological behaviour that is imperfectly understood. This chapter highlights the properties of rubber relevant to the research aims and objectives outlined in the previous chapter. The areas which will be reviewed in subsequent sections include:

1. A definition of general polymer properties which have relevance to this study.
2. A description of how theories for calculating the energy in a rubber network were derived and how they account for swelling of the network.
3. The effect of swelling on the stress-strain behaviour of rubber, including chemical and mechanical based treatments of the problem by others.
4. A summary of elastomeric fatigue behaviour, particularly with respect to dynamic equi-biaxial fatigue and swelling.

Other properties of elastomers, such as hyperelasticity and viscoelasticity and the phenomenological theories developed to describe them are contained in Appendix 4.

2.1.1 Definition of general polymer properties

Before entering into further detailed descriptions of elastomer properties, the general properties of polymers, of which rubbers are a group, should be discussed.

Chain types and Cross Linking

Polymers can consist of two different types of chain, straight or branched. Crosslinking polymer chains will result in an increase in strength by creating chemical bonds at junction points of different chains. Solvent swelling can have the effect of breaking these links. On drying, links can reform, but at different locations. The effect of solvent swelling on rubber properties will be discussed in detail in subsequent sections.

Chain Density

The density of polymer chains in a material can affect its physical properties. Polyethylene can be used to describe the effect on properties that polymer chain type and density can have. Low density polyethylene consists of polymer chains which are branched. A limited number of these chains can occupy a discrete space. High density polyethylene consists mainly of straight chains of polymers. More of these straight chains can occupy a discrete space than branched chains, thereby resulting in a denser material, with increased intermolecular forces, tensile strengths and higher glass transition temperatures.

Molecular Weight

The molecular weight of a polymer atom gives an indication of its properties. With increasing molecular weight, the mechanical properties, such as hardness, will increase and physical properties such as melting point will also increase.

Physical Forces - Intermolecular Action/Forces

Intermolecular physical, as opposed to chemical forces, in typical polymers in increasing order are:

Van der Waals forces - These are also known as non-polar forces and are the weak attractions between the atoms in one polymer chain and the atoms in another adjacent chain. These forces exist in materials having chains containing carbon and hydrogen atoms.

Polar forces - These are attractions between polymer chains having chlorine (or fluorine) atoms, where the negatively charged chlorine atoms on the side of one polymer chain are attracted to the positively charged carbon atoms on the corresponding side of an adjacent polymer chain.

Hydrogen Bonding - These bonds take place in polymer structures containing Nitrogen (N), Oxygen (O) or Sulphur (S). There is a chemical attraction between the N, O and S atoms in the polymer chains and hydrogen atoms in adjacent chains.

2.2 Thermodynamical analysis of a rubber network and development of statistical theory

It was first reported by Gough in 1805 that rubber generates heat when stretched and cools upon contracting. He also noted that rubber strip under a constant load contracted when heated and elongated when cooled.

Following the formation of the second law of thermodynamics, Joule in 1859 interpreted data on vulcanised rubber in terms of thermodynamics. The experimental findings of Gough and Joule could only be interpreted phenomenologically until the development of the molecular theory of rubber

elasticity. The derivation of the thermodynamic theory has been summarised elsewhere, notably by Treloar [9].

As heat is generated by a stretched rubber, from the first law of thermodynamics the change in internal energy dU is given by:

$$dU = dQ + dW \tag{1}$$

where dQ is the heat absorbed by the system and dW is the work done on it.

The second law defines the entropy change dS in a reversible process by the relation:

$$TdS = dQ \tag{2}$$

From equation (2), for a reversible process:

$$dU = TdS + dW \tag{3}$$

The Helmholtz free energy, which will be discussed in more detail in 2.3.3, is defined by the relation:

$$A = U - TS \tag{4}$$

For a change taking place at a constant temperature:

$$dA = dU - TdS \tag{5}$$

Combining (4) with equation (3), we get:

$$dA = dW \tag{6}$$

When observing the mechanical treatment of a swollen rubber in section 2.2.3, the significance of equation (6) will become evident.

Also, referring to equation (3), it can be seen that the work done on the specimen (-dW), exceeds the increase in internal energy dU. The entropy of deformation, given by $dS = dQ/T$ for a reversible process (which is carried out very slowly) decreases. This entropy differs from that of the total system (e.g. the elastomers and its surroundings)

If $dU = 0$, $-TdS = dW$, meaning that the work on the specimen will result in a decrease in entropy at a constant temperature.

Consider a unit cube strained so that it has 3 unequal edge lengths λ_1, λ_2 and λ_3. It can be shown that the change in entropy for a constant volume deformation can be represented by the following equation:

$$\Delta S = -\frac{1}{2} Nk(\lambda_1^2 + \lambda_2^2 + \lambda_3^2 - 3) \tag{7}$$

If we assume that there is no change in internal energy U on deformation, then from (5) and (6),

$$W = -TdS \tag{8}$$

Then (7) can be shown to be,

$$W = -\frac{1}{2}G(\lambda_1^2 + \lambda_2^2 + \lambda_3^2 - 3) \tag{9}$$

Where

$$G = nkT \tag{10}$$

2.2.2 Extension of theories to swollen rubber

Treloar outlined the basis of this theory in his treatment of the elastic properties of a swollen rubber [9]. It is assumed that the unswollen sample is a unit cube which contains N chains per unit volume. The swelling degree is defined in terms of the volume fraction υ_2 of the rubber in the mixture of elastomer and liquid. The volume swelling ratio is $1/\upsilon_2$ and the linear dimensions of the swollen sample are $\lambda_0=1/\upsilon_2^{1/3}$, assuming a linear swelling ratio.

The parameter υ_2 is introduced as a means of defining the state of swelling of the network, regardless of whether or not this state is the equilibrium state with respect to the absorption of liquid. The nature of the swelling liquid, or how and if equilibrium swelling is determined is not of consequence at this stage.

Again swelling corresponds to an isotropic expansion of the network and will therefore be accompanied by a reduction in the entropy of the network, as can be seen, from equation (7).

Applying a stress to the swollen rubber results in further reduction in network entropy, due to further deformation of the swollen network. This total reduction in network entropy can be looked on as being the sum of two separate terms, that due to swelling and that due to the subsequent strain in the system.

The second of these terms is the one of primary importance, as the mechanical properties of the swollen rubber are determined from it.

$$\Delta S' = \Delta S'_0 - \Delta S_{0,} \tag{11}$$

where,

$\Delta S'_0$ is the total entropy change in passing from the unstrained swollen state to the strained swollen state.

ΔS_0, is the entropy of deformation associated with the initial isotropic swelling.

$\Delta S'$ is the difference between $\Delta S'_0 - \Delta S_{0,}$

ΔS is the entropy of deformation per unit volume of swollen rubber and can be expressed as:

$$\Delta S = \upsilon_2 \Delta S' \tag{12}$$

These terms are related as follows:

$$\Delta S_0' = -\frac{1}{2} Nk(l_1^2 + l_2^2 + l_3^2 - 3) \tag{13}$$

where l_1, l_2 and l_3 are the lengths of the edges of the original unit cube, i.e. the principal extension ratios referred to the unswollen state.

The change of entropy ΔS_0 associated with the initial isotropic swelling, corresponding to the linear extension ratio λ_0, is

$$\Delta S_0 = -\frac{1}{2} Nk\,(3\lambda_0^2 - 3) = -\frac{1}{2} Nk\,(3\nu_2^{-\frac{2}{3}} - 3) \tag{14}$$

The entropy of deformation ΔS_0 of the swollen network is the difference between these two quantities, i.e.

$$\Delta S' = \Delta S'_0 - \Delta S_0 = -\frac{1}{2} Nk(l_1^2 + l_2^2 + l_3^2 - 3\nu_2^{-\frac{2}{3}}) \tag{15}$$

The extension ratios λ_1, λ_2 and λ_3 are defined with reference to the unstrained swollen state, so that $l_1 = \lambda_1\lambda_0 = \lambda_1\upsilon_2^{1/3}$, etc. so that the following expression is obtained:

$$\Delta S' = -\frac{1}{2} Nk\nu_2^{-\frac{2}{3}}(\lambda_1^2 + \lambda_2^2 + \lambda_3^2 - 3) \tag{16}$$

This is the entropy of deformation per unit volume of the original unswollen rubber. The entropy of deformation ΔS per unit volume of the swollen rubber is given by:

$$\Delta S = \nu_2 \Delta S' = -\frac{1}{2} Nk\nu_2^{\frac{1}{3}}(\lambda_1^2 + \lambda_2^2 + \lambda_3^2 - 3) \qquad (17)$$

The corresponding strain-energy density function for the swollen rubber thus becomes

$$W = -T\Delta S = \frac{1}{2} NkT\nu_2^{\frac{1}{3}}(\lambda_1^2 + \lambda_2^2 + \lambda_3^2 - 3) \qquad (18)$$

This equation represents the properties of the swollen rubber in terms of the extension ratios measured in the swollen state and the volume fraction of rubber υ_2. It should be noted that N is the number of chains per unit volume of the unswollen rubber.

Comparison of the result expressed by (18) with the corresponding expression for the unswollen rubber shows the dependence of the stored energy on strain to be the same in both cases, the only difference being in the value of the shear modulus. If G and G' are the respective moduli in the unswollen and in the swollen states, then

$$G' = G\upsilon_2^{1/3} = \rho RT/M_c\, \upsilon_2^{1/3} \qquad (19)$$

Where ρ is the density in the unswollen state. The resultant stress-strain relations for the swollen rubber are of the form

$$t_1 - t_2 = G\upsilon_2^{1/3}(\lambda_1^2 - \lambda_2^2) = G'(\lambda_1^2 - \lambda_2^2) \qquad (20)$$

and show a corresponding difference. These results imply that the only effect of the swelling is to reduce the modulus in inverse proportion to the cube root of the swelling ratio, without changing the form of the stress-strain relation.

By the use of a different method of calculating the entropy of deformation, based on the consideration of the entropy of formation of the network from a corresponding set of independent chains, the following result was obtained:

$$\Delta S'_0 = - \tfrac{1}{2}Nk \{l_1^2 + l_2^2 + l_3^2 - 3 - \ln (l_1 l_2 l_3)\} \qquad (21)$$

Which differs from (13) by the inclusion of the term $-\ln (l_1 l_2 l_3)$. (13) and (21) become identical for the case of an unswollen rubber for which $\ln (l_1 l_2 l_3) = 0$, while for a swollen rubber the effect of the additional term is in most practical cases rather small.

2.2.3 The dependence of swelling on strain

This problem of determining the equilibrium degree of swelling in the presence of a stress was first solved by Flory and Rehner [8] and clarified in later work by Gee [10] for the case of a simple tensile stress.

The results of the studies showed that the effect of the tensile stress is to increase the amount of swelling compared with that for the stress free rubber.

Consider a specimen of crosslinked material, as shown in Figure 2.1, originally in the form of a unit cube. This cube is in contact with a liquid and is constrained by normal forces applied to its faces having dimensions l_1, l_2, and l_3.

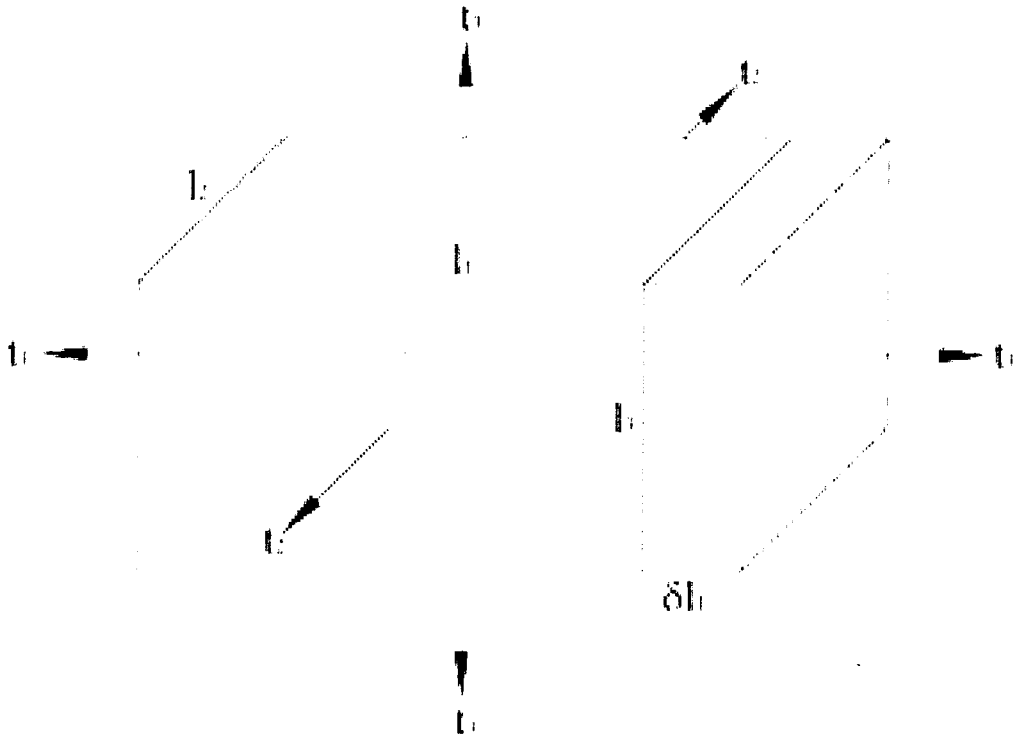

Figure 2.1. Equilibrium of swollen rubber under stress

If the volumes of the polymer and liquid are assumed to be additive:

$$l_1 l_2 l_3 = 1/\nu_2 = 1 + n_1 V_1 \qquad (22)$$

n_1 is the number of moles in the liquid in the swollen polymer

V_1 is the molar volume of the liquid

ν_2 is the volume fraction of the polymer

Consider now the absorption of a further quantity δn_1 moles of liquid, under the condition that l_2 and l_3 are held constant, while l_1 increases by the amount δl_1. The stress t_1 acts on the area $l_2 l_3$. The corresponding force on this area is therefore $t_1 l_2 l_3$.

Since no work is done by t_2 and t_3, the total work done by the external forces is

$$\partial W = t_1 l_2 l_3 = t_1 V_1 \partial n_1 \tag{23}$$

If we treat the total change of free energy of the system as the sum of two free energies:-

i) The free energy of mixing of polymer and liquid molecules and

ii) The free energy of network deformation (entropy)

We get:

$$\Delta G = \Delta G_m + \Delta G_e \tag{24}$$

We already know from 2.2 that for a reversible process at a constant temperature:

$$\Delta A = \Delta W \tag{25}$$

A small displacement in equilibrium will be equal to the work done by the applied forces:

$$\partial \Delta A = \delta W \tag{26}$$

The relation between Gibbs free energy ΔG and ΔA under conditions of constant pressure and temperature is:

$$\Delta G = \Delta A + p\Delta V \tag{27}$$

If the net volume change of liquid plus polymer is assumed to be zero, then $\Delta G = \Delta A$, then:-

$$\partial \Delta G = \partial W = t_1 V_1 \partial n_1 \tag{28}$$

Rearranging,

$$(\frac{\partial \Delta G}{\partial n_1})_{l_2 l_3} = t_1 V_1 \tag{29}$$

Applying to (25) we get,

$$(\frac{\partial \Delta G}{\partial n_1})_{l_2 l_3} = \frac{\partial \Delta G_m}{\partial n_1} + (\frac{\partial \Delta G_e}{\partial n_1})_{l_2 l_3} \tag{30}$$

It is known that the Flory-Huggins parameter χ in this notation can be shown as,

$$\frac{\partial \Delta G_m}{\partial n_1} = RT\{\ln(1-\nu_2) + \nu_2 + \chi \nu_2^2\} \tag{31}$$

We know that the elastic free energy of a swollen network referred to the unswollen state is,

$$\Delta G_e = W = \frac{\rho RT}{M_c}(l_1^2 + l_2^2 + l_3^2 - 3) \tag{32}$$

Using this expression with (22) we get,

$$(\frac{\partial \Delta G_e}{\partial n_1})_{l_2 l_3} = (\frac{\partial \Delta G_e}{\partial l_1})(\frac{\partial l_1}{\partial n_1})_{l_2 l_3} = \frac{\rho RT}{M_c} l_1 \frac{V_1}{l_2 l_3} = \frac{\rho V_1 RT}{M_c} \nu_2 l_1^2 \qquad (33)$$

Combining (32) and (33) and arranging in the form of (30) to get the total free energy of dilution and introducing the equilibrium condition (29) the result is:

$$t_1 = \frac{RT}{V_1}\{\ln(1-\nu_2) + \nu_2 + \chi \nu_2^2 + \frac{\rho V_1}{M_c} \nu_2 l_1^2\} \qquad (34)$$

Corresponding equations exist for t_2 and t_3, in terms of l_2 and l_3.

From the three equations, by subtraction three general stress-strain relations for swollen rubber can be written in the form:

$$t_1 - t_2 = \frac{\rho RT}{M_c} \nu_2 (l_1^2 - l_2^2) = \frac{\rho RT}{M_c} \nu_2^{\frac{1}{3}} (\lambda_1^2 - \lambda_2^2) \qquad (35)$$

In which λ_1, λ_2 and λ_3 are the extension ratios referred to the swollen unstrained state.

It should be noted here that in an incompressible material (whether swollen or unswollen), the volume and hence the state of strain is unaffected by the by the superposition of an arbitrary hydrostatic pressure. In a compressible rubber, or a rubber considered to be in equilibrium with respect to the swelling liquid, this is

not true, since any such hydrostatic pressure will reduce the volume or liquid content.

In this respect therefore, a swollen rubber in continuous equilibrium with a surrounding liquid may be regarded as having mechanical properties equivalent to those of a compressible material.

2.2.3.1 The case of hydrostatic pressure

In the case of a simple hydrostatic pressure p applied to the polymer, (but not to the liquid),

$$t_1 = t_2 = t_3 = -p \tag{36}$$

$$l_1 = l_2 = l_3 = v_2^{-\frac{1}{3}} \tag{37}$$

For equilibrium, from (34),

$$\frac{RT}{V_1}\{\ln(1-v_2) + v_2 - \chi v_2^2 + \frac{\rho V_1}{M_c} v_2^{\frac{1}{3}}\} = -p \tag{38}$$

The pressure p is equivalent to the swelling pressure.

2.2.3.2 The case of simple tension

For simple elongation, with a tensile stress t_1 acting in the direction l_1

$$t_1 = t_2 = 0\,,\; l_{12}^2 = l_{13}^2 = 1/\nu_2 \tag{39}$$

Using the expression for t_2 based on (34), the equilibrium becomes,

$$t_2 = \frac{RT}{V_1}\{\ln(1-\nu_2) + \nu_2 + \chi\nu_2^2 + \frac{\rho V_1}{M_c l_1}\} = 0 \tag{40}$$

The equation may be solved for ν_2 for a specified value of l_1, the length in the direction of the applied force. If l_1 is greater than $\nu_2^{-\frac{1}{3}}$, the force is tensile, if less than, the force is compressive. If the terms are equal, the tensile stress is zero and free swelling exists.

2.2.3.3 The case of equi-biaxial extension

For simple elongation, with a tensile stress t_1 acting in the direction l_1

$$t_2 = t_3\,,\; t_1 = 0\,,\; l_{12}^2 = l_{13}^2 = 1/l_1\nu_2 \tag{41}$$

Using the expression for t_2 based on (35), the equilibrium becomes,

$$t_1 = \frac{RT}{V_1}\{\ln(1-\nu_2) + \nu_2 + \chi\nu_2^2 + \frac{\rho V_1}{M_c l_2^4}\} = 0 \tag{42}$$

In this expression l_1 is the stretch ratio in the plane of the stretched sheet, referred to the unswollen unstrained dimensions.

2.2.4 Swelling and Extension Ratios – Alpha Terms

The following derivation has also been used in the past for the mechanical treatment of swollen rubbers by Krigbaum and Roe [11] and Treloar [12] where an 'α' term is used instead of stretch ratios.

It is commonly assumed [13] that the Helmholtz free energy can be represented as follows:

$$A = A_{el} + A^{+} \tag{43}$$

Where the Helmholtz free energy A is defined as the useful work of a closed thermodynamic system at a constant temperature. A_{el} represents the elastic or configuration free energy, which depends on such parameters as the number of network chains, conditions of network formation, temperature, effect on specimen's dimensions by surface tractions and swelling. The term A^{+} is related to intermolecular interactions and is considered to be independent of the deformation.

The change in the elastic free energy of a network subject to deformation can be determined using the following equation derived elsewhere [14]

$$\Delta A_{el} = (\nu kT/2)[(V/V_0)^{2/3}(\alpha_1^2 + \alpha_2^2 + \alpha_3^2) - 3] \tag{44}$$

where $(\alpha_1^2 + \alpha_2^2 + \alpha_3^2) = 1$, regardless of the magnitude of V.

To represent volume changes resulting from swelling or de-swelling the following equation was derived:

$$\Delta A_{el} = (\nu kT/2)[(V/V_0)^{2/3}(\alpha_1^2 + \alpha_2^2 + \alpha_3^2) - 3 - B\ln(V/V_0)] \quad (45)$$

This equation can be applied to a swollen elastomer, an elastomer formed in the presence of a solvent and to an elastomer obtained from the latter by extraction of the solvent, or addition of more solvent.

Consider a rectangular (length L_u, width W_u, thickness T_u) specimen of rubber in the undeformed state (Figure 2.2).
When a pure homogeneous deformation is imposed, its dimensions become L, W and T.

The state of deformation can be specified by the principal extension ratios:

$$\lambda_1 = L/L_u, \quad (46)$$

$$\lambda_2 = W/W_u, \quad (47)$$

$$\lambda_3 = T/T_u, \quad (48)$$

And it follows that

$$\lambda_1\lambda_2\lambda_3 = V/V_u, \quad (49)$$

Where V and V_u are the deformed and undeformed specimen volumes.

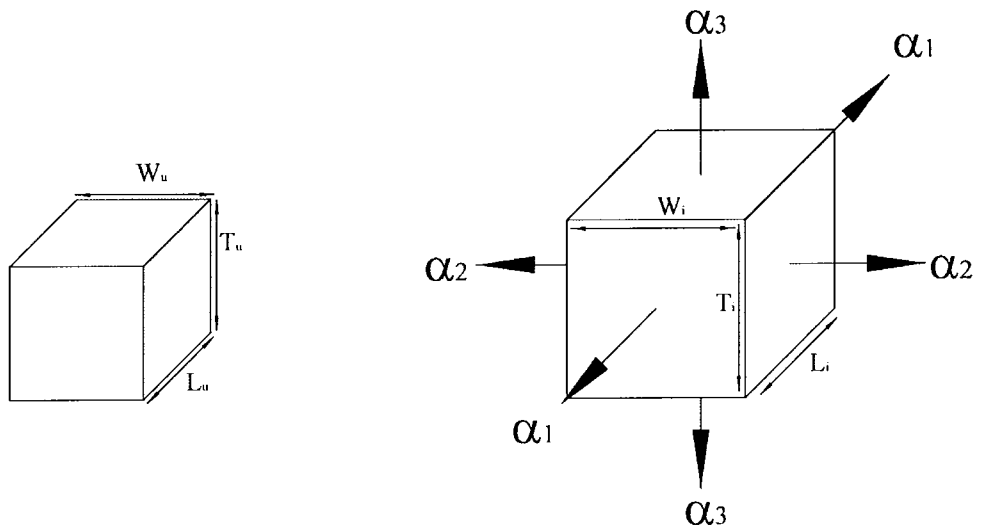

Figure 2.2. Unit cube of rubber (a) and (b), the same cube subject to a homogeneous deformation (tensile).

Consider a swollen cuboid specimen in its isotropic state, $\lambda_1 = \lambda_2 = \lambda_3$ and hence $\lambda_1^3 = \lambda_2^3 = \lambda_3^3 = V/V_u = 1/\upsilon_r$, where V is the volume of the swollen specimen and υ_r is the volume fraction of the network in the swollen specimen.

To allow precise determination of the increase in size due to swelling, it is useful to introduce another set of extension ratios related to the λ's as follows:

$$\alpha_1 = (V_u/V)^{1/3}\lambda_1, \tag{50}$$

$$\alpha_2 = (V_u/V)^{1/3}\lambda_2, \tag{51}$$

$$\alpha_3 = (V_u/V)^{1/3}\lambda_3, \tag{52}$$

where,

$(V_u/V)^{1/3} = \upsilon_r^{1/3} = L_u/L_i = W_u/W_i = T_u/T_i$, where $L_i = W_u/W_i = T_u/T_i$ represent the dimensions of the specimen in its isotropic state at volume V, as shown in figure 2.3. Specifically $\alpha_1 = L/L_i$ and similarly for α_2 and α_3.

It follows that

$$\alpha_1\alpha_2\alpha_3 = 1 \qquad (53)$$

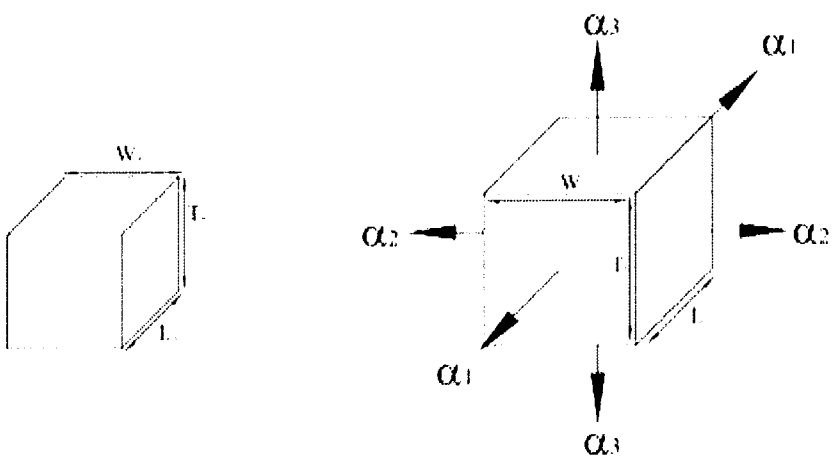

Figure 2.3. Unit cube of rubber at a volume V_u (a) and (b), the same cube subject to deformation due to swelling, occupying a volume V.

When a volume change results from the swelling or de-swelling of a specimen, the α's may differ considerably from the λ's. In cases where a specimen is subject to stress, α's may differ slightly from the λ's, because V is somewhat dependant on the applied stress.

2.3 The influence of swelling on rubber-like materials

2.3.1 Introduction

When a rubber is vulcanised, there exists a three-dimensional structure of polymeric chains which occupy the entire elastomer system in question. This structure may be treated at a macroscopic level as one large molecule, provided the elastomer system is dry, e.g. no solvent/diluent is present. During the crosslinking process, at a molecular level every primary molecule in the rubber couples with other molecules through chemical bonds at a large number of sites. As a result of the crosslinking process, all of these primary molecules become part of one continuous molecular structure. Due to the existence of these bonds after vulcanisation, the polymer network will not dissolve in a solvent, as would the network for a rubber which had not been crosslinked. However, the network will allow solvent absorption and a finite amount of swelling to take place.

Organic liquids such as oil tend to weaken elastomers by physical means only, whereas corrosive liquids, such as acids and alkalis tend to attack chemically.

The rate of swelling is diffusion controlled and an elastomers resistance to swelling increases as a square of its thickness and with increasing viscosity of the swelling liquid. The mechanical behaviour of a rubber depends largely on its crosslink density. The more crosslinks per unit volume in an elastomer, the less the material is prone to swelling when immersed in a solvent. Rubbers and solvents, when of the appropriate compatibility, can be used to determine the crosslink density of an unswollen rubber. By determining this property of the elastomer, the modulus of the material may also be estimated. Section 2.3.2 details the development of the theory of swelling phenomenon, from the early experimental research to the development of the thermodynamical theories for

swelling of rubbers subjected to mechanical strain [12] and the compatibilities of polymer solvent mixtures [15], as well as the significance and use of the Flory-Rehner equation [8] in the understanding of network structure. The use of swelling in the investigation into dynamic mechanical properties of elastomers is also discussed in detail.

2.3.2 Early Research into swelling phenomenon

The literature in the late 1920's and early 1930's shows that researchers were beginning to look at swelling in a scientific manner, with Scott producing a number of time swelling curves for rubbers immersed in different solvents [16]. This was based on swelling rubber in different liquid combinations and taking the increase of weight of the rubber as being the weight of the liquid absorbed. This new weight, combined with the specific gravities of the rubber and liquid in question, allowed the swelling of the rubber to be expressed in terms of the volume of liquid absorbed as a percentage of the volume of the original rubber. The experiments showed that the volume of the swollen rubber sample was equal to the sum of the volumes of the dry rubber and the absorbed liquid.

One aspect of behaviour noted was a time swelling curve. The saturation curve describes a simple saturation of the rubber with liquid, with a relatively rapid absorption of the liquid by the rubber, then proceeding to a maximum value or saturation point, while the increment curve is a very slow, practically uniform increase in swelling, which the author attributed to a progressive change in the properties of the rubber. From these two curves, the time-swelling curve is described. The existence of the increment was attributed to a gradual depolymerisation of the rubber brought about by the atmospheric oxygen

dissolved in the swelling liquid, where the author defined depolymerisation as an alteration of the rubber, with the breaking down of larger structures into smaller structures. In terms of swelling and mechanical properties of the rubber, Scott concluded that "swelling may be regarded as a form of deformation equivalent to a small linear extension". He determined that there was a relationship between the swelling maximum and the percentage, but no obvious relationship between this swelling maximum and tensile strength, resilience or permanent set.

During these early years of research into swelling phenomenon, there were no machines for testing the tensile strength, elongation at break and tear and abrasion resistance of swollen elastomers and these properties were determined rudimentarily by physically stretching the specimen to estimate changes in tensile strength, while a knife was used to estimate changes in tear and abrasion resistance. However, in his investigation into the swelling of rubbers in oil, Hayden noted that the swelling of the rubber in the oil was restricted by mechanical pressure and that when the rubber was strained, the rate of oil absorption increased [17].

2.3.3 Further Research of Swelling Phenomenon - Development of the thermodynamics of swelling

In studies by Whitby [18] carried out on vulcanised rubber immersed in a wide range of liquids, a supposed relationship was thought to exist between the swelling power of the liquid for rubber and its cohesive energy density.

Other research carried out by Gee and Treloar, [15] described experimental studies of mixtures of benzene and unvulcanised rubber over the widest possible range of vapour pressures. The results they obtained were used to calculate

Gibbs free energy of dilution ΔG_1, the heat of dilution ΔH_1 and the entropy of dilution ΔS_1. The work on benzene showed that the ready absorption of most organic liquids by rubber is not to be taken as evidence of any mutual affinity, but is due essentially to the large increase of entropy which results from mixing.

Further studies into this phenomenon were carried out by Gee [19-24] who attempted to derive a thermodynamic basis to describe the mechanism of rubber swelling. Gee stated that the entropy of swelling of vulcanised rubber can be estimated and was assumed independent of the nature of the swelling liquid. The heat of swelling is related to the cohesive energies of the liquid and rubber. The swelling power of a liquid can be calculated approximately if its cohesive energy and molecular volume are known. When investigating the mixing of two liquids, consider that at the molecular level the molecules of a liquid are close together and therefore exert strong forces on one another. This is the origin of the latent heat of evaporation, which represents the work done in overcoming the cohesive energy of the molecules. As different liquids do not have the same molar latent heats, it must be concluded that their molecules cohere with different energies. This difference depends partly on the chemical nature of the molecules and partly on the way they pack together.

Following the use of a statistical thermodynamic method to describe the swelling of rubbers in single liquids, Gee extended the method to mixed liquids. From this work, there were two primary conclusions:

i. Of two liquids of equal molecular volume, the one whose heat of mixing (per cc) with the polymer is the smaller, will be preferentially absorbed.

ii. Of two liquids of whose heats of mixing with the rubber (per cc) are identical, the one of smaller molecular volume will be absorbed.

Agreement with this hypothesis was good for natural rubber, but was less so for synthetic rubbers. This was later attributed to block polymerisation, where block copolymers, made up of blocks of different polymerised monomers, undergo microphase separation to form periodic nanostructures [24].

Further discussion of the thermodynamics of rubber swelling and cohesive energy densities is contained in Appendix 4.

2.3.4 Determination of Crosslinking in Rubbers

The work of Gee and Treloar into the thermodynamics of swelling derives from work carried out by Flory on polymer solutions [8].

As already discussed, non-crosslinked rubbers swell in compatible solvents until they lose all cohesive strength and go into solution. However, a level at which the volume of a polymer cannot be increased by absorbing a solvent, referred to as equilibrium swelling, is reached in crosslinked rubbers. The greater the crosslinking, the less the material is prone to swelling. Hence, establishing a correlation between equilibrium swelling and crosslink density provides information about the inter-molecular forces in an elastomer. The Flory-Rehner equation can be shown in the following form:

$$-\ln(1-V_2)+V_2+\chi V_2^2=(V_1/\upsilon M_c)(1-2M_c/M)(V_2^{\frac{1}{3}}-V_2/2) \qquad (54)$$

Where

M_c = Mean chain molecular weight

V_2 = volume fraction of polymer in the swollen network (ratio of swollen volume to initial volume)

υ, the average crosslink density.

χ = Solvent-Polymer interaction parameter (Constant for a given polymer-solvent mixture)

Flory and Rehner derived (54) from experimental and theoretical derivations. The equation permits the relationship between crosslink density and swelling to be determined. Additionally it gives an indication of the constraints, including the presence of entanglements and filler interactions in an elastomeric network. Further derivation of the equation by Flory and Rehner showed the effect of swelling on elastic properties. This is discussed in section 2.3.6.2.

Crosslink density is fundamental for polymeric networks as it determines many of the physical properties of the resulting material. Crosslink density can be divided into two sub-parts: chemical and physical crosslink density. The former is the contribution of the pure chemical crosslinks that result from vulcanisation. It should be noted that methods other than the Flory-Rehner equation exist for determining crosslink density and include stress-strain measurements, determining the elastic modulus at a certain temperature in the rubbery plateau zone and using nuclear magnetic resonance (NMR).

2.3.5 Swelling of Rubber - Oil Resistance

Elastomers can be broadly divided into two categories, oil resistant and non oil resistant [25]. EPDM, SBR and NR are all at the lower end of the scale with

respect to oil resistance. Therefore, they will tend to swell appreciably in hydrocarbon based solvents.

Natural rubber consists of polymer chains having a cis-1,4 structure, it is also called cis-1,4 polyisoprene. It crystallises on stretching, resulting in a high gum tensile strength. It has excellent mechanical properties, but poor resistance to heat, ozone and sunlight, along with poor resistance to oil, gasoline and hydrocarbon solvents.

Styrene-butadiene copolymers are synthesised mainly by free radical emulsion polymerisation. SBR has similar properties to natural rubber and is the lowest cost and highest volume elastomer available. It has very good mechanical properties, but possesses very little resistance to oil, gasoline and hydrocarbon solvents.

EPDM is synthesised by the polymerisation of ethylene, propylene and diene. It has very good resistance to heat, ozone and sunlight, has good flexibility at lower temperatures and has good resistance to acids, alkalis and oxygenated solvents. It has poor resistance to oil, gasoline and hydrocarbon solvents.

Elastomers will swell to a certain extent in all solvents. However the swelling potential can be estimated to determine if a polymer will dissolve in a solvent.

The solubility parameter δ, is defined as the square root of the cohesive energy density, which was discussed in Section 2.3.3.

If the following relationship exists between the solvent and the polymer, then the polymer will dissolve in the solvent.

$$(\delta_1 - \delta_2)^{\frac{1}{2}} < 1 \qquad (55)$$

Where,

δ_1 = Solubility parameter of the solvent.

δ_2 = Solubility parameter of the polymer.

The solubility parameters for most solvents and rubbers/polymers has been determined by experiment. In general, the lower the difference between the solubility parameters of the oil and the rubber, the lower the oil swell. Raising the temperature will also increase the level of swelling. Increasing the crosslink density will also theoretically limit the swell, by providing tie-points that limit the amount of solvent that can be absorbed by the network, but this will be at the expense of the elastic properties of the rubber.

Crystalline regions of a polymer are difficult to dissolve because of the resistance to solvent diffusion into the network due to close packing of the chains. Crystallinity is related to glass transition temperature T_g. In plastics, this temperature is relatively high, while in elastomers it is relatively low. Therefore, hard plastics will tend to be resistant to swelling in a solvent at room temperature, while rubber will be more susceptible to swelling.

Chlorine atoms, which have strong cohesion, can have the effect of raising the value of the glass transition temperature. Several commercial oil resistant elastomers have polymer chains which contain chlorine in their chemical structure.

Figure 2.4 illustrates the various elastomers types and their relative heat and oil resistance when tested with ASTM standard oil (ASTM D471-06, Standard Test Method for Rubber).

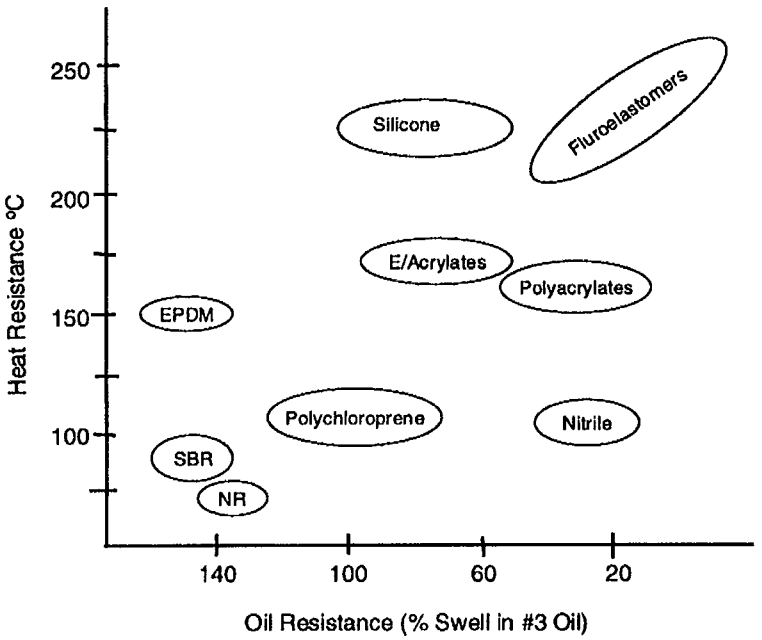

Figure 2.4. Heat and oil resistance of commercial elastomers [25].

2.3.6 Swelling and determination of rubber mechanical properties

The preceding sections gave an overview of how the available network energy is reduced in a swollen network and also how swelling and modulus are related. While the use of swelling as a means of estimating the cross link density of elastomers is commonplace, there has also been a great deal of research carried out in the area of the effect of swelling on the mechanical behaviour of filled rubbers, especially in the area of static testing and relaxation. Research into the dynamic testing of swollen elastomer is less common and will be discussed in a subsequent section.

2.3.6.1 Stress-Strain Behaviour of Swollen Vulcanised Rubbers

Tiltman and Porritt [26] carried out early studies on the stress strain behaviour of vulcanised rubber. They treated the rubber by allowing the absorption of the

vapour of a solvent by the rubber and then carried out load-extension testes on the samples. They looked at the effect of varying the solvent quantity on the stress-strain curve of the rubber and also investigated whether the swelling had any permanent effect on the material, after it had been removed by drying. Stresses were based on the dimensions of the original dry rubber. The results showed that the rigidity of the vulcanised rubber was progressively reduced by the absorption of the solvent vapour. There was little effect on the breaking elongation, but the breaking stress was considerably reduced. The absorption of the solvent, followed by complete drying seemed to produce a 'slight but technically negligible effect' on the stress-strain curve, when compared to a dry rubber sample tested in a similar fashion.

The investigation into the stress-strain relation of swollen rubbers was continued by Tanaka, Kambara and Noto [27], who looked into the stress-strain behaviour of vulcanised rubber in the liquid swollen state. They used a mixture of ethyl alcohol and benzene as the swelling medium. The stress-strain curves they generated showed a marked decrease in ultimate tensile strength, percentage elongation and modulus with increasing amounts of swelling.

Studies by Parris and Scott [28], showed an increase in swelling time with advancing vulcanisation. Swelling was also found to reduce the hardness, increase the elasticity and reduce 'fragility' (presumably weakness or the inverse of strength) of the hard rubber. They also examined the solvent action of the liquid. Liquids left at the end of long-period tests were evaporated and the residual solid matter was weighed and calculated as a percentage of the original dry weight of the hard rubber. The extracted matter was usually quite small for the liquids used. The maximum extracted matter being 4.5% of original dry

weight for xylene, but much less that this for other liquids, in the range of 0 - 1.1% and no attempt was made to correct the swelling figures for this extracted matter.

2.3.6.2 Determination of Elastic Properties Using Swelling – Stress Relaxation

When rubber reacts with the molecules of the solvent, there is partial destruction of the intermolecular bonds. With very high solvent swelling, all the bonds of the three dimensional network are destroyed [29]. Analysis on swollen rubbers was therefore of interest to researchers because vulcanised rubber, when swollen tended not to deviate to any great extent from the statistical theory.

The statistical theory leads to the following expression for the force of retraction in stretched rubber as a function of temperature, elongation and network structure:

$$\tau = RT(\frac{\nu}{V})(\alpha - \frac{1}{\alpha^2}) \qquad (56)$$

where,

T = Absolute temperature.

ν = Effective number of chains extending between crosslinkages within the volume V of the rubber.

α = Length of stretched rubber relative to its unstretched length

τ = Retractive force per unit initial unstretched area.

Equation (56) is derived from work carried out by Flory and Rehner [8], who following on from their determination of cross link densities from swelling, studied the elastic properties of a swollen network.

Further work by Gee [30], Flory [31] and Dogadkin and Gul [29] considered the dependence of the force of retraction on the degree of crosslinking in a given rubber. Gee and Flory carried out separate experiments where samples were held in place with two clamps and a glass tube enclosed the sample under test. The test apparatus was set to zero load and the zero load specimen length was noted. The lower clamp was adjusted to give the desired elongation of the test-piece. The glass tube around the sample was filled with solvent and swelling allowed to proceed for 10 minutes. The solvent was then removed and the sample was dried in air/nitrogen and the force was observed. It was noted that the distance between the marks had not substantially altered, but the force of retraction had reduced. It was known at the time that for a dry rubber without solvent 'equilibration', the stress would continue to relax over an indefinitely long period. However, after the solvent equilibration, the force of retraction remains constant for many hours. Gee and Flory both carried out further tests where specimens were held in tension at a given extension and swollen in a swelling agent for a period of 1 to 2 days. The volume fraction of the rubber was then determined by removing a portion for the strained specimen and determining v_2. This was carried out in an attempt to describe a function for a swollen elastic modulus χ,

where,

$$\chi = \frac{f}{TA_0(l/l_0 - l_0^2/l^2 v_2)} \tag{57}$$

The tension in the test-piece of swollen rubber of length l was represented by f, at a volume fraction of rubber of ν_2 at a temperature T, where l_0 and A_0 were the dimensions of the dry unstrained rubber.

When χ was plotted against percentage elongation, Gee found that it fell with increasing extension and swelling, but tended to a limiting value independent of the nature of the liquid and was substantially independent of temperature for a given natural rubber.

Flory concluded that the force of retraction increased with an increase in specimen cross link density. This was in agreement with statistical theory, albeit the increase was not as pronounced experimentally as the theory would suggest. This was attributed by Flory to entanglements in the network structure restraining the chains when the rubber was elongated.

Dogadkin and Gul [29] carried out mechanical measurement on vulcanised rubbers swollen in the vapours of solvents. They measured the relaxation of stress in swollen rubbers rings at given elongations and compared the results against similar elongations in dry rubbers, finding that the form of the relaxation curve did not change appreciably, but was of a lower value for the swollen rubbers. They related the deviation of the stress σ at a given deformation α, with the degree of swelling ν from the Flory Rehner equation,

$$\sigma = \frac{\rho RT}{M_c}(\alpha - \frac{1}{\alpha^2}) \qquad (58)$$

They reasoned that the deviation was due to the variation in the mean value of the molecular weight of the segments of the chain molecules between two adjoining bonds in the network.

2.3.6.3 Investigations into swelling and filler interactions

Zapp and Guth [32], investigated the effect of filler loading on the elastic properties of rubber networks. They looked at Butyl Rubber with both carbon and mineral fillers. The elastic properties of swollen and unswollen networks were compared, with emphasis on the filler interaction with the rubber network. They investigated how the solvent affected the filler in the network and suggested that the average linear extension of the polymer chains was proportional to the cubed root of the volume increase. Therefore, they applied an extra compensating strain to the unswollen samples, based on the hypothesis that these samples must be given additional stretch to compensate for the extension due to swelling in the swollen samples. By looking at the modulus for each type of test they determined the effect of solvent action on material modulus. The results showed that the carbon black remains as part of the structure and contributes to the strength of the rubber network, even in the swollen state, while the surface bonds of the mineral filler were broken down by solvent action.

2.3.6.4 Investigations into swelling and modulus

Both Treloar [33] and Mullins [34], examined the relationship between the stress strain properties of highly swollen vulcanised natural rubbers and their equilibrium swelling values. Mullins carried out the tests using a swelling agent

which had a low vapour pressure, which allowed the loss of swelling liquid during the tests to be largely ignored. The values of the modulus for the swollen rubber were converted to an equivalent modulus for dry rubber, by multiplying by a factor of $\nu_2^{-1/3}$, providing the equation:

$$f = 2A_0\nu_2^{-1/3}(\lambda - \lambda^{-2})(C_1 + \lambda^{-1}C_2) \tag{59}$$

At high values of swelling, C_2 reduces to zero, so re-arranging gives:

$$C_1 = \frac{f}{2A_0\nu_2^{-1/3}(\lambda - \lambda^{-2})} \tag{60}$$

It was proposed that C_1=NRT, thereby allowing a comparison with crosslink measurements to be made. Mullins plotted the values of C_1 against volume swelling ν_2, for a series of swollen rubbers. His experimental results showed good correlation with theories developed by Flory and Huggins. He concluded that values of C_1 obtained for dry unswollen rubber should be preferred to those obtained for swollen rubber. At high degrees of swelling the limited extensibility of the network could produce a significant increase in the modulus, even for small extensions, giving values 10% higher than those obtained on dry rubber.

Treloar's investigation into the effect on strains on the degree of swelling is covered in section 2.2.3.2. The equations shown in sections 2.3.6.2 and 2.3.6.4 which characterise reduced stresses in swollen elastomers are still in use. In their research, Queslel and Mark [35], defined the reduced stress or modulus f^* for a swollen rubber under strain as:

$$f^* = \frac{f v_2^{1/3}}{A_v(\alpha - \alpha^{-2})} \tag{61}$$

Where

f = Equilibrium Retractive Force

A_v = Cross Sectional area of a dry isotropic sample

ν_2 = Volume Fraction of Polymer

$$\alpha = \frac{L^*}{Li^*} = \frac{\text{Length of sample in swollen deformed state}}{\text{Length of sample in swollen isotropic state}} \tag{62}$$

2.3.7 Carbon Black and Dynamic Testing of Swollen Rubber

Dynamic analysis of rubber is typically limited to deformations not exceeding 25%. The dynamic properties are usually measured after several pre-conditioning cycles, so that the initial Mullins effect is not of consequence. When a rubber is undergoing sinusoidal deformation, the stress can be resolved into the elastic stress, which is in phase with the strain and the viscous stress which is out of phase.

If a spring-dashpot model is used to represent the material behaviour, the elastic stress is due to the spring, while the viscous stress is due to the dashpot.

The following terms are important in respect of dynamic analysis of rubber:

- Strain Amplitude – This is half the minimum to maximum strain.
- Double Strain Amplitude (Strain Range) – Peak to trough deformation of the sample, typically expressed as a %.

- Elastic Modulus – Also called storage modulus, G' where,

$$G' = \frac{\text{Elastic stress amplitude}}{\text{Strain amplitude}} \tag{63}$$

- Loss Modulus – Also called viscous modulus, G'' where,

$$G'' = \frac{\text{Viscous stress amplitude}}{\text{Strain amplitude}} \tag{64}$$

- The complex modulus G* is defined as:

$$G^* = G' + iG'' \tag{65}$$

- and its absolute, or resultant value is

$$|G^*| = \sqrt{G'^2 + G''^2} \tag{66}$$

- Loss Tangent can be defined as:

$$\tan\delta = \frac{G''}{G'} \tag{67}$$

In the context of elastomers, carbon black can be considered to consist of aggregates which are formed by fusion of particles under heat. The aggregates are clustered into agglomerates and (under normal loading), a network, which

can be completely separated into the constituent aggregates by deformation of the rubber compound.

An important property of carbon black is the specific surface area, expressed in m^2/g. Research in the 1940's [36] and 1950's [37] established that increased loading and surface area of carbon black resulted in a increase in the complex modulus and loss tangent, as well as a dependence of the complex modulus on amplitude, where it was found that the initial dynamic modulus was almost fully recoverable with decreasing amplitude. Fletcher and Gent [38] discovered that the dynamic viscosity of a carbon black filled natural rubber first decreased, then increased before ultimately decreasing with increasing amplitude. Tan δ was found to decrease slightly at very low amplitudes and then increase up to a maximum. This phenomenon became known as the 'Fletcher-Gent Effect'.

Payne [39][40] showed decreases in G' after strain amplitudes exceeded values of approximately 0.5%, tending to an apparent constant value at higher amplitudes, irrespective of the filler content. The phase angle for each blend also tended to remain constant up to 0.5% strain amplitude, before increasing to a maximum between 0.1-1% strain amplitude, for a given blend. The idealised curve shown in Figure 2.5 shows the elastic modulus levelling off at a value of G_∞ at high amplitude and at G_0 at low amplitude.

The influence of carbon black at the high amplitude was thought to be associated with a combination of a hydrodynamic effect and additional effective crosslinks due to rubber filler bonds. The difference between G_∞ and G_0 was attributed to the physical structure of the carbon black, 'filler-filler linkages which are broken down by straining', in other words, interaggregate association by physical forces.

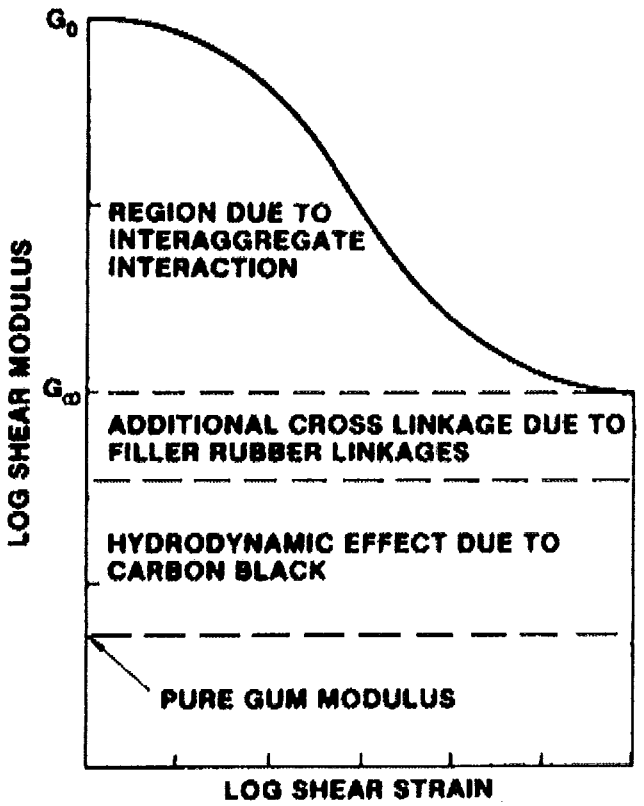

Figure 2.5. Qualitative interpretation of strain amplitude dependence of G' [40].

With regard to swollen rubber, Neogi *et al* [41] investigated how the dynamic properties change after swelling the network in a solvent, after previous studies showed that hysteresis due to carbon black was reduced by swelling the elastomers in question in a good solvent. Storage modulus, loss modulus and tan δ were shown to be a function of structure and surface area of carbon black along with their dependence on amplitude, temperature and frequency.

Neogi investigated how the dynamic properties changed after swelling the network in a solvent. Tests were carried out on NR and SBR using paraffin oil and xylene as the swelling fluids. The tests were carried out at varying temperatures and storage modulus, loss modulus and tan δ were recorded as a function of temperature. Dynamic strain was set at 0.125%. For the unswollen

samples, the storage modulus decreases with the increase in temperature and with the decrease in loading and surface area of carbon black filler.

On partial swelling, the effects were reduced significantly and for equilibrium swelling the storage modulus becomes independent of surface area and loading. The loss modulus of unswollen samples followed the same trend, except for samples swollen in xylene, where the modulus increased due to contributions from the solvent and the rubber matrix. The loss tangent decreased with the increase in temperature and with the decrease in loading of carbon black filler and a limiting value of storage modulus was determined for all the filled samples.

Busfield *et al* [42] looked at the effect of swelling on the dynamic properties of filled natural rubber as a function of pre-strain, where a static tensile strain was applied to swollen and dry rubber strips and small oscillations were superimposed. The study showed that both storage modulus ($G^{'}$) and loss modulus ($G^{''}$) reduced when the specimen was swollen and that the dependence of $G^{'}$ and $G^{''}$ was much greater for specimens containing higher levels of filler. This was attributed to the diluent effect of adding a liquid, combined with the influence of altering the free volume available for the movement of the rubber chains.

In terms of fatigue testing of swollen elastomers, Gul *et al* [43] were responsible for much of the early research. Their experiments showed that there is an initial increase in fatigue resistance, followed by a decrease with increases in the degree of swelling. Their work will be discussed in more detail in Section 2.4.6.

2.4 Fatigue of Materials

Fracture of engineering components due to fatigue is the most common cause of service failure, since virtually all critical components are subject to cyclic stressing. Fatigue failures will occur under loading conditions where the fluctuating stress is below the tensile strength of the material and in most cases, well below the elastic limit of the material. Fatigue tests are usually carried out under conditions of rotating-bending with a zero mean stress, or with a push-pull type loading. A Wöhler machine is used in the first case [44], while a Haigh machine is used in the latter [45].

The following parameters are typically used in fatigue tests to describe the loading pattern the specimen is subjected to.

$$\text{Stress Range, } \sigma_r = 2\sigma_a \tag{68}$$

$$\text{Mean Stress, } \sigma_m = \frac{\sigma_{\max} + \sigma_{\min}}{2} \tag{69}$$

$$\text{Alternating stress amplitude, } \sigma_a = \frac{\sigma_{\max} - \sigma_{\min}}{2} \tag{70}$$

$$\text{Stress Ratio, } R_s = \frac{\sigma_{\min}}{\sigma_{\max}} \tag{71}$$

Stress is not the only parameter that is plotted in fatigue tests. Simple mechanical histories applied to laboratory specimens are usually characterised by parameters

such as maximum, alternating, minimum and mean loading, and/or the R-ratio [46]. These parameters are illustrated in Figure 2.6.

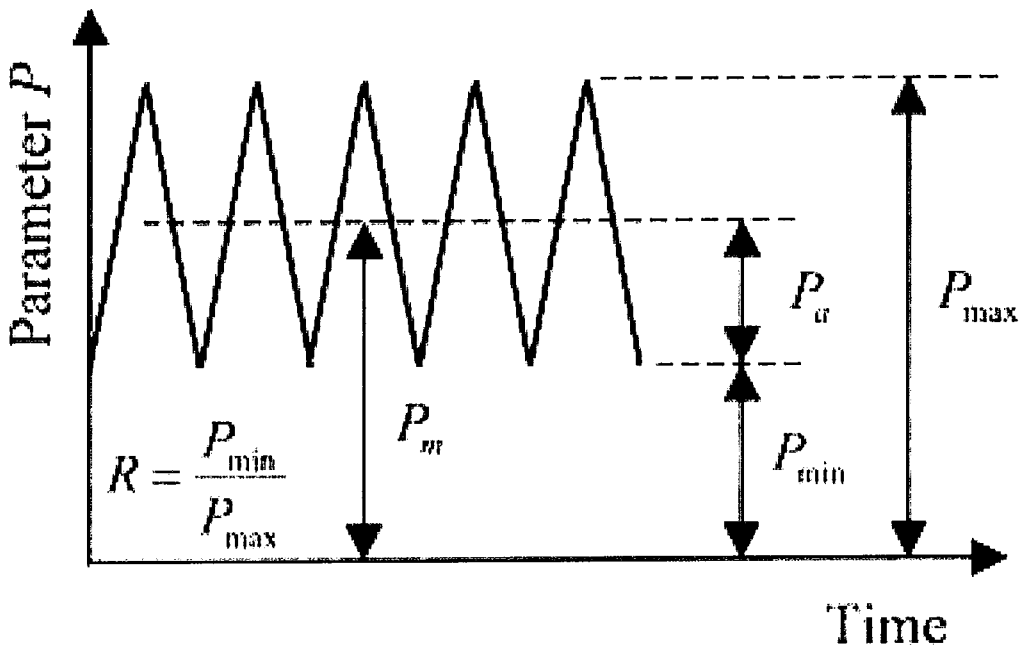

Figure 2.6. Parameters used in the description of constant-amplitude mechanical loading history [46].

The equations for these parameters are similar to (68-71) and from Figure 2.6 it can be seen that

P_{min} = Minimum Load (72)

P_{max} = Maximum Load (73)

P_a = Average Load = $0.5(P_{max} - P_{min})$ (74)

$R = R_{Ratio} = P_{min}/P_{max}$ (75)

When plotting fatigue cycles against alternating or maximum load, it is important that the minimum loading (or mean or R ratio) is also stated. This completely specifies the cycle limits. Typical fatigue data is presented as an S/N, or Wöhler curve, where the stress amplitude is plotted against cycles to failure, as shown in Figure 2.7.

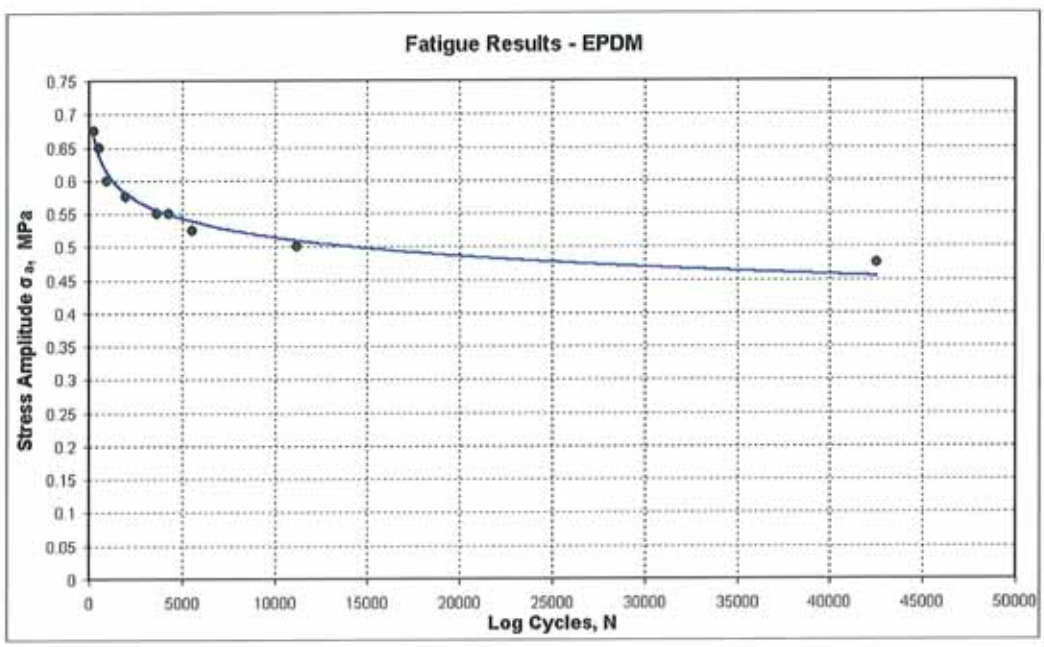

Figure 2.7. Typical S/N curve for a material, in this case EPDM Shore A70 E9566 EPDM rubber.

2.4.1 Fracture Mechanics and Crack Propagation

A basic principle in thermodynamic theory is that a system will move to a state where the free energy of the system is lower. From this, a simple premise for crack growth in a material can be formulated. It is assumed that a crack will only grow if there is a decrease in the free energy of the system comprising the cracked body and the loading mechanism. This assumption was developed by Griffith [47].

Griffith showed that if this decrease in energy was greater than the energy required to produce new crack faces, then there would be a net decrease in energy and the crack would propagate [48].

2.4.2 Crack Propagation and its application to elastomers

The basis of the fracture mechanics approach to elastomers is the use of the strain energy release rate, or the tearing energy and both terms are interchangeable.

The tearing energy (typically reported in units of kJ/m^2) is defined as:

$$T = -\frac{dW}{dA} \tag{76}$$

Where W (equivalent to U in elastic materials), is the total elastic strain energy stored in an elastomer containing a crack and A is the area of one fracture surface of the crack where it is assumed that the external forces do no work. For the approach to be useful, it is necessary that the rate of growth be uniquely defined by T. This has been found to be so for most (but not all) elastomers.

When applied to test-pieces which have been developed for the investigation of crack growth in elastomers [49], T can have different forms, depending on the test-piece configuration. More details on the forms of these test-pieces are contained in Appendix 4 Part 4). Rivlin and Thomas [50-51] carried out fatigue tests on specimens with different geometries in an attempt to determine if the tearing energy at the instant of tearing was independent of the specimen geometry. The primary conclusion of this work was that the relationship between

the tearing energy and the rate of tearing was a fundamental property of the material and independent of the method of testing.

Further tests carried out by Lake and Lindley demonstrated that when a pre-crack was applied to a test-piece, there was a relationship between the tearing energy and the crack growth rate per cycle, which was independent of the specimen geometry [52].

2.4.3 Fatigue Crack Growth

Following the establishment of the fracture mechanics approach for rubber, both fatigue crack growth and fatigue crack nucleation studies have been carried out under conditions of fully reversed cyclic loading in tension (R_{Ratio}=0) and the results are often shown against maximum loading, where the amplitude is one half of the maximum loading.

When plotted as a function of maximum energy release rate, R = 0, fatigue crack growth behaviour in rubber conforms to an approximate sigmoid, or S-shape. Using this approach, four types of material behaviour can be described: a sub-threshold regime, a transition regime, a power-law regime and a failure regime in which unstable crack growth occurs.

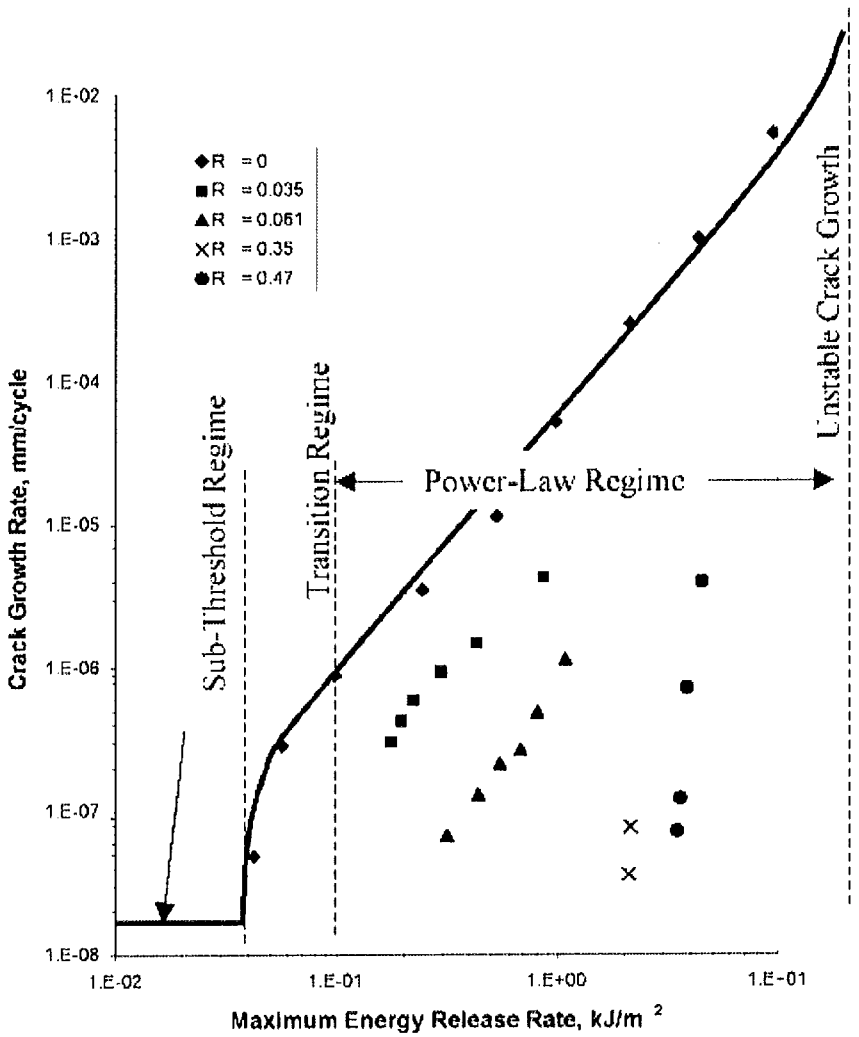

Figure 2.8. Lindley's [53] fatigue crack growth results for unfilled natural rubber, showing typical regimes of behaviour, and the effects of R > 0 loading.

If Figure 2.8 is studied with respect to the conditions where R=0 only, the regimes of material behaviour may be explained as follows:

Sub-threshold regime

In this regime, when the maximum load remains below the mechanical threshold of the material, cracks or flaws do not grow due to mechanical fatigue. In this case, the specimen in question would be assumed to have an infinite life. Other

factors may eventually cause mechanical failure of the specimen. These factors can be environmental in nature, such as crack growth due to ozone or chemical attack, changes to the operating load, or changes to the fatigue crack growth threshold.

Power Law Regime

When the part is loaded below the crack growth threshold, but below the value that results in sudden fracture, a power law relationship has been observed. This relationship exists both in fatigue crack nucleation tests (load versus life) and in fatigue crack growth tests (load versus crack growth rate). An analytical relationship between fatigue crack growth tests and crack nucleation tests in this regime has been derived.

Unstable Crack Growth Regime

Above a critical load, the fatigue crack growth rate accelerates rapidly to unstable fracture. For small cracks in crystallising rubbers at high strains, the bulk material may strain crystallise before the point of unstable crack growth is reached. When this occurs, the strength can be increased by more than a factor of two.

2.4.4 Fatigue of Non-Strain Crystallising Elastomers – Non Relaxing Tests

Lindley [54], investigated the crack growth for SBR in terms of the tearing energy T, the energy available for crack growth. Under relaxing conditions (R=0), he postulated a relationship between the crack growth per cycle and T at the maximum deformation. He superimposed his results for non-relaxing

conditions onto the results from the relaxing conditions using a scaling factor applied to the static and dynamic aspects of the crack growth behaviour. He put forward a 'tentative' explanation for this factor, which was used mainly for the convenient way it allowed the non-relaxing data to be presented, but was qualified as not being accurate at lower rates, where the static component could not be easily described.

Further studies by others [55-58] have continued Lindley's investigations into crack growth in fatigued rubber components.

2.4.5 Fatigue Live Determination – Recent Investigations

Recent studies by Abraham into fatigue life prediction of dry filled elastomers have demonstrated the amplitude dependence of fatigue life in filled non strain-crystallising rubbers [3-5]. In addition, the effect of mean stress amplitude and consequently dynamic stored energy on fatigue life has been shown on EPDM and SBR specimens tested cyclically in uniaxial tension.

The main objective of Abraham's work [3] was to characterise the dependence of fatigue on stress amplitude and minimum stress in non strain crystallising elastomers. Materials with and without filler were used in the investigation. This allowed investigation into the effects of reinforcement, stress softening and the Payne-effect of filled systems. The second objective of the research was to clarify the question of which criteria (related to some value of stress, strain or energy) most accurately characterised the fatigue properties of elastomeric materials.

Abraham's investigations [3-4] observed that in non-strain crystallising rubbers containing filler for a given stress amplitude an increase in fatigue resistance

occurred when the specimen was pre-stressed. Rubber without filler did not experience any increase in fatigue life with an increase in minimum stress for a given stress amplitude.

All specimens were tested under a range of loading conditions. Two different test procedures were used. The first procedure used tests with a minimum load of zero and a set of different load amplitudes. The second procedure included tests with constant load amplitudes and different minimum loads.

The uniaxial tests conducted on filled EPDM resulted in large increases in fatigue life when tensile pre-loads were applied using the second test procedure, as Figure 2.9 illustrates. It was shown that different load amplitudes and pre-stressing produced increases in fatigue life of a magnitude of 11 (0-400N stress range) to 16 (0-500N stress range).

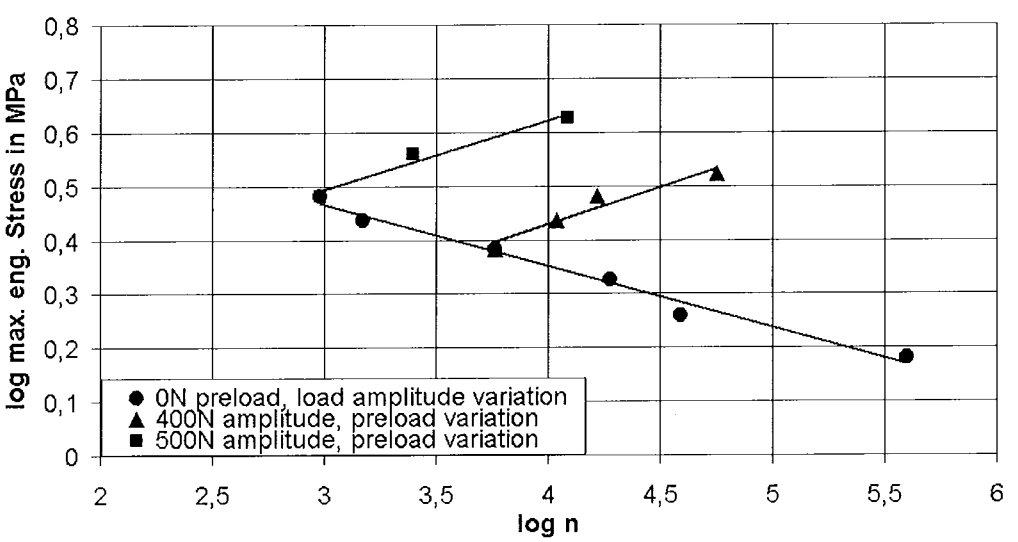

Figure 2.9. Fatigue properties of filled EPDM (maximum stress dependency) [3].

Abraham found good correlation between the dynamic stored energy in the specimen and the cycles at failure at different numbers of cycles throughout the tests, (Figure 2.10) and proposed the use of dynamic stored energy as a plausible fatigue life predictor [3]. The dynamic stored energy is the area bounded by the unloading portion of the stress-strain curve during the cycle measured, where the energy was reported in units of Nmm.

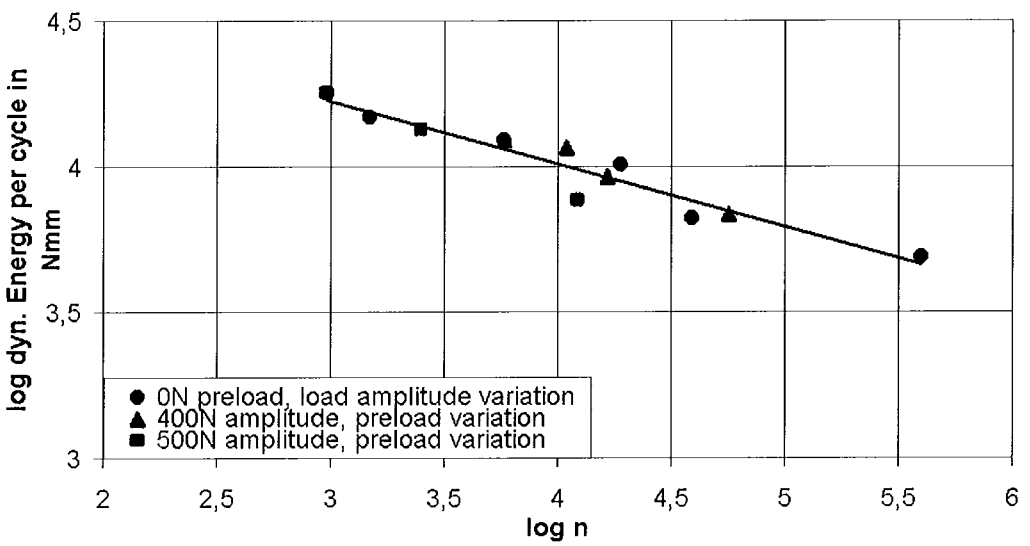

Figure 2.10. Fatigue properties of filled EPDM (energy dependency) [3].

A principle of the testing of swollen rubbers, loaded equi-biaxially in fatigue, was to broaden the range of testing available to study the dynamic behaviour of swollen elastomers, while investigating if the application of energy criteria for predicting the fatigue life of swollen elastomers applied.

2.4.6 Fatigue of Swollen Rubber – Previous Research

Gul *et al* [43] studied the fatigue resistance (measured in hours) of swollen vulcanised natural rubber under constant deformation and constant load, when

swollen with paraffin oil and dibutyl phthalate. Under constant deformation, the modulus of the swollen rubber decreased with swelling, leading them to conclude that this decrease was evidenced by the reduction in the mechanical work required to achieve the deformation. They surprisingly found that at constant strain amplitudes the relative fatigue resistance improved in swollen rubbers.

For constant load deformations [59] they reported an irregular change in fatigue resistance with the increase of the degree of swelling in the solvents (Figure 2.11). Fatigue resistance initially increases to a maximum when plotted against degree of swelling, before falling away for higher values. They attributed this to two processes; an initial increase in fatigue resistance due to the reduction in mechanical losses and a subsequent decrease due to a decrease in tensile strength proportional to the higher degree of swelling.

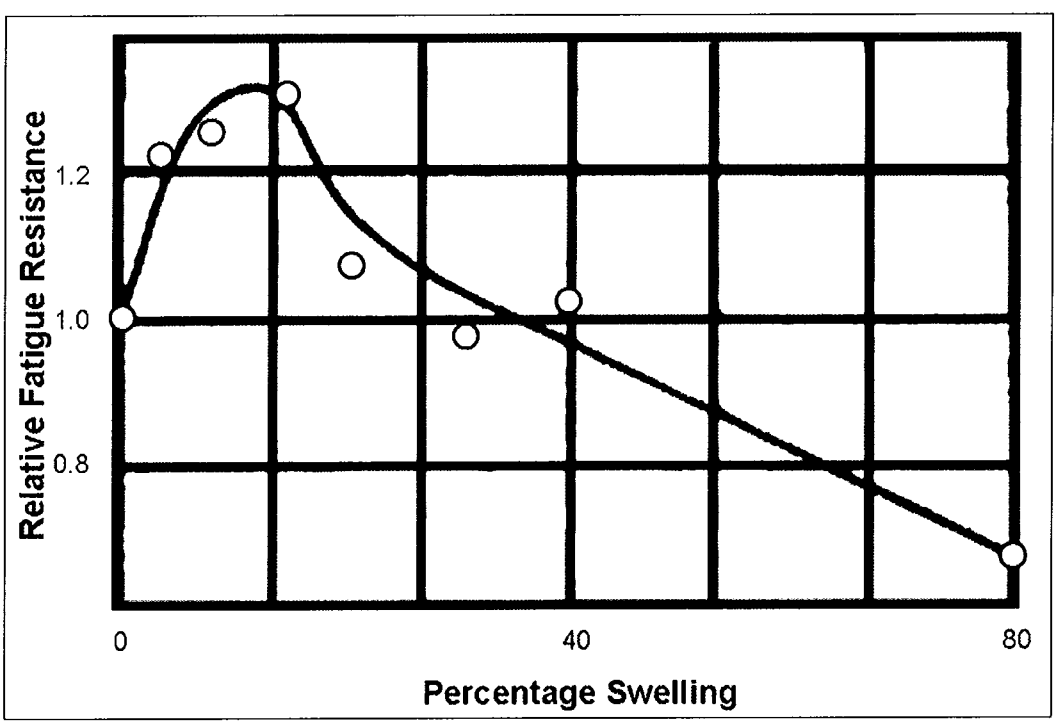

Figure 2.11. Relation of fatigue resistance, y to the degree of swelling of vulcanised natural rubber in paraffin oil [59].

Further studies [60] investigated the phenomenon of fatigue resistance for constant 'stress-work' amplitudes with a range of degrees of swelling for a given rubber-solvent combination.

A combination of solvents with varying polarity were applied to vulcanised natural rubber. The solvents were plasticisers commonly used in compounding of elastomers. Different levels of swelling were applied to the specimens for each type of solvent. Tests were carried out under equal loading and frequency conditions and dynamic fatigue was characterised by the relative fatigue resistance, which was defined as:

$$\text{Relative Fatigue Resistance} = \frac{\text{Time to destruction of swollen sample}}{\text{Time to destruction of dry sample}} \qquad (77)$$

The constant 'stress work' tests were carried out in the following manner:

For rubbers with different modulus values, the specimens were cycled at constant amplitude until the rubber reached 'dynamic equilibrium'. For a given set of test specimens, this was carried out at 5-6 different strain amplitudes and a 'quasi equilibrium' relationship was determined between the stress and the strain.

They then tested the samples using what seemed to be a constant work amplitude test, where they used a testing machine capable of 'constant swing', which was reported in units of kg.m, which when multiplied by the gravitational constant 'g' of 9.81 m/s^2 is dimensionally equivalent to Joules.

The results of these tests showed that the relative fatigue resistance of the natural rubber decreased with an increase in the degree of swelling, regardless of the rubber-solvent combination used, as illustrated in Figure 2.12.

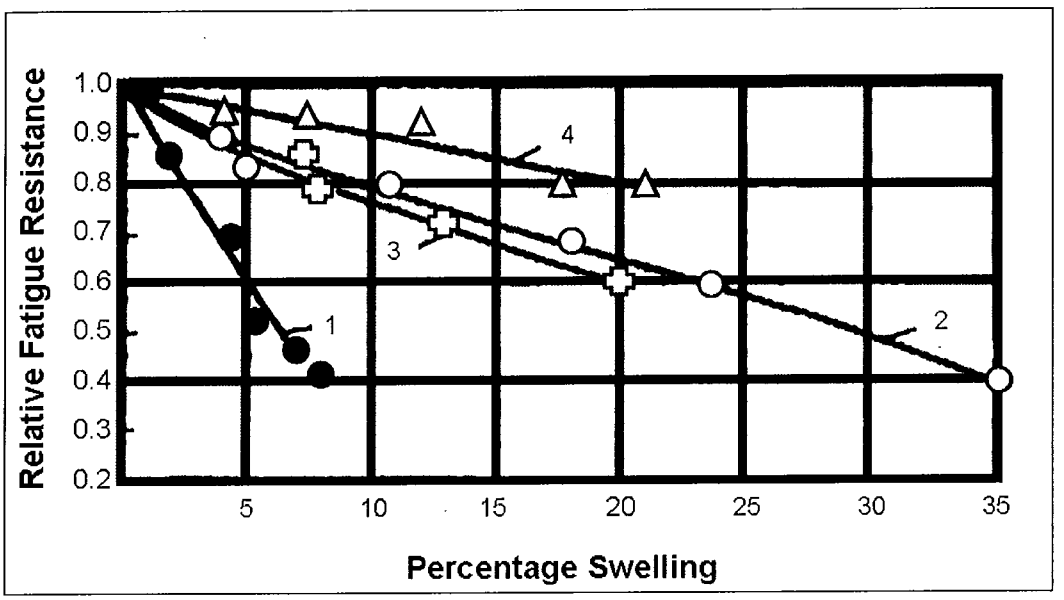

Figure 2.12. Change in relative fatigue resistance with increase in % volume swell for natural rubber swollen in four different solvents [57].

The decrease in fatigue resistance with increased swelling was attributed to a change in the 'intermolecular action' in the rubber. This was supported by changes in material properties with swelling, such as a decrease in the glass transition temperature, as well as an increase in elastic rebound.

The effects of heat build-up in specimens was reduced in the constant 'stress-work' tests by using specimens of a thin cross-section (1.5mm thickness) to increase heat transfer from the inside of a specimen to the surroundings. However it could be seen from the results that the frequencies the tests were carried out at were in excess of 4 Hz, which would inevitably lead to heat build up [49], particularly in the thicker samples and some subsequent thermal degradation of the rubber network would have occurred. There was no reference to the larger sample dimensions, so this can only be speculated. It should also be mentioned that this research did not take account of crack growth formation, but this would constitute a relatively small number of the total cycles to failure.

Following this first set of 'stress-work' tests on swollen vulcanised rubber, equivalent volumes of solvent/softener were added to the rubber stock prior to vulcanisation and the rubber produced from the process was dynamically tested in fatigue. The results of the tests showed that again, the relative fatigue resistance dropped with an increase in the amount of softener added to the stock. It was concluded that fatigue results obtained by swelling of vulcanised rubber could be used to characterise plasticised rubbers consisting of the equivalent vulcanisate-solvent combination.

However, it should be noted that the above recommendation was not in total agreement with previous tests on the effect of plasticisers on the static mechanical properties of elastomers which had been carried out on natural rubber compounds by Williams [61]. Williams found that compounds vulcanised in the presence of oil were soft and remained so, even after the oil had been removed. This was in contrast to rubber which had been vulcanised in the absence of oil, which had a higher modulus than the former, even after oil had been diffused into the compound. This indicated that a small amount of inert softener in the compound can influence the network formation before vulcanisation, but once a network is formed, the subsequent introduction of softener will not destroy it.

Further work on fatigue of swollen rubber was carried out by Cho *et al* [62] who investigated fatigue crack growth of elastomers, specifically on two types of SBR swollen in mineral oil and fatigue tested in pure shear with a sharp stress raiser (pre-crack) and a strain applied cyclically at magnitudes of 10-35%. The crosslink density was different for each specimen type. Tearing energy and crack growth rate were measured and compared against specimens that were not swollen. Using a modified version of equation (88), the tearing energy was

multiplied by the square of the linear swelling ratio, λ^2, to take into account the reduction in the number of molecular chains per unit fracture plane. The study found that the fatigue resistance of the elastomer was decreased in the presence of low-viscosity fluid in proportion to the degree of swelling. The reasons for this reduction in fatigue resistance were attributed to a number of factors.

Firstly, internal friction was reduced between network strands during deformation in the swollen test-pieces. Less energy could be dissipated by hysteresis, as would normally be the case in a dry rubber. Secondly, SEM micrographs of the failure surface, shown in Figure 2.13, revealed that the surface of the swollen test-pieces were smoother than those of the dry specimens. This would suggest a sharp tear for the swollen specimens, with blunt tearing taking place in the dry test-pieces.

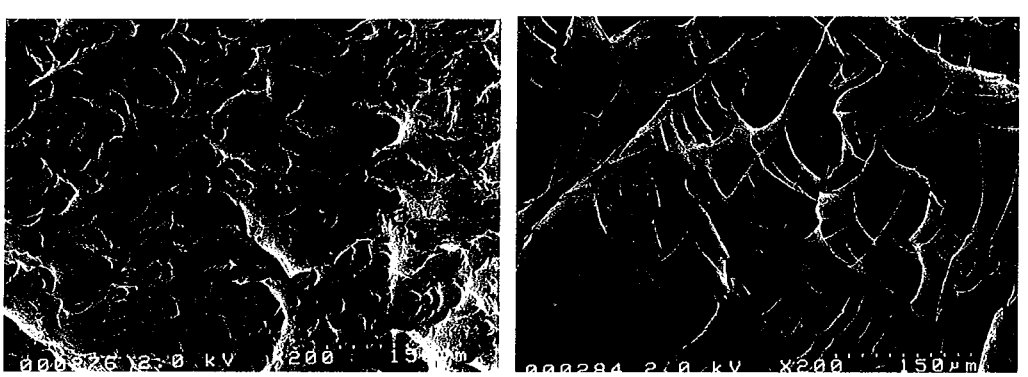

(a) (b)

Figure 2.13. Scanning electron micrographs of torn surface for SBR-H vulcanisates, (a) in dry condition, (b) in swollen condition [59].

Thirdly, they concluded that the crosslink type, rather than the crosslink density contributed to the fatigue resistance of the SBR. The SBR with a higher crosslink density, but thought to contain more polysulphidic linkages, had a lower fatigue

resistance. These linkages are thought to break and reform in a dry rubber, but the solvent would inhibit this reformation in swollen specimens.

The primary conclusions were that the variation of the fatigue resistance of the elastomer in the swollen state was due to the reduction in viscoelastic energy loss and sharpening of the crack tip in the swollen state.

2.5. Summary of Literature Review

It is clear that a wealth of information has been gathered in the analysis of the physical properties of dry and swollen rubber in the last century. The main findings of these various investigations include:

1. Derivation of theories to calculate rubber network strain energy, in both the dry and swollen cases.
2. The relationship between swelling and modulus allows the degree of crosslinking of a rubber to be estimated and allows comparison between batches of the same compound.
3. The stress-strain and stress relaxation behaviour of a rubber can be more fully understood by comparing the specimens in the dry and swollen conditions.
4. The effect of swelling on filler interaction and damping properties has been investigated and the dynamic response of a compound may be described in both the dry and swollen cases.

However, dry and swollen rubbers subjected to dynamic equi-biaxial loading have not received the same levels of scrutiny in respect of experimental testing and analysis as the uniaxial and shear loading cases.

This is due to fatigue of rubber only receiving notable attention by researchers in the last two decades, coupled with the fact that dynamic multiaxial testing apparatus has only been generating reliable test results for a few years, with the multiaxial data for the loading case of combined tension and torsion testing [46][57][58]. These multi-axial studies have concentrated on crack growth rates and differ from the fatigue tests carried out by Abraham [3], which observed changes in the properties of the elastomers over the whole lifetime of the material, rather than close to its fatigue life limit, as is the case for typical crack propagation studies.

The next chapter discusses the theory of bubble inflation and its application in the characterisation of the stress-strain behaviour of elastomers. Additionally, the development of the dynamic bubble inflation rig is discussed, along with the justification for the selection of ASTM reference oils for equi-biaxial fatigue testing of swollen rubbers.

Chapter 3 An Equi-biaxial Fatigue Rig

3.1 Evolution of the rig

Stretch frames, used for the biaxial tensile testing of rubber are limited by the specimen dimensions which have to be used, as well as the extension ratios which can be achieved [63]. These disadvantages include clamping effects, specimen dimensions, extension ratios that can be achieved and loading frequencies for dynamic tests.

If an elastomeric specimen is strained using the bubble inflation method, then deformations can be obtained of a magnitude which will result in rupture of the specimen in equi-biaxial tension.

As part of research carried out by Robert Bosch GmbH in collaboration with Coventry University, a method of investigating axi-symmetric bubble inflation of elastomers by an optical measuring system and determination of local stress and strain properties in biaxial deformation was developed [64]. Both the surface displacement and the bubble contour were observed optically on-line during a continuous inflation process. The relations between internal pressure, bubble height and local shell stress and strain were analysed. As stresses toward the pole of the bubble gradually increased throughout the inflation process, the experimental method permitted an investigation into material properties at high equi-biaxial deformations and the determination of physical constants for any of the current competing material models. The conclusion of this research was that simple assumptions relating local stress and strain levels to bubble inflation height and radius of curvature could not be made.

3.1.1 Bubble Inflation Method

While bubble inflation can utilise either compressible or incompressible media, the test procedure applied in the rig used in this research applies pressure hydraulically to the test-piece, although pneumatic inflation is also possible. Hydraulic inflation is required as it eliminates lag which is introduced to the system if compressed air is used. For inflation, the specimen is fixed uniformly around its full circumference to allow deformation at the centre. The diameter of the circular inflation orifice is 35 mm and a clamping method is applied at the circumference allowing no protrusion. This clamping method allows a free bubble to form resulting in uninhibited bubble development. The only constraint occurs where the specimen is held as shown in Figure 3.1.

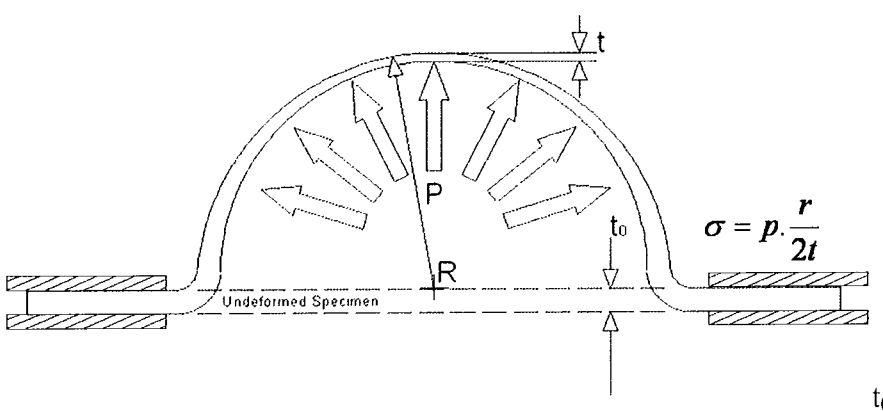

t_0, original sheet thickness; t, inflated sheet thickness; R, Bubble Radius; P, Pressure.

Figure 3.1 Free bubble inflation.

3.1.2 Bubble Inflation Theory

Bubble inflation is considered to comply with theory for applying pressure to a thin shell structure possessing negligible bending stiffness, alternatively described as membrane theory. For an ideal isotropic material and an axi-

symmetric set-up, the bubble contour exhibits rotational symmetry and therefore the deformation at the pole is equi-biaxial as shown in Figure 3.2.

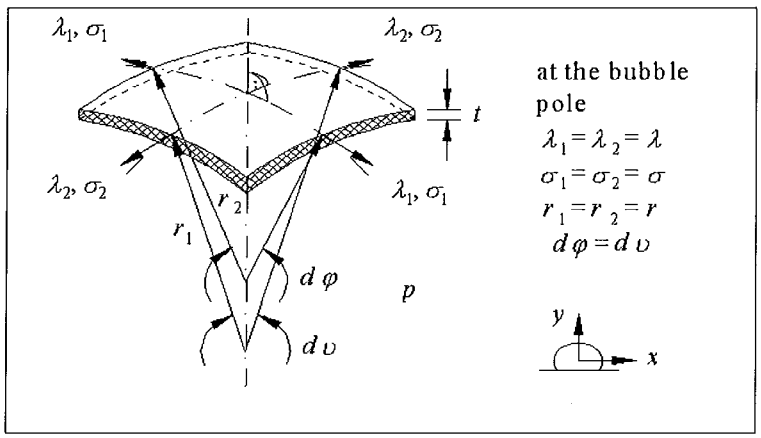

Figure 3.2 Bubble inflated shell element [61].

Pressure p is applied to inflate a thin sheet with thickness t_0 to produce a bubble shell. From the measurement of pressure p and the radius of curvature r, the equation for stress at the pole can be determined from Equation (78).

$$\sigma = p.\frac{r}{2t} \tag{78}$$

The first instance of experimental investigation into strains in an inflated rubber sheet was carried out by Flint and Naunton [65], who determined that inevitably the shape of the bubble becomes non-hemispherical at larger strains. Treloar [66] looked at the state of strain over the surface of an inflated rubber sheet, to determine over what area the extension could be regarded as uniform. He concluded that the pole was in a state of simple tensile strain with the clamped

edge being in pure shear strain, with the material in-between these two extremes occupying an intermediate state of strain.

This was confirmed in subsequent publications devoted to the contour analysis of inflated membranes [67-72].

The initial bubble shape is approximately hemispherical, but continued inflation (when the bubble height exceeds the radius of the inflation orifice) results in the bubble assuming an elliptical shape, if failure does not occur during the hemispherical phase of inflation. The form of the elliptical contour depends on the compound, the clamping mechanism and the shape of the inflation orifice. When the elliptical shape is formed, inflation in the transverse direction occurs at a different rate to that in the vertical direction. This is due to specimen clamping effects, non-linear material behaviour and the equi-biaxial deformation state in the rubber shell. In the case where inflation is carried out using a circular inflation orifice, thinning of the material along the meridian occurs and an increase of strain towards the pole results from the specimen fixing [9]. The meridian cross-section of a bubble contour can be expressed in polar co-ordinates R,φ, by a two dimensional tensor or as an ellipsoid function.

$$R = \left(a^2.\cos^2\varphi + b^2.\sin^2\varphi\right)^{\frac{1}{2}} \tag{79}$$

The cross-section of the axi-symmetrical ellipsoid is described in Cartesian co-ordinates by the simple equation

$$\frac{x^2}{a^2} + \frac{y^2}{b^2} = 1 \tag{80}$$

The centre of the ellipsoid is located at the intersection of the x and y axis whereas the symmetry of rotation is about the y axis. The axis interception to the equator is formed by parameter a and the segment to the bubble pole by b. Both parameters describe the radius of curvature at the pole.

$$r_1 = r_2 = \frac{a^2}{b} \tag{81}$$

The strain at the pole in a region approximately within ±10° of the pole in polar co-ordinates is equi-biaxial even at values of high strain, as verified by experimentation [73].

The local stretch ratios at the pole can be determined using Equation (82)

$$\lambda = ((x_{cir} - x_{orig})/x_{orig}) + 1 \tag{82}$$

where λ is the principal stretch ratio, x_{cir} is the circumferential point spacing at the bubble pole and x_{orig} is the original point spacing. Using Equations (78) and (82), plots of engineering stress versus stretch ratio can be generated.

By substituting the instantaneous thickness for the original thickness in Equation (78), values of true stress may also be calculated. The relationship between the principal stretch ratios for equi-biaxial tension and how the instantaneous thickness is calculated from the circumferential strain is described in Appendix 4 (See Equation A.4.4).

3.1.3 Development of the bubble inflation fatigue rig

A typical uniaxial test allows the calculation of material constants for finite element analysis (FEA) although the material models will probably be implausible. It is desirable to test rubber in a variety of stress-strain modes to improve the accuracy of material parameters and by fully defining the material properties to allow complex equi-biaxial component deformations to be modelled. A more stable regression analysis results from using plausible data and the inclusion of equi-biaxial deformation tests allows a more accurate determination of physical properties.

Biaxial deformation of elastomers is commonly achieved by using a mechanical frame having a mechanism for loading in two mutually perpendicular directions. The advantage of the bubble inflation method over mechanical stretch frames is that it allows a full stress-strain curve to failure to be achieved in equi-biaxial deformation and minimises variations in stress distribution towards the specimen centre. Stress concentrations in the test-piece are less than those occurring in stretch frame tests and the inertia and friction effects inherent in the frame method are avoided [68]. Clearly, in dynamic testing, particularly in those tests that cycle to failure in fatigue, the limitations imposed by friction and inertia are exacerbated. Also, gripping the disc specimen is improved in bubble inflation due to the clamping area of the original disc remaining constant during the stretch process. As a result, large localised deformations in equi-biaxial strain can be achieved.

The rig developed as part of this research gives a method of determining the mechanical properties of elastomers in equi-biaxial deformation under fatigue conditions, rather than to observe a single pressure loading to failure, although

the test rig can also be used to provide stress-strain data from single cycle tests. As part of the research, a basic pressure control system was developed and a prototype vision system was tested. A number of enhancements were made to the rig as part of this and other research programmes and the modified machine operates as illustrated in Figure 3.3.

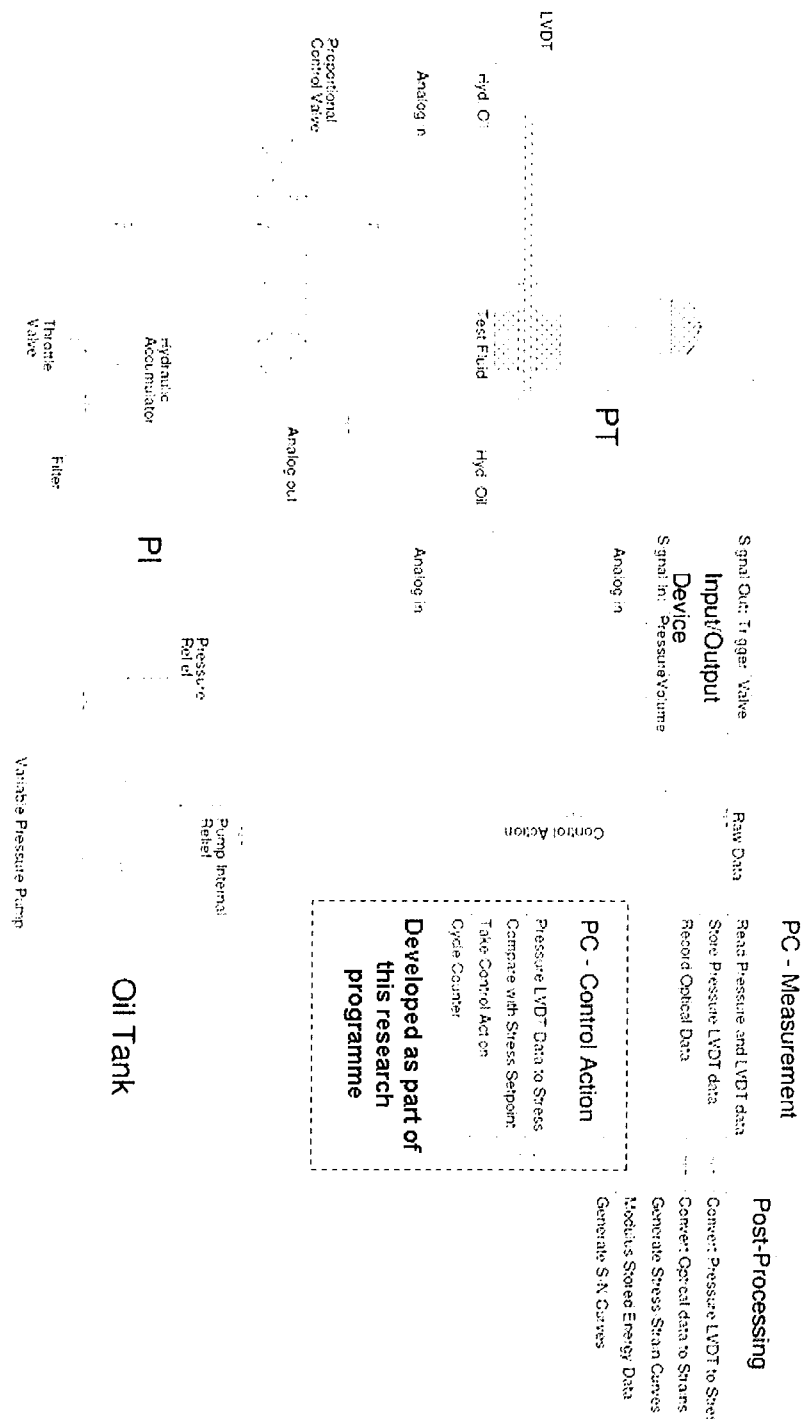

Figure 3.3 Bubble Inflation Rig Process Overview.

The principal components of the dynamic bubble inflation rig are the hydraulic system, the control program and the vision system.

Hydraulic System and Control Program

The hydraulic system utilises a hydraulic power unit, with a pressure compensated vane pump, pressure filter and accumulator. To allow bubble rupture at high volumes, a cylinder with an available volume of 250 cc is used for inflation and deflation. Inflation and deflation is carried out using a proportional flow directional control valve. The dynamic testing facility is integrated with the rig control programme which allows cycling between pre-set pressures of 0-10 Bar. Changing the inflation medium is a simple process and complete air bleeding of the system can be achieved. The specimen clamp ensures an evenly distributed force around the clamped portion of the sample, eliminating specimen slippage during testing. A cycle counter records the cycles to failure. A manual incremental inflate and deflate option is also available on the rig. Details of the control system program are contained in Appendix 2.

Vision System

The vision system is based on two charge coupled device (CCD) cameras connected to a PC. The cameras are mounted over the specimen and the output from each camera is combined to allow 3-dimensional data to be determined. The set-up is shown in Figure 3.4.

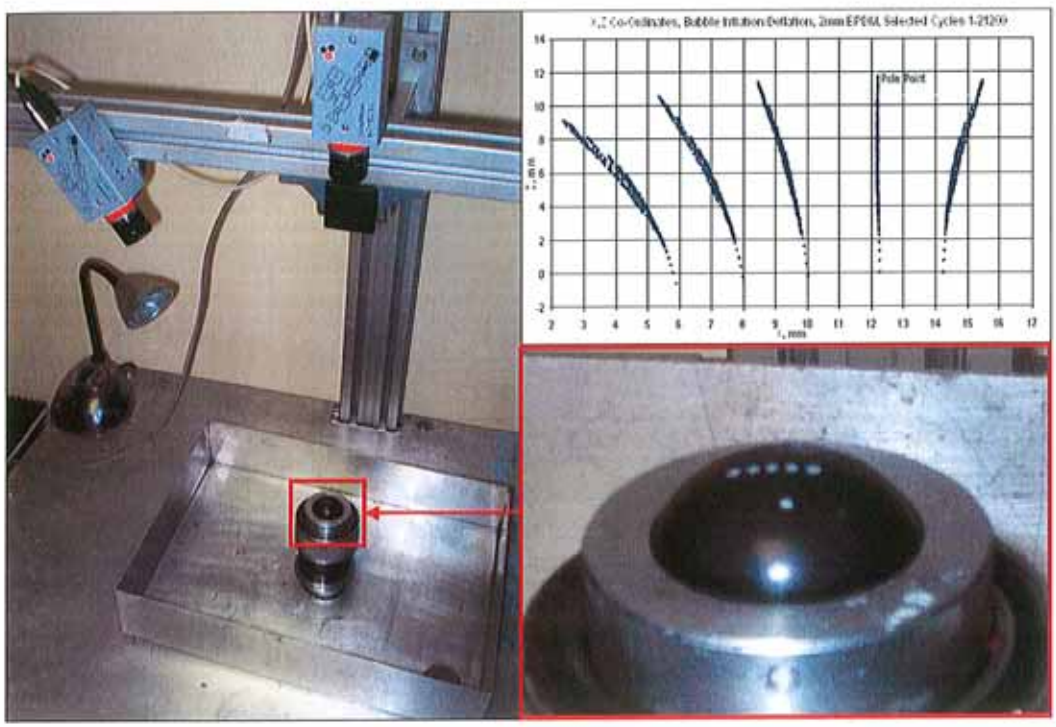

Figure 3.4 Bubble inflation rig, showing camera set-up and subsequent co-ordinate extraction.

A calibration routine is required to ensure that the co-ordinates as measured by each camera can be related to each other. The raw measured X,Y,Z data is output in pixel coordinates and this data must be combined for each camera and rotated, translated and scaled using constants generated as part of the calibration process. Details of a typical calibration are contained in Appendix 3. Once scaled into millimetres, the X, Y, Z data is used for two purposes. Firstly, the radius of the bubble is calculated using a least squares fit through the X, Z co-ordinates for a particular frame. Secondly the X data for a particular frame is combined with the corresponding radial data to calculate the circumferential spacing of the markings on the surface of the test-piece.

Pressure readings are synchronised with the cameras during the image capture sequences, by taking a pressure measurement every time a trigger signal is output

to the cameras to signal image capture. Values of the bubble volume are also taken at the same time. The volume is measured using a linear variable differential transducer (LVDT), which was retro-fitted to the rig, following identification of the requirement for constant stress controlled tests, which will be discussed in detail in Chapter 4. When the co-ordinate information is combined with the associated pressure values, stress strain data can be calculated at each measurement point in an inflation and deflation cycle. Examples of the spreadsheet calculations which were used to generate values of engineering and true stress and stretch ratios are contained in Appendix 3.

3.2 Swelling phenomenon in equi-biaxial fatigue

In equi-biaxial fatigue, consideration must be given to the effect of the inflation medium on the test-piece. As discussed in Chapter 2, inducing a strain into a rubber specimen will render it more susceptible to swelling. During the course of a fatigue test, if a fluid compatible with the test-piece (i.e. having good swelling potential) was used as an inflation fluid, the volume fraction of the rubber would change with progressive cycling of the test-piece. This led to a proposal to use the inflation media in two different ways in the execution of the fatigue tests.

Test Method 1

Firstly, specimens would be subjected to no pre-swelling and then dynamically tested using an incompatible inflation fluid. While all rubbers will swell to some degree in an inflation fluid, the level of volume increase is much lower with an incompatible fluid. This would allow the fatigue behaviour of an essentially 'dry' rubber in equi-biaxial fatigue to be evaluated.

Test Method 2

Secondly, the specimen would be swollen to a known value and then placed in the test-rig. The specimen would then be fatigued using the different parameters discussed (constant pressure, volume amplitudes), using an inflation fluid which would be incompatible with the specimen. To illustrate this, imagine an EPDM sample swollen with hydraulic oil, a compatible fluid with the rubber. The swollen test-piece would then be dynamically tested in the rig using silicone brake fluid as the inflation media, silicone brake fluid being incompatible with EPDM with respect to swelling. This would allow the rubbers to have their volume fractions 'arrested' at a known amount and then subjected to dynamic testing.

It was also suggested that a specimen would be subjected to no pre-swelling and then fatigued using a compatible fluid as an inflation media. This would allow the fatigue behaviour of a rubber swollen due to combined swelling and fatigue effects to be evaluated and described. However, this was discounted as a testing method, as the increase in swelling during the fatigue test would be difficult to estimate, as the test-piece would have to be removed and weighed throughout the test to measure the change in swelling ratio (the swelling ratio being the ratio of dry weight to swollen weight). In this case, the test would not replicate the loading history applied to a dry specimen.

3.2.1 Selection of appropriate swelling media for EPDM

In terms of oil and rubber compatibility, it is important to consider that an oil is made up of several different components. The compatibility can be made complex by such variables as fillers and plasticisers, rubber molecular structure,

selective swelling action by fluid components, time-temperature effects on swelling rates and chemical degradation of the elastomer or fluid. Elastomers can preferentially absorb solvent fractions in the oil. This can also work in reverse, where plasticisers in the rubber can be extracted by the swelling fluid.

As discussed in Section 2.3.5, all rubber will swell to some extent in oil, but the degree of swelling can be estimated for a particular oil-rubber combination, if the solubility parameters δ, for both components of the mixture are known. If the square root of the difference between the solubility parameters of the rubber and the oil is less than 1, as shown in equation (55), then the rubber will swell appreciably in that oil. It is clear that there can be difficulties in accurately determining the solubility parameter for a fluid when it consists of two or more fractions.

Powers and Billmeyer [74] found that the aniline point of hydrocarbon oils and solvents could be used as an index of the swelling of oil resistant synthetic rubber compositions, where the logarithm of the percentage volume increase varied inversely with the aniline point up to 100 per cent swelling. The aniline point is defined as the lowest temperature at which equal volumes of aniline and hydrocarbon sample are completely miscible for selected oils. The slopes by Powers and Billmeyer generated from their experimental data were specific to the rubbers they tested and were not affected by filler loading, temperature or degree of cure. They found that tensile strength was not greatly affected at swelling levels below 100% swelling, but the properties rapidly deteriorated above this value.

Following these findings, Beerbower *et al* [24] discovered by experiment that that the solubility parameter for a hydraulic fluid may be estimated from other

known physical properties which are readily available. One of their experiments allowed the relationship between the solubility parameter and the aniline point of the oils being tested to be plotted as an empirical linear relationship, as illustrated in Figure 3.5.

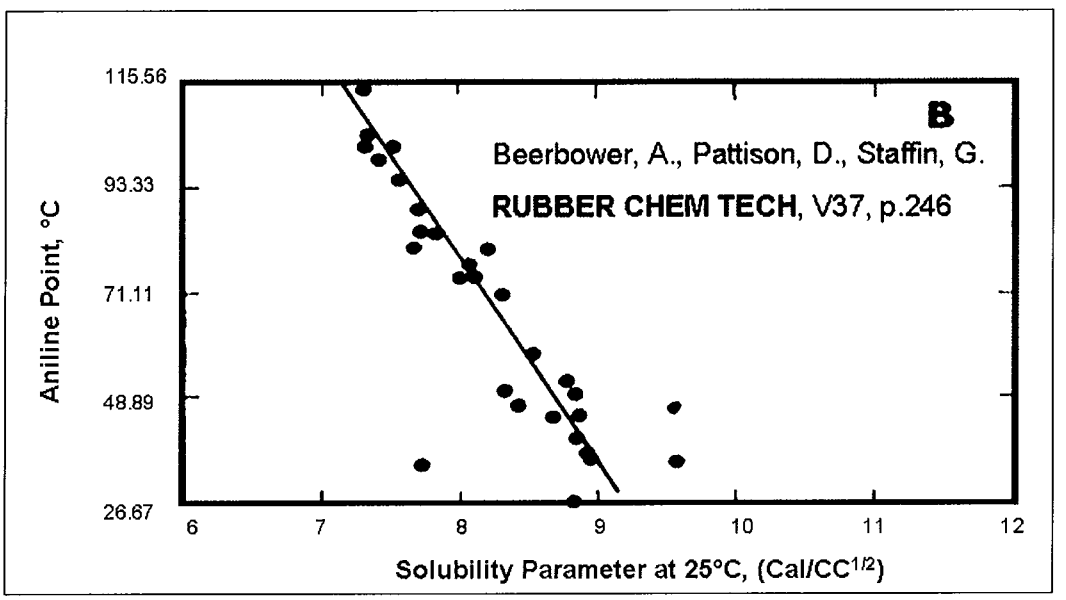

Figure 3.5. Aniline Point versus Solubility Parameter [24].

In order to best demonstrate the effects of swelling in typical hydraulic oils it is therefore necessary to use hydraulic fluids where the properties have been pre-determined and thus can consequently be used as a reference. From the ASTM standards for rubber liquid compatibility [75] the reference oil IRM 903 is the most appropriate choice of oil for high swelling of EPDM. Its aniline point has been determined and can be compared with the solubility parameter for the test material to allow rubber-liquid compatibility to be gauged. Moreover, it is generally comparable with typical hydraulic oils in terms of liquid properties. In addition, by using another reference oil, IRM 902, which imparts medium swell

effects, the influence of different oil solubilities on rubber properties may also be investigated. The properties of these liquids are summarised in Table 3.1.

	IRM 902	**IRM 903**
Boiling Point	> 316°C	> 249°C
Vapour Pressure	<0.001 mm Hg @ 20°C	<0.001 mm Hg @ 20°C
Specific Gravity	0.93 (Water = 1)	0.92 (Water = 1)
Molecular Weight	460	319
Viscosity	20.48 cST @ 99°C	33.3 cST @ 99°C
Aniline Point	92.7°C	70.6°C

Table 3.1 Reference oil properties.

3.2.2 Variation of dynamic strain energy in swollen rubber subjected to fatigue

As discussed in Chapter 2, it can be shown that the modulus of rubber, as well as its strain energy will decrease with swelling. By extension, this would suggest that the dynamic strain energy for cycled samples will be reduced by the swelling action.

The introduction of a solvent into the rubber-filler matrix has been shown to alter the behaviour by reducing the rubber-filler interaction and as a consequence hysteresis is lessened. As discussed in Chapter 2, expressions to describe the mechanical behaviour of a swollen rubber in terms of reduced stress have been developed. It was envisaged that the results of the fatigue testing carried out as part of this research would clarify whether the swollen rubber fails at a lower value of dynamic stored energy than that of the dry rubber.

Chapter 4 presents results recorded during the development of the dynamic test rig and describes how the test procedures evolved to provide the final results presented in Chapter 5 of this thesis.

Chapter 4 Methodology and Test Procedure Evolution

4.1 Preliminary Testing

During the course of this research a number of studies were carried out in parallel with the development of the equi-biaxial testing system. These investigations included:

1. Comparing the dependency of fatigue life on minimum pressure and pressure amplitude for biaxially deformed elastomers with existing data for uniaxially loaded elastomeric test-pieces, [3][76].
2. Determining the effects of stress softening in EPDM cycled biaxially between preset pressure limits [77].
3. Determining the effect of toluene on the dynamic equi-biaxial behaviour of EPDM [78].
4. Determining the effects of oil on the equi-biaxial behaviour of EPDM subjected to pressure controlled fatigue loading [79].
5. Determining the effect of specimen size on the dynamic equi-biaxial deformation of EPDM [80].

A comprehensive description of the aforementioned investigations is contained in Appendix 1.

The results of these tests allowed the methodology to be established for the fatigue tests that would be carried out on the dry and swollen rubber samples and satisfied the first four objectives of the research programme, as listed in Chapter 1.

Figure 4.1 shows the fatigue testing schedule which was carried out to meet the objectives of this research and refers to the corresponding chapters where the test results are discussed in detail.

		FATIGUE TESTING MATRIX							
		Dry		Toluene Swelling		Medium Oil Swelling		High Oil Swelling	
		Pressure Control Fatigue Tests	σ_{Eng} Control Fatigue Tests	Pressure Control Fatigue Tests	σ_{Eng} Control Fatigue Tests	Pressure Control Fatigue Tests	σ_{Eng} Control Fatigue Tests	Pressure Control Fatigue Tests	σ_{Eng} Control Fatigue Tests
TEST MATERIALS	C-14	Ch 4		Ch 4					
	E-1-M	Ch 4		Ch 4					
	E9566	Ch 4	Ch 5			Ch 5	Ch 5	Ch 5	Ch 5

Figure 4.1. Testing matrix for equi-biaxial bubble inflation fatigue tests.

4.2 Initial equi-biaxial fatigue testing– Pre-Pressurisation Tests

In a study to determine if pre-stressing led to increases in the fatigue life of EPDM compounds cycled using biaxial bubble inflation, a number of dynamic pressure controlled tests were carried out. EPDM rubber containing 110 pphr (parts per hundred rubber) low activity carbon black and 70 pphr softener was initially chosen for the investigation (C-14 material, see Appendix 6). The bubble specimen was initially a flat rubber disc having a diameter of 50 mm (35 mm unclamped diameter) and a thickness of 2mm. The test-piece in the first of these tests was cycled from a zero minimum pressure with a range of constant pressure amplitudes. Thereafter, test-pieces were cycled from a minimum pressure of 0.5 MPa with a similar range of pressure amplitudes to that used in the zero minimum pressure tests. All of the tests were carried out until failure occurred.

Figure 4.2 shows that for pre-pressurisation there was a decrease in fatigue life as pressure amplitudes increased.

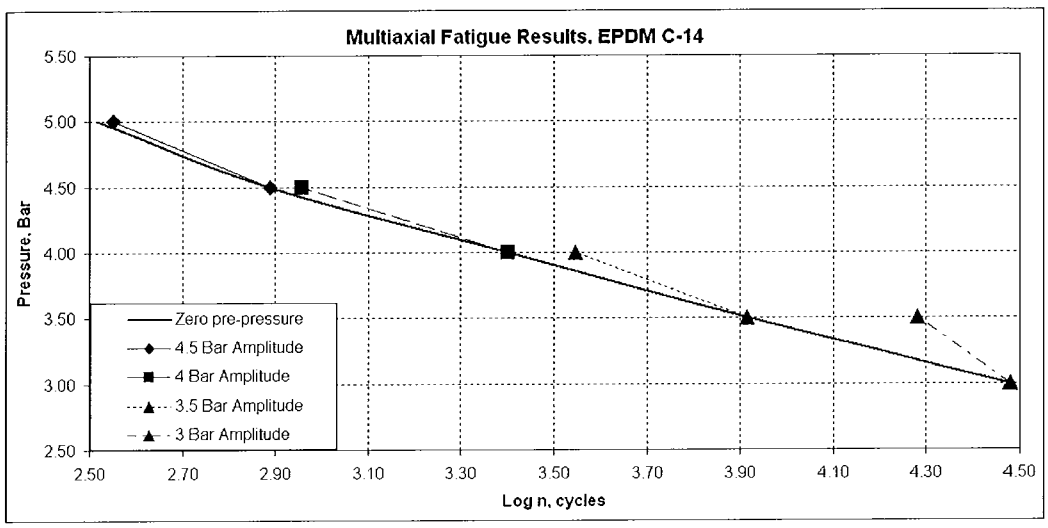

Figure 4.2. Plot of Pressure versus log of cycles for fatigued 2mm C-14 EPDM with zero and non-zero minimum cycling pressure.

This appeared to be at variance with Abraham's findings for uniaxial tests (see Figure 2.9) and further investigation into the results resolved this contradiction. In equi-biaxial bubble inflation, both the engineering stress and the true stress-pressure relationships changed as a function of radius and it was found that the true stress increased as the complex modulus decreased with the accumulation of cycles. This was due to increases in radius for constant applied pressure limits leading to increased thinning of the specimen at the bubble pole. Figure 4.3 illustrates the difference between the engineering and true stress for cycles 1-1000 of a pressure controlled specimen. This is explained by the different relationship between true stress and engineering stress for bubble inflation and the uniaxial case. In bubble inflation, the true stress is equal to the engineering stress multiplied by λ^2, while in the uniaxial case the true stress is equal to the

engineering stress multiplied by λ [7][76]. However, these initial findings led to the belief that engineering stress could possibly be achieved by continuing to use pressure as the control parameter.

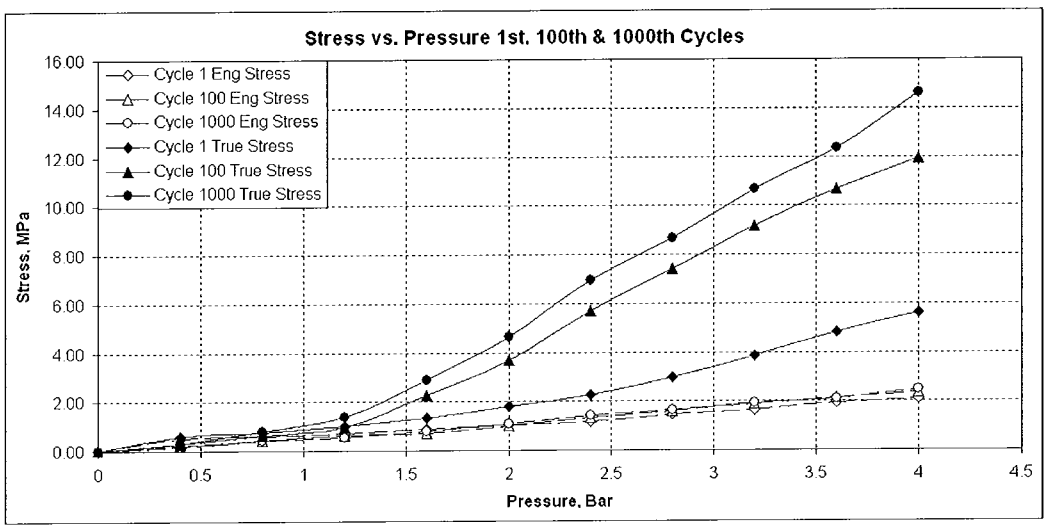

Figure 4.3. Plot of increasing pressure and stress for 2mm C-14 EPDM showing relationship in terms of true stress and engineering stress.

The shape of the fracture resulting from fatigue failures could be observed in the tests using constant pressure control. Single shot inflations to failure tended to rupture in a star or cloverleaf pattern [64][81] as shown in Figure 4.4(a). However, during the series of cyclic tests, rupture due to fatigue was predominantly in the form of a slit in a single direction running through the bubble pole as shown in Figure 4.4(b). The splits emanated from a region at the pole where maximum stress occurred.

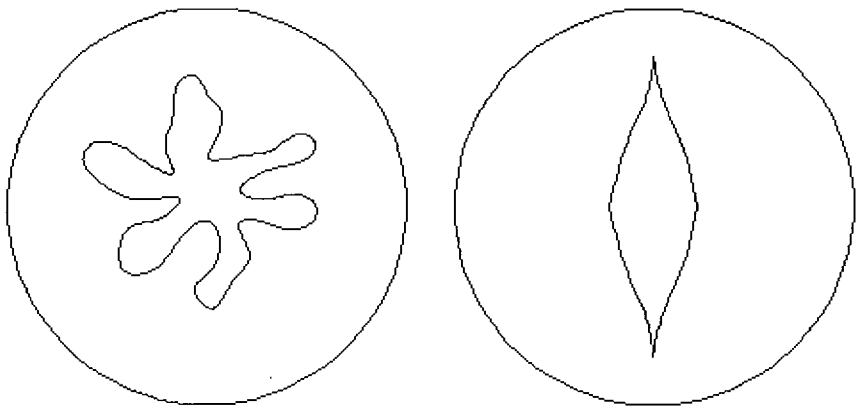

(a) (b)

Figure 4.4. Typical specimen failures modes which occurred during equi-biaxial tests.

4.3 Initial equi-biaxial fatigue testing – Stress-Strain Analysis

Further tests were carried out to investigate if the engineering stress remained constant throughout the fatigue test [76]. A plot of stress strain behaviour for a 2mm EPDM E9566 specimen is depicted in Figure 4.5 for a short-term failure, where short-term is defined as being less than 2000 cycles (test duration of approximately 30 minutes at 1 Hz).

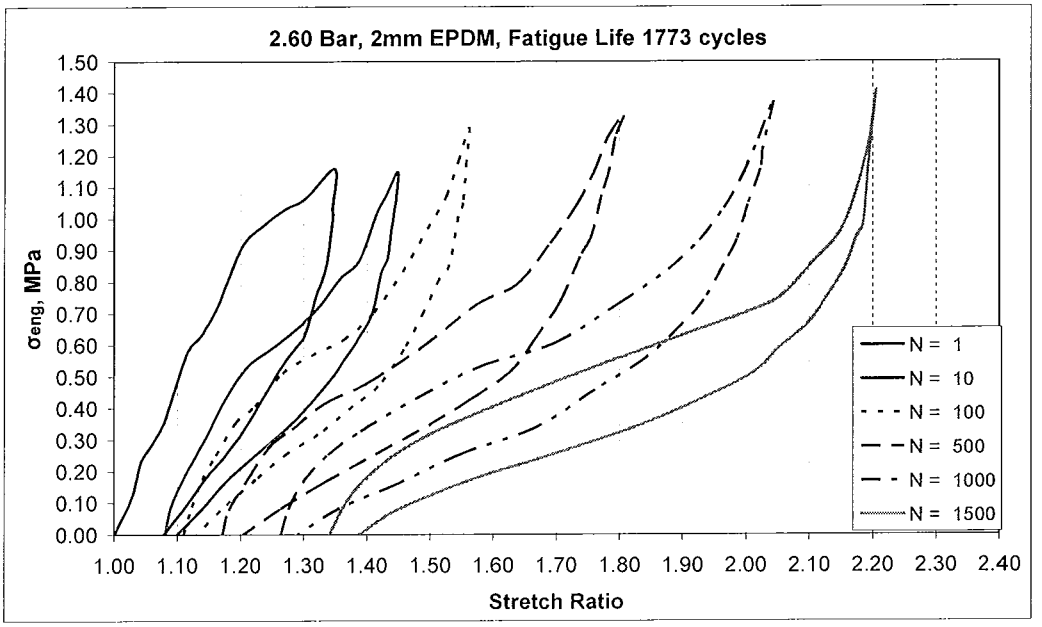

Figure 4.5. Low fatigue life behaviour at constant pressure, 2mm E9566 EPDM specimen.

Following analysis of the short fatigue life specimen, medium-term failures were analysed, where medium-term is defined as greater than 10000 cycles and less than 50000 cycles (test duration of approximately 2.75 - 14 hours at 1 Hz).

The upper stresses in the 2mm specimens in the medium-term fatigue samples did not increase as rapidly as in the short-term samples, as Figure 4.6 illustrates. The upper stresses in the 2mm specimens in the medium failure region remained relatively constant up to 10000 cycles. However, when long term cyclic testing was undertaken, large increases in engineering stress occurred during the latter half of the test. When 4000 cycles had been accumulated, there was a 10% increase in engineering stress. The stress continued to climb throughout the test and at 25200 cycles; 500 cycles before failure, the engineering stress had increased by over 50% of its initial value.

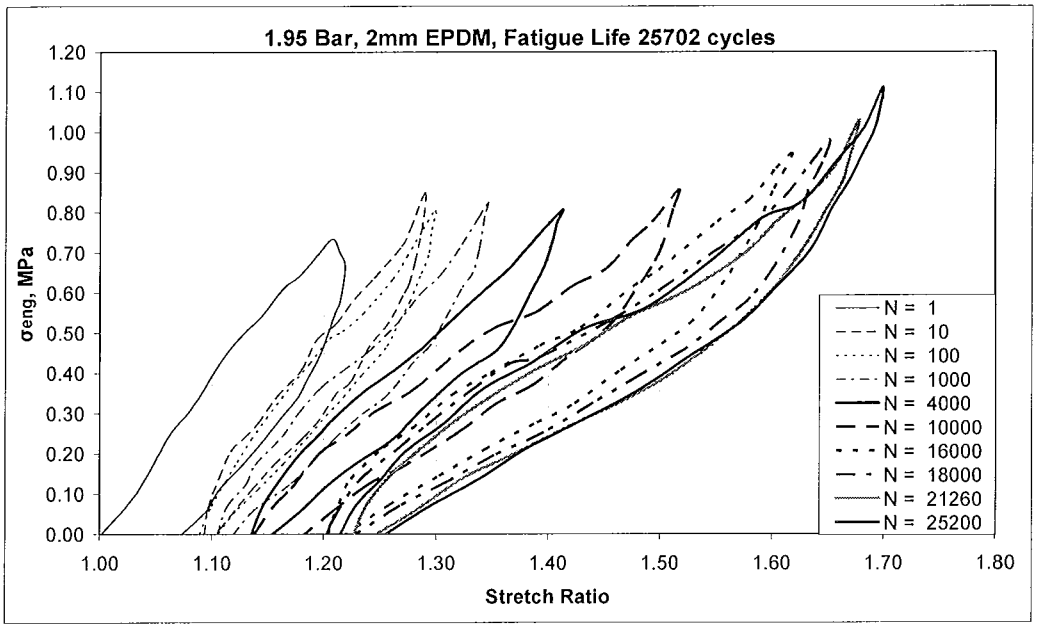

Figure 4.6. Medium fatigue life behaviour at constant pressure, 2mm E9566 EPDM specimen.

This investigation demonstrated that when constant pressure was used as a control mechanism during dynamic cycling of the equi-biaxially loaded EPDM test-pieces, the engineering stress increased throughout the test for a given applied pressure. For initial test cycles, constant pressure control gave a reasonable approximation of constant engineering stress control and it was concluded that it could be used to investigate equi-biaxial stress softening for a discrete number of cycles, allowing valid material models to be obtained. However, constant engineering stress control is essential where accurate long-term lifetime predictions for components subjected to complex loading are required.

4.4 Fatigue and Swelling Tests using Toluene

The first tests incorporating swelling and equi-biaxial bubble inflation provided plots of fatigue life against pressure for two types of EPDM elastomer. Dry and toluene swollen specimens were fatigued to failure in this investigation. Initially three specimens of each elastomer were weighed and then immersed in toluene. Following this, the weight of each specimen was recorded daily until equilibrium-swelling conditions were attained (typically after several days). The weight of the specimens at equilibrium swelling was noted and from this, υ_e, the average crosslink density (XLD) was calculated for each elastomer by using a rearranged version of the Flory-Rehner equation (54), where the effects of filler were accounted for.

$$N' = -\frac{1}{2V_s}\frac{\ln(1-v_r)+v_r+\chi v_r^2}{v_r^{1/3}-v_r/2} \tag{83}$$

where

N' = Number of moles of crosslinks per unit volume,

V_s = Molar volume of the swelling solvent,

v_r = The volume fraction of rubber in the swollen gel

χ = The polymer-solvent interaction parameter.

While equation (83) does not correct for the presence of reinforcing filler it allows comparison between the two compounds. Table 4.1 shows the average values of crosslink density for each elastomer used in the testing.

C14	Density	phr	Volume	M	c		
	g/cm^3		cm^3	g/mol	10^{-5}mol/cm^3		
Polymer	0.91	140.00	153.85	3200*	21.88		
Carbon Black	3.60	141.00	39.17	12.01*	5871.64		
ZnO	5.60	4.00	0.71	81.37	24.59		
Stearicacid	0.85	2.00	2.37	284.47	3.52		
Sulphur	2.07	0.70	0.34	32.06	10.92		
TBBS	1.28	1.00	0.78	33.06	15.13		
TBzTD	1.28	3.50	2.73	34.06	51.39	Density Mixture	
Total		292.20	199.95		5999.07	1.46	
E1M	Density	phr	Volume	M	c		
	g/cm3		cm3	g/mol	10-5mol/cm3		
Polymer	0.86	100.00	116.28	3200*	15.63		
Carbon Black	3.60	110.00	30.56	12.01*	4580.71		
ZnO	5.60	5.00	0.89	81.37	30.73		
Stearicacid	0.85	1.00	1.18	284.47	1.76		
Sulphur	2.07	1.50	0.72	32.06	23.40		
TBBS	1.28	1.00	0.78	33.06	15.13		
TBzTD	1.28	0.80	0.63	34.06	11.75	Density Mixture	
Total		219.30	151.04		109.56	1.45	
Toluene	0.87		106.29	92.14			
Swelling after 2 days / 48 h	Weight before Swelling	Weight after Swelling	m Polymer	m LM	ϕ 1,2	χ 1,2	Crosslink Density, ν_e (x 10^{-5} mol/cm^3)
C14	4.22	7.30	3.92	3.08	0.57	0.32	300.63
E1M	4.13	7.55	3.81	3.42	0.52	0.32	229.11
* Estimates							

Table 4.1. Crosslink densities of EPDM specimens.

Following swelling of the rubber, specimens were placed in a vacuum drying apparatus and dried until all volatiles were removed from the elastomer. The vacuum system consisted of a vacuum tank and a residual gas analyser (mass spectrometer system). The specimen was placed in the vacuum tank and the residual gas in the tank was analysed to ensure all volatile gases had been removed to acceptable levels prior to removal of the specimen from the tank. Figure 4.7 shows the gas spectrum from the vacuum rig, with atomic weight plotted on the x-axis and the current produced by one gas at a specific mass plotted on the y-axis. By selecting an atomic weight on the graph, the current of the gas at the specific mass can be converted to a partial pressure in mbar. The final toluene content in the vacuum chamber was measured as having a partial

pressure of 6.383 x 10^{-14} mbar (atomic mass of toluene = 92), showing that the toluene had been removed from the EPDM sample.

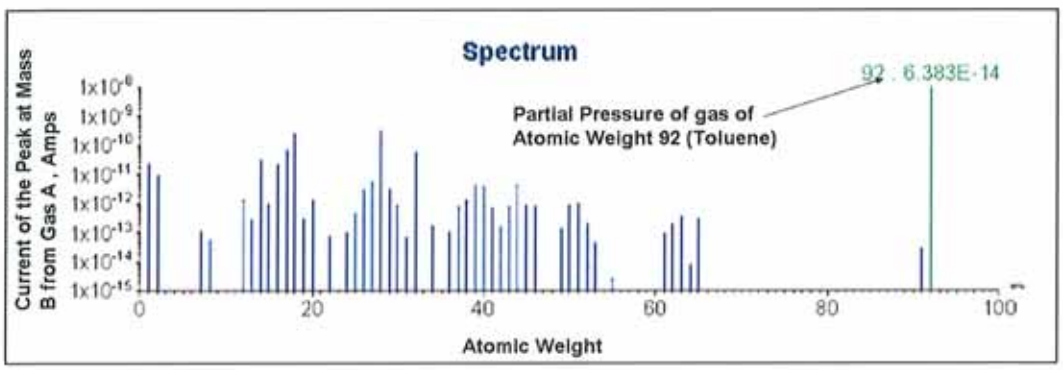

Figure 4.7. Gas spectrum from vacuum rig showing toluene content in mbar. X-axis shows atomic weight and y-axis peak current in amps.

After initial drying of the solvent from the specimens it was noted that the specimen diameter and thickness had reduced. This was thought to be due to extraction of the soluble fraction of the elastomer by the toluene and did not affect the test diameter of the specimens, as the test diameter was less than the reduced outside diameter of the specimen. Consequently the specimen clamp was able to grip the specimen. However, the reduced specimen thickness had an influence on the test results.

Both the untreated and vacuum dried specimens for each elastomer were cycled between 0 bar and pre-set upper pressure limits and the number of cycles to failure was recorded. The results in Figure 4.8 show the fatigue results for the two types of EPDM.

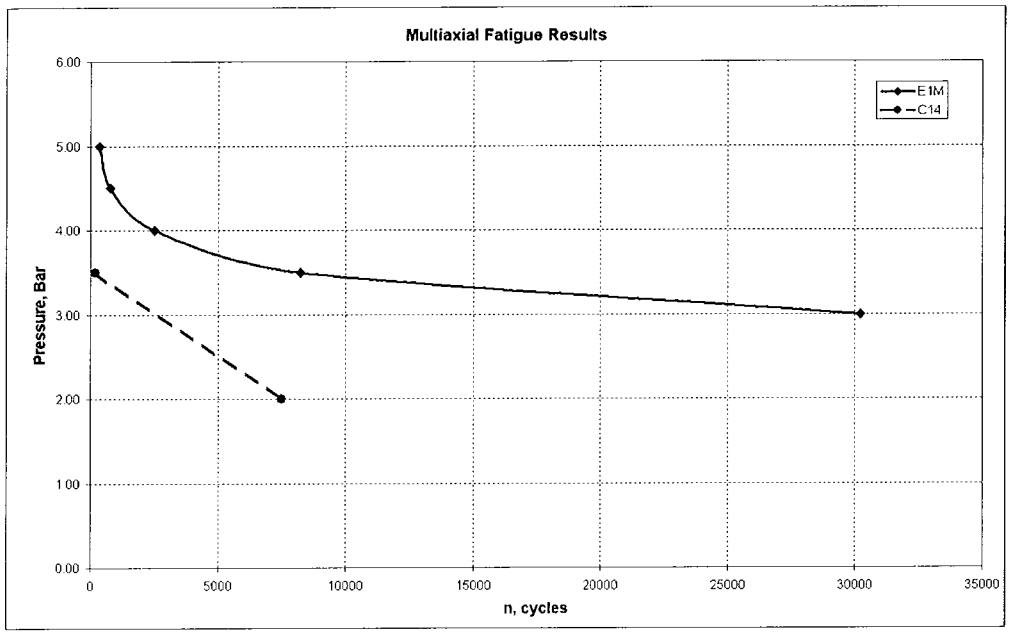

Figure 4.8. Fatigue results for equi-biaxial tests on the two EPDM types (E-1M and C-14), with a minimum cycling pressure of zero bar (2mm original specimen thickness).

As expected, failure occurred rapidly at high pressure amplitudes, while fatigue life increased for lower maximum pressure amplitudes in tests carried out with constant pressure ranges. It is also clear that elastomers with a greater degree of crosslinking had greater fatigue resistance, when subjected to cyclic pressure loads. Failure of both type of specimen after relatively few cycles can be attributed to the fact that equal pressure amplitudes resulted in far higher magnitudes of engineering stress than would be experienced in conventional biaxial loading of the material. Moreover, as the radius of curvature increased in successive cycles due to stress softening, this caused more thinning of the test piece at the bubble pole and as a consequence, an increase in true stress occurred. There was a marked difference in fatigue life between the two types of EPDM C14 specimens, one of which was swollen in toluene and then vacuum dried.

The average fatigue life for the specimens not swollen in toluene was 7496 cycles, compared with 2265 for the swollen and vacuum dried specimens. The fatigue tests for this set of experiments were carried out at pressure limits of 0-2 bar and a frequency of 1Hz. As stated, after drying the swollen samples had a smaller diameter and thinner cross-section, which meant that less cross-section was available to resist the applied pressure during the test. Also, changes in the network structure of the rubber as a result of the solvent treatment, would have influenced the rigidity of the material.

Figure 4.9 shows the difference in stress-strain behaviour between the EPDM C14 specimens, one of which was swollen in toluene. The stress-strain data for each of these curves was taken for the 2000^{th} cycle during a 0-2 bar test. The greater difference between true stress and engineering stress at higher numbers of fatigue cycles for both materials is apparent. The toluene swollen EPDM is a stiffer material, with a higher initial modulus E*, a lower maximum stress and less elongation for a pressure of 2 bar. The hysteresis curve and hence energy of deformation for the swollen EPDM is smaller, suggesting that there are less crosslinks resisting the loading. The untreated specimens by comparison, were more elastic materials, with much greater elongations for the maximum pressure applied.

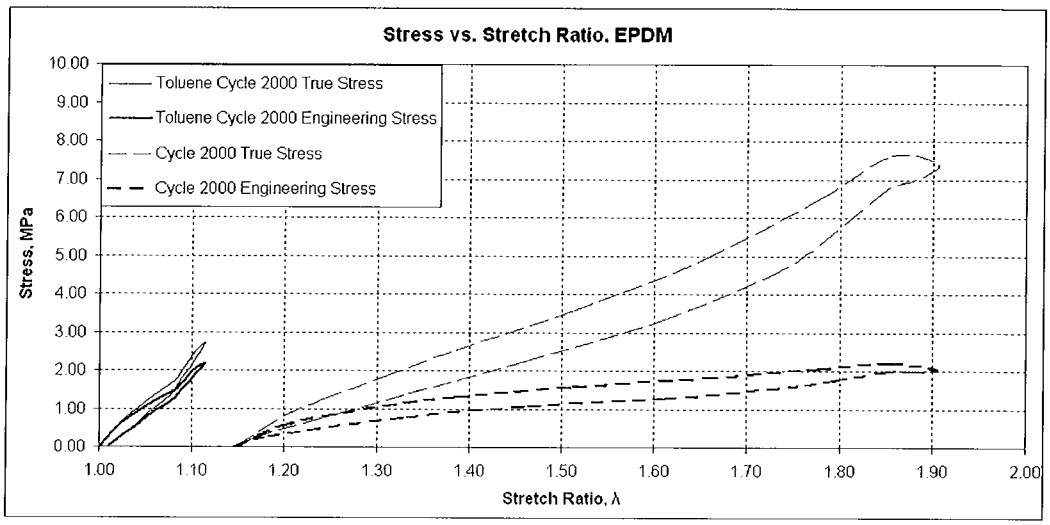

Figure 4.9. Comparison of fatigue lives of swollen and unswollen C-14 EPDM 2mm specimens, for a 0-2 bar test.

These results highlight the significance of elastomer swelling when used as a means of characterising rubber material behaviour. Swelling two different types of EPDM and using the Flory-Rehner equation allowed the degree of crosslinking of each material to be determined. As shown, the material with a greater degree of crosslinking exhibited a higher fatigue life. The average fatigue life under equal loading conditions for the C14 EPDM specimens swollen in toluene and vacuum dried was 30% of that of the C14 EPDM which was untreated. This can be attributed to a number of factors. Specimen thickness influences the stress greatly and the post swelling phenomenon of thinner specimen section, combined with chemical changes in the material as a result of rubber-solvent interaction, both contributed to the reduced fatigue life of the vacuum dried samples. There is a notable difference in the stress-strain behaviour of the vacuum dried and the untreated specimens, with the vacuum dried specimens having a much stiffer initial modulus and less dynamic stored energy than the untreated samples. For the purposes of the fatigue tests, it was therefore

of importance to use a solvent that swelled the specimen, did not extract large amounts of soluble matter and had a higher vapour pressure than the toluene while retaining good compatibility. This further strengthened the argument for using hydrocarbon based oils as a swelling medium.

4.5 Fatigue and Swelling with Reference Oils

Following the toluene fatigue tests and validation of the test rig vision system, further swelling tests were carried out using reference oils on a commercial (Semperit E9566) Shore A 70 hardness EPDM, containing carbon black filler and sulphur crosslinked. A series of dynamic tests were carried out on two types of EPDM specimens. The first type was not subjected to any pre-treatment, while the second type was subjected to oil swelling. Swollen specimens were prepared by immersing them in reference mineral oil for a known duration, temperature was measured and the degree of swelling calculated. Following this, both sets of test-pieces were cycled to failure in fatigue, using constant pressure control. It should be noted that these tests were carried out in parallel with those in Section 4.3. The stress-pressure relationship was determined for both the swollen and unswollen specimens. Test pressures were selected which allowed comparable levels of maximum engineering stress to be applied to each specimen type. The number of cycles to failure for a given maximum stress amplitude were plotted for both dry and swollen specimens. Each specimen type was analysed at a given pressure amplitude and changes in complex modulus as cycles accumulated were compared.

4.5.1 Oil Swelling Test Procedure

Swelling experiments were carried out by immersing the specimens in reference oil IRM 903, at an elevated temperature of 100°C for a period of one hour, in accordance with ASTM standard D471. The properties of IRM 903 have been previously described in Table 3.1.

The specimens were removed from the hot oil and cooled in oil at ambient temperature for a short period, before being wiped dry and weighed. An average swelling ratio of 1.11 (11% increase in mass) was calculated for the samples. Following swelling calculations, the swollen test-pieces were inflated to failure under equi-biaxial fatigue loading, again using silicone fluid to inflate the test-pieces.

4.5.2 Oil Fatigue and Swelling Test Results

The relationship between applied pressure and measured engineering stress was used to generate plots of stress-amplitude versus cycles to failure for both the swollen and unswollen test-pieces. The pressure-stress relationship for the swollen rubber is shown in Figure 4.10. It can be seen that for the cycles shown and for lower inflation pressures, this relationship was found to be linear.

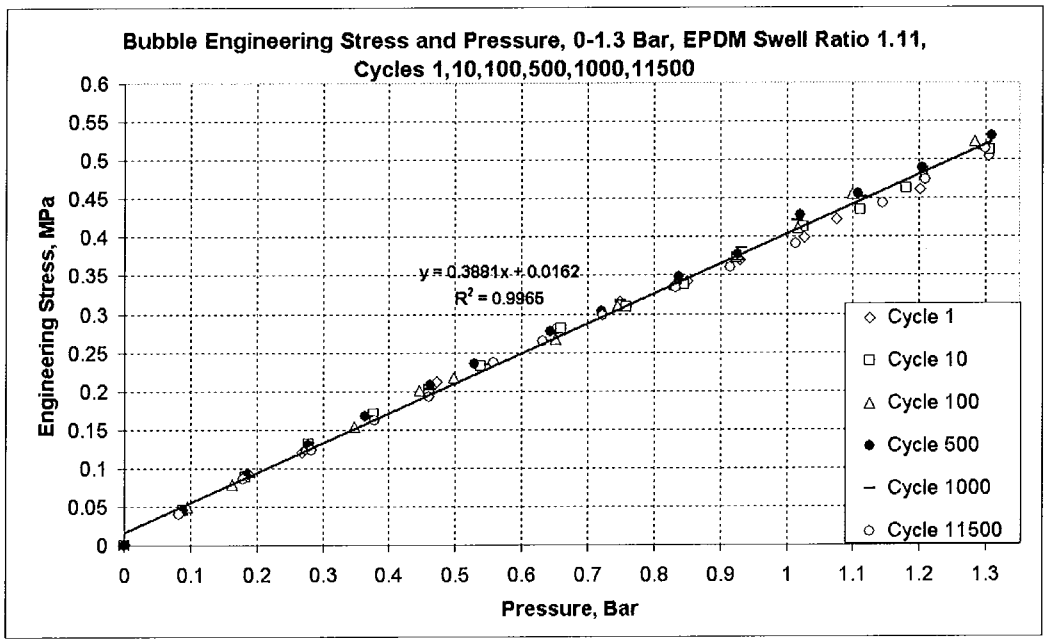

Figure 4.10. Pressure-Engineering Stress relationship for swollen 2mm E9566 rubber (0-0.6 MPa).

The plot of stress amplitude versus cycles to failure is shown in Figure 4.11. Unsurprisingly, the unswollen specimens exhibited greater fatigue resistance than the swollen test-pieces. This can be attributed to the swollen test-pieces having a larger bubble radius and hence a higher engineering stress for a given applied pressure. It should be noted however, that the pressure-stress relationship does not remain constant, so the S-N curves generated as part of this investigation would have questionable validity.

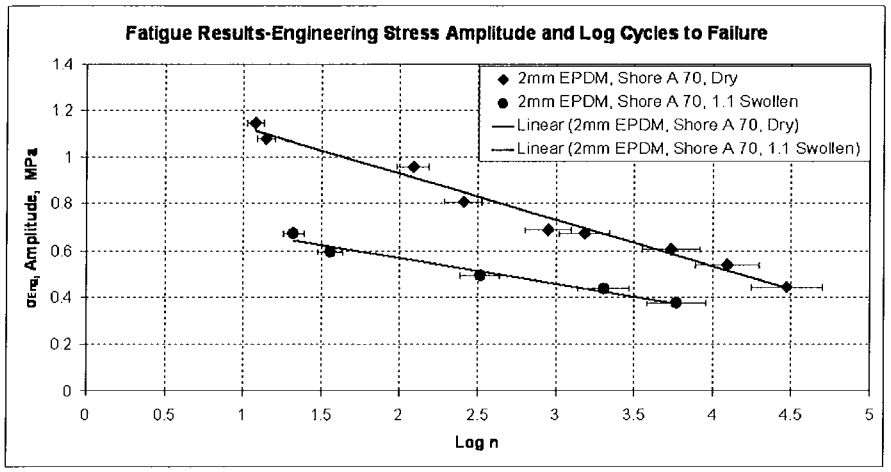

Figure 4.11. Stress amplitude versus cycles to failure, swollen/unswollen 2mm E9566 EPDM.

When the stress-strain behaviour of the two specimen types is analysed, it can be seen that the unswollen test-pieces exhibited higher stiffness than the swollen specimens. This is shown in Figure 4.12, where the change in the deformation behaviour of the two sample types is shown for cycles 10 and 1000, for an upper engineering stress of 0.6 MPa.

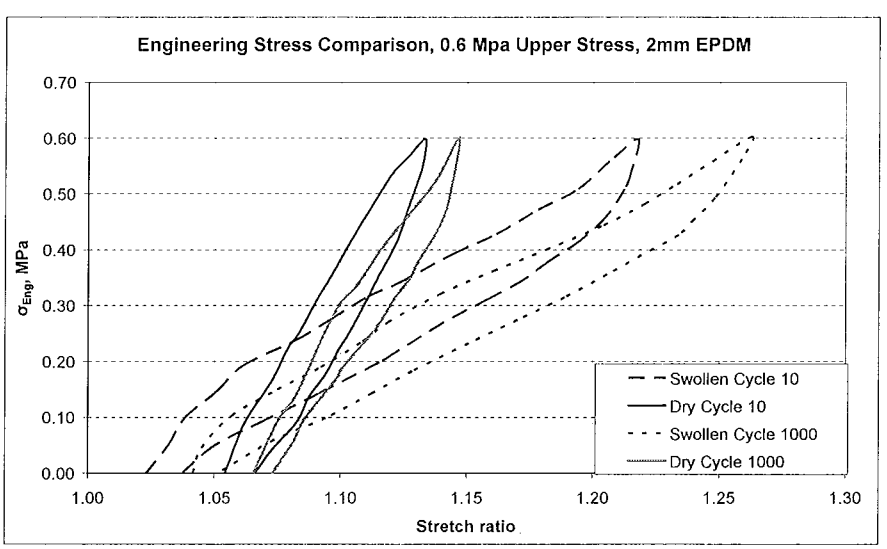

Figure 4.12. Stress-strain curves, swollen and unswollen 2mm E9566 EPDM, 0.6 MPa upper engineering stress, cycles 10 and 1000.

The initial modulus of the unswollen test-piece was greater than that of the swollen specimen. However, the rate of decrease in modulus in the unswollen specimens appeared to be greater than that of the swollen specimens with the accumulation of cycles. It was not possible to have confidence in this outcome due to uncertainties associated with rig control at the time of testing, where some samples were unavoidably subjected to random over-pressurisation during testing. Modifications to the rig obviated this failing in further tests.

4.6 Development of Constant Stress Controlled Tests

The tests outlined previously in this chapter highlighted the requirement for control of engineering stress during the test. A system was developed to make this possible. A linear variable differential transducer (LVDT) was fitted to the inflation/deflation cylinder and incorporated in the control system circuit. The LVDT allowed the cylinder stroke/bubble volume to be monitored and controlled. By controlling the output of the system to a set-point based on both the inflation pressure and the bubble volume, values of engineering stress can be monitored throughout a cycle and subsequently could be used to initiate inflation or deflation of the bubble. The graph in Figure 4.13 shows the change in bubble radius represented as a voltage proportional to an applied cylinder stroke/volume for the dry 2mm E9566 EPDM. By applying a fourth order polynomial fit to this data a master curve for volume and radius was generated and used in the control program as a function to convert cylinder stroke length to radius. By multiplying this radius value by the pressure and dividing by the original thickness, the instantaneous engineering stress could be calculated. Similar curves were generated for the swollen specimen sets, with each type of material having

different volume/radius behaviour. However, when carrying out stress controlled tests in this manner, it is essential that no inflation fluid escapes the system during testing, as this will introduce an error into the control method. It should also be noted that any calibration curve is specific to both the material and the sample thickness of that material. There was a noticeable set in the EPDM material during fatigue testing, meaning that the points on the calibration curve below 0.2 Volts were only used for control on the initial cycles. However, for more elastic materials this would not be the case and this portion of the curve would be used for control between lower engineering stress limits.

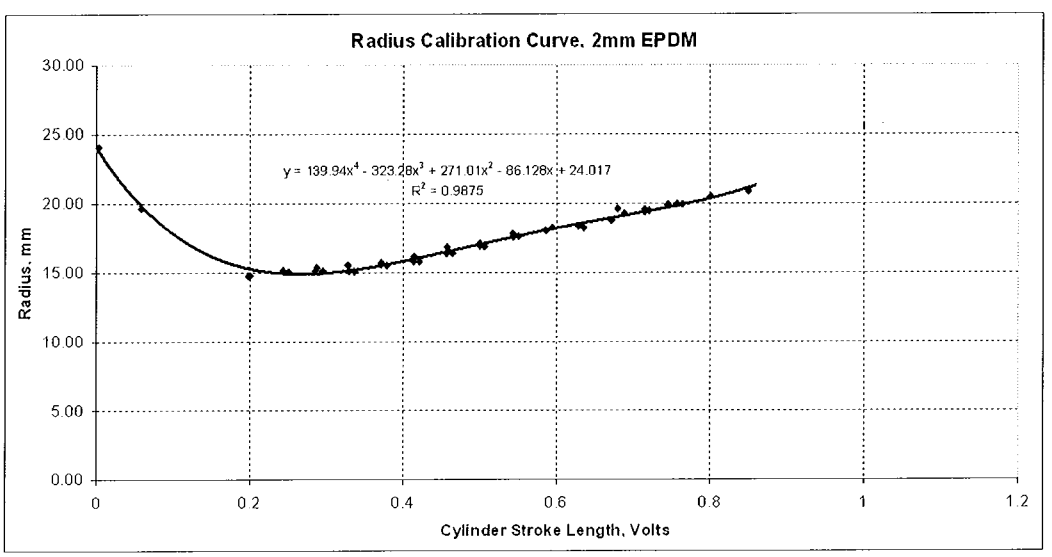

Figure 4.13. Relationship between bubble radius and applied volume, in this case for unswollen 2mm E9566 EPDM.

This method of control allowed the upper engineering stress limit to be maintained, within limits of ±5% throughout the test, as Figure 4.14 illustrates. This control method allowed many of the objectives of the research programme to be completed.

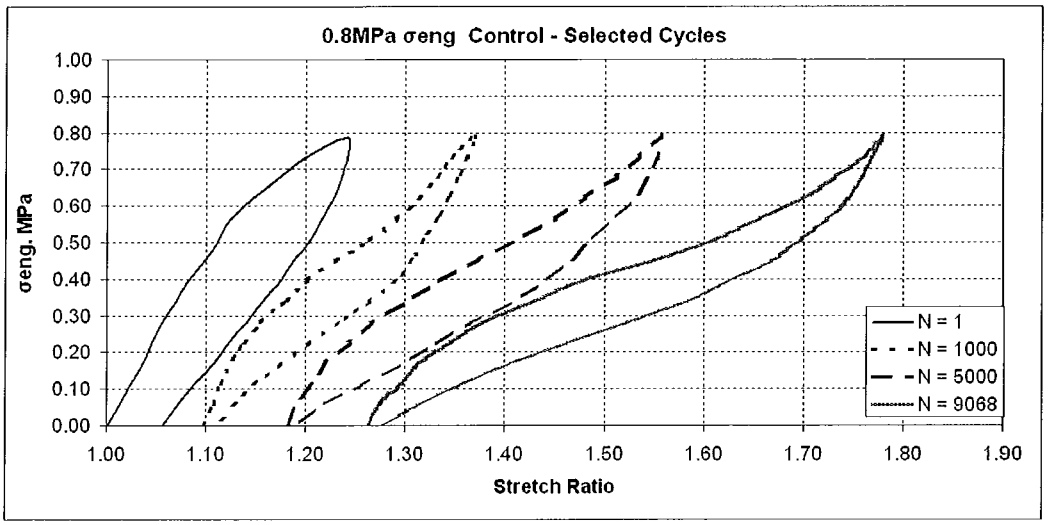

Figure 4.14. Stress-strain behaviour of 2mm E9566 EPDM for a stress controlled fatigue test for selected cycles, 1-9068.

Following the validation of these changes to the control system, a final series of dynamic equi-biaxial tests were carried out on dry E9566 EPDM and two specimens sets swollen using the reference oils. Control of the engineering stress throughout the fatigue test permits plausible analysis of the changes in the dynamic properties of the material such as the complex elastic modulus E* and dynamic stored energy. Fatigue results for dry and swollen E9566 EPDM and the changes in these properties with cyclic loading will be evaluated in Chapter 5.

Chapter 5 Equi-biaxial fatigue and Swelling – Results

5.1 Test Schedule

Following the tests conducted on EPDM samples described in Chapter 4, a final schedule of testing was devised. It was proposed to test three different EPDM specimen sets in equi-biaxial fatigue, between pre-set maximum and zero minimum engineering stress limits. By testing using engineering stress control, changes in the material properties of the EPDM, such as complex elastic modulus E* and dynamic stored energy in a cycle could be directly related to a maximum engineering stress which did not increase throughout the test. This permitted realistic comparison with results obtained for EPDM in load controlled uniaxial fatigue tests [3]. Moreover, the effect of different swelling ratios on the mechanical properties of the EPDM could be analysed.

The test specimens were in two conditions:

1. Dry specimens, fatigued to failure. The inflation fluid for these tests was chosen to cause minimal swelling effects.
2. Specimens swollen in two different reference oils, IRM 902 and IRM 903 for one hour at 100°C. Following removal from the swelling medium, test-pieces were equi-biaxially tested to failure in fatigue, using a silicone based inflation fluid which minimises swelling effects during the dynamic tests.

5.2 Test Preparation – Swelling Tests

Again, swelling experiments were carried out by immersing the specimens in reference oils at elevated temperature of 100°C for a period of one hour. The specimens were removed from the hot oil and cooled in oil at ambient

temperature for a short period, before being wiped dry and weighed. An average swelling ratio was calculated for the samples, where the swelling ratio Q can be expressed as,

$$Q = W_s / W_d, \tag{84}$$

where W_s is the weight of the swollen elastomer sample and W_d is the weight of dry elastomer before swelling.

A swelling ratio of 1.10 (10% increase in mass) was calculated for the EPDM swollen in IRM 903 and a ratio of 1.042 (4.2% increase in mass) for the EPDM swollen in IRM 902. Following swelling calculations, the swollen test-pieces were inflated to failure under equi-biaxial fatigue loading, using silicone fluid to inflate the test-pieces. Using the same procedure as before, radius calibration curves were generated for the three specimen sets, (dry, high swell and medium swell, as previously defined).

5.3 Equi-biaxial Fatigue Tests – S-N Curves, Stress Control

To allow the peak engineering stress in a cycle to be maintained at the same value for all cycles throughout the test, the pressure set-point was adjusted continually. By using this method of control, practical S-N curves could be obtained to compare the fatigue lives of the dry versus swollen rubbers.

Plots were generated of stress-amplitude versus cycles to failure for both the swollen and unswollen test-pieces. All fatigue tests were carried out with zero

minimum stress in each cycle. The plot of stress amplitude versus cycles to failure for all three specimen sets is shown in Figure 5.1. For each data point on the S-N plot, three tests were typically carried out at the stress amplitude in question and the average fatigue life was then used.

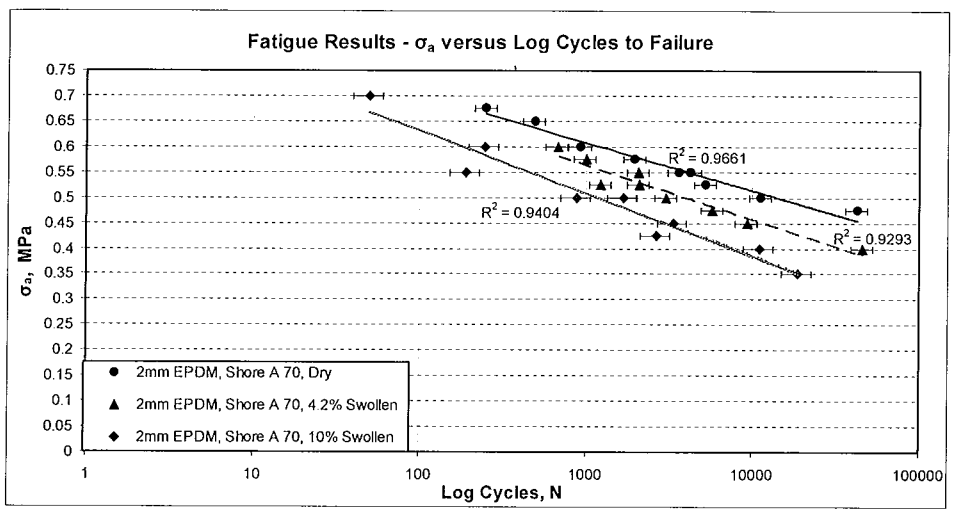

Figure 5.1 – Plot of stress amplitude versus cycles to failure for the dry and swollen 2mm E9566 EPDM specimens.

Unsurprisingly, the unswollen specimens exhibited greater fatigue resistance by comparison with the swollen test-pieces. It can be seen that the fatigue life of the EPDM is reduced in proportion to the degree of swelling.

5.4 Analysis of Results – Elastic Modulus

The fatigue behaviour of the three specimen sets was studied further. The complex modulus, E* of both specimen sets was analysed, where E* was approximated by calculating the slope of the loading curve from zero stress and minimum strain to peak engineering stress and maximum strain for the cycle in question.

Abraham observed in his tests [82] that the material failed after a material specific loss in complex modulus E*. This predictor (termed $E^*_{residual}$ in this work) can be represented as:

$$E^*_{residual} = (E^*)/ E^*_{conditioning}.100\% \quad (85)$$

Abraham noted that $E^*_{residual}$ appeared to be independent of the magnitude and frequency of the applied loading. The dry and swollen specimens were analysed using this approach, where the percentage drop in $E^*_{residual}$ was plotted versus cycles to 95 % of the fatigue life of the specimen. The values for denoting 100% of E* were defined as the modulus of the material after 10 conditioning cycles (termed $E^*_{conditioning}$). The plot of decrease in $E^*_{residual}$ is shown for the dry EPDM in Figure 5.2. $E^*_{residual}$ was found to have an average value of 33% ±10% of its original value at 95% of the fatigue life of each specimen.

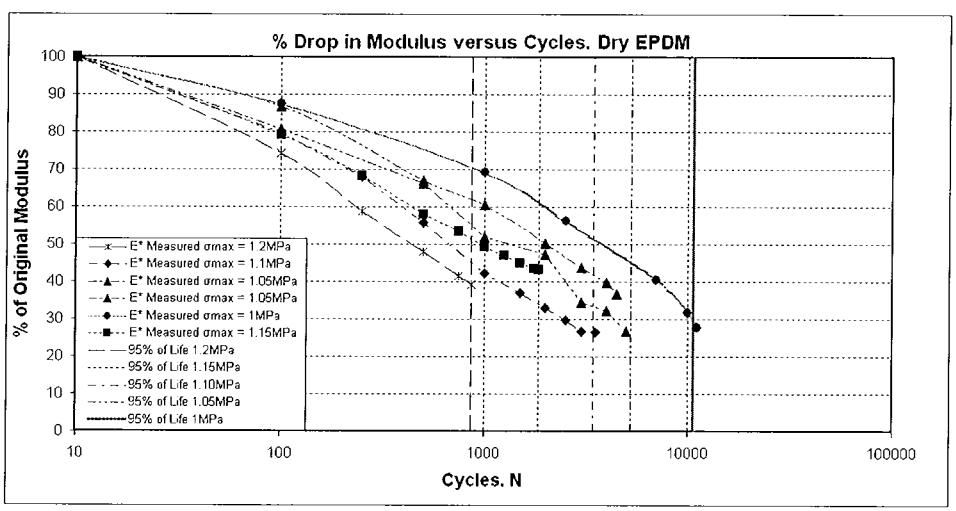

Figure 5.2. Percentage drop in Specific Modulus for Dry 2mm E9566 EPDM during fatigue testing.

When the values of E* are compared for the three specimen sets at a similar stress amplitude, it is clear that the dry specimens have a higher initial modulus. It should be noted however, that the rate of decrease is also more rapid in the dryer specimens, as shown in Figure 5.3.

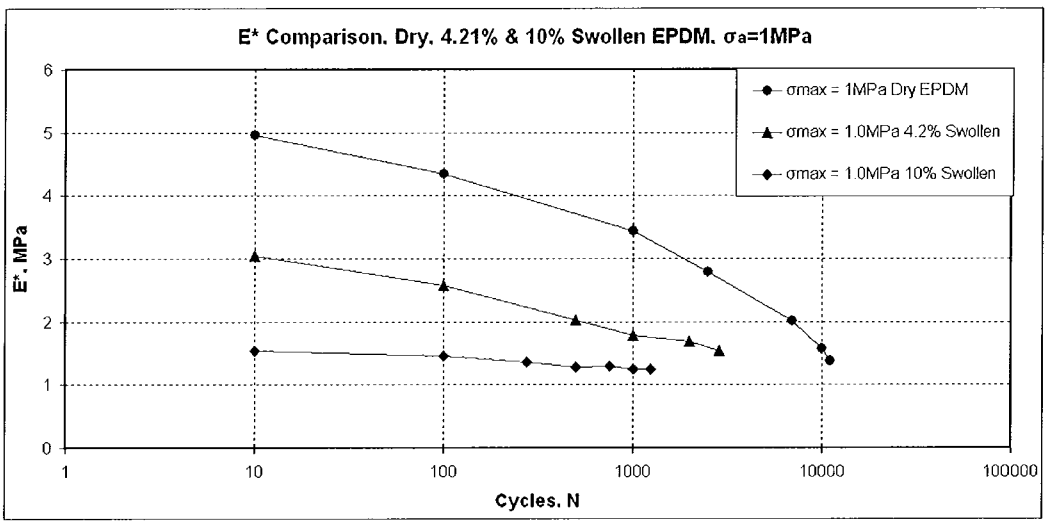

Figure 5.3. Comparison of E* versus cycles for the three specimen sets at σ_a = 1MPa.

Again, considering the change in $E^*_{residual}$, results for the EPDM swollen by 4.2% showed an average limiting value of $E^*_{residual}$ of 54% at 95% of specimen life, as depicted in Figure 5.4. This higher percentage value of specific modulus is attributed to the reduction in initial modulus caused by the swelling. Figure 5.5 shows that the EPDM swollen by 10% had an average specific value of $E^*_{residual}$ of 59.8% at 95% of specimen life.

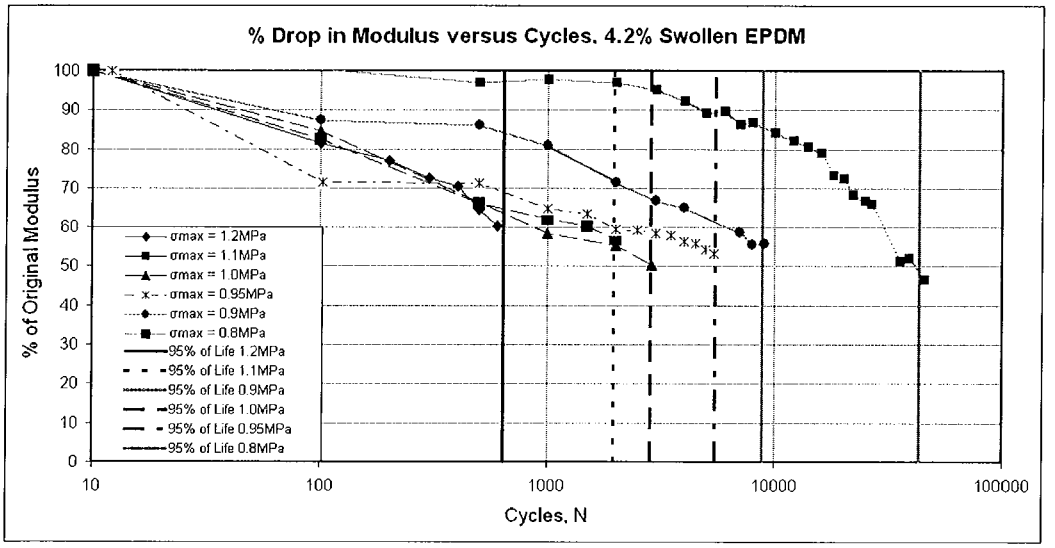

Figure 5.4. Percentage drop in $E^*_{residual}$ versus cycles for 4.2% Swollen 2mm E9566 EPDM during fatigue testing.

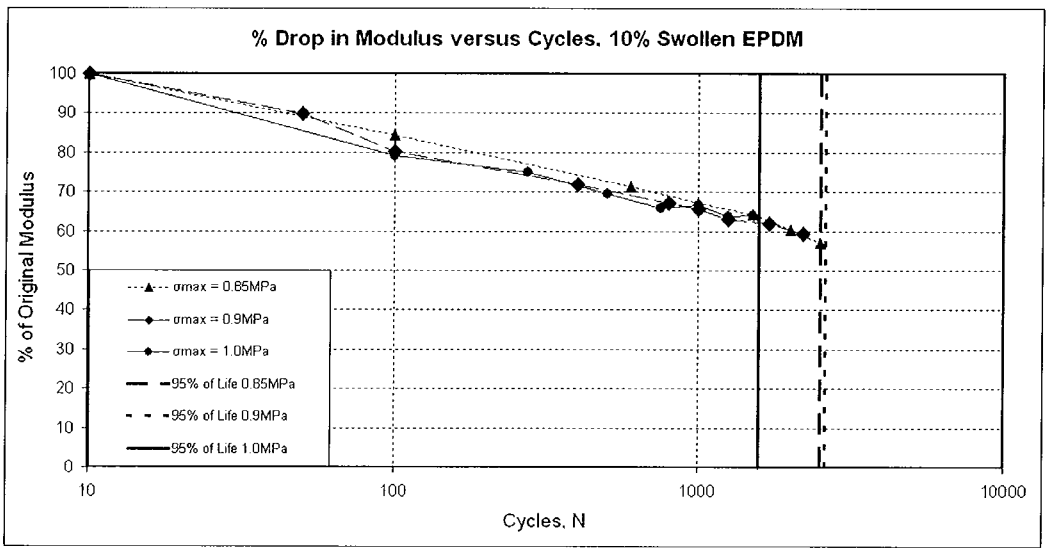

Figure 5.5. Percentage drop in $E^*_{residual}$ versus cycles for 10% Swollen 2mm E9566 EPDM during fatigue testing.

The dry and 4.2% swell specimen sets were then compared at similar stress amplitudes, where the 100% initial modulus value ($E^*_{conditioning}$) was assumed to be the value at 10 conditioning cycles in the dry specimens, for each respective

stress amplitude. The trends for each specimen set are shown for four stress amplitudes in Figure 5.6.

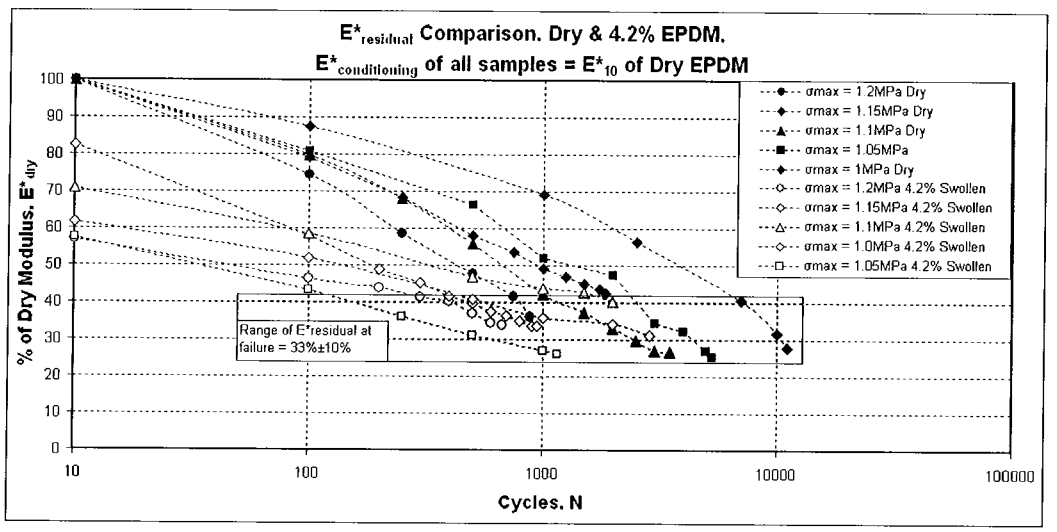

Figure 5.6. Percentage drop in Specific Modulus versus cycles for the dry and 4.2% swollen specimens sets at four different stress amplitudes, where $E^*_{conditioning}$ is based on that of the dry 2mm E9566 EPDM.

There is an average $E^*_{residual}$ at failure of 33% ±10% for these sets of specimens, at the four different stress ranges. It can be argued that by knowing the initial modulus ($E^*_{conditioning}$) for the dry specimens, an approximation of the failure modulus for the swollen test-pieces may be made.

When comparing the three specimen sets at similar stress amplitudes, the number of samples which could be analysed was limited, due to the 10% swollen specimens having short lives at higher stress amplitudes and the dry specimens having extremely long fatigue lives at lower stress amplitudes, with many of these tests typically ending with failures at the clamp edge. However, at an amplitude of 1MPa, comparison can be made between all three sample sets in terms of the decrease in specific modulus. Figure 5.7 plots the decrease in

$E^*_{residual}$ for each sample type at σ_a = 1MPa, where again the initial modulus used for each sample was that of the dry EPDM after 10 conditioning cycles. The values of $E^*_{residual}$ were found to fall within the 33% ±10% range at failure for each of the three specimens. Hence, for a stress amplitude that could be applied to all specimens to allow a realistic comparison of $E^*_{residual}$ at failure, this value of $E^*_{residual}$ was similar irrespective of the levels of swelling.

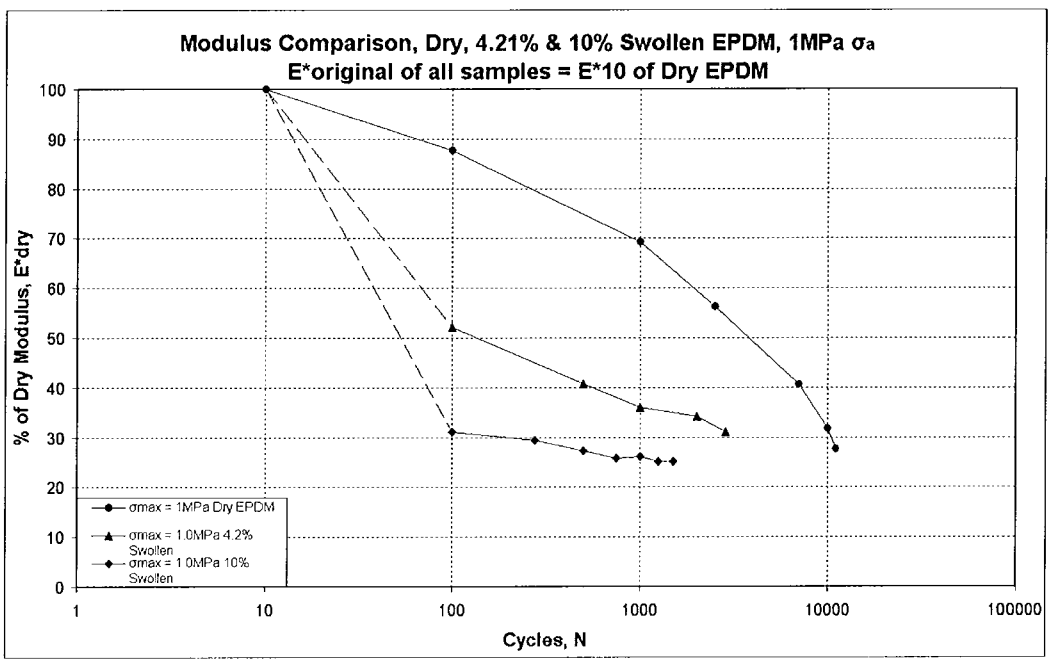

Figure 5.7. Percentage drop in $E^*_{residual}$ versus cycles for the 3 specimens sets at σ_a = 1MPa, where $E^*_{conditioning}$ is based on that of the dry 2mm E9566 EPDM.

5.4.1 Modelling of Decreases in Modulus

Models were generated to describe the decrease in elastic modulus due to swelling and fatigue. Figure 5.8 below shows the experimental data for dry, 4.2% swollen and 10% swollen test-pieces, with models also shown replicating the

decrease in modulus with cycling of the test-piece. The models were based on the following equation:

$$E^* = E^*_{Conditioning} - ZM\ln(N) \qquad (86)$$

Where,

Z = Loading Factor (Non-linear function of σ_a)

M = (1 - % Increase in mass due to swelling)

N = Number of cycles

$E^*_{conditioning}$ = E* after conditioning (typically, 10-15 cycles)

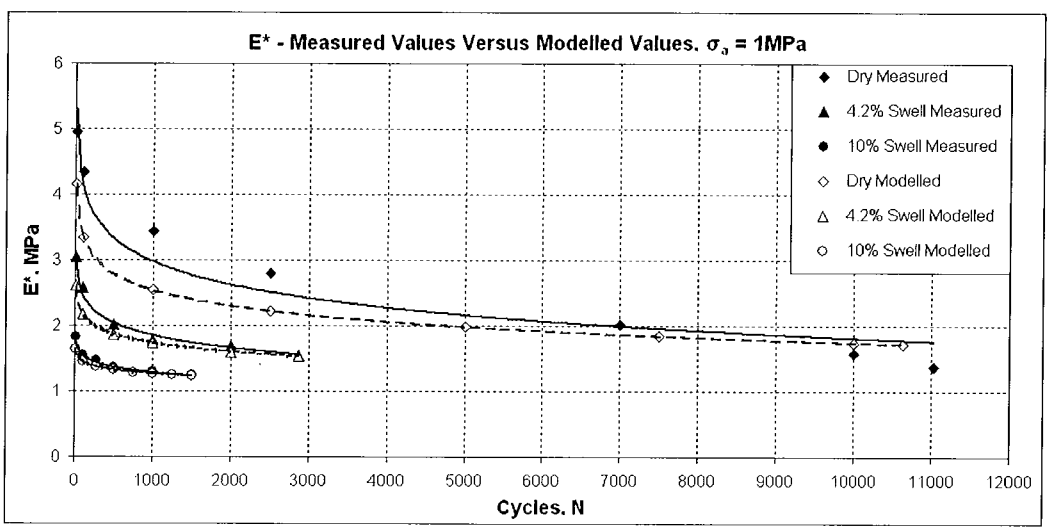

Figure 5.8. Experimental and modelled E* plots for three specimen sets at a stress amplitude of 1MPa.

The models generated using equation (86) fit the data reasonably well. Figure 5.9 shows a plot of Z versus stress amplitude (σ_a). It should be noted that the loading factor Z varies as a function of the stress amplitude and its value is offset by the swelling ratio. Further plots of E* models are contained in Appendix 5.

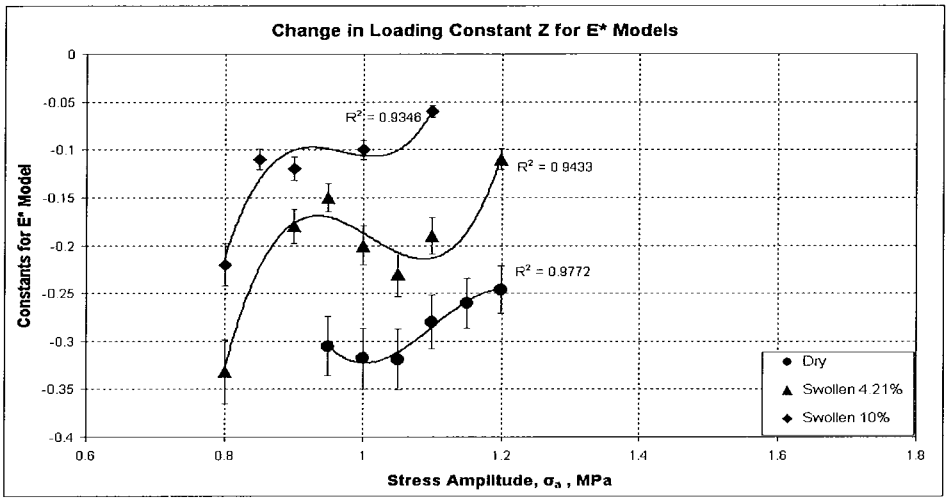

Figure 5.9. Plot of loading factor Z versus applied stress for the three specimen sets.

The change in the loading factor Z with respect to the stress amplitude can be represented by the 3rd order polynomial function shown in Equation (90)

$$Z = Ax^3 + Bx^2 + Cx + D \tag{87}$$

where constants A, B and C are multipliers and constant D is an offset which is a function of the initial modulus. The values of Z increase with an increase in swelling for a given stress amplitude. Table 5.1 lists the values of these constants for the three specimen sets.

	Constant A	Constant B	Constant C	Constant D
0% Swelling (Dry)	19.778	65.348	-71.39	25.498
4.20% Swelling	24.847	- 75.328	75.681	- 25.388
10% Swelling	28.947	-84.132	81.339	- 26.262

Table 5.1 Table of constants to describe form of loading factor Z.

5.5 Analysis of Results – Dynamic Stored Energy

The results for the fatigued specimens presented in this work were analysed with respect to the dynamic stored energy in a similar manner to analysis carried out by Abraham [79], where the energy was reported in units of Nmm. Figure 5.10 shows how the different energies were calculated from the stress strain (or stretch ratio) data.

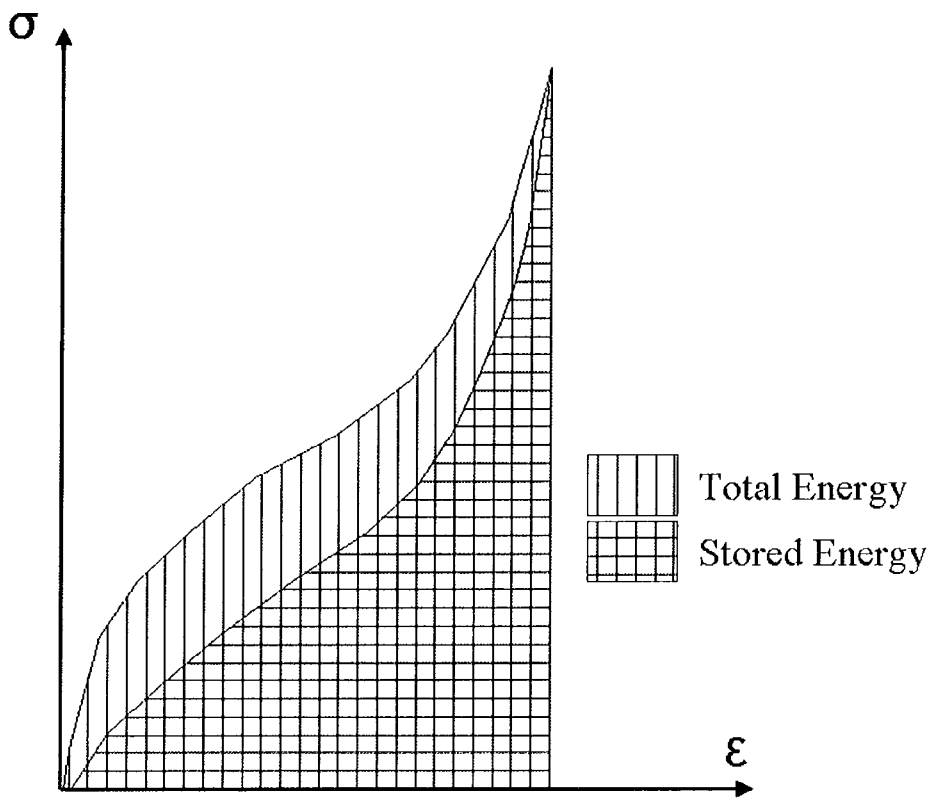

Figure 5.10. Basis of Calculation of Dynamic Stored Energy from Stress-Strain Data.

During fatigue testing, a number of stress-strain measurements were made at intervals throughout the test. The dynamic stored energy in a cycle was subsequently calculated for these measured cycles. When plotted against the cycles to failure, the dynamic stored energy was found to increase linearly,

following conditioning of the test-piece. Figure 5.11, shows the plot of dynamic stored energy for the dry EPDM specimens. Similar plots were generated for the 4.2% and 10% swollen EPDM.

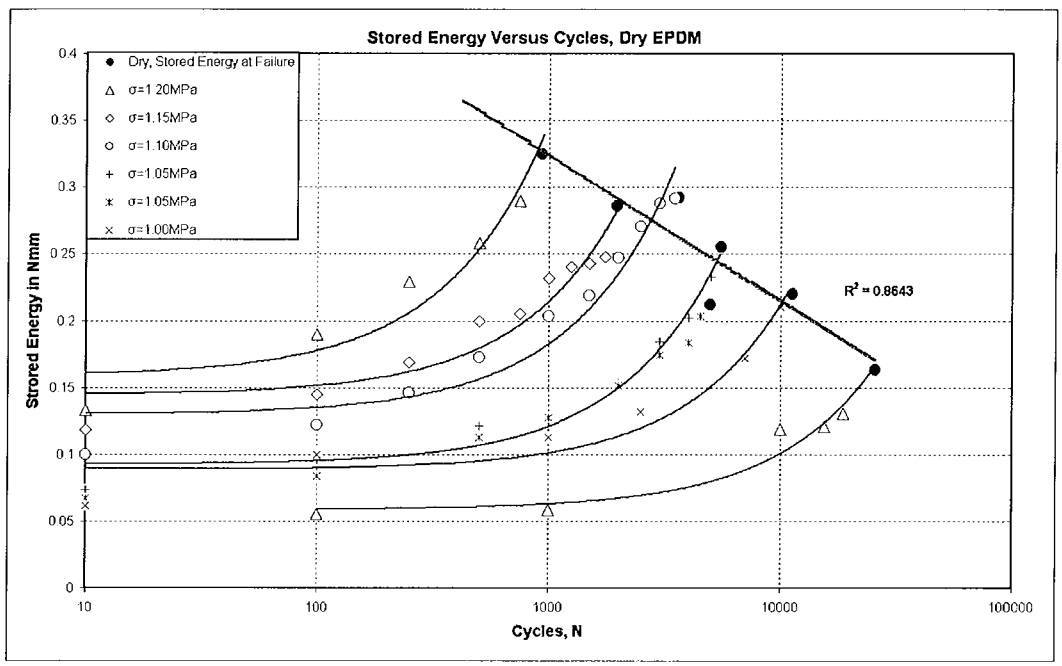

Figure 5.11. Plot of Dynamic Stored Energy at Failure for dry 2mm E9566 EPDM.

When shown on one graph, as in Figure 5.12, the impact of swelling on the property of dynamic stored energy can be described. At similar stress amplitudes, the dry EPDM samples had higher dynamic stored energy at failure, by comparison with the swollen specimens, with the 10% swollen rubber having the lowest dynamic stored energy for a given stress amplitude. This result can be attributed to the strain energy that can be absorbed by filler-filler bonds, which exist in fewer numbers for an increase in the degree of swelling.

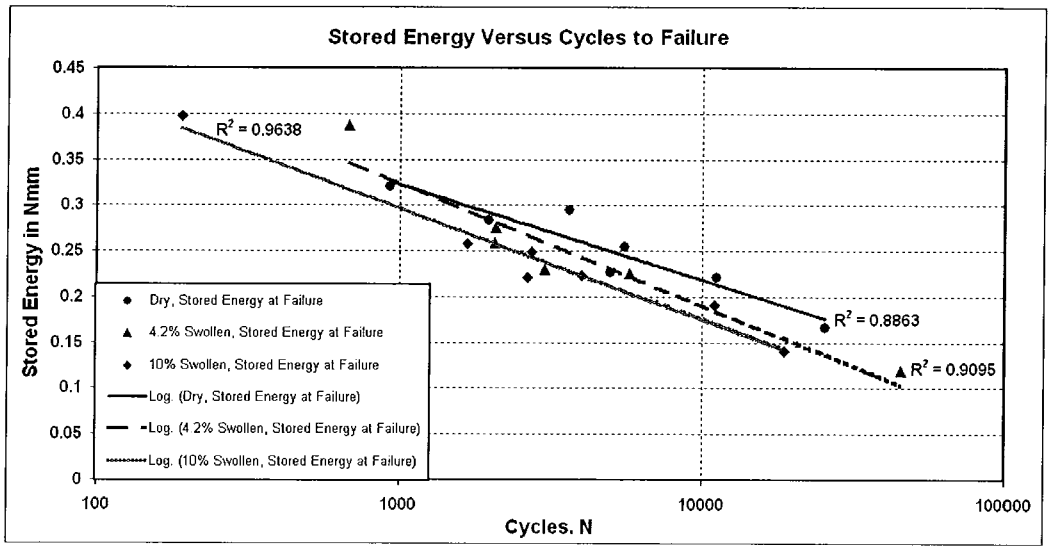

Figure 5.12. Trends of Dynamic Stored Energy at Failure for all three 2mm E9566 EPDM specimen sets.

These curves of stored energy for the dry and swollen specimens may have a relationship to each other, which could be described by applying a shift factor to the dry stored energy curve, with the shift factor being a function of the degree of oil swelling. A similar approach using shift factors was used by Ronan *et al* in the characterisation of long term stress relaxation in elastomers [83][84].

5.6 Analysis of Results - Microscopy of Failure Surfaces

Initially, the fracture surfaces of the dry samples were analysed using a digital imaging microscope. A magnification factor of X200 was used to view failure surfaces. For low cycle lives of less than 100, the type of failure is more akin to that of a single cycle test to destruction, with the surface morphology fibrous in nature and in some instances showing delamination at the failure surface. Failures at cycles greater than this show clear evidence of crack propagation and subsequent rupture. In most fatigue failures, the cracks appear on the surface of

the bubble and continue to grow until total failure. This behaviour was common to both the swollen and unswollen specimens. Surface morphologies for both dry and swollen fatigued specimens are shown in Figure 5.13. In the dry samples there is a coarser failure surface at lower cycles than for failures at higher cycles. The morphology of the failure surfaces of the swollen EPDM samples differed from those of the dry test-pieces for all stress ranges.

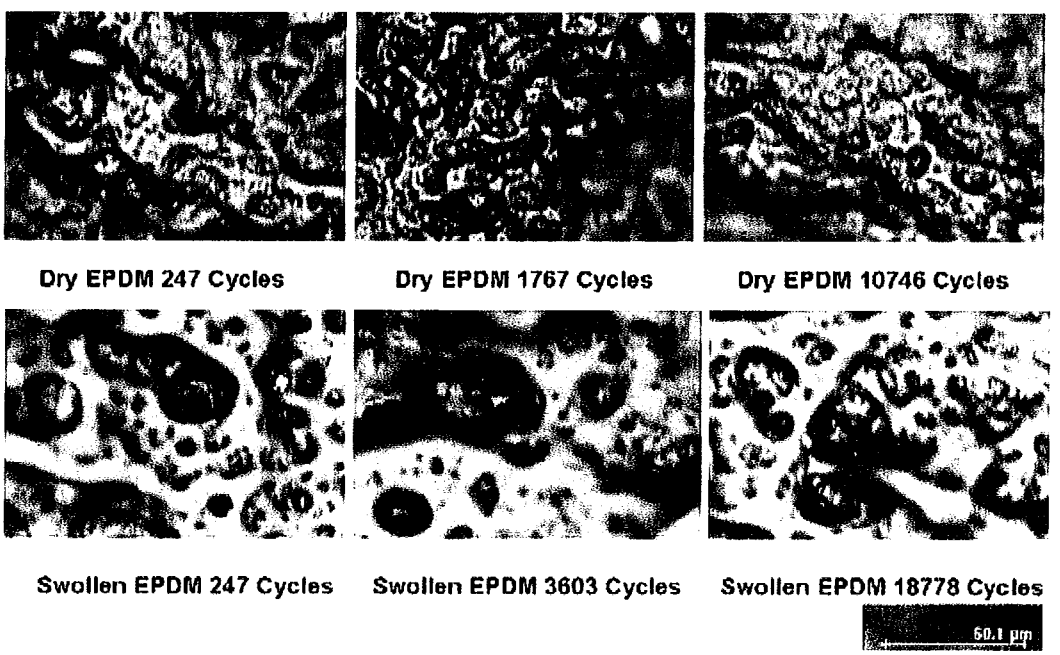

Figure 5.13 – Fracture surface of dry and swollen E9566 2mm EPDM specimens, magnification factor X200.

Scanning electron microscopy (SEM) was used to investigate the sample fractures at higher magnifications. All SEM images were taken at 2.0kV, using a Jeol JKA-8600 Superprobe. The images of the fracture surfaces for the three specimen sets are shown in Figure 5.14 at a magnification of X140, where all three samples were fatigued at a stress amplitude of σ_a = 1MPa.

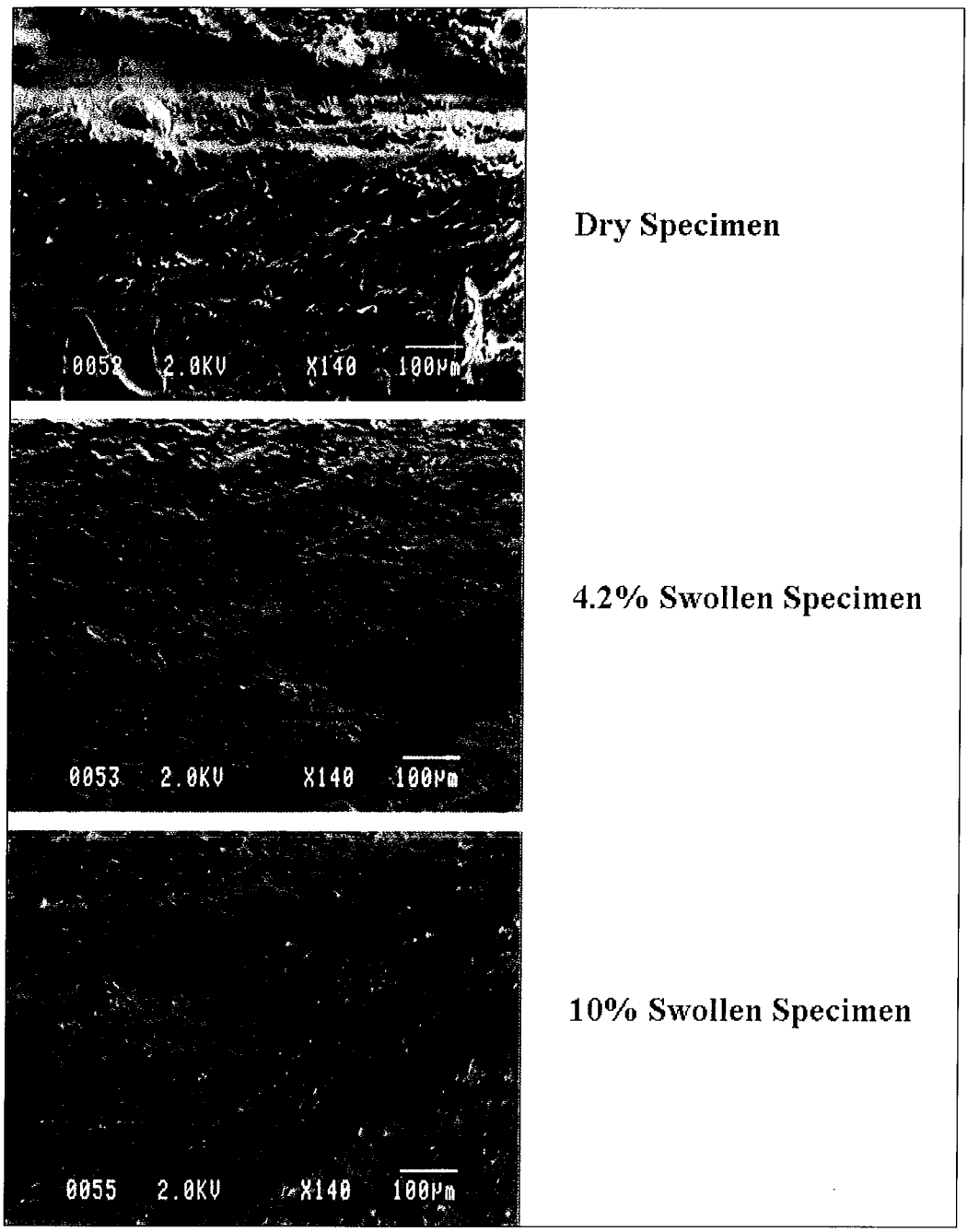

Figure 5.14 – SEM Imaging of fracture surface of dry, 4.2% and 10% swollen 2mm E9566 EPDM specimens, magnification factor X140.

Additional SEM images of the 10% swollen and dry specimen fractures are shown in Figure 5.15 at a magnification of X190 and in Figure 5.16 at a magnification of X400. These images were taken for samples which had similar fatigue lives.

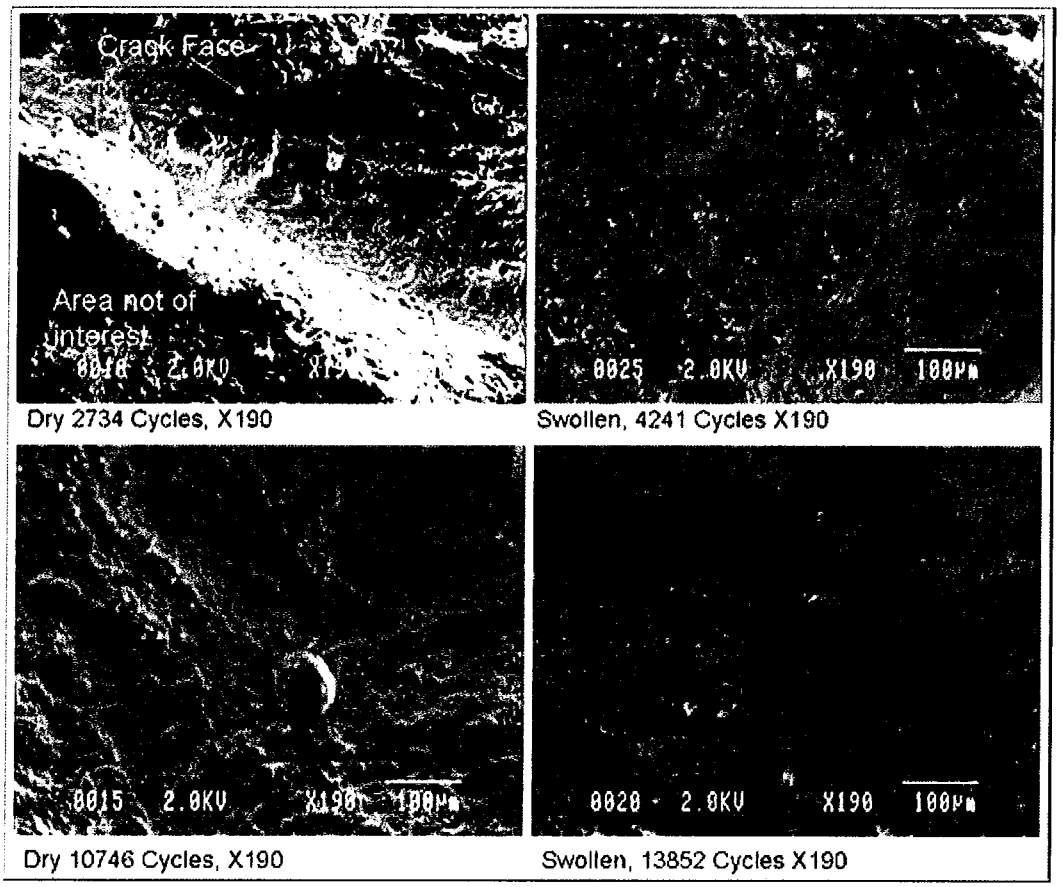

Figure 5.15 – SEM Imaging of fracture surface of dry and 10% swollen 2mm E9566 EPDM specimens, magnification factor X190.

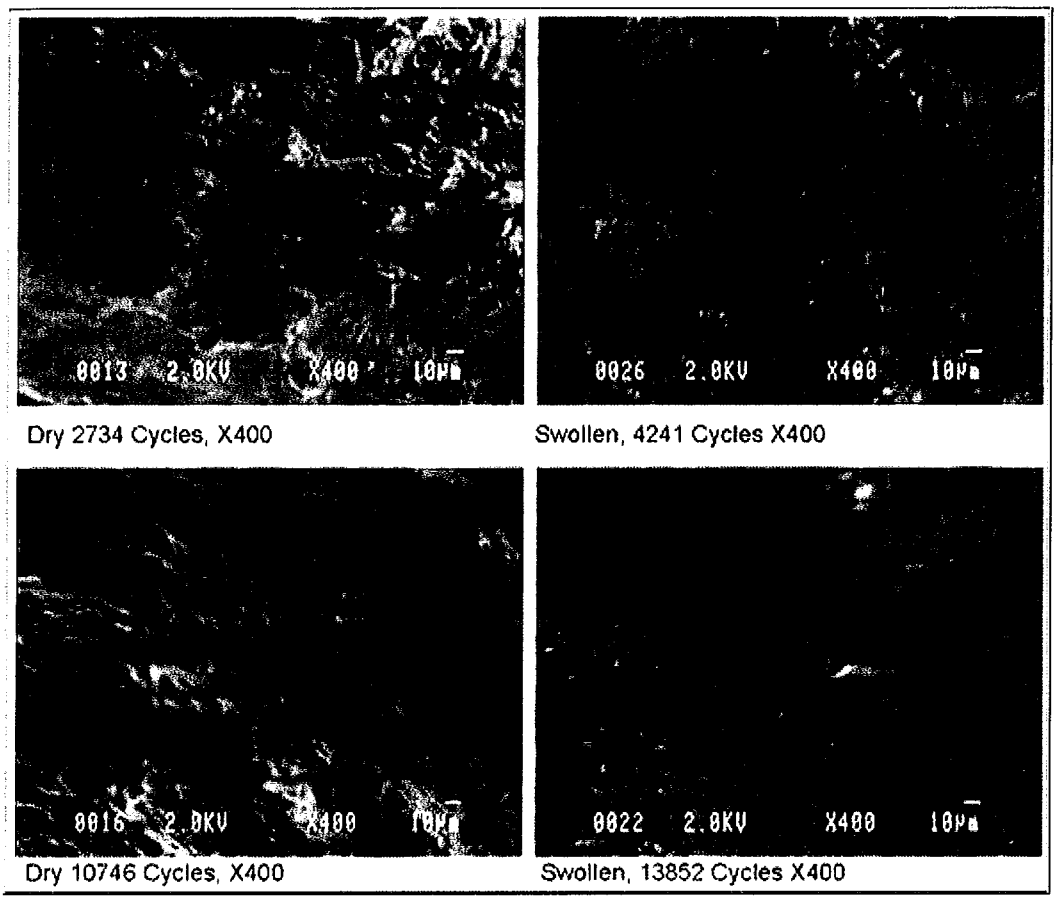

Figure 5.16 – SEM Imaging of fracture surface of dry and swollen 2mm E9566 EPDM specimens, magnification factor X400.

In all instances, evidence of blunter tearing was observed on the fracture surfaces of the dryer samples. This can be contrasted with the smoother fracture surfaces of the more swollen EPDM samples. This blunt tearing could be attributed to more polymer-filler interaction in the dry material, with the material being tougher for a given applied stress. The fractures in the swollen samples appear to show that the failure surfaces flowed more readily over each other than did those of the dryer specimens. These results correlate with those reported by Cho *et al* [62] in shear tests on specimens which were fatigued to failure with a pre-crack. Their study reported that the surface morphology of the dry samples indicated blunt tearing, while the morphology of the swollen test-pieces indicated sharp

tearing. It can also be seen that there is a greater instance of flaws in the swollen material, which can be attributed to the swelling effects of the oil breaking down filler-filler bonds. Due to the presence of these flaws the probability of crack growth being initiated at these flaws would be expected to be high, with these areas potentially less stiff than other points in the network.

Chapter 6 Conclusions

As stated in Chapter 1, there were a number of objectives for the research including:

1. To determine if a reduction in fatigue life due to swelling in the equi-biaxial case agreed with findings for uniaxial loading.
2. To develop a method of controlling engineering stress limits during fatigue testing of EPDM specimens.
3. To generate equi-biaxial Wöhler (S/N) curves for the specimens tested.
4. To determine what were the relationships between equi-biaxial fatigue cycles to failure and dynamic modulus and stored energy.
5. To confirm if any or each of the fatigue life predictors postulated by Abraham *et al* [3] of dynamic stored energy and limiting residual modulus were applicable when determining the service life of compounds subjected to constant pressure and constant stress amplitude in the swollen and unswollen states.

Firstly, it was found that the fatigue life results for the equi-biaxial case agreed with those for the uniaxial case; that is, the fatigue life of the specimens reduced in proportion to the amount of swelling induced in the test-pieces. These findings also allowed completion of the second objective of the research, the generation of S/N curves for three different specimen sets subjected respectively to no swelling, medium swelling and high swelling. One principal finding made when carrying out the fatigue tests in respect of comparison with load-controlled

uniaxial tests was the requirement for constant stress control when carrying out dynamic bubble inflation tests. Initially it was thought that constant pressure amplitudes would correlate reasonably well with maintaining constant engineering stress ranges throughout the fatigue test. However, from experiments this was found not to be so. Modifications to the test rig, where the volume of the bubble was measured and synchronised with the associated pressure and material strain, allowed the relationship between the volume of the bubble and the bubble radius to be determined. By reading the volume and pressure values simultaneously, they could be converted to a stress value and this value used as the control parameter. This meant continual reduction of the pressure set-point as the bubble volume (and by extension its radius) increased to maintain the value of the maximum stress in the cycle.

A relationship was found to exist between the dynamic stored energy and the cycles to failure for the dry E9566 EPDM. This confirms Abraham's suggestion of using it as a predictor for non-strain crystallising rubber when fatigued with a zero minimum load. The dynamic stored energy and cycles to failure relationship is altered by swelling the test-pieces, with the energy at failure reduced for increases in the degree of swelling. It may be possible to relate the swollen predictor curve to the dry predictor curve by some shift factors similar to those employed by Ronan *et al* [83][84] to determine long term stress relaxation in elastomers.

A more practical approach is to use the limiting value of the residual modulus. In the analysis conducted in Chapter 5, it was found that if the residual modulus for the swollen test-pieces was based on a calculation using the initial conditioned modulus of the dry rubber at a similar stress amplitude, good agreement was

found for the limiting value of $E^*_{residual}$, with a limiting value of 33% ±10% found to exist for both the dry and swollen specimens using this approach. The deviation of ±10% can probably be attributed to the quality of the testing material, with a commercial compound used for the testing, which would not have been subject to the same quality controls as the materials used by Abraham in his tests. By knowing this limiting value of $E^*_{residual}$, the effect of swelling on fatigue life can be calculated, if the value of $E^*_{conditioning}$ is known at a particular stress amplitude. E* for different states of swelling can also be calculated using models generated using the same approach adopted in Section 5.4.1.

This could have practical significance in the design of elastomeric components subjected to fatigue loading conditions. Consider a component manufactured from a similar compound to the E9566 EPDM used in these tests. If the part was loaded within a constant engineering stress range and the value of $E^*_{conditioning}$ at that stress range was known, it could be proposed that once the value of $E^*_{residual}$ fell below a material specific value of 43% after operating under normal working conditions, then replacement of the part would be recommended.

Significantly, the fatigue life of an EPDM sample under dynamic equi-biaxial loading can be greatly reduced in the presence of the oil in the rubber network, even for relatively small amounts of swelling. Despite being in contact with the oil for only one hour at 100°C, the dynamic properties such as the complex modulus E* and the dynamic stored energy are fundamentally altered for the swollen material tested when compared with the dry material. The changes in these properties and the lower fatigue lives of the swollen specimens can be attributed to a number of factors, both physical and chemical in nature.

Physical factors include the presence of larger voids in the network due to the swelling action which in turn leads to a lower initial complex modulus. The presence of these flaws in the elastomer network structure was confirmed by SEM imaging, which showed that the failure surfaces for each set of samples is markedly different in the dry and swollen cases.

Chemical factors which explain the difference in the dynamic mechanical properties of the unswollen specimens include changes in the network structure due to oil swelling, where there is a reduction in the number of crosslinks resisting the tensile force, while the reformation of polysulphidic linkages during a loading cycle can be inhibited in the presence of swelling fluid.

It has been shown that the dynamic bubble inflation method can provide repeatable stress-strain data for EPDM sample cycled between constant engineering stress limits. While this method is capable of providing more relevant dynamic equi-biaxial data than is currently achievable using stretch frames, bubble inflation was found to be subject to some minor limitations, namely:

i. The bubble volume/radius relationship must be determined for each material tested and it is essential that no inflation fluid escapes the system during testing, as this introduces an error into the engineering stress control method.
ii. The most reliable fatigue results were achieved when the sample assumed the hemispherical bubble shape in early cycles. In some cases (although they are very infrequent), the LVDT value can reduce during a test, due

to the calculated radius being higher at lower voltages. This was more prevalent in cases where the specimen had not been scragged before testing.

iii. For similar reasons to those outlined in the previous point, failures in the clamp region can occur at low stress amplitudes. If the bubble volume required to achieve the upper engineering stress is low, levels of flexing of the sample at the clamp edge may result in the higher stress occurring at the clamp edge instead of at the bubble pole due to a combination of the applied stress and the stress concentration.

These effects were most noticeable in the dry specimens tested. It would be expected that these effects would be less common in EPDM rubbers that have a lower Shore A hardness than 70.

The practical significance of this study is to highlight the effect of oil swelling on the mechanical performance of non-strain crystallising elastomers under realistic loading conditions. EPDM components are commonly used in automotive applications, where they have the advantage of having more functionality at higher temperatures than SBR or natural rubber. However, some of these advantages are offset by their poor resistance to the numerous fluids used in vehicles. The results presented here illustrate that if a risk of oil contamination is sufficiently high and the automotive design engineer has failed to recognise them by fully taking swelling into account, safety factors and life expectations may be unrealistically high and components will lack the residual mechanical strength to withstand levels of fatigue loading.

Chapter 7 Outlook

In addition to validating the results presented as part of this PhD thesis, the following studies are required to more fully characterise the behaviour of elastomers subjected to dynamic equi-biaxial loading.

1. Further testing and analysis of the equi-biaxial fatigue behaviour of EPDM should be continued to determine if a limiting value of E* can be used as a predictor of useful component life for cases where there is a non-zero minimum stress. These tests should use compounds manufactured under controlled conditions to ensure the minimum amount of scatter in the results, though setting limits for design purposes will require a determination of the variability in quality of the compound.
2. For the compound tested it should be investigated if it is prudent and feasible to set a life limiting value of $E^*_{residual}$ of say, 45% of that of the dry conditioned material. Furthermore, it should be determined if this limiting value is applicable to compounds manufactured with lower hardness values.
3. Tests should be carried out to determine if there is a correlation between different forms of the engineering stress control calibration curve and different sample thicknesses.
4. With regard to the compounds used in this study, the changes in material properties due to swelling in oil should be validated by dynamic uniaxial testing.

5. Tests should be carried out on EPDM compounds with a lower hardness than Shore A 70, for example, compounds with hardness of say, Shore A 55 and Shore A 35.
6. Failure modes and crack growth rate in bubble inflated samples should be analysed with respect to rate of crack growth for an applied stress. Verification should be obtained that cracks can occur randomly on either side of the specimen surface, or may be initiated from a flaw within the material.
7. Radial and circumferential strains should be compared for a number of loading cycles to determine if the area of the bubble considered to be in equi-biaxial tension increases or decreases.
8. Detailed stress softening tests should be carried out on test-pieces loaded equi-biaxially and dry specimen behaviour should be compared with that of swollen test-pieces.
9. Testing of other materials should also be investigated, including, but not limited to SBR, Natural Rubber and Biomaterials (Myocardium).
10. Testing of materials should be carried out at different temperature ranges.

At the time of writing, further developments in dynamic bubble inflation testing technology are underway in the Dublin Institute of Technology. DYNAMET, a dynamic equi-biaxial testing machine is being built as part of an Enterprise Ireland 'Proof of Concept' funding programme. This machine will bear a number of similarities to the machine used to carry out the tests presented in this research, but will also have a range of improvements including:

- High speed image acquisition for better synchronisation of pressure data with vision data and with improved camera calibration routines.
- The inclusion of Matrox software which will allow rapid conversion of image data into material strain information.
- A new hydraulic unit which will allow faster inflation rates, a facility for inflation of elastomers with aggressive fluids and the potential for testing of biomaterials.
- Improved clamping mechanisms which will allow different specimen diameters to be tested, as well as reducing the number of spurious test-piece failures due to clamping effects.

Glossary

Aliphatic. Organic compounds in which carbon atoms are joined together in straight or branched chains or in rings. Can be either saturated or unsaturated, but not aromatic.

Anisotropy. Having properties that are different in all directions in a material at a point.

Aniline Point. This is the lowest temperature at which equal volumes of aniline and hydrocarbon sample are completely miscible. Aniline Point determination is useful in characterising pure hydrocarbons. Aromatic hydrocarbons exhibit the lowest aniline points and paraffinic hydrocarbons exhibit the highest values. Cycloparaffins and olefins exhibit values that lie between those of paraffins and aromatics. In a homologous series, the aniline point increases with increasing molecular weight. The aniline point for mixtures of hydrocarbons, such as diesel oils and mineral oils serves as a guideline for determining the aromatic hydrocarbon content of an oil and for comparing oils.

Aromaticity. This is a chemical property of molecules. An example of an aromatic compound is benzene (C_6H_6), which has a structure consisting of six carbon atoms in the form of a ring, with each carbon atom linked by a double carbon bond, with a hydrogen atom linked to each carbon atom by a single bond.

Boltzmann's constant. The physical constant relating energy and temperature at the particle level1.38×10^{-23} J /K

Bulk modulus of elasticity. Ratio of stress to change in volume of a material subjected to axial loading. Related to modulus of elasticity (E) and Poisson's ratio (υ) by the following equation: $K=E\upsilon/3(1-2\upsilon)$.

Bursting strength. Measure of ability of materials in various forms to withstand hydrostatic pressure.

Carbon-black. An amorphous form of finely divided carbon

Cauchy stress. True stress (Force/deformed area)

Co-efficient of friction. Friction is a resistive force that prevents two objects from sliding freely against each other. The coefficient of friction (μ) is a number that is the ratio of the resistive force of friction (F_r) divided by the normal or perpendicular force (F_n) pushing the objects together.

CCD Camera. Charge-coupled device camera. In this text, a camera that is connected to a computer system to digitise information from the images produced

Conditioning. Taking a test-piece through a number of stress cycles to remove stress softening to a level where the material is considered to be at a consistent level of rigidity.

Coefficient of elasticity. Alternative term for modulus of elasticity.

Complex modulus. Measure of dynamic mechanical properties of material taking into account energy dissipated as heat during deformation and recovery. It is equal to the sum of static modulus of a material and its loss modulus. In the case of shear loading it is called dynamic modulus. See also damping capacity.

Convergence. Convergence occurs when an FEA program successfully computes an analysis.

Copolymer. A polymer that comprises chains made up of two or more chemically different repeating units

CPU. Central Processing Unit

Deformation energy. Energy required to deform a material by a specified amount. It is the area enclosed by the stress-strain diagram.

Drop weight test. Method for determining the nil-ductility transition temperature of steel. Results are reported as temperature above which specimens no longer show brittle fracture after specified shock loadings. (ASTM E-208).

Dynamic creep. Creep that occurs under fluctuating load or temperature.

Dynamic modulus. Complex modulus of material under dynamic shear loading. It is equal to the sum of static shear modulus and loss modulus. Dynamic modulus takes into account energy dissipated as heat when material is deformed.

Elastic hysteresis. Difference between strain energy required to generate a given stress in a material and elastic energy at that stress. It is the energy dissipated as heat in a material in one cycle of dynamic testing. Elastic hysteresis divided by elastic deformation energy is equal to damping capacity.

Elasticity. Ability of a material to return to its original shape when load causing deformation is removed.

Elongation. Measure of the ductility of a material determined in a tensile test. It is the increase in gauge length (measured after rupture) divided by original gauge length. Higher elongation indicates higher ductility. Elongation cannot be used to predict behaviour of materials subjected to sudden or repeated loading.

Endurance limit. Alternative term for fatigue limit.

Engineering stress. Load applied to a specimen in a tension or compression test divided by the unstrained cross sectional area of the specimen. The change in cross sectional area that occurs with increases and decreases in applied load is disregarded in computing engineering stress. It is also called conventional stress.

EPDM. Ethylene-Propylene Diene Monomer, a type of synthetic rubber.

Extensometer. Instrument for measuring changes in linear dimensions. Also called a strain gauge.

Fatigue. Permanent structural change that occurs in a material subjected to fluctuating stress and strain. However, in the case of glass, fatigue is determined by long-term static testing and is analogous to stress rupture in other materials. In general, fatigue failure will occur with stress levels below the elastic limit.

Fatigue life. Number of cycles of fluctuating stress and strain of a specified nature that a material will sustain before failure occurs. Fatigue life is a function of the magnitude of the fluctuating stress, geometry of the specimen and test conditions. An S-N diagram is a plot of the fatigue life at various levels of fluctuating stress.

Fatigue limit. Maximum fluctuating stress that a material can endure for an infinite number of cycles. It is usually determined from an S-N diagram and is equal to the stress at the asymptote of the locus of points corresponding to the fatigue life of a number of fatigue test specimens. An alternative term is endurance limit.

Fatigue notch factor. Ratio of fatigue strength of a specimen with no stress concentration to fatigue strength of a specimen with a notch or other stress raiser. Fatigue notch factor is usually lower than the theoretical stress concentration factor because of stress relief due to plastic deformation. An alternative term is strength reduction ratio.

Fatigue ratio. Ratio of fatigue strength or fatigue limit to tensile strength. For many materials fatigue ratio may be used to estimate fatigue properties from data obtained in tensile tests.

Fatigue strength. Magnitude of fluctuating stress required to cause failure in a fatigue test specimen after a specified number of cycles of loading. Usually determined directly from an S-N diagram.

Fatigue strength reduction factor. An alternative term for fatigue notch factor.

Fracture stress. True stress generated in a material at fracture.

Fracture test. Visual test wherein a specimen is fractured and examined for grain size, case depth, etc.

Gaussian error function. Error function complying with the bell shaped probability curve developed by K.F. Gauss.

Gibbs free energy. The thermodynamic potential of an isothermal, isobaric thermodynamic system.

Hardness. Measure of a materials resistance to localised plastic deformation. Most hardness tests involve indentation, but hardness may be reported as resistance to scratching (file test), or rebound of a projectile bounced off the material.

Helmholtz free energy. The useful work of a closed thermodynamic system at a constant temperature

Hookean. Conforming to Hooke's Law that relates stress to strain linearly.

Hooke's law. Stress is directly proportional to strain. Hooke's law assumes perfectly elastic behaviour. It does not take into account plastic or dynamic loss properties.

Hoop stress. Circumferential stress in a cylinder subjected to internal hydrostatic pressure. For thin walled cylinders it can be calculated by Barlow's formula: $S = PD/2t$ where S is hoop stress; P, applied pressure; D, cylinder outside diameter;

and t, wall thickness. Barlow's formula cannot be used for thick-wall cylinders where stress variation across wall thickness must be considered.

Indentation hardness. Resistance of material to surface penetration by an indentor. See hardness.

International rubber hardness degrees (IRHD). Measure of indentation hardness of rubber. For substantially elastic isotropic rubbers IRHD is related to Young's modulus by the equation: F/M = 0.00017 R0.65 Pl.35 where F is indenting force in kg; M, Young's modulus in kg/sq cm; R, radius of indentor in cm, and P, penetration in hundredths of mm. IRHD of a rubber is approximately equal to durometer hardness determined on the Shore hardness scales. A standard test method for determining IRHD is given in ASTM D-1415.

Invariant. Non-varying quantity irrespective of the Cartesian axis system chosen.

Isochoric. Volume retaining, incompressible.

Isotropic. Having properties that are the same in all directions in a material at a point. Most metallic alloys and thermoset polymers are considered isotropic, where by definition the material properties are independent of direction. Such materials have only 2 independent variables (i.e. elastic constants) in their stiffness and compliance matrices.

Limit of Proportionality. Highest stress at which stress is directly proportional to strain. It is the highest stress at which the curve in a stress-strain diagram is a straight line and is equal to elastic limit for many metals.

Load-deflection diagram. Plot of load vs. corresponding deflection.

Loss factor. Ratio of the real and imaginary components of complex modulus. The term is used in connection with dynamic tests to determine damping capacity of materials and combinations of materials. An alternative term is loss tangent.

Loss modulus. Imaginary component of complex modulus. It takes into account mechanical energy dissipated as heat during deformation of a material under dynamic loading.

Loss tangent. An alternative term for loss factor.

Mean stress. Algebraic difference between maximum and minimum stress in one cycle of fluctuating loading as in a fatigue test. Tensile stress is considered positive and compressive stress negative.

Mechanical hysteresis. Alternative term for elastic hysteresis.

Modulus of elasticity. Rate of change of strain as a function of stress. The slope of the straight line portion of a stress-strain diagram. The tangent modulus of elasticity is the slope of the stress-strain diagram at any point. The secant modulus of elasticity is stress divided by strain at any given value of stress or strain. It also is called stress strain ratio. Tangent and secant modulus of elasticity are equal up to the proportionality limit of a material.

Modulus used alone generally refers to tensile modulus of elasticity. Shear modulus can be determined by plane or torsional shear testing and in both cases the term modulus of rigidity is used.

Moduli of elasticity at a point is given by direct stress divided by direct strain. For linear materials in tension and compression values are approximately equal. It is also termed Young's modulus. Modulus of rigidity is related to Young's modulus by the equation: $E = 2G (1 + \upsilon)$ where E is Young's modulus, G is

modulus of rigidity and υ is Poisson's ratio. Modulus of elasticity also is called elastic modulus and coefficient of elasticity.

Modulus of rigidity. Rate of change of strain as a function of stress in a specimen subjected to shear or torsional loading. It is the elastic modulus determined from a torsion test. Alternative terms are modulus of elasticity in torsion and modulus of elasticity in shear.

Modulus of rupture. Ultimate strength determined in a flexure or torsion test. In a flexure test, modulus of rupture in bending is the maximum fibre stress at failure. In a torsion test, modulus of rupture in torsion is the maximum shear stress in the extreme fibre of a circular member at failure. Alternative terms are flexural strength and torsional strength.

Monomer or (mer). The single unit that with others joined chemically end to end makes up a polymer chain.

Necking. Localised reduction of cross section area of a specimen under tensile load. It is disregarded in calculating engineering stress but considered in determining true stress.

Nominal stress. Stress calculated on the basis of the net cross section of a specimen without taking into account the effect of geometric discontinuities such as holes, grooves, fillets, etc.

Notch sensitivity. Measure of reduction in load-carrying ability caused by stress concentration in a specimen.

Offset yield strength. Arbitrary approximation of elastic limit. It is the stress that corresponds to the point of intersection of a stress-strain curve and a line parallel to the straight line portion in the diagram. Offset refers to the distance between the origin of the stress-strain diagram and the point of intersection of the

parallel line and the zero stress axis. Offset is expressed in terms of strain (often 0.2%).

Operating stress. Stress imposed on a part in service.

Overstressing. In the context of this research, the application of high fluctuating loads at the beginning of a fatigue test and lower loads toward the end. It is a means for speeding up a fatigue test.

Penetration. Depth to which the striker of a rebound pendulum penetrates a rubber specimen. It is an index of the dynamic stiffness or complex modulus of rubber specimens.

Permanent set. Extent to which a material is permanently deformed by a specified load. Usually expressed as % and calculated by dividing the difference in dimensions in the direction of loading prior to loading and after the load is removed by the original dimension and multiplying by 100.

Plane strain. Having zero strain in one direction (usually the 'z' direction).

Plastic deformation. Deformation that remains after the load causing it is removed. It is the permanent part of the deformation beyond the elastic limit of a material. It is also called plastic strain and plastic flow.

Plasticity. Tendency of a material to remain deformed after reduction of the deforming stress to a value equal to or less than its yield strength.

Plastometer test. Method for determining ability of rubber to be compressed at an elevated temperature and to recover at room temperature. Results are reported as plasticity number and recovery. Test differs from compressibility and recovery test in that the latter measures behaviour of material subjected to short-time loading at room temperature.

Poisson's ratio. Ratio of lateral strain to axial strain in axial loaded specimen. It is the constant that relates modulus of rigidity to Young's modules in the equation: $E = 2G (\upsilon + 1)$ where E is Young's modulus; G, modulus or rigidity and υ, Poisson's ratio. The formula is valid only within the elastic limit of a material.

Proof stress. Stress that will cause a specified permanent deformation.

Rate of strain hardening. Rate of change of true stress as a function of true strain in a material undergoing plastic deformation. An alternative term is modulus of strain hardening.

Recovery. Index of a material's ability to recover from deformation in the compressibility and recovery test (ASTM F-36), the deformation under load test (ASTM D-621) and the plastometer test (ASTM D-926). In the compressibility and recovery test it is usually reported with compressibility and given as %. It is calculated by dividing the difference between recovered thickness and thickness under load by the difference between original thickness and thickness under load. In the deformation under load test it indicates the extent to which a non-rigid plastic recovers from prolonged compressive deformation at elevated temperature. It is given as % and is calculated by dividing the difference between height recovered 1½ hours after load is removed and height after 3 hours of loading by the change in height under load. In the plastometer test it indicates the extent to which an elastomer recovers from compressive loading at elevated temperature. It is equal to plasticity number minus recovered height. See also Rockwell recovery.

Reduction of area. Measure of the ductility of metals obtained in a tensile test. It is the difference between original cross section area of a specimen and the area of

its smallest cross section after testing. It is usually expressed as % decrease in original cross section. The smallest cross section can be measured at or after fracture. For metals it usually is measured after fracture and for plastics and elastomers it is measured at fracture.

Relaxation. Rate of reduction of stress in a material due to creep. An alternative term is stress relaxation.

Rupture resistance. Indication of the ability of rubber to withstand tensile loading. It is the load required to rupture a rubber specimen under conditions set out in ASTM D-530.

Rupture strength. Nominal stress developed in a material at rupture. It is not necessarily equal to ultimate strength and since necking is not taken into account in determining rupture strength, it seldom indicates true stress at rupture.

S-N diagram. Plot of stress (S) against the number of cycles (N) required to cause failure of similar specimens in a fatigue test. Data for each curve on an S-N diagram are obtained by determining fatigue life of a number of specimens subjected to various amounts of fluctuating stress. The stress axis can represent stress amplitude, maximum stress or minimum stress. A log scale is almost always used for the N scale and sometimes for the S scale. An alternative term is Wöhler curve.

Secant modulus of elasticity. Ratio of stress to strain at any point on a curve in a stress-strain diagram. It is the slope of a line from the origin to any point on stress-strain curve.

Shear modulus of elasticity. Tangent or secant modulus of elasticity of a material subjected to shear loading. Alternative terms are modulus of rigidity and

modulus of elasticity in shear. Also, shear modulus of elasticity is usually equal to torsional modulus of elasticity.

Shear strength. Maximum shear stress that can be sustained by a material before rupture. It is the ultimate strength of a material subjected to shear loading. It can be determined in a torsion test where it is equal to torsional strength. The shear strength of a plastic is the maximum load required to shear a specimen in such a manner that the resulting pieces are completely clear of each other.

Recovery. Degree to which a material returns to its original shape after deformation.

Scragging. See conditioning

Stretch ratio. The ratio of deformed to original length (i.e. $1+\varepsilon$)

Stiffness. Measure of resistance of plastics to bending. It includes both plastic and elastic behaviour, so it is an apparent value of elastic modulus rather than a true value.

Strain. Change per unit length in a linear dimension of a part or specimen, usually expressed in %. Strain as used with most mechanical tests is based on original length of the specimen. Shear strain is the change in angle between two lines originally at right angles.

Strain crystallising. The property of forming crystals with an associated change in size.

Strain energy. Measure of energy absorption characteristics of a material under load up to fracture. It is equal to the area under the stress-strain diagram, and is a measure of the toughness of a material.

Strain rate. Time rate of elongation.

Strain relaxation. Alternative term for creep of rubber.

Strength reduction ratio. Alternative term for fatigue notch factor.

Stress. Load on a specimen divided by the area through which it acts. As used with most mechanical tests, stress is based on original cross section area without taking into account changes in area due to applied load. This sometimes is called conventional or engineering stress. True stress is equal to the load divided by the instantaneous cross sectional area through which it acts.

Stress amplitude. One-half the range of fluctuating stress developed in a specimen in a fatigue test. Stress amplitude is often used to construct an S-N diagram.

Stress concentration factor. Ratio of the greatest stress in the area of a notch or other stress raiser to the corresponding nominal stress. It is a theoretical indication of the effect of stress concentrations on mechanical behaviour. Stress concentration factor usually is higher than the empirical fatigue notch factor or strength reduction ratio because it does not take into account stress relief due to local plastic deformation.

Stress ratio. Ratio of minimum stress to maximum stress in one cycle of loading in a fatigue test. Tensile stresses are considered positive and compressive stresses negative.

Stress relaxation. Decrease in stress in a material subjected to prolonged constant strain at a constant temperature. Stress relaxation behaviour is determined in a creep test. Data often is presented in the form of a stress vs. time plot. Stress relaxation rate is the slope of the curve at any point.

Stress-strain diagram. Graph of stress as a function of strain. It can be constructed from data obtained in any mechanical test where a load is applied to

a material and continuous measurements of stress and strain are made simultaneously. It is constructed for compression, tension and torsion tests.

Stress-strain ratio. Stress divided by strain at any load or deflection. Below the elastic limit of a material it is equal to tangent modulus of elasticity. An alternative term is secant modulus of elasticity.

Stripping strength is an alternative term for peel strength.

T. Absolute temperature in degrees Kelvin.

Tangent modulus of elasticity. Instantaneous rate of change of stress as a function of strain. It is the slope at any point on a stress-strain diagram.

Tensile strength. Ultimate strength of a material subjected to tensile loading. It is the maximum stress developed in a material in a tensile test.

Tensile test. Method for determining behaviour of materials under axial stretch loading. Data from test are used to determine elastic limit, elongation, modulus of elasticity, proportional limit, reduction in area, tensile strength, yield point, yield strength and other tensile properties. Tensile tests at elevated temperatures provide creep data.

Time for rupture. Time required to rupture specimen under constant stress and temperature in a creep test.

Torsional modulus of elasticity. Modulus of elasticity of material subjected to twist loading. It is approximately equal to shear modulus and is also called modulus of rigidity.

Torsional strain. Strain corresponding to a specified torque in the torsion test. It is equal to torsional deformation multiplied by the radius of the specimen.

Torsional strength. Measure of the ability of a material to withstand a twisting load. It is the ultimate strength of a material subjected to torsional loading and is

the maximum torsional stress that a material sustains before rupture. Alternative terms are modulus of rupture and shear strength.

Torsional stress (τ). Shear stress developed in a material subjected to a specified torque in a torsion test. It is calculated by the equation: $\tau = Tr/J$ where T is torque, r is the distance from the axis of twist to the outermost fibre of the specimen and J is the polar moment of inertia.

Torsional Yield strength. Yield strength of material under twist loading.

True strain. In terms of linear (engineering) strain, as long as $\delta l_1 << \delta l_0$ it is possible to write the strain in terms of engineering strain. In cases where a body is deformed twice (cumulative deformation), and $\delta l_1 >> \delta l_0$, the final strain ε_f will be slightly different than the sum of the two strains ε_1 and ε_2. In this case, true strain can be used to express the amount of deformation, where $\varepsilon_T = \ln(l_f/l_0)$.

True stress. Applied load divided by actual area of the cross section through which load operates. It takes into account the change in cross section that occurs with changing load.

Ultimate elongation. Alternative term for elongation of material at rupture under tensile loading.

Ultimate strength. Highest engineering stress developed in material before rupture. Normally, changes in area due to changing load and necking are disregarded in determining ultimate strength.

Van der Waal's forces. Relatively weak forces between atoms that are not the result of chemical bond formation that hold non-polar molecules together.

Volatility. A measure of the tendency of a liquid (or solid) to evaporate into a gaseous form. Higher volatility indicates a higher tendency to evaporate and a lower volatility infers a lesser tendency to evaporate.

Vulcanisation. The process of forming crosslinks between long chain molecules by chemical reaction, achieved by heating rubber in the presence of sulphur and/or other reagents.

Wöhler Curve is an alternative term for an S-N curve.

Yield point. Stress at which strain increases without accompanying increase in stress. Only a few materials (notably ferrous metals) have a yield point and generally only under tensile loading.

Yield point elongation. Strain at yield point of a material. It is an indication of ductility.

Yield strength. Indication of maximum stress that can be developed in a material without causing plastic deformation. It is the stress at which a material exhibits a specified permanent deformation and is a practical approximation of elastic limit.

Offset yield strength is determined from a stress-strain diagram. It is the stress corresponding to the intersection of the stress-strain curve and a line parallel to its straight line portion offset by a specified strain. Offset is usually specified as 0.2 %, i.e., the intersection of the offset line and the zero-stress axis is at 0.2 % strain.

Yield strength elongation. Extension corresponding to the yield strength of the material. It is an indication of ductility.

Yield value. Stress in an adhesive joint at which a marked increase in deformation occurs without an increase in load.

Young's modulus. Alternative term for modulus of elasticity in tension or compression.

References

1. http://www.jsae.or.jp/e07pub/jaso_e.html, (2007)
2. Datamonitor - Global Tires and Rubber, Industry Profile, Ref 0199-2148, March 2007.
3. Abraham, F, Alshuth, T, Jerrams, S., "Parameter Dependence and Prediction of Fatigue Properties of Elastomer Products". Rubber Chemistry and Technology Journal, Volume 75, Issue 4, p 365, September/October (2002).
4. Abraham, F., Alshuth, T, Jerrams, S., "Dependence on Mean Stress and Stress Amplitude of Fatigue life of EPDM Elastomers". The Journal of Plastics, Rubber and Composites, Institute of Materials, Vol 30 No. 9 pp 421-425, (ISSN 1465-8011) (2001).
5. Abraham, F. Alshuth, T, Jerrams, S., "Ermüdungsbeständigkeit von Elastomeren – Einfluss der Spannungsamplitude und der Unterspannung Teil 2". KGK Kautschuk Gummi Kunststoffe, pp 674-678 (2002).
6. Muhr, A.H., Thomas, A.G., "Determination of crack growth characteristics using the angled testpiece", Rubber Chemistry and Technology Journal, Vol 62, p 219-233, (1989).
7. Johannknecht, R, Jerrams, S. Clauss, G., "Determination of non-linear, large equal biaxial stresses and strains in thin elastomeric sheets by bubble inflation". Proceedings of the Institute of Mechanical Engineers, Vol 216 Part L, No L4, (ISSN 1464-4207) Journal of Materials, Design and Applications (2002).
8. Flory, P. J., Rehner, J., "Statistical Mechanics of Cross-Linked Polymer Networks II. Swelling", J. Chem. Phys. 11, 521 (1943).

9. Treloar, L.R.G., "The Physics of Rubber Elasticity", Clarendon Press, Oxford University Press, London (1975).
10. Gee, "Interaction between rubber and liquids IX. The elastic behaviour of dry and swollen rubbers", Rubber Chemistry and Technology, Volume 20, p.442-456, (1947).
11. Krigbaum, W.R., and Roe, R.J., "The Contribution of Internal Energy to the Elastic Force of Natural Rubber", Rubber Chemistry and Technology, Volume 38, p.351-364, (1963).
12. Treloar, L.R.G., "Volume changes and mechanical anisotropy of strained rubbers", Polymer, Volume 10, p.279-289, (1969).
13. Flory, P.J., "Thermodynamic relations for high elastic materials", Trans. Faraday Soc. 57, 829 (1961).
14. Smith, T.L., "Molecular Aspects of Rubber Elasticity", Treatise on Materials Science and Technology Volume 10 Part A: Properties of Solid Polymeric Materials", Schultz, J.M. (Editor), Academic Press.
15. Gee, G., Treloar, L.R.G., "Interaction between rubber and liquids I. Thermodynamical study of the system rubber-benzene", Rubber Chemistry and Technology, Volume 16, p89-110. (1943).
16. Scott, J.R. "The Swelling of Vulcanised Rubber in Liquids", Rubber Chemistry and Technology, Volume 3, p.3-18, (1930).
17. Hayden, O.M., "The Testing of Rubber and Rubber-like Materials for Oil-Resistance", Rubber Chemistry and Technology, Volume 7, p.657-662, (1934).
18. Whitby, Evans and Pasternack, Trans. Faraday Soc. 38, 269 (1942).

19. Gee, "Interaction between rubber and liquids II. The thermodynamical basis of the swelling and solution of rubber", Rubber Chemistry and Technology, Volume 15, p545-552 (1942).
20. Gee, "Interaction between rubber and liquids III. The swelling of vulcanised rubber in various liquids", Rubber Chemistry and Technology, Volume 16, p263-267 (1943).
21. Gee, "Interaction between rubber and liquids IV. Factors governing the absorption of oil by rubber", Rubber Chemistry and Technology, Volume 16, p818-833 (1943).
22. Gee, "Interaction between rubber and liquids V. The osmotic pressures of polymer solutions in mixed solvents", Rubber Chemistry and Technology, Volume 18, p236-241 (1945).
23. Gee, "Interaction between rubber and liquids VI. Swelling and solubility in mixed liquids", Rubber Chemistry and Technology, Volume 18, p241-255 (1945).
24. Beerbower, A., Pattison, D.A., Staffin, G.D., "Predicting Elastomer-Fluid Compatibility for Hydraulic Systems", Rubber Chemistry and Technology, Volume 37, p.246-260, (1964).
25. Abhimanyu, P., Coolbaugh, T., "Elastomers: A Literature Review with Emphasis on Oil Resistance", Rubber Chemistry and Technology, Volume 78, p.516-535, (2005).
26. Tiltman, H.A., Porritt, B.D., "The effect of solvents on the stress-strain curve of vulcanised rubber", India Rubber Journal, Vol.78, p345-346 (1929).

27. Tanaka, Y., Kambara, S., Noto, J., "The Oil Resistance of Rubber I. Study of the Swelling of Vulcanised Rubber", Rubber Chemistry and Technology, Volume 9, 70-73, (1936).
28. Parris, R.W., Scott, J.R., "Properties of Hard Rubber, IX. Swelling in various liquids (Part XIII of Swelling of Rubber)", Rubber Chemistry and Technology, Vol 15, p.280-300, (1942).
29. Dogadkin, B.A., Gul, V., "The Role of Intermolecular Forces in the Mechanism of High Elastic Deformation III. Effect of Swelling on the Mechanical Properties of Vulcanised Rubber", Rubber Chemistry and Technology, Volume 24, P.344-353, (1951).
30. Gee, "Interaction between rubber and liquids IX. The elastic behaviour of dry and swollen rubbers", Rubber Chemistry and Technology, Volume 20, p.442-456, (1947).
31. Flory, P., Rabjohn, N., Shaffer, M., "Dependence of Elastic Properties of Vulcanised Rubber on the Degree of Cross-Linking", Rubber Chemistry and Technology, Volume 23, p.9-26, (1950).
32. Zapp, R.L., Guth, E., "Elastic Modulus and Swelling of Butyl Vulcanizates", Rubber Chemistry and Technology, Vol 24, P.894-913 (1951).
33. Treloar, L.R.G., "The Swelling of Cross-Linked Amorphous Polymers under Strain", Rubber Chemistry and Technology, Vol 24, P.290-298, (1951).
34. Mullins, L., "Determination of Degree of Crosslinking in Natural Rubber Vulcanizates. Part I", Rubber Chemistry and Technology, Vol 30, P.1-10, (1957).

35. Queslel, J.P., Mark, J.E., "Theoretical Equilibrium Moduli and Swelling Extents for Elastomers Crosslinked in Solution", Rubber Chemistry and Technology, Vol 63, P.46-55, (1990).

36. Dillon, J.H., Prettyman, J.B., Hall, G.L., "Hysteretic and Elastic Properties of Rubberlike Materials under Dynamic Shear Stresses", Journal of Applied Physics, Volume 15, P.309-323 (1944).

37. Gui, K.E., Wilkinson, C.S., Gehman, S.D., "Vibration Characteristics of Tread Stocks", Industrial & Engineering Chemistry, Volume 44, P.720-723, (1952).

38. Fletcher, W.P., Gent, A.N., "Nonlinearity In The Dynamic Properties Of Vulcanized Rubber Compounds", Transactions of The Institution of the Rubber Industry, Volume 29, P.266-280, (1953).

39. Payne, A.R., "The Dynamic Properties Of Carbon Black Loaded Natural Rubber Vulcanizates. Part I", Rubber Chemistry and Technology, Volume 36, p.432-443, (1963).

40. Payne, A.R., "The Dynamic Properties Of Carbon Black Loaded Natural Rubber Vulcanizates. Part II", Rubber Chemistry and Technology, Volume 36, p.444-450, (1963).

41. Neogi, C, Bhattacharya, A.K., Bhowmick, A.K., "Dynamic Mechanical Analysis of Carbon-Black-Filled Rubber Vulcanizates under Swollen Conditions", Rubber Chemistry and Technology, Volume 63, p651-659 (1990).

42. Busfield, J.J.C., Deeprasertkul, C., Thomas, A.G., "The effect of liquids on the dynamic properties of carbon black filled natural rubber as a function of pre-strain", Polymer 41, p9219-9225 (2000).

43. Gul, V, Dorokhina, T.V., Dogadkin, B.A., "Changes of Fatigue Resistance of Vulcanised Natural Rubbers during Swelling", Rubber Chemistry and Technology, Volume 26, p70-77 (1953).
44. Wöhler A., Journal: Bauwesen, 20 (1870) 73-106.
45. Warnock, F.V., Benham, P.P., "Mechanics of Solids and Strength of Materials", pp 485-491, First Edition, Pitman Paperbacks, ISBN: 273 40371 0 (1967).
46. Mars, W. V., Fatemi, A., "Factors That Affect the Fatigue Life of Rubber: A Literature Survey", Rubber Chemistry and Technology, Vol 77, p391-412 (2004).
47. Griffith, A.A., "The phenomena of rupture and flow in solids", Proc. Roy. Soc., A, 221 (1920).
48. Hearn, E.J., "Mechanics of Materials: An Introduction to the Mechanics of Elastic and Plastic Deformation of Solids and Structural Materials: V. 1", Third Edition, Butterworth-Heinemann Ltd, ISBN-13: 978-0750632652 (2004).
49. Seldén, R., "Fracture Mechanics Analysis of Fatigue Of Rubber-A Review", Progress In Rubber And Plastics Technology, Vol.11, No.1, The Institute of Materials/RAPRA, (1995).
50. Thomas, A.G., "The Development of Fracture Mechanics for Elastomers", Rubber Chemistry and Technology, Volume 67, P.G50, (1994).
51. Rivlin, R.S., Thomas, A.G., J. Polym. Sci. 10, 291 (1953).
52. Lake, G., "Fatigue and Fracture of Elastomers", Rubber Chemistry and Technology, Volume 68, P.435-460, (1995).

53. Lindley, P. B., "Relation between hysteresis and the dynamic crack growth resistance of natural rubber", International Journal of Fracture, Volume 9, Number 4, P.449-462, (1973).

54. Lindley, P., "Non-Relaxing Crack Growth and Fatigue in A Non-Crystallising Rubber", Rubber Chemistry and Technology, Volume 47, P.1253-1264, (1974).

55. Verron, E., Andriyana., "Definition of a New Predictor for Multiaxial Crack Nucleation in Rubber". Journal of the Mechanics and Physics of Solids (2007), doi:10.1016/j.jmps.2007.05.019.

56. Hainsworth, S.V., "An Environmental Scanning Electron Microscopy Investigation of Fatigue Crack Initiation and Propagation in Elastomers", Polymer Testing, Volume 26, P.60-70, (2007).

57. Harbour, R.J., Fatemi, A., Mars, W.V., "Fatigue Life Analysis and Predictions for NR and SBR under Variable Amplitude and Multiaxial Loading Conditions", International Journal of Fatigue (2007), doi10.1016/j.ijfatigue.2007.08.015.

58. Mars, W.V., Fatemi, A., "Multiaxial Stress Effects on Fatigue Behaviour of Filled Natural Rubber", International Journal of Fatigue, Volume 28, P.521-529, (2006).

59. Gul, V., Fedyukin, D., Dogadkin, B.A., "Investigation of the Role of Intermolecular Forces in the Mechanism of High-Elastic Deformation. VII. The Effect of Molecular Interaction on The Fatigue Resistance of High Polymers Having Highly Developed Spatial Structures", Rubber Chemistry and Technology, Vol 27, p363-373 (1954).

60. Gul, V., Fedyukin, D., Dogadkin, B.A., "The Influence of Intermolecular Action on the Dynamic Fatigue of Rubbers", Rubber Chemistry and Technology, Vol 32, p.454-462 (1959).

61. Williams, I., "The Effect of Softeners in Rubber", Rubber Chemistry and Technology", Volume 26, P.152-155, (1953).

62. Cho, K., Wook, J.J., Daeho, L., Hyunaee, C., Young-Wook, C., "Fatigue crack growth of elastomers in the swollen state", Polymer 41, p179-183 (2000).

63. Charlton, D.J, Yang, J., "A review of methods to Characterise Rubber Elastic Behaviour for the use in Finite Element Analysis", Rubber Chemistry and Technology, 67, pp. 481-503, (1994).

64. Johannknecht, R. The Physical Testing and Modelling of Hyperelastic Materials for Finite Element Analysis, PhD Dissertation, Coventry University, (1999).

65. Flint, C., Naunton, W. J. S., "Physical Testing of Latex Films", Transactions of The Institution of the Rubber Industry, Volume 12, P.367-406, (1937).

66. Treloar, L.R.G, "Strains in an Inflated Rubber Sheet, and the Mechanism of Bursting", Rubber Chemistry and Technology, Volume 17, p957-967 (1944).

67. Bhate, P, Kardos, J., "A Novel Technique for the Determination of High Frequency Equi-biaxial Stress-Deformation Behaviour of Viscoelastic Elastomers", Polymer Engineering and Science, Vol. 24, No. 11 (1984).

68. Dickie, R, Smith, T., "Ultimate Tensile Properties of Elastomers. VI. Strength and Extensibility of a Styrene-Butadiene Rubber Vulcanizate in

Equal Biaxial Tension", Journal of Polymer Science, Vol. 7, Part A-2, 687-707, (1969).

69. Kong, D., White, J.L., "Inflation Characteristics of Unvulcanised Gum and Compounded Rubber Sheets", Rubber Chemistry and Technology, Volume 59, p.315-327, (1986).
70. Song, W, Mirza, F, Vlachopoulos, J., "Finite element analysis of inflation of an axisymmetric sheet of finite thickness", The Society of Rheology, Inc., (1991).
71. Khayat, R, Derdouri, A., "Stretch and Inflation of Hyperelastic Membrane as Applied to Blow Molding", Polymer Engineering and Science, Vol. 35, No. 23, (1995).
72. Adkins, J, Rivlin, R. 1952. "Large elastic deformations of isotropic materials. XI The deformation of thin shells", F.R.S., Vol. 244, A. 888.
73. Mott, P., Roland, C. M., Hassan, S., "Strains in an Inflated Rubber Sheet", Rubber Chemistry and Technology, Volume 76, p.326-333, (2003).
74. Powers, P., Billmeyer, B., "Swelling of Synthetic Rubbers in Mineral Oils Effect of Temperature and Aniline Point", Rubber Chemistry and Technology, Volume 18, p.452-459, (1945).
75. ASTM Standard D471-95, "Standard Test Method for Rubber Property-Effect of Liquids", Annu. Book ASTM Stand. 08.01, 86 (1995).
76. Murphy, N., Hanley, J., McCartin, J., Lanigan, B., McLoughlin, S.D., Jerrams, S., Clauss, G., Johannknecht, R., "Determining multiaxial fatigue in elastomers using bubble inflation", proceedings of the 4th European Conference on Constitutive Models for Rubber, Stockholm,

June 2005 and a chapter in the book 'Constitutive models for rubber IV' edited by P.-E. Austrell and L. Kari, pp 65-70, (Published by A. A. Balkema, ISBN 0415383463), (2005).

77. McCartin, J., Murphy, N., Hanley, J., Jerrams, S., Lanigan, B., "Determining levels of stress softening in multi-axial deformation", Poster for German Institute of Rubber Technology (DIK) 7th Fall Rubber Colloquium (KHK 2006), Hannover, November 2006 and subsequently published in KGK Kautschuk Gummi Kunststoffe 2007.
78. Hanley, J., Murphy, N., Ali, H., Jerrams, S., "The effect of swelling on the properties of elastomers subjected to multiaxial fatigue using bubble inflation", Proceedings of the 6th International Conference on Materials-Energy-Design (MED06), Dublin, March 2006.
79. Hanley, J., Murphy, N., Ali, H., Jerrams, S., "Swelling Effects in Multiaxial Fatigue of Elastomers", (Paper presented at Polymeric Materials in Automotive, Bratislava, May 2007 and submitted to Polymers for Advanced Technologies, 2007).
80. Murphy, N., Hanley, J., Ali, H., Jerrams, S., "The Effect of Specimen Geometry on the Multiaxial Deformation of Elastomers", proceedings of the 5th European Conference on Constitutive Models for Rubber, Paris, September 2007 and a chapter in the book 'Constitutive models for rubber V' edited by A.Boukamel, L.Laiarinandrasana, S.Méo and E.Verron, pp 61-65. (Published by Taylor & Francis, ISBN 0415454425), (2007).
81. Hallett, J.F. Multiaxial Strength and Fatigue of Rubber Compounds, PhD Dissertation, Loughborough University, (1997).

82. Abraham, F, "The influence of Minimum Stress on the Fatigue Life of Non-Strain Crystallising Elastomers". PhD Dissertation, Coventry University, (2002).

83. Ronan, S., Alshuth T., Jerrams, S., Murphy, N., "Long-term stress relaxation prediction of elastomers using the time-temperature superposition method", Journal of Materials and Design, Vol 28, Issue 5, 2007, pp 1513-1523.

84. Ronan, S., Alshuth T., Jerrams, S., Murphy, N., "An approach to estimating the long-term stress relaxation of elastomers and separating relaxation processes", Kautschuk Herbst Kolloquium, Hannover, Nov 2006 and subsequently published in KGK Kautschuk Gummi Kunststoffe 2007.

85. Andre, N., Cailletaud, G., Piques, R., "Haigh Diagram for Fatigue Crack Initiation Prediction of Natural Rubber Components", KGK Kautschuk Gummi Kunststoffe, 52. Jahrjang, Nr 2/99, p120 (1999)

86. Hildebrand, "Solubility", Reinhold Publishing Co., New York, 1936, p.73.

87. Gent, A.N., "Engineering with Rubber", Hanser Publishers, ISBN 3-446-17010-3 (1992).

88. Carman, F., P. Powers, P., Robinson, H., "Swelling of Synthetic Rubbers in Mineral Oils", Rubber Chemistry and Technology, Volume 13, p.936-941, (1940).

89. Continental Annual Report 2006, (http://report.contionline.com/en/02_corporate_profile/chapter_2_04_en.html).

90. Grest, G.S., Pütz, M., Everaersc, R., Kremerc, K., "Stress–strain relation of entangled polymer networks", Journal of Non-Crystalline Solids, Volume 274, P.139-146, (2000).

91. Hanley, J., Murphy, N., Ali, H., Jerrams, S., "The Effect of Oil Swelling on the Fatigue Life of Elastomers subjected to Cyclic Bubble Inflation", KGK Kautschuk Gummi Kunststoffe, (In Press), 2007.

92. Hanley, J., Murphy, N., Ali, H., Jerrams, S., "The Effect of Oil Swelling on the Fatigue Life of Elastomers subjected to Multi-axial Fatigue using Bubble Inflation", 11th International Seminar of Elastomers ISE 2007, Freiberg, Germany, September 2007.

93. Hanley, J., Murphy, N., Ali, H., Jerrams, S., "The Effect of Oil Swelling on the Multi-Axial Fatigue Life of EPDM", High Performance & Speciality Elastomers, (In Press), 2007.

94. Hearn, E.J., "Mechanics of Materials: The Mechanics of Elastic and Plastic Deformation of Solids and Structural Materials: V. 2", Third Edition, Butterworth-Heinemann Ltd, ISBN-13: 978-0750632669 (1997).

95. Javořik, J., Dvořàk, Z., "Equibiaxial Test of Elastomers", KGK Kautschuk Gummi Kunststoffe, September 2007, P.456-459 (2007)

96. Johannknecht, R. Jerrams, S, Clauss G. 1999 "The uncertainty of implemented curve fitting in finite element analysis: Finite element analysis of elastomers". Boast, D. & Coveney V. (ed) Professional engineering publishing London 141-151 ISBN 1 86058 171 4.

97. Johannknecht, R. Jerrams, S. 1999 "The need for equi-biaxial testing to determine elastomeric material properties". 1st European Conference on

Constitutive Models for Rubber (ECCMR), August 1999, Vienna, Austria.

98. Lake, J., "Fatigue and Fracture of Elastomers", Rubber Chemistry and Technology, Volume 68, P.435-460, (1995).

99. Medalia, A., "Effect of Carbon Black on Dynamic Properties of Rubber Vulcanizates", Rubber Chemistry and Technology, Volume 51, p.437-523, (1978).

100. Murphy, N. Spratt, C. Ronan, S. Jerrams, S. Johannknecht, R. "A method for determining equi-biaxial fatigue in elastomers." 3rd European Conference on Constitutive Models for Rubber (ECCMR), 2003, London, England.

101. Ogden R.W. "Large Deformation Isotropic Elasticity: On the Correlation of Theory and Experiments for Incompressible Rubber-like Solids". Proceedings of the Royal Society Vol A (326) pp 556-585 (1992).

102. Rachik, M., Schmidt, F.M., Reuge, N., Le Maoult, Y., Abbe, F., "Elastomer biaxial characterization using bubble inflation technique. II: Numerical investigation of some constitutive models", vol. 41, no3, pp. 532-541, (2001).

103. Reuge, N., Schmidt, F.M., Le Maoult, Y., Rachik, M., Abbe, F., "Elastomer Biaxial Characterization Using Bubble Inflation Technique. I: Experimental Investigations", Polymer Engineering and Science, vol. 41, no3, pp. 522-531, (2001).

104. Rijke, A.M., Taylor, G.L., "Stress-Strain Behavior of Swollen Polymeric Networks", Rubber Chemistry and Technology, Volume 42, P.572-579, (1969).

105. Thomas, A.G., "The Development of Fracture Mechanics for Elastomers", Rubber Chemistry and Technology, Volume 67, G50-G60, (1994).

106. Mullins, L., "Softening of rubber by deformation", Rubber Chemistry and Technology, Volume 42, 339-362. (1969).

107. Mooney, M. Journal of Applied Physics, Vol 11, p 582 (1940).

108. Jerrams S.J. and Bowen J. "Modelling the behaviour of rubber-like materials to obtain correlation with rigidity modulus tests" CMEM 95, Capri (1995).

109. Rivlin R.S. "Rheology, theory and applications.", (Ed. Eirich F.R.) Academic Books, London p 351 (1956).

110. Ogden R.W. "Non-linear Elastic Deformations", pp 482-520, First Edition, Ellis Horwood Limited, ISBN-13: 0-85312-273-3 (1984).

111. Rivlin R.S., Saunders D.W. Phil. Trans. Royal Society, Vol A243, p 251 (1951).

112. James A.G., Green A. and Simpson G.M. "Strain energy functions of rubber, 1: Characterisation of gum vulcanisates". Journal of Applied Polymer Science, 19, (1975).

113. Tschoegl N.W. Journal of Polymer Science Vol A1 9 p 1959 (1959).

114. Yeoh O.H. "Characterization of Elastic Properties of Carbon-Black-Filled Rubber Vulcanizates", Rubber Chemistry and Technology, Vol 63, No. 5, pp 792-805 (1990).

115. Jerrams S, Johannknecht R, Hookes DE, "Modelling Surface Deformations Resulting from Rigid Punch Indentation in Rubber", Computer Applications in Industry, December 1995, Cairo, Egypt.

116. Jerrams S, Kaya M, Soon KF, "The Effects of Strain Rate and Hardness on the Material Constants of Nitrile Rubbers", Journal of Materials and Design, Vol 19 No 4, August 1998.

117. Dick, John. S., "Rubber Technology – Compounding for Testing and Performance", Hanser Publishers Munich, ISBN 3-446-19186-0 (2001).

118. Grinberg, F., Garbaczyk, M., Nestle, N., Kuhn, W., Jurga, S., "A Novel Approach to the Determination of the Cross-link Density in Rubber Materials using the Dipolar-correlation Effect in Low Magnetic Fields", Journal of Polymer Science Part B: Polymer Physics 39, 2207-2216 (2001),

119. Charalambides M.N., Wanigasooriya L., Williams J.G., Chakrabarti S., "Biaxial deformation of dough using the bubble inflation technique. I. Experimental". Rheologica Acta, 41, 532-540 (2002).

120. Charalambides M.N., Wanigasooriya L., Williams J.G., "Biaxial deformation of dough using the bubble inflation technique. II. Numerical modelling". Rheologica Acta, 41, 541-548 (2002).

121. Campion, R.P. "Durability review of elastomers for severe fluid duties," Rubber Chemistry and Technology, Volume 76, no. 3, p. 719 (2003).

122. Ignatz-Hoover, F., To, B.H., Datta, R.N., De Hoog, A.J., Huntink, N.M., Talma, A.G., "Chemical additive migration in rubber," Rubber Chemistry and Technology, Volume 76, no. 3, p. 747 (2003).

123. Shinyoung Kaang, Young Woong Jin, Yang-il Huh, Wan-Jin Lee, Wan Bin Im, "A test method to measure fatigue crack growth rate of rubbery materials", Polymer Testing 25, P.347–352 (2006).

Appendix

Appendix 1 – Published Papers Relevant to the Research

Appendix 2 – Control Program Process Description

Appendix 3 – Vision System Details and Stress-Strain Calculations

Appendix 4 – Supplemental Literature Review

Appendix 5 – Plots of E* Models

Appendix 6 – Test Materials Specifications

Appendix 1 – Published Papers Relevant to the Research

List of Publications and Conference Contributions:

1. N. Murphy, J. Hanley, S. Jerrams, J. McCartin. B. Lanigan, S.D. McLoughlin, G. Clauss, R. Johannknecht. "*Determining multiaxial fatigue in elastomers using bubble inflation*". Paper presented at the 4th Conference for Constitutive Models for Rubber (ECCMR), June 27-29th 2005, Stockholm, Sweden and subsequently as a chapter in the book 'Constitutive models for rubber IV' edited by P.-E. Austrell and L. Kari, pp 65-70, (Published by A. A. Balkema, ISBN 0415383463), 2005.
2. J. Hanley, N. Murphy, H.Ali & S. Jerrams. "*The effect of swelling on the properties of elastomers subjected to multiaxial fatigue using bubble inflation*". Paper presented at International Conference on Materials Energy and Design, March 14^{th}-17^{th}, 2006, Dublin, Ireland.
3. J. McCartin, N. Murphy, J. Hanley, S. Jerrams, B. Lanigan, "*Determining levels of stress softening in multi-axial deformation*", Poster for German Institute of Rubber Technology (DIK) 7th Fall Rubber Colloquium (KHK 2006), Hannover, November 2006 and subsequently published in KGK Kautschuk Gummi Kunststoffe 2007.
4. N. Murphy, J. Hanley, H. Ali, S. Jerrams, "*The Effect of Specimen Geometry on the Multiaxial Deformation of Elastomers*", presented at the 5th European Conference on Constitutive Models for Rubber, Paris, September 2007 and subsequently as a chapter in the book 'Constitutive models for rubber V' edited by A.Boukamel, L.Laiarinandrasana, S.Méo

and E.Verron, pp 61-65. (Published by Taylor & Francis, ISBN 0415454425), 2007

5. J. Hanley, N. Murphy, H. Ali, S. Jerrams, "*Swelling Effects in Multiaxial Fatigue of Elastomers*", (Paper presented at Polymeric Materials in Automotive, Bratislava, May 2007 and awaiting publication in Polymers for Advanced Technologies (In Press).
6. J. Hanley, N. Murphy, H. Ali, S. Jerrams, "*The Effect of Oil Swelling on the Fatigue Life of Elastomers subjected to Multi-axial Fatigue using Bubble Inflation*", 11th International Seminar of Elastomers ISE 2007, Freiberg, Germany, September 2007 and awaiting publication in KGK Kautschuk Gummi Kunststoffe (In Press).
7. J. Hanley, N. Murphy, H. Ali, S. Jerrams, "*The Effect of Oil Swelling on the Multi-Axial Fatigue Life of EPDM*", High Performance & Speciality Elastomers, (In Press), 2007.
8. S. Jerrams, J. Hanley, N. Murphy, H. Ali, "Equi-Biaxial Fatigue of Elastomers – The Effect of Oil Swelling on Fatigue Life" Rubber Chemistry and Technology, Under Peer Review at Time of Writing, February 2008.

1. N. Murphy, J. Hanley, S. Jerrams, J. McCartin. B. Lanigan, S.D. McLoughlin, G. Clauss, R. Johannknecht. "*Determining multiaxial fatigue in elastomers using bubble inflation*". Paper presented at the 4th Conference for Constitutive Models for Rubber (ECCMR), June 27-29th 2005, Stockholm, Sweden and subsequently as a chapter in the book 'Constitutive models for rubber IV' edited by P.-E. Austrell and L. Kari, pp 65-70, (Published by A. A. Balkema, ISBN 0415383463), 2005.

Determining multiaxial fatigue in elastomers using bubble inflation

N. Murphy, J. Hanley, S. Jerrams & J. McCartin.
Dublin Institute of Technology, Dublin, Ireland.

B. Lanigan & S.D. McLoughlin.
National University of Ireland, Maynooth, Ireland.

G. Clauss.
Heilbronn University of Applied Science.

R. Johannknecht.
Robert Bosch GMBH.

ABSTRACT: This paper describes results obtained from tests using an axi-symmetric bubble inflation rig. The rig allows the determination of real time stress/strain data for thin elastomeric sheets subjected to cyclic loading by bubble inflation. A fully integrated hydraulic pressure control system inflates and deflates the test-piece between preset pressure limits. Local strains are determined from displacements recorded by an optical measuring system at inflation and deflation points throughout the cycle and the corresponding pressure data is used to calculate local stress. The data is collected in real time and subsequently dynamic stress/strain behaviour for each or any cycle can be represented by hysteresis curves, allowing the energy of deformation to be determined. The measured data will be used to produce accurate mathematical models of hyperelastic and viscoelastic material behaviour during cyclic loading leading to failure. Recent research has highlighted the dependency of the fatigue life of non strain-crystallising elastomers during uniaxial deformation on applied stress amplitude as well as minimum stress. Tensile pre-stressing of tests pieces was shown to increase fatigue life if stress amplitude remained unchanged. In this work results from the rig are presented for specimens of non strain-crystallising elastomers, subjected to pre-pressures and cycled at ranges allowing a comparison with the uniaxial tests. The potential of the rig to determine other multi-axial viscoelastic properties of materials using different inflation media has led to a widening of the programme.

1 INTRODUCTION

The function of most rubber components means that they are subjected to complex loading conditions in service. Uniaxial load test data is consequently unrepresentative of actual component behaviour. In order to obtain accurate service life predictions, multiaxial testing methods are necessary and though stretch frames provide a simple biaxial test method, results are inaccurate and stretch ratios limited (Charlton and Yang, 1994).

Bubble inflation (Johannknecht *et al.* 2002, 1999) provides a method of obtaining controllable, repeatable and quantifiable equibiaxial deformation of rubber sheet to failure in fatigue (Murphy *et al.* 2003).

Non strain crystallising elastomers exhibit higher fatigue lives when pre-stressed uniaxially (Abraham *et al.* 2001, 2002, 2001). One of the aims of the research is to investigate whether this phenomenon is replicated for multi-axial fatigue. Bubble inflation of elastomeric sheets is a method of determining equibiaxial stresses and strains for large deformations which does not possess the disadvantages exhibited by stretch frames. The dynamic bubble inflation rig is capable of cycling between pre-set pressure limits and this work investigates the influence of pre-pressurising for large equibiaxial deformations. This text describes a series of tests on Ethylene-Propylene-Diene (EPDM) material in the form of 35mm test diameter discs of 2mm thickness, which were cycled to failure using bubble inflation for both zero minimum and non-zero minimum pressure conditions. The stresses and strains can be calculated at any point throughout the test and hysteresis curves were plotted periodically, allowing dynamic stored energy and complex modulus to be determined.

In addition, the number of cycles to failure was recorded for each test. Results are presented which can be compared with those for uniaxially loaded EPDM specimens and show the influence of stress softening on material behaviour throughout a biaxial fatigue test. Finally, the potential of the rig to deliver information about other viscoelastic phenomena during equi-biaxial deformation is discussed.

2 THEORY

Bubble inflation is assumed to comply with theory for applying pressure to a thin spherical shell structure possessing negligible bending stiffness, alternatively described as membrane theory. For an ideal isotropic material and axi-symmetric deformation, the bubble contour exhibits rotational symmetry and therefore the strain at the pole is equibiaxial as shown in Figure 1.

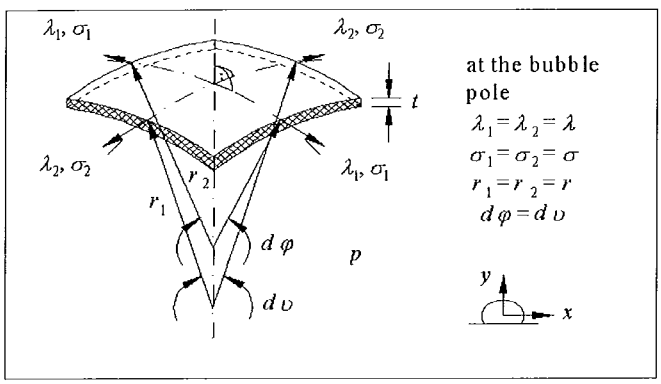

Figure 1. Bubble inflated shell element.

Pressure p is applied to inflate a thin sheet with thickness t to produce a bubble shell. From the measurement of pressure p and the radius of curvature r the equation for stress at the pole can be determined from Equation 1.

$$\sigma = p.\frac{r}{2t} \tag{1}$$

The initial bubble shape is approximately hemispherical. Previous publications on the contour analysis of inflated bubbles refer to numerical solutions (Bhate & Kardos 1984, Dickie & Smith 1969, Song *et al.* 1991, Khayat & Derdouri 1995, Adkins & Rivlin 1952). However, due to specimen clamping effects, non-linear material behaviour and the multiaxial deformation state in the rubber shell, the inflated contour will not be perfectly spherical when the bubble height exceeds the radius of the inflation orifice. Thinning of the material along the meridian occurs and an increase of strain towards the pole results from the specimen fixing (Treloar 1975). The meridian cross-section of a bubble contour can be expressed in polar co-ordinates R,φ, by a two dimensional tensor or as an ellipsoid function.

$$R = \left(a^2.\cos^2\varphi + b^2.\sin^2\varphi\right)^{\frac{1}{2}} \tag{2}$$

The cross-section of the axi-symmetrical ellipsoid is described in Cartesian co-ordinates by the simple equation

$$\frac{x^2}{a^2} + \frac{y^2}{b^2} = 1 \tag{3}$$

The centre of the ellipsoid is located at the intersection of the x and y axis whereas the symmetry of rotation is about the y axis. The axis interception to the equator is formed by parameter 'a' and the segment to the bubble pole by 'b'. Both parameters describe the radius of curvature at the pole as shown in equation 4.

$$r_1 = r_2 = \frac{a^2}{b} \tag{4}$$

3 OBJECTIVES

The primary aims of this investigation are:

1. To compare the dependency of fatigue life on minimum pressure and pressure amplitude for biaxially deformed elastomers with existing data for uniaxially loaded elastomeric test-pieces, (Abraham et al. 2001).
2. To determine the effects of stress softening in EPDM cycled biaxially between preset pressure limits.

4 MATERIALS

EPDM rubber containing 110 pphr low activity carbon black and 70 pphr softener was initially chosen for the investigation. This allows direct comparisons between dynamic biaxial test results and those from the dynamic uniaxial tests carried out by Abraham. The bubble specimen consists of a rubber disc having a diameter of 50 mm (35 mm unclamped diameter) and a thickness of 2mm. For uniaxial tension, standard dumbbells conforming to S2 ISO 37 were used. The tests carried out by Abraham used the same EPDM material in the form of cylindrical dumbbells to allow a uniaxial cyclic load to be imparted.

5 METHODOLOGY

A circular sheet of rubber is clamped around its edges and an air tight seal is formed. Pressure is then applied to one side of the sheet causing it to in-

flate in a balloon like manner. An optical system is used to record the movements of specific points on the surface of the sheet during deformation. Stress values calculated from the applied pressure and bubble geometry are combined with the strain data from the optical system to provide biaxial stress/strain relations.

A dynamic testing facility is integrated with the rig control programme which allows cycling between pre-set pressures of 0-10 Bar. Changing the inflation medium is a simple process and complete air bleeding of the system can be achieved. The specimen clamp design (Figure 2), ensures an evenly distributed force around the clamped portion of the sample, eliminating specimen slippage during testing.

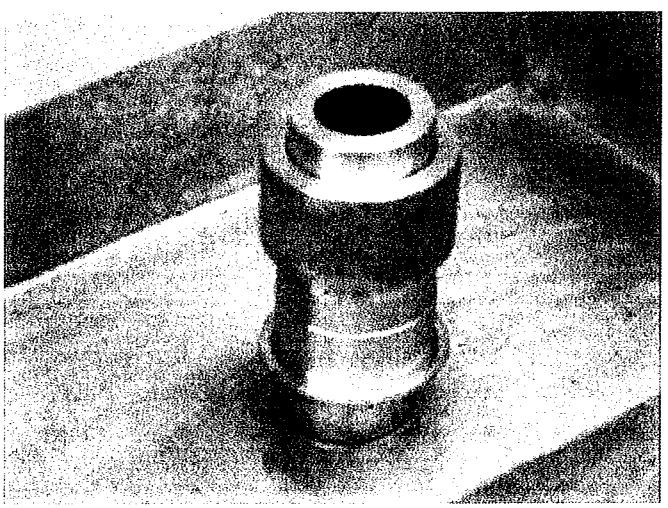

Figure 2. Specimen in rig clamp.

A bi-directional flow-regulating valve, linked to a pressure sensor is employed to maintain steady inflation and deflation rates during the cycles. When maximum pressure is reached on the inflation cycle, the programme initiates the deflation cycle.

The vision system is based on two charge coupled device (CCD) cameras connected to a PC. A calibration routine is used to build a correction matrix to compensate for camera misalignment and lens distortion. Values for strain are obtained by calculating the surface distance between feature points on the bubble surface using three dimensional position co-ordinates obtained by the vision system.

The pressure readings are synchronised with the cameras during the image capture sequences. Trigger signals are sent to the camera PC during the measurement cycle to initiate image capture. Figure 3 show how inflation and deflation cycles are integrated with the image acquisition system.

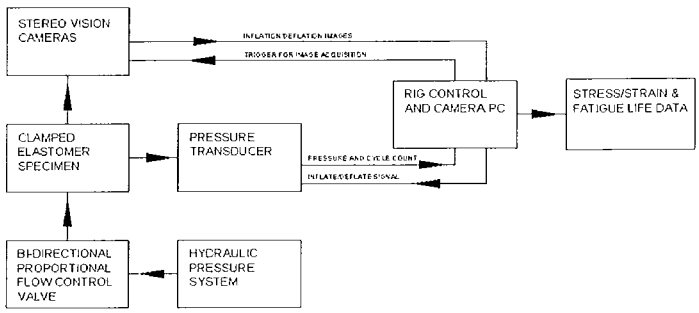

Figure 3. Test process schematic.

X, Y and Z pixel co-ordinates are calculated for each point and converted to linear real co-ordinates. When this co-ordinate information is combined with the associated pressure values, reliable stress/strain data is available on an accurate and repeatable basis.

6 TEST RESULTS AND DISCUSSION

6.1 Results of multiaxial fatigue testing of EPDM

Single shot inflations to failure tend to rupture in a star or cloverleaf pattern (Johannknecht *et al.* 2002) as shown in Figure 4(a). However, during the series of tests presented, rupture due to fatigue was predominantly in the form of a single line fracture running through the bubble pole as shown in Figure 4(b). These splits emanate from a region at the pole where maximum stress occurs.

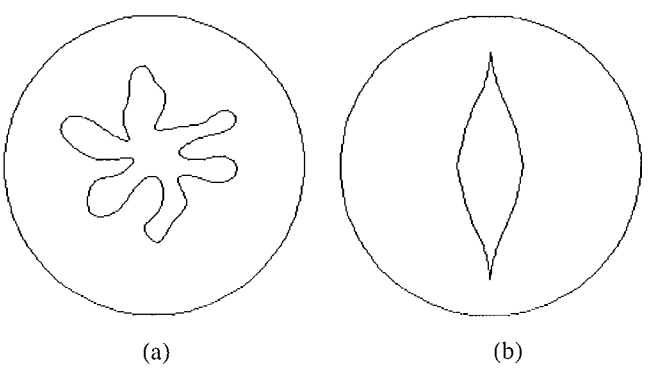

Figure 4. Typical specimen failures modes which occurred during multiaxial tests.

6.2 Typical results of multiaxial fatigue testing of EPDM

The uniaxial tests conducted by Abraham (Abraham *et al.* 2001, 2002) resulted in large increases in fatigue life when tensile pre-loads were applied. Representative results are shown in Figure 5, where different load amplitudes and pre-stressing produce increases in fatigue life of a magnitude of 11 (0-400N) to 16 (0-500N).

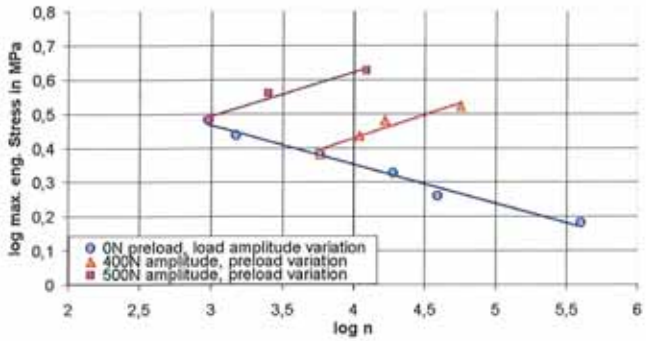

Figure 5. Fatigue results from uniaxial tests on EPDM, showing increase in fatigue life with pre-stressing.

6.3 Uniaxial load control tests - some considerations

In the tests conducted by Abraham *et al* 'engineering stress' (σ_{eng}) was used in preference to 'true (Cauchy) stress' (σ_{true}) when determining parameter dependence for fatigue life calculations. At first consideration this is acceptable, but σ_{eng} and σ_{true} are not directly proportional when strain is increasing or decreasing throughout a load cycle.

i.e. for uniaxial deformation of an incompressible material

where $\lambda_1 = \lambda, \quad \lambda_2 = \lambda_3 = \lambda^{-0.5}$ (5)

if $\lambda_1 = 2$ (100% strain)

then $\lambda_2 =$ (at the test piece diameter 'D') $= 0.707$

$$\sigma_{eng} = L/(\pi D^2/4) \quad (6)$$

and $$\sigma_{true} = L/[\pi(0.707D^2)/4)] \quad (7)$$

Therefore $$\sigma_{eng} = 0.5\sigma_{true} \quad (8)$$

Showing that true stresses will be greater than engineering stresses for uniaxial load amplitudes by a ratio of σ_{true} to σ_{eng} of λ.

Hence, equal load amplitudes for cycles with a zero minimum and a non-zero minimum do not produce equal true stress amplitude – tensile pre-stressing will produce a larger true stress due to greater reduction in diameter in the higher stress range. This strengthens Abraham's argument that pre-stressing in the uniaxial case leads to increases in fatigue life in non-strain crystallising rubbers. The phenomenon observed in the tests would have been accentuated if equal 'true' stress amplitudes had been used. Moreover, due to successive loss of modulus in each cycle the test-piece will stretch more, reduce in diameter and increase true stresses further.

6.4 Equi-biaxial tests

In an initial investigation to show if the phenomenon exhibited in uniaxial fatigue tests can be shown to occur in EPDM cycled using biaxial bubble inflation, a number of dynamic pressure controlled tests were carried out. The test-piece in the first of these tests was cycled from a zero minimum pressure with a range of constant pressure amplitudes. The results in Figure 6 show that failure occurs quite early at high pressure, while fatigue life increases with lower pressure amplitudes, as expected.

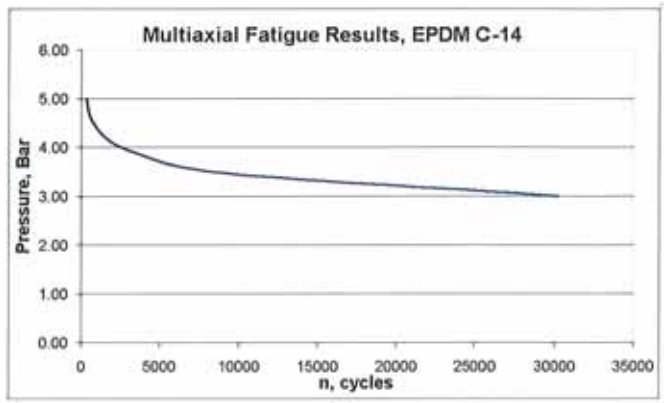

Figure 6. Fatigue results for multi-axial tests on EPDM, with a minimum cycling pressure of zero bar.

Thereafter, test-pieces were cycled from a minimum pressure of 0.5 MPa with a similar range of pressure amplitudes to that used in the zero minimum pressure tests.

All of the tests were carried out until failure occurred. Figure 7 shows that for pre-pressurisation there was a decrease in fatigue life at all pressure amplitudes.

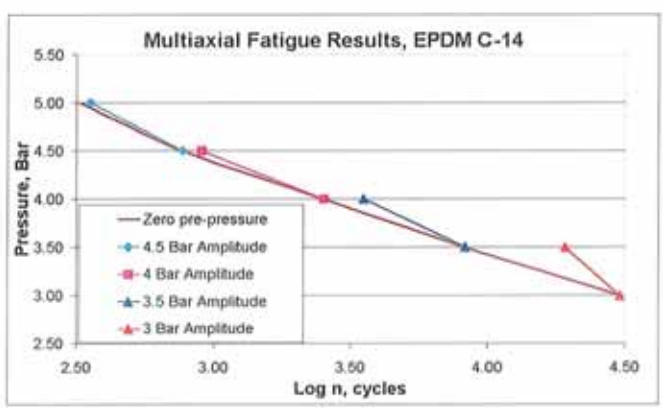

Figure 7. Plot of Pressure versus log of cycles for fatigued EPDM with zero and non-zero minimum cycling pressure.

6.5 Equi-biaxial pressure controlled tests - some considerations

Let the bubble inflation method receive similar consideration as the uniaxial case in Section 6.3. Constant pressure amplitudes, for initial conditions of zero pressure and non-zero positive pressure, are analogous to constant load amplitudes in the uniaxial case. The engineering and true membrane stresses at the bubble pole are given respectively by the formulae:

$$\sigma_{eng} = pr/2t_0 \quad (9)$$

and

$$\sigma_{true} = pr/2t \quad (10)$$

where t_0 is unstrained membrane thickness at the pole and t is the strained thickness.

Again, true stresses will be greater than engineering stresses for higher amplitudes, but for bubble inflation the ratio of σ_{true} to σ_{eng} is λ^2.
This means that equal pressure amplitudes will result in far higher magnitudes of true stress with pre-stressing, so correlation with the uniaxial tests is not achieved. Moreover, the radius of curvature will increase in successive cycles due to stress softening, causing more thinning of the test piece and further accentuate the difference between pressure amplitude and engineering stress and true stress.
Thus, to accurately replicate true stress amplitudes in the bubble inflation case requires greatly reduced pressure amplitudes for non-zero minimum stress cases.

6.6 Stress softening results

The first, hundredth and thousandth cycles for an EPDM specimen are shown in Figure 8 for a dynamic bubble inflation test with a pressure range of 0-4 bar. Throughout this range and for subsequent constant pressure cycles, the maximum true stress continually increased.

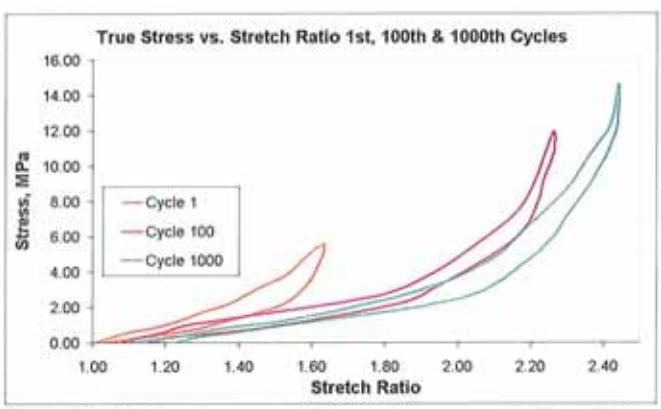

Figure 8. Hysteresis curve of true stress vs. stretch ratio for EPDM, showing stress softening in the 1st, 100th and 1000th cycles.

Figure 9 shows that while engineering stress also rises in subsequent pressure cycles, the ratio of engineering stress (σ_{eng}) to true stress (σ_{true}) becomes quite significant for bubble inflation, i.e. σ_{true} is greater than σ_{eng} by a factor of λ^2, as discussed in Section 6.5.

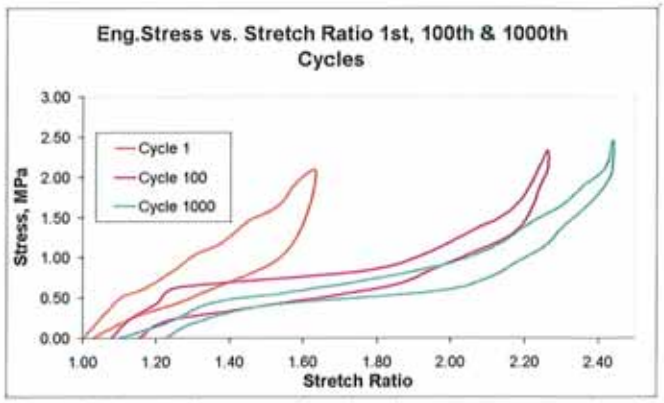

Figure 9. Hysteresis curve of engineering stress vs. stretch ratio for EPDM, showing stress softening in the 1st, 100th and 1000th cycles.

7 FURTHER PROPOSED TESTING

In equi-biaxial bubble inflation the stress pressure relationship changes as a function of radius and this is increased as the complex modulus decreases with the accumulation of cycles as shown in Figure 10. Also, the ratio of strained membrane thickness to unstrained thickness for the equi-biaxial specimens requires that for comparability with uniaxial fatigue testing, the pre-set controlled parameter should not be pressure alone but should be stress and preferably true stress. To control stress amplitude in this manner requires that the pressure and stress relationship must be monitored and adjusted throughout the test.

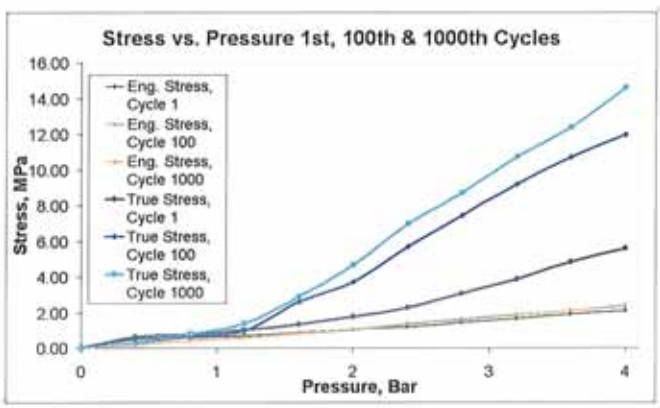

Figure 10. Plot of increasing pressure and stress showing relationship in terms of true stress and engineering stress.

Until the control of the machine assimilates constant true stress amplitudes, comparing dynamic stored energy and change in complex modulus for specimens fatigued using bubble inflation with the results achieved in uniaxial tests is of limited benefit.

Further testing is scheduled which will attempt to definitively answer some of the following questions:

- Does pre-stressing an elastomer subjected to equi-biaxial loading in fatigue improve the material's fatigue life if constant true stress limits are maintained?

- Is there a level of complex modulus (E*) reached in equi-biaxial fatigue loading at which particular elastomers will fail irrespective of the stress induced and the form of the loading cycles?
- Are research findings relating fatigue life in non strain-crystallising elastomers to dynamic stored energy in uniaxial extension supported for multi-axial deformation?
- Can finite element codes be provided with an option to accurately model viscoelastic and cyclic three-dimensional behaviour?

8 CONCLUSIONS

The tests carried out in this work using controlled pressure amplitude have shown that pre-pressurising non-strain crystallising EPDM will not increase the fatigue life for a specific pressure amplitude. Using pressure as the controlled parameter for the tests ignores hyperelastic and viscoelastic influences on true stress, both throughout a cycle and in subsequent cycles. In order to definitively answer whether pre-stressing will increase fatigue in non-strain crystallising EPDM and other non-strain crystallising rubbers subjected to equi-biaxial fatigue, true stress is the preferred controlled parameter for testing.
A comprehensive test programme devoted to determining the influence of pre-stressing of rubbers subjected to multi-axial deformation is underway. Further fatigue tests on EPDM will be carried out where a constant 'true stress' amplitude will be maintained during the test and where consequently the inflation pressure amplitude will be varied throughout the test. The current programme has led to a consideration of viscoelastic behaviour in elastomers subjected to complex loading considered from a wider perspective. The rig will be utilised to investigate the Mullins effect for low cycles for a range of both strain crystallising and non-strain crystallising elastomers. Stress relaxation and creep have been induced in specimens using the rig and will form the basis of further investigations. Additionally, the influence of swelling phenomenon on the physical characteristics of equi-biaxially loaded test pieces subjected to fatigue will be determined by using a range of inflation media and a selection of elastomers.

9 ACKNOWLEDGEMENTS

The authors would like to thank the Faculty of Engineering and the Research Support Unit in the Directorate of Research and Enterprise in the Dublin Institute of Technology. They are also indebted to the Departments of Experimental Physics and Computer Science in the National University of Ireland, Maynooth.

REFERENCES

Abraham, F, Alshuth, T, Jerrams, S. 2001 "Parameter Dependence and Prediction of Fatigue Properties of Elastomer Products". Rubber Chemistry and Technology Journal, Vol 75, Issue 4, p 365, September/October 2002

Abraham, F., Alshuth, T, Jerrams, S. 2001 "Dependence on Mean Stress and Stress Amplitude of Fatigue life of EPDM Elastomers". The Journal of Plastics, Rubber and Composites, Institute of Materials, Vol 30 No. 9 pp 421-425, (ISSN 1465-8011)

Abraham, F. Alshuth, T, Jerrams, S. 2002 "Ermüdungsbeständigkeit von Elastomeren – Einfluss der Spannungsamplitude und der Unterspannung Teil 2". KGK Kautschuk Gummi Kunststoffe, pp 674-678.

Adkins, J, Rivlin, R. 1952. Large elastic deformations of isotropic materials. XI The deformation of thin shells, F.R.S., Vol. 244, A. 888.

Bhate, P, Kardos, J. 1984. "A Novel Technique for the Determination of High Frequency Equi-biaxial Stress-Deformation Behaviour of Viscoelastic Elastomers", Polymer Engineering and Science, Vol. 24, No. 11.

Charlton, D.J, Yang, J. 1994 "A review of methods to Characterise Eubber Elastic Behaviour for the use in Finite Element Analysis", Rubber Chemistry and Technology, 67, pp. 481-503

Dickie, R, Smith, T. 1969 Ultimate Tensile Properties of Elastomers. VI. Strength and Extensibility of a Styrene-Butadiene Rubber Vulcanizate in Equal Biaxial Tension, Journal of Polymer Science, Vol. 7, Part A-2, 687-707.

Johannknecht, R. Jerrams, S, Clauss G. 1999 "The uncertainty of implemented curve fitting in finite element analysis: Finite element analysis of elastomers". Boast, D. & Coveney V. (ed) Professional engineering publishing london 141-151 ISBN 1 86058 171 4.

Johannknecht, R. Jerrams, S. 1999 "The need for equi-biaxial testing to determine elastomeric material properties". 1st European Conference on Constitutive Models for Rubber (ECCMR), August 1999, Vienna, Austria.

Johannknecht, R, Jerrams, S. Clauss, G. 2002 "Determination of non-linear, large equal bi-axial stresses and strains in thin elastomeric sheets by bubble inflation". Proceedings of the Institute of Mechanical Engineers, Vol 216 Part L, No L4, (ISSN 1464-4207) Journal of Materials, Design and Applications.

Khayat, R, Derdouri, A. 1995. "Stretch and Inflation of Hyperelastic Membrane as Applied to Blow Molding, Polymer Engineering and Science, Vol. 35, No. 23.

Murphy, N. Spratt, C. Ronan, S. Jerrams, S. Johannknecht, R. "A method for determining equi-biaxial fatigue in elastomers." 3rd European Conference on Constitutive Models for Rubber (ECCMR), 2003, London, England.

Song, W, Mirza, F, Vlachopoulos, J. 1991. Finite element analysis of inflation of an axisymmetric sheet of finite thickness, The Society of Rheology, Inc.

Treloar, L. 1975. The Physics of Rubber Elasticity, Clarendon Press, Oxford University Press, London.

2. J. Hanley, N. Murphy, H.Ali & S. Jerrams. "*The effect of swelling on the properties of elastomers subjected to multiaxial fatigue using bubble inflation*". Paper presented at International Conference on Materials Energy and Design, March 14th-17th, 2006, Dublin, Ireland.

The effect of swelling on the properties of elastomers subjected to multiaxial fatigue using bubble inflation

J. Hanley[1], N. Murphy[1], H.Ali[2] & S. Jerrams[3]

[1] *School of Manufacturing Engineering, Dublin Institute of Technology, Dublin, Ireland.*
[2] *School of Chemistry, Dublin Institute of Technology, Dublin, Ireland.*
[3] *Research Support Unit, Directorate of Research and Enterprise, Dublin Institute of Technology, Dublin, Ireland.*

Abstract

The mechanical behaviour of a rubber depends largely on its cross-link density. The more cross-links per unit volume in an elastomer, the less the material is prone to swelling when immersed in a solvent.

Previous research into the mechanical behaviour of elastomers swollen by solvents showed that in uniaxial and bi-axial extension, swelling is increased by the application of tensile strain, while in compression the swelling is reduced.

Another investigation carried out on test-pieces loaded uniaxially, considered the behaviour of swollen rubbers in fatigue. Results showed that an increase in elastomer swelling was accompanied by a decrease in fatigue resistance.

There is a paucity of results for fatigue testing of swollen elastomers subjected to multi-axial loading between constant pressure limits and little or nothing has been published.

The results presented in this paper were obtained from tests carried out using a multi-axial bubble inflation rig. Three different types of testing were carried, out all of which incorporated different aspects of the swelling phenomenon.

Firstly, specimens of two different elastomers had their cross-link densities calculated. Rubber samples of each elastomer type were swollen in a solvent until equilibrium swelling was attained. They were then dried, weighed and the degree of cross-linking was calculated. Test-pieces were then cycled dynamically between controlled pressure limits at a constant frequency with varied upper pressure limits applied to each data set. Subsequently, the fatigue resistance for each elastomer type was compared with its cross-link density.

Secondly, EPDM specimens from one elastomer type were exposed to the solvent 'toluene' for an extended period of time, to allow for maximum absorbance of the solvent by the elastomer. Thereafter, the test-pieces were vacuum-dried to remove the solvent. These samples were then fatigued in a similar manner to those in the first tests and the fatigue results from both test types were compared.

Thirdly, the stress strain behaviour of samples from the first and second tests was plotted and analysed.

Previous fatigue results of specimens tested using bubble inflation highlighted the need to test between constant true stress limits, since constant pressure or engineering stress ranges did not provide equal stress states for successive cycles. The results presented in this paper show the influence of this phenomenon on rubbers which have been swollen in a solvent.

Keywords: Elastomers and rubber, chemical and solvent resistance

1 Introduction

Non cross-linked rubbers swell in compatible solvents until they lose all cohesive strength and go into solution. However, in cross-linked rubbers there is a level at which the volume of a polymer cannot be increased by absorbing a solvent. When the material has reached this level it is referred to as being in a state of equilibrium swelling. The greater the cross-linking in the rubber, the less it is prone to swelling by the solvent. Flory [1] discovered a correlation between equilibrium swelling and cross-link density. The development of the Flory-Rehner equation allowed the degree of cross-linking in an elastomer to be determined by measuring the amount of a solvent that can be absorbed by an elastomer.

In terms of solubility, rubber can be considered as a liquid. This is because the rubber molecules have a high level of freedom to slip past one another, which is a similar characteristic to that associated with liquids. At a molecular level, the molecules of a liquid are close together and exert strong forces on each another. This is the origin of the latent heat of evaporation, which represents the work done in overcoming the cohesive energy of the molecules. As different liquids do not have the same molar latent heats, their molecules cohere with different energies. This difference depends on the chemical nature of the molecules and also on the way they pack together. Thus the heat of swelling is related to the cohesive energies of the liquid and rubber. The swelling power of a liquid can be calculated approximately if its cohesive energy and molecular volume are known. It is known that toluene and EPDM have similar cohesive energy densities (C.E.D). Therefore toluene will swell EPDM appreciably. It was for this reason that toluene was chosen as a solvent for the tests described in this research.

There have been some investigations into the mechanical behaviour of rubbers subjected to swelling. Treloar [2] showed that in uniaxial and bi-axial extension, the swelling is increased by the strain, while in compression it is reduced. Gul et al. [3] showed that there is an initial increase in fatigue resistance, followed by a decrease as the degree of swelling increases. Neogi et al. [4] investigated how the dynamic properties change after swelling the network in a solvent after previous studies showed that hysteresis due to carbon black was reduced by swelling the elastomers in question in a good solvent.

These mechanical treatments of the swelling phenomenon in rubbers were based on testing rubbers which were saturated with solvent. Part of this particular study incorporates dynamic testing of solvent swollen rubber, which has subsequently been dried.

As already stated, swelling a rubber and weighing it before and after equilibrium swelling allows the cross-link density of that particular rubber to be calculated. In addition to this, the swelling process can alter the physical behaviour of the material.

Consequently, the objectives of the research are as follows:

- To compare the multi-axial fatigue lives of two differently cross-linked elastomers, where the degree of cross-linking has been determined using the Flory-Rehner equation.
- To compare the fatigue lives of test-pieces subjected to swelling when loaded multi-axially for an EPDM elastomer, compared with that of fatigued test-pieces which have not been immersed in a solvent.
- To compare stress-strain behaviour of multi-axially loaded specimens of an elastomer which have been immersed in solvent with samples that are untreated.

Bubble inflation of elastomeric sheets provides a method of determining equibiaxial stresses and strains for large deformations [5]. The dynamic bubble inflation rig used for this study is capable of cycling between preset pressure limits. The stresses and strains can be calculated at any point throughout the test and strain energy of the rubber can be determined.

2 Materials and Specimen Preparation

Two types of EPDM rubber containing low activity carbon black were chosen for this investigation. A number of specimens were weighed and then immersed in toluene. Following this, the weight of each specimen was determined daily until equilibrium-swelling conditions were attained. The weight of the specimens at equilibrium swelling was noted and from this, υ_e, the average crosslink density (XLD) was calculated for each elastomer by using the Flory-Rehner equation:

$$-\ln(1 - V_2) + V_2 + XV_2^2 = (V_1/\upsilon M_c)(1 - 2M_c/M)(V_2^{1/3} - V_2/2) \qquad (1)$$

Table 1 shows the average values of cross-link density for each elastomer type used in the testing.

Elastomer	**Crosslink Density, XLD x 10^{-5} mol/cm^3**
E1M, EPDM	229.11
C-14, EPDM	300.63

Table 1. Cross-link densities of EPDM specimens.

3 Testing Methodology

A bubble inflation rig consisting of a dynamic testing facility which interfaces with a control programme was used to test the specimens. The control programme allows cycling of a test-piece between pre-set pressure limits. During a measurement cycle, the pressure readings can be synchronised with an optical measurement system, consisting of two charge coupled device (CCD) cameras. Trigger signals are sent to the cameras during measurement cycles and images are captured which correspond with discrete pressures at a point in an individual inflation and deflation cycle.

Two different types of tests were carried out using the bubble inflation rig:

- Dynamic fatigue testing of specimens to pre-set pressure limits.
- Single cycle inflation and deflation of specimens to high upper pressure with optical measurement of displacements.

3.1 Tests for comparison of cross link density and fatigue life

For the testing described in this paper, a hydraulic inflation medium was selected which did not react with EPDM. The first series of tests allowed fatigue life to be plotted against pressure for each elastomer type tested. A specimen with an effective test sample diameter of 38mm was clamped in place. All samples were bonded to the clamp to prevent specimen slippage. The specimen was cycled between a lower pressure of 0 bar and pre-set upper pressure limits and the number of cycles to failure was recorded.

3.2 Fatigue behaviour of solvent treated and vacuum dried elastomers

Specimens were cut from 2mm rubber sheet and immersed in toluene. Following swelling of the rubber, a specimen was placed in a vacuum drying apparatus and dried until all volatiles were removed from the elastomer. The gas from the vacuum rig can be analysed to ensure all volatile gases have been removed to acceptable levels. Figure 1 shows the gas spectrum from the vacuum rig, with the final toluene content having a partial pressure of 6.383×10^{-14} mbar (atomic mass of toluene = 92).

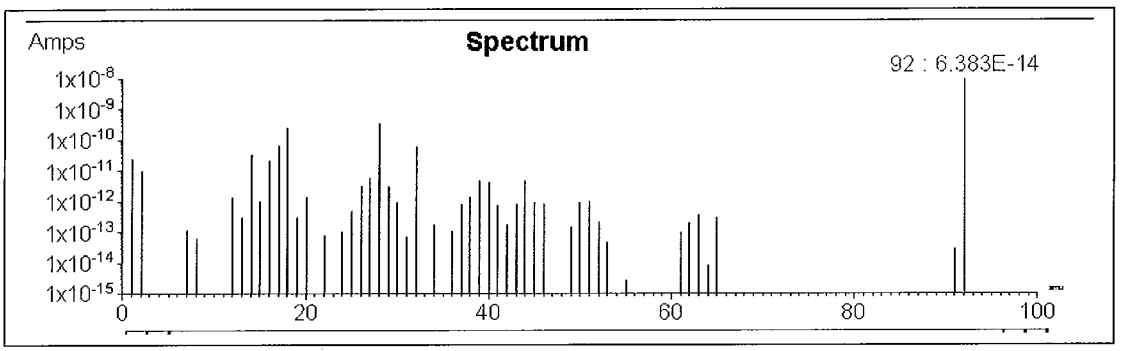

Figure 1. Gas spectrum from vacuum rig showing toluene content in mbar. x-axis shows atomic weight and y-axis partial pressure in mbar.

As in the first set of tests, the vacuum dried specimens were cycled between 0 bar and pre-set upper pressure limits and the number of cycles to failure was recorded. After initial drying of the solvent from the specimens it was noted that specimen geometry had reduced. This did not affect the test diameter of the specimens, as the test diameter was less than the reduced outside diameter of the specimen and consequently the specimen clamp was able to grip the specimen. However, the reduced specimen thickness had an influence on the test results as will be discussed in subsequent sections.

3.3 Stress-strain measurement of samples

A specimen with a test diameter of 38mm was clamped in place. Again, samples were bonded to the clamp to prevent slippage. A pattern of dots was applied to the test-piece, in order that an optical system could record the movements of specific points on the surface of the sheet during deformation. This is illustrated in Figure 2. This series of tests was carried out to determine the stress-strain behaviour of the material being investigated. The sheet was inflated, pressure data was continuously monitored and image capture took place at incremental values of pressure. Once the upper pressure limit was reached, the deflation portion of the cycle was initiated by the rig control programme and image capture continued.

The stress-strain relation during bubble inflation is assumed to comply with membrane theory where, from the measurement of pressure p and the radius of curvature r, the equation for stress at the pole can be determined using Equation 2.

$$\sigma = pr/2t \qquad (2)$$

Stress values were calculated from the measured pressure and bubble geometry data from the optical system. The optical system was also used to measure displacement on the specimen surface, from which strain data could be calculated. Combining these sets of data allowed the determination of biaxial stress/strain relations.

Figure 2. Specimen in rig clamp showing pattern for optical measurement.

4 Test Results

4.1 Comparison of multi-axial fatigue lives versus cross-link density

The results in Figure 3 allow a comparison to be made between the two types of EPDM tested.

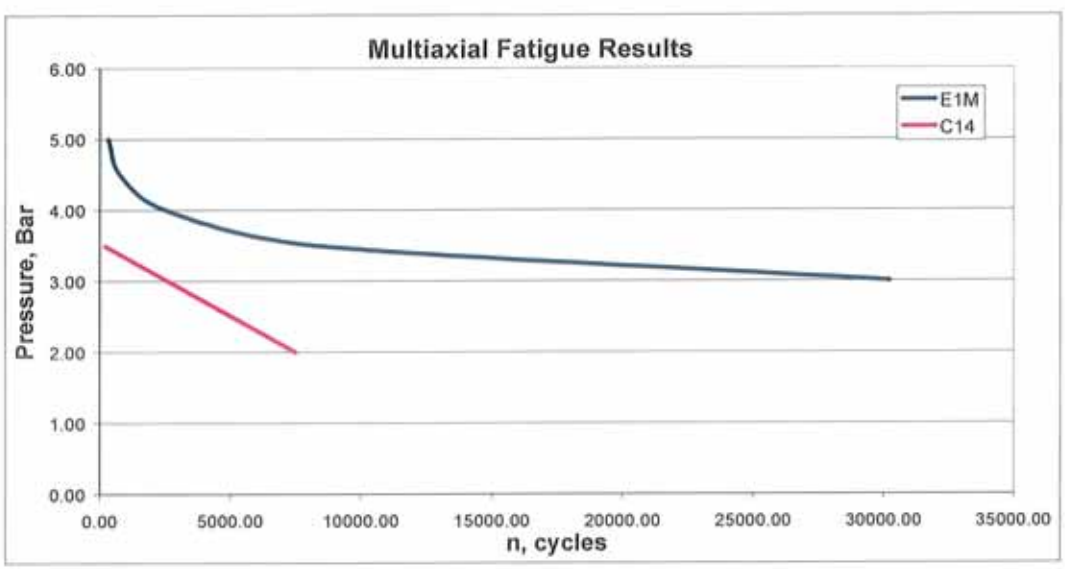

Figure 3. Fatigue results for multi-axial tests on the two elastomer types, with a minimum cycling pressure of zero bar.

As expected, failure occurred rapidly at high pressure, while fatigue life increased at lower maximum pressures for tests carried out with constant pressure ranges. It is also clear that the elastomer with a greater degree of cross-linking had greater fatigue resistance, when subjected to a cyclic pressure load. Failure of both specimens after relatively few cycles can be attributed to the fact that equal pressure amplitudes resulted in far higher magnitudes of true stress than would be experienced in

conventional bi-axial loading of the material. Moreover, the radius of curvature increased in successive cycles due to stress softening, causing more thinning of the test piece at the bubble pole and as a consequence, an increase in true stress occurred.

4.2 Elastomer fatigue live – Swollen and unswollen specimens

There was a marked difference in fatigue life between the two types of EPDM C14 specimens, one of which was swollen in toluene, and then vacuum dried. The average fatigue life for the specimens not swollen in toluene was 7496 cycles, compared with 2265 for the swollen and vacuum dried specimens. The fatigue test for this set of results was carried out at pressure limits of 0-2 bar at a frequency of 1Hz. As stated, after drying the swollen samples had both a smaller diameter and thinner cross-section, which meant that less material was present to resist the applied pressure during the test. Also, changes in the network structure of the rubber, as a result of the solvent treatment would have influenced the rigidity of the material.

4.3 Stress-strain behaviour – Swollen and unswollen specimens

Figure 4 shows the difference in stress-strain behaviour between the EPDM C14 specimens, one of which was swollen in toluene. The stress strain data for each of these curves was taken at 2000 cycles during a 0-2 bar test. The phenomenon of the greater difference between true stress and the engineering stress at higher numbers of fatigue cycles for both materials is apparent. As can be seen. the swollen EPDM is a stiffer material, with a higher initial modulus 'G', a lower maximum stress and less elongation for a pressure of 2 bar. The hysteresis curve for the swollen EPDM is smaller, suggesting that there are less cross-links to be broken during loading of the specimen. The untreated specimen by comparison, is a more elastic material, with much greater elongation for the maximum pressure applied.

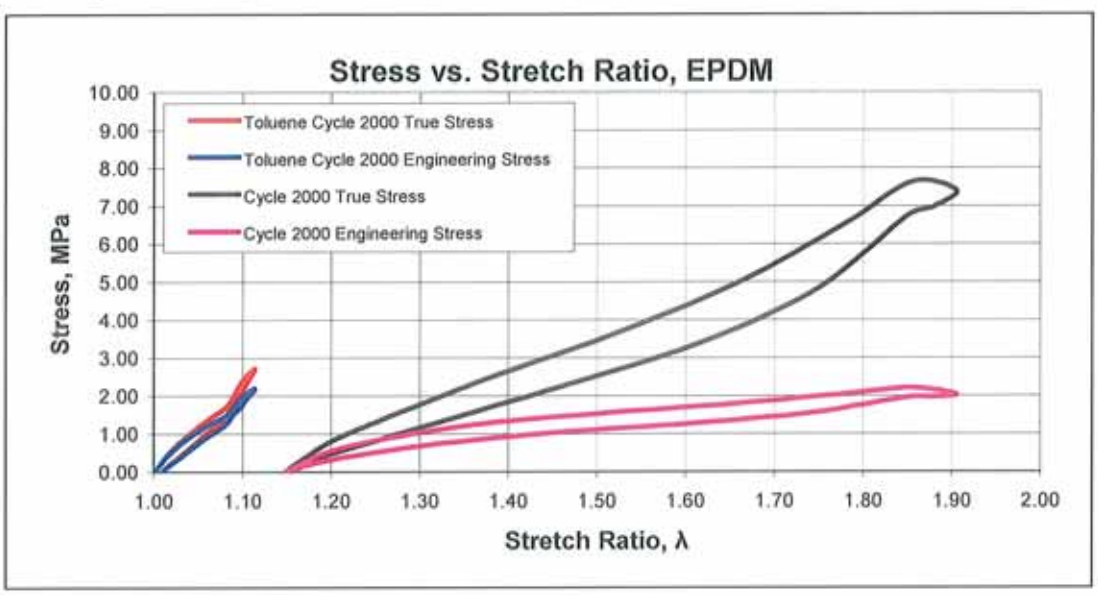

Figure 4. Comparison of fatigue lives of swollen and unswollen specimens, for a 0-2 bar test.

Conclusions

A series of results have been presented which highlight the significance of elastomer swelling when used as a means of quantifying rubber material behaviour. Swelling two different types of EPDM and using the Flory-Rehner equation allowed the degree

of cross-linking of each material to be determined. As shown, the material with a greater degree of cross-linking exhibits a higher fatigue life.
The average fatigue life for the specimens swollen in toluene and vacuum dried was 30% of that of the elastomer which was not treated. This can be attributed to a number of factors. Previous studies by the authors have shown that using pressure as the controlling parameter for the tests ignores hyperelastic and viscoelastic influences on true stress. The stress-pressure relationship changes as a function of radius and this is increased as the complex modulus decreases with the accumulation of cycles. Specimen thickness influences the stress greatly and the post swelling phenomenon of thinner specimen section, combined with molecular changes in the material as a result of rubber-solvent interaction, both contribute to the reduced fatigue life of the vacuum dried samples.
There is a notable difference in the stress-strain behaviour of the vacuum dried and the untreated specimens, with the vacuum dried specimens having a much stiffer initial modulus and less dynamic stored energy than the untreated samples. This particular facet of the research will require further investigation.
Further work is underway in this area of fatigue testing and elastomer swelling. Subsequent investigations will clarify the fatigue performance of elastomers swollen in different types of hydraulic media and the degree of cross-linking throughout the section of a bubble inflated specimen.

Acknowledgements
The authors would like to thank the Dublin Institute of Technology for the use of facilities in the Faculty of Engineering and the Research Support Unit in the Directorate of Research and Enterprise. They are also indebted to the Department of Experimental Physics in NUI Maynooth.

References
1. Flory, P. J., Rehner, J., "Statistical Mechanics of Cross-Linked Polymer Networks II. Swelling", J. Chem. Phys. 11, 521 (1943).
2. Treloar, L.R.G, "The Elasticity and Related Properties of Rubbers", Rubber Chemistry and Technology, Volume 47, p625-695 (1974).
3. Gul, V, Dorokhina, T.V., Dogadkin, B.A., "Changes of Fatigue Resistance of Vulcanised Natural Rubbers During Swelling", Rubber Chemistry and Technology, Volume 26, p70-77 (1953).
4. Neogi, C, Bhattacharya, A.K., Bhowmick, A.K., "Dynamic Mechanical Analysis of Carbon-Black-Filled Rubber Vulcanizates under Swollen Conditions", Rubber Chemistry and Technology, Volume 63, p651-659 (1990).
5. Hanley, J., Murphy, N., McCartin, J., Lanigan, B. McLoughlin, S., Jerrams, S.J., Clauss, G., Johannknecht, R, "Determining multiaxial fatigue in elastomers using bubble inflation", Proceedings of the 4th European Conference on Constitutive Models for Rubber, Stockholm, June 2005.
6. Porritt, B., Tiltman, H., "The Effect of Solvents on the Stress-Strain Curve of Vulcanized Rubber", Rubber Chemistry and Technology, Volume 3, p19-21 (1930).
7. Gee, "Interaction between rubber and liquids III. The swelling of vulcanised rubber in various liquids", Rubber Chemistry and Technology, Volume 16, p263-267 (1943).
8. Murphy, N. Spratt, C. Ronan, S. Jerrams, S. Johannknecht, R. "A method for determining equi-biaxial fatigue in elastomers." 3rd European Conference on Constitutive Models for Rubber (ECCMR), 2003, London, England.

9. Johannknecht, R, Jerrams, S. Clauss, G. 2002 "Determination of non-linear, large equal bi-axial stresses and strains in thin elastomeric sheets by bubble inflation". Proceedings of the Institute of Mechanical Engineers, Vol 216 Part L, No L4, (ISSN 1464-4207) Journal of Materials, Design and Applications.
10. Abraham, F, Alshuth, T, Jerrams, S. 2001 "Parameter Dependence and Prediction of Fatigue Properties of Elastomer Products". Rubber Chemistry and Technology Journal, Vol 75, Issue 4, p 365, September/October 2002.

3. J. McCartin, N. Murphy, J. Hanley, S. Jerrams, B. Lanigan, "*Determining levels of stress softening in multi-axial deformation*", Poster for German Institute of Rubber Technology (DIK) 7th Fall Rubber Colloquium (KHK 2006), Hannover, November 2006 and subsequently published in KGK Kautschuk Gummi Kunststoffe 2007.

Determining levels of stress softening in multi-axial deformation

J. McCartin[†], N. Murphy[†], J. Hanley[†], S. Jerrams[†], B. Lanigan[‡]
[†] Dublin Institute of Technology, Ireland.
[‡]National University of Ireland, Maynooth, Ireland.

Introduction

A method for obtaining stress softening data for multi-axially loaded rubber test-pieces and some preliminary results are described. Multi-axial loading was achieved by subjecting rubber disc membranes to a dynamic bubble inflation process. To produce test data allowing the calculation of complex modulus (E*) in successive cycles, a hydraulically controlled system was used to cyclically inflate and deflate the rubber membranes between preset pressure limits. Thereafter, values of E* were determined in the same manner employed by Abraham *et al* in their research into uniaxial fatigue of non-strain crystallising rubbers [1]. Stress-strain data for the upper membrane surface was acquired using an integrated optical system and associated in-house software. Graphical representation of the load cycles was used to show the reduction in rigidity in a non strain-crystallising elastomer and hence provide information about the Mullins Effect in conditions similar to those experienced by membranes in many practical situations.

Virtually all of the current information about stress softening in filled rubber is taken from uniaxial tests [2] and results are well documented. However, most rubber components are subjected to complex multi-axial loading conditions in service and uniaxial load test data is consequently unrepresentative of actual component behaviour. In order to obtain accurate predictions of dynamic viscoelastic behaviour, multi-axial testing methods are necessary. Industry has a requirement for multi-axial stress softening data. This text describes a viable method for obtaining such data and presents some preliminary results.

The research programme

The objectives of the research programme are;

1. To determine levels of stress softening in test-pieces subjected to multi-axial loading applied by the bubble inflation method.
2. To correlate these levels of stress softening to those achieved in uniaxial cyclic testing.
3. To study multi-axial stress softening phenomenon for a range of rubber compounds resulting from stress softening obtained using a process of bubble inflation.

Materials

The material used during this investigation was Ethylene-Propylene-Diene Polymer (EPDM) consisting of 110phr low activity carbon black and 70phr softener. The test-piece original configuration was a 50mm disc of 2mm thickness. The effective unclamped diameter of the specimen was 35mm.

Equipment

The rubber disc clamping method allowed an air tight seal to be formed at the disc periphery and also ensured an evenly distributed retaining force around this periphery. Consequently specimen slippage was eliminated during testing. Pressure was applied to the sample causing it to inflate in a balloon like manner. A control valve linked to a pressure sensor was used to obtain continuous cycling of the specimen between two preset pressure limits. When maximum pressure was reached on the inflation cycle, an integrated control system initiated the deflation cycle.

An optical system and in-house software, based on two charge coupled device (CCD) cameras connected to a PC, were used to record the movement of specific points on the surface of the sheet during deformation. Stress values calculated from the applied pressure and bubble geometry were simultaneously combined with the strain data from the optical system to provide multi-axial stress/strain relations over high strain ranges. This data also allowed the graphical depiction of hysteresis effects occurring during the stress softening process.

Methodology

The controlled parameter in this investigation was pressure. The rubber specimen was clamped and cycled between the preset pressure limits of 0-2 bar. Pressure is related to stress at the bubble pole by the simple relationship given in Equation 1, where p is the pressure used to inflate the specimen, t is the thickness of the rubber sheet and r is the radius of curvature.

$$\sigma = p\frac{r}{2t} \qquad (1)$$

Most mechanical tests evaluate engineering stress (σ_{eng}), where the original cross-sectional area is used in determining stress for all strain values during the test. The use of σ_{true} would provide more relevant predictions of viscoelastic behaviour. However, the stress values calculated during this study were σ_{eng} since the calculation of true stress values requires the change in the radius of curvature 'r' and the thickness of the specimen 't' to be constantly monitored. The procedure for achieving this in real time is still under development.

The use of pressure as a control parameter produces results which approximate to tests using constant maximum σ_{eng} [3] for the test specimens under investigation. For this reason initial tests using pressure as a control parameter can be taken as analogous to maximum σ_{eng} control. However, this gives rise to a situation where each subsequent cycle during the early stages of the test produces a large increase in σ_{true}.

Results

Figure 1 shows increased stress softening as the test progressed. The Mullins effect is pronounced in equi-biaxial tests due to the large increase in σ_{true} as bubble growth occurs. In order to produce data that can be compared with

existing uniaxial data for stress softening, it is necessary to control pressure in subsequent cycles to provide constant true stress ranges. Figure 2 depicts typical values of E^* plotted against accumulated cycles for uniaxial [1] and multi-axial testing. During multiaxial testing, carried out over a similar engineering stress range to those in the uniaxial tests of Abraham *et al*, the complex modulus (E*) was higher at low cycles, indicating the greater energy required to deform a test-piece multi-axially. However E^* falls more rapidly with increased cycles than in uniaxial testing and was at a similar level for both uniaxial and multi-axial specimens at higher cycles.

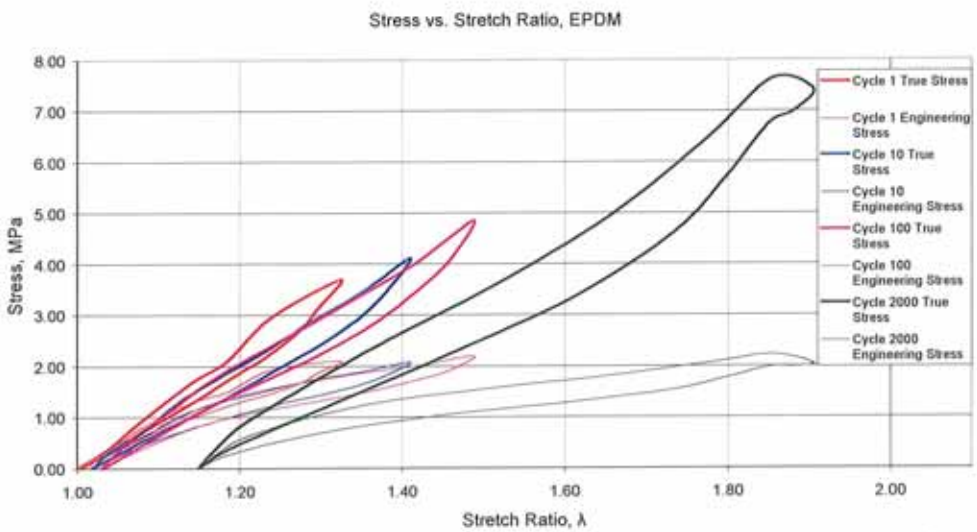

Figure 1: The Mullins effect in an EPDM sample for the 1st, 10th, 100th and the 2000th cycle of multi-axial testing

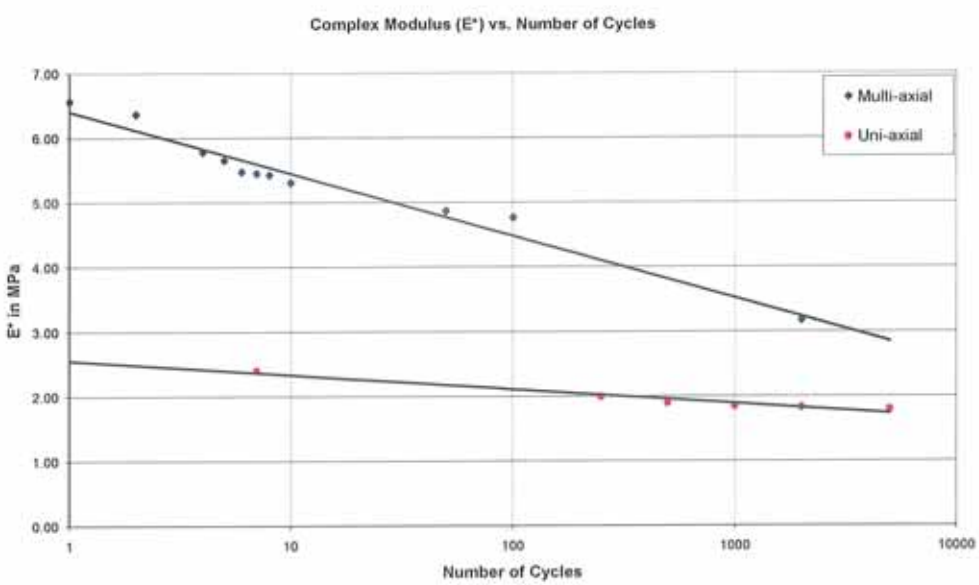

Figure 2: Graph of reduction in complex modulus against number of cycles during uniaxial [1] and multi-axial testing

Conclusions

Cyclic bubble inflation is a viable method of determining stress softening (and other viscoelastic phenomena) in multi-axial deformation of rubber. Multi-axially deformed rubbers initially exhibit greater stiffness than those strained uniaxially, but for higher accumulated cycles (> 2500) in tests on this compound, values for each method of loading converge.

In order to provide comprehensive data in respect of stress softening under multi-axial cyclic loading it is proposed that constant true stress tests be devised and carried out. Two methods are proposed.

1. Samples of the material to be tested are dynamically inflated to various pressures to obtain a relationship between the required inflation pressure and the resulting σ_{true} for specific cycles during the test. These individual tests are used to obtain a mathematical function to enable the pressure to be reduced for each subsequent inflation cycle to maintain constant σ_{true}.

2. Strain data obtained from the vision system will be used to calculate the true stress in real time during each cycle. This gives a direct method of using σ_{true} as a control parameter without the need for calibration data from pre-test samples. The difficulty with this system is that the cycle rate is limited by the time required for image capture and calculation at each control point. Methods are currently being evaluated to reduce the processing time to a practical level.

References

[1] Abraham, F, Alshuth, T, Jerrams, S. 2001 "Parameter Dependence and Prediction of Fatigue Properties of Elastomer Products". Rubber Chemistry and Technology Journal, Vol 75, Issue 4, p 365, September/October 2002

[2] Mullins, L., 1969. Softening of rubber by deformation. Rubber chem. Technol. 42, 339-362.

[3] Murphy, N., Hanley, J., McCartin, J., Lanigan, B., McLoughlin, S., Jerrams, S.J., Clauss, G., Johannknecht, R. Determining multiaxial fatigue in elastomers using bubble inflation. 4th European Conference on Constitutive Models for Rubber, Stockholm, June 2005.

4. N. Murphy, J. Hanley, H. Ali, S. Jerrams, "*The Effect of Specimen Geometry on the Multiaxial Deformation of Elastomers*", presented at the 5th European Conference on Constitutive Models for Rubber, Paris, September 2007 and subsequently as a chapter in the book 'Constitutive models for rubber V' edited by A.Boukamel, L.Laiarinandrasana, S.Méo and E.Verron, pp 61-65. (Published by Taylor & Francis, ISBN 0415454425), 2007.

The Effect of Specimen Geometry on the Multiaxial Deformation of Elastomers

N. Murphy & J. Hanley
School of Manufacturing Engineering, Dublin Institute of Technology, Dublin, Ireland.
H. Ali
School of Chemistry and Pharmaceutical Science, Dublin Institute of Technology, Dublin, Ireland.
S.J. Jerrams
Directorate of Research and Enterprise, Dublin Institute of Technology, Dublin, Ireland.

ABSTRACT: The effect of specimen thickness on the characterisation of physical properties of EPDM rubber during multi-axial deformation is presented. It has been shown that the thickness of rubber specimens loaded in uni-axial tension influences the stress-strain relationship and hence, complex modulus and tensile strength in dynamic tests. Previous research carried out by the authors involved the determination of the pressure-stress-strain relationship of multi-axially loaded elastomers in single cycle and dynamic tests. In this investigation, a series of tests were carried out on EPDM specimens of two different thicknesses, loaded in equi-biaxial tension. Elastomeric discs were bonded in a clamping device and loaded multi-axially using an automatic hydraulic pressure inflation system. Specimens were loaded to failure, both in single and multi-cycle inflation tests. The dynamic stress-strain relations were analysed to provide insight into size effect in multi-axial elastomeric deformation under cyclic loading. The change in complex modulus for a specimen at a given stress amplitude was determined and compared for two specimen thicknesses. This research is part of a larger programme investigating multi-axial material behaviour of elastomers. Further studies will be published on stress-softening, swelling phenomenon and fatigue of rubber compounds loaded in equi-biaxial tension.

1 INTRODUCTION

The difficulty in predicting stress-strain relationships for rubber is epitomised by the occurrence of increases in measured tensile strength with decreases in cross-sectional area. Bartenev and Gul (1) found disparities of 70-80% for butadiene-styrene rubber test-pieces having a range of thickness between 2.2 and 0.4 mm, while Nazeni (2) also observed this phenomenon in extensive tests.

The method of dynamic bubble inflation was used to investigate if the thickness of the test specimen influenced the multi-axial material behaviour of non-strain crystallizing rubber subjected to multiple cycles.

This text describes a series of experiments carried out on EPDM in the form of 35mm diameter test discs of two different thicknesses, which were subjected to cyclic loading, with the cycles having a controlled upper pressure limit and a lower limit of zero pressure. The stress-strain and stress-pressure relationships were determined for each specimen thickness throughout the tests and in each case the number of cycles to failure was recorded.

As the tests progressed, using constant upper pressure limits as a control parameter resulted in an increase in engineering stress in subsequent cycles.

It was necessary to introduce a control system which allowed constant engineering stress limits to be used as a control parameter. Results are presented for each specimen thickness, showing multi-axial stress softening with increasing cycles. The effect of specimen thickness is discussed with respect to change in complex modulus for similar engineering stress levels.

2 OBJECTIVES

The objectives of this investigation were:

1 To determine specimen size effect on the stress-strain behaviour of test-pieces subjected to both uni-axial and equi-biaxial tension in static tests.
2 To determine the stress-strain and stress pressure relationships for EPDM samples of 2 different thicknesses, subjected to dynamic loading conditions.
3 To determine the effect of specimen geometry on the material behaviour of elastomers subjected to multi-axial cyclic loading under constant upper engineering stress conditions.

3 MATERIALS

EPDM rubber of 70 Shore A hardness, containing 110 pphr low activity carbon black and 70 pphr softener was initially chosen for the investigation.

The bubble specimen consisted of a rubber disc having a diameter of 50 mm (35 mm clamped diameter). Two different specimen thicknesses were tested as part of the experimentation; 2mm and 1mm.

4 METHODOLOGY

Initially the uni-axial stress-strain behaviour of the two specimen thicknesses was determined by loading in uni-axial tension to failure.

Thereafter, dynamic multi-axial tests to failure were conducted. The multi-axial tests were carried out by clamping a circular specimen around its edges and applying pressure to one face of the disc causing it to inflate in a balloon like manner.

Bubble inflation is considered to comply with theory for applying pressure to a thin shell structure possessing negligible bending stiffness, alternatively described as membrane theory, where stresses and stretch ratios at the bubble pole can be determined from the local radius, applied pressure and local strains (Murphy *et al.* 2005).

Once upper pre-defined pressure limits are reached, deflation of the bubble is initiated. An optical system is used to record the movements of specific points on the surface of the sheet during this deformation. Stress values calculated from the applied pressure and bubble geometry are combined with the strain data from the optical system to provide multi-axial stress-strain relations. Figure 1 shows the displacement of specimen markings for a series of inflation and deflation cycles.

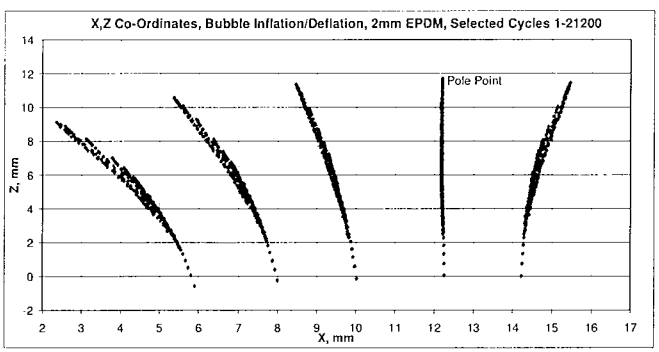

Figure 1. Displacement of specimen markings in absolute co-ordinates for selected inflation/deflation cycles.

When inflating rubbers using liquids, the properties of the liquid must be considered. If the square root of the difference between the solubility parameters of a rubber and fluid is less than 1, the rubber will swell appreciably in that fluid (Abhimanyu *et al.* 2005). Therefore, it is important to select an inflation fluid which will not cause swelling of the test-piece with the accumulation of cycles. Furthermore, the swelling effects in elastomers in contact with most liquids are less pronounced at normal ambient temperatures. Silicone based fluids will not swell EPDM appreciably. Therefore, fluids having the appropriate composition were chosen as the inflation media for the testing.

Specimens were loaded multi-axially to upper pressure limits under fully relaxing conditions until failure occurred. Stress-strain behaviour was recorded for the specimens throughout these tests.

5 TEST RESULTS AND DISCUSSION

5.1 *Single Cycle Tests to Failure*

Initially static tests were carried out on the two specimen thicknesses to look at the specimen size effects on samples tested uni-axially to failure. In addition, specimens were loaded to failure in multi-axial tension. The average maximum measured tensile strength of the two specimen types is shown in Table 1. This illustrates the variation in tensile strengths in specimens having different cross sectional areas. It should be noted that for comparison with the uni-axial results, the multi-axial values were scaled by the stretch ratio at peak stress (Johannknecht *et al.* 2002).

Table 1. Average maximum tensile strength values for the two specimen types.

Specimen Size	Uniaxial	Bubble Inflated Multi-Axial (Scaled)
	N/mm²	N/mm²
2 mm	5.78	4.67
1 mm	7.40	4.99

5.2 *Multi-axial Fatigue Tests*

Figure 2 shows fatigue results for the two specimen thicknesses cycled between constant pressure limits under fully relaxing conditions. Unsurprisingly, the 2mm specimens exhibited greater fatigue resistance when subjected to higher pressure amplitudes.

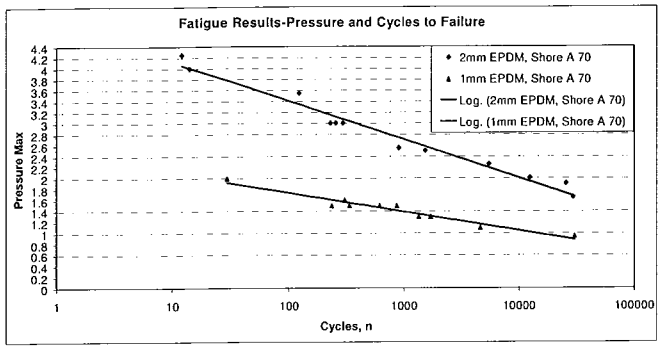

Figure 2. Pressure Amplitude versus log of cycles to failure for 1mm, and 2mm specimens.

The stress-strain behaviour of both sets of samples was analysed in two different regions of the pressure versus cycles shown in Figure 2. The first was defined as the high pressure-rapid failure region (0-2000 cycles) and the second defined as the medium-term region (10000-30000 cycles).

5.2.1 *Stress-Strain Behaviour - Rapid Failures*

The samples analysed in the rapid failure region had comparable engineering stress levels for the first stress cycle.

The stress-strain curves for a 1mm specimen loaded between constant pressure limits of 0-1.35 Bar is shown in Figure 3. The engineering stress increased continually throughout the test until failure occurred.

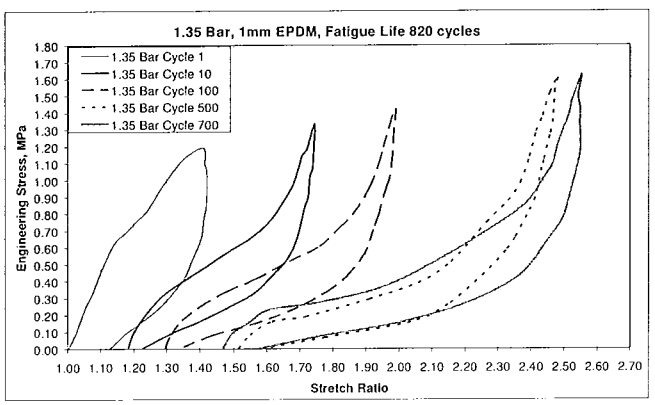

Figure 3. Low fatigue life behaviour at constant pressure, 1mm specimen.

A plot of stress strain behaviour for a 2mm specimen is depicted in Figure 4. The specimen was subjected to similar engineering stresses to those for the 1mm sample in the first cycle of the test. However, the increase in engineering stress and set in the 2mm sample occurred at a slower rate than in the 1mm test-pieces.

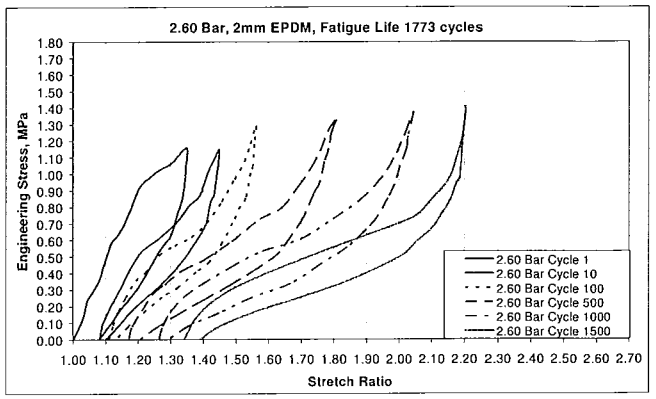

Figure 4. Low fatigue life behaviour at constant pressure, 2mm specimen.

5.2.2 *Stress-Strain Behaviour - Medium Failures*

Following analysis of the rapid failure specimens, medium-term failures were analysed. Again, specimens were chosen having similar upper engineering stress levels in the first cycle.

The results for a 1mm specimen are shown in Figure 5. In this case the upper engineering stress did not increase appreciably during the early stages of the test. However, an 11% increase in engineering stress occurred by cycle 4000 and there was a 25% increase by cycle 10150.

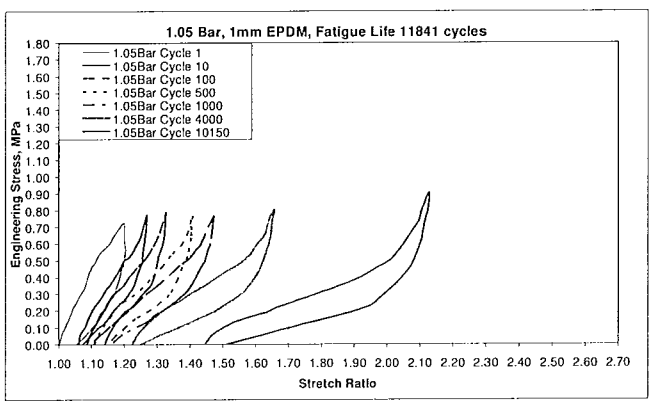

Figure 5. Medium fatigue life behaviour at constant pressure, 1mm specimen.

The upper stresses in the 2mm specimens in the medium failure region did not increase as rapidly as in the 1mm specimens, as Figure 6 illustrates.

The upper stresses in the 2mm specimens in the medium failure region stay relatively constant up to 10000 cycles. However, when long term cyclic testing was undertaken, it can be seen that large increases in engineering stress occurred during the latter half of the test.

When 4000 cycles had been accumulated, there was a 10% increase in engineering stress. The stress continues to climb throughout the test and at 25200 cycles; 500 cycles before failure, the stress had increased by over 50% of the initial engineering stress value.

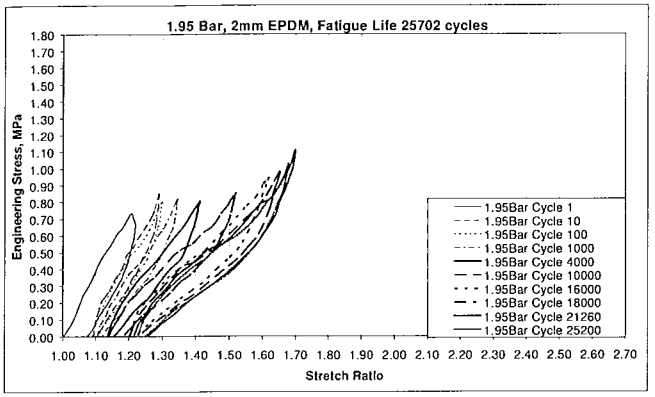

Figure 6. Medium fatigue life behaviour at constant pressure, 2mm specimen.

These increases in engineering stress with cycles are studied more closely in Figure 7. It was found that the 2mm specimens allowed more cycles to be accumulated with a less pronounced increase in engineering stress which did not occur until later in the cycle. This can be attributed to reduction in the amount of set that took place in the material with cycling, leading to lower increases in bubble radius at peak pressures.

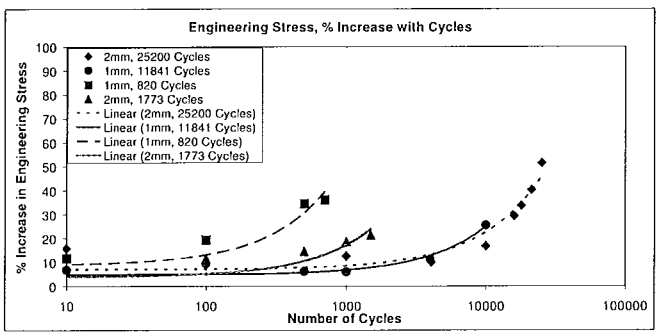

Figure 7. Percentage increase in engineering stress with cycles for 1mm and 2mm specimens.

5.3 *Controlled Engineering Stress Tests*

Following the tests at constant pressure, specimens were subjected to fatigue tests using constant engineering stress as the upper control limit. Figure 8 shows the change in stress-strain response for a 2mm specimen subjected to the same upper engineering stress as that in the initial inflation cycle of the first pressure controlled 2mm specimen, shown in Figure 4. As can be seen, the fatigue life when constant engineering stress control was used increased to 2722 cycles, as opposed to 1773 cycles when constant pressure control was used.

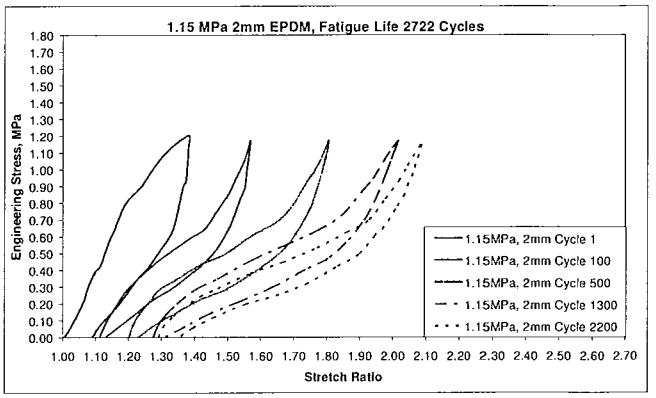

Figure 8. 2mm sample cycled between constant engineering stress limits, selected cycles 1-2200.

When specimens of different thicknesses were subjected to dynamic cycling, controlled at similar upper engineering stress limits, the effect of specimen geometry became apparent. This is illustrated in Figure 9, where stress softenening occurred in the 1mm specimens at a greater rate than that of the 2mm test-pieces. Note the close agreement between the initial modulus values given by the slope of the loading curve in the first cycle.

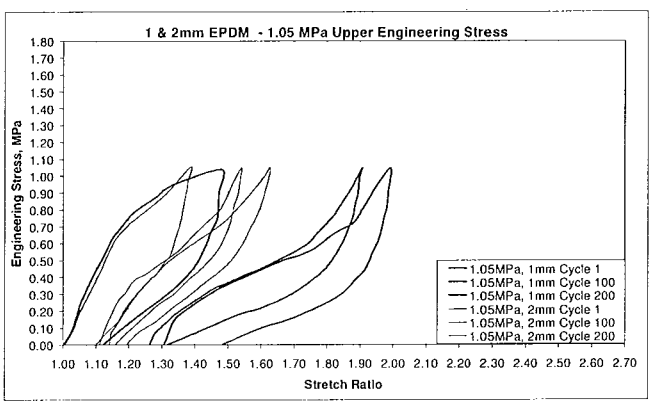

Figure 9. 1mm and 2mm samples cycled between constant engineering stress limits cycles, 1-200.

6 CONCLUSIONS

It was shown that when constant pressure is used as a control mechanism during dynamic cycling of multi-axially loaded EPDM test-pieces, engineering stress increased throughout the test for a given applied pressure. However, for initial test cycles, constant pressure control can gave a reasonable approximation of constant engineering stress control and thus can be used to investigate multi-axial stress softening for a discrete number of cycles, allowing valid material models to be obtained.

Specimen size selection was shown to have a large influence on the above phenomenon. For the material used, 2mm test-pieces exhibited less set, stress softening and as a consequence, less increases in peak stress with the accumulation of cycles than 1mm samples when the two specimen geometries

were analysed with respect to similar first cycle upper stresses.

In summary, constant engineering stress control is essential where accurate long-term lifetime predictions for components subjected to complex loading is required. However, for short-term testing, good agreement exists between the engineering stress levels for tests controlled by constant pressure and tests controlled by constant engineering stress.

It is important when using constant engineering stress control, to consider the influence of specimen geometry. The rate of decrease of complex modulus was shown to be greater in 2mm samples cycled at comparable peak engineering stress levels than in 1mm samples, but further testing of this behaviour is required and these tests should be extended to other compounds

7 PROPOSED FURTHER WORK

Further analysis of multiaxial fatigue will incorporate investigation into the structure of the failure surface of specimens fatigued multi-axially using constant stress control. In addition, results will be published on fatigue resistance in swollen rubbers loaded in equi-biaxial tension.

8 ACKNOWLEDGEMENTS

The authors would like to thank the Faculty of Engineering and the Directorate of Research and Enterprise in the Dublin Institute of Technology.

This work was made possible by funding from Enterprise Ireland under its 'Proof of Concept' programme.

REFERENCES

Abhimanyu, P., Coolbaugh, T. 2005. Elastomers: A Literature Review With Emphasis on Oil Resistance. *Rubber Chemistry and Technology*, 78: 516.

Abraham, F, Alshuth, T, Jerrams, S. 2002. Parameter Dependence and Prediction of Fatigue Properties of Elastomer Products. *Rubber Chemistry and Technology* 75(4): 365.

Bartenev, G.M., Gul, V.E. 1961. *Soviet Plastics* 1: 46.

Hanley, J., Murphy, N., 2007. Swelling Effects in Multiaxial Fatigue of Elastomers, *Presentation at Polymeric Materials in Automotive, PMA 2007*, Bratislava, Slovakia.

Johannknecht, R, Jerrams, S. Clauss, G. 2002. Determination of non-linear, large equal bi-axial stresses and strains in thin elastomeric sheets by bubble inflation. *Proceedings of the Institute of Mechanical Engineers, Journal of Materials, Design and Applications* 216(Part L, No L4), (ISSN 1464-4207).

Mars, W. V., Fatemi, A. 2004. Factors that affect the Fatigue Life of Rubber: A Literature Survey. *Rubber Chemistry and Technology* 77: 391-412.

Mott, P., Roland, C. M., Hassan, S. 2003. Strains in an Inflated Rubber Sheet. *Rubber Chemistry and Technology* 76: 326-333.

Murphy, N. Spratt, C. Ronan, S. Jerrams, S. Johannknecht, R. 2003. A method for determining equi-biaxial fatigue in elastomers. *3rd European Conference on Constitutive Models for Rubber (ECCMR)*, London, England.

Murphy, N., Hanley, J., McCartin, J., Lanigan, B., McLoughlin, S., Jerrams, S., Clauss, G., Johannknecht, R. 2005. Determining multiaxial fatigue in elastomers using bubble inflation. *4th European Conference on Constitutive Models for Rubber (ECCMR)*, Stockholm.

Nazeni, D.I. 1960. *Deutsche Kautshauk-Gesellschaft*, Vortragstagung, Berlin.

D412-06a. 2006. Standard Test Methods for Vulcanized Rubber and Thermoplastic Elastomers-Tension, ASTM Book of Standards Volume: 09.01.

D471-06. 2006. Standard Test Method for Rubber Property-Effect of Liquids, ASTM Book of Standards Volume: 09.01. 1.

5. J. Hanley, N. Murphy, H. Ali, S. Jerrams, "*Swelling Effects in Multiaxial Fatigue of Elastomers*", (Paper presented at Polymeric Materials in Automotive, Bratislava, May 2007 and awaiting publication in Polymers for Advanced Technologies (In Press).

Swelling Effects in Multiaxial Fatigue of Elastomers

J. Hanley[1*], N. Murphy[1], H. Ali[2], S. Jerrams[3]
[1]*School of Manufacturing and Design Engineering, Dublin Institute of Technology, Dublin, Ireland.*
[2]*School of Chemistry and Pharmaceutical Science, Dublin Institute of Technology, Dublin, Ireland.*
[3]*Directorate of Research and Enterprise, Dublin Institute of Technology, Dublin, Ireland.*

email: John Hanley (john.hanley@dit.ie)

*Correspondence to J. Hanley, School of Manufacturing and Design Engineering, Dublin Institute of Technology, Dublin, Ireland.

Keywords
Elastomers • Swelling • Fatigue

Abstract
This paper describes more fully the dynamic behaviour of rubber with respect to oil resistance for non-strain crystallising elastomers cycled to fatigue in multi-axial tension between constant pressure limits. A series of dynamic tests were carried out on two types of EPDM specimens, the first type was not subjected to any pre-treatment, while the second type was subjected to oil swelling. Swollen specimens were prepared by immersing them in reference mineral oil for a specified duration and temperature and the degree of swelling was calculated for each specimen. Following this, both sets of test-pieces were cycled to failure, using a bubble inflation system, with a constant pressure control system. The stress-pressure relationship was determined for both the swollen and unswollen specimens. Test pressures were selected which allowed comparable levels of maximum engineering stress to be applied to each specimen type. The number of cycles to failure for a given maximum stress amplitude was plotted for both dry and swollen specimens. Each specimen type was analysed at a given engineering stress amplitude and changes in complex modulus with the accumulation of cycles were compared. The fatigue resistance of the EPDM was significantly reduced in the swollen state. However, the rate of decrease in complex modulus at a given cyclic stress was found to be greater in the unswollen sample.

Introduction

In terms of oil and rubber compatibility, it is important to consider that in any practical application both the oil and the rubber are made up of several different components. The compatibility can be made complex by such variables as fillers and plasticisers, rubber molecular structure, selective swelling action by fluid components, time-temperature effects on swelling rates and chemical degradation of the elastomer or fluid. All rubber will swell to some extent in oil (Abhimanyu *et al.* (2005)), but the degree of swelling can be estimated for a particular oil-rubber combination, if the solubility parameters δ, for both substances are known. If the square root of the difference between the

solubility parameters of the rubber and the oil is less than one, then the rubber will swell appreciably in that oil. It is clear that there can be difficulties in accurately determining the solubility parameter for a fluid when it consists of two or more fractions. Previous research (Beerbower *et al.* (1964)) discovered by experiment that the solubility parameter for a hydraulic fluid may be estimated from known physical properties which are readily available. The experiments allowed the relationship between the solubility parameter and the aniline point of the oils being tested to be plotted as an empirical linear relationship. In order to best demonstrate the effects of swelling in typical hydraulic oils it is therefore necessary to use hydraulic fluids where the properties have been determined and can be used as a reference. From the ASTM standards for rubber liquid compatibility, the reference oil IRM 903 is the most appropriate choice for use as a high swelling oil for the physical testing of swollen rubbers. Its aniline point has been determined and can be compared with the solubility parameter for the test material to allow rubber-liquid compatibility to be gauged. Moreover, it is generally comparable with typical hydraulic oils in terms of liquid properties. The properties of the oil are summarised in Table 1.

In terms of fatigue of swollen elastomers, previous research (Gul et al. (1959)) investigated the phenomenon of fatigue resistance for constant 'stress-work' amplitudes with a range of degrees of swelling for a given rubber-solvent combination, using rubber plasticisers as the solvents. The results of these uniaxial tests showed that the relative fatigue resistance of the natural rubber decreased with an increase in the degree of swelling, regardless of the rubber-solvent combination used.

Further work on fatigue of swollen rubber (Cho et al. (2000)), investigated fatigue crack growth of elastomers on two types of SBR swollen in mineral oil and fatigue tested under conditions which replicated pure shear with sharp stress raisers (pre-cracks) and strains applied cyclically at magnitudes of 10-35%. Tearing energy and crack growth rate were measured and compared against specimens that were not swollen. The study found that the fatigue resistance of the elastomers was decreased in the presence of low-viscosity fluid, in proportion to the degree of swelling. This variation of the fatigue resistance of an elastomer in the swollen state was due to the reduction in viscoelastic energy loss and sharpening of the crack tip when the swollen.

The tests presented in this work differ from those of Gul and Cho in a number of respects. Firstly, test frequencies were maintained at 1Hz, as opposed to frequencies in excess of 4 Hz, which would have led to heat build-up and consequent thermal degradation (Seldén, R., (1995)). Secondly, virtually all components are complexly loaded in service, so constant stress-work or simulated pure shear do not give a complete picture of the fatigue behaviour of swollen elastomers. Many rubber parts can be at risk from oil contamination, where component reliability may be compromised in the event of a fluid leak in service. EPDM components are commonly used in automotive applications, where they have the advantage of having more functionality at higher temperatures than SBR or natural rubber. However, these advantages are offset by their poor resistance to numerous fluids used in vehicles. By using reference oils, the properties of the oil are comparable such fluids and the parameters of the swelling liquid can be reported with the test results.

Experimental

EPDM rubber of 70 Shore A hardness, containing 110 pphr low activity carbon black and 70 pphr softener was initially chosen for the investigation. The bubble specimen consisted of a rubber disc having a thickness of 2mm and a diameter of 50 mm (35 mm clamped diameter). Dynamic multi-axial tests were carried out by clamping a circular specimen around its edges and applying pressure to one face of the disc causing it to inflate in a balloon like manner. Bubble inflation is considered to comply with theory for application of pressure to thin shell structures possessing negligible bending stiffness, alternatively described as membrane theory, where stresses and stretch ratios at the bubble pole can be determined from the local radius, applied pressure and local strains (Murphy *et al.* 2005). The relationship between pressure, bubble radius and surface strain is illustrated in Figure 1.

Before the tests started, pre-defined pressure limits were selected. Thereafter, the specimen was inflated and deflated between these pressure limits. During these deformations, the movements of markings on the surface of the sheet were recorded using an automatic vision system. Stress values calculated from the applied pressure and bubble geometry were combined with the strain data from the optical system to provide multi-axial stress-strain relations.

When inflating rubbers using liquids, the swelling potential of the inflation media must be taken into account. Silicone based fluids will not swell EPDM appreciably. Following swelling tests to confirm this, fluids of this composition were chosen as the inflation media and all fatigue tests were carried out at temperatures of 15°C. Firstly, the unswollen tests-pieces were fatigued to failure under multi-axial loading conditions. Stress-strain relations were recorded at different cycles and the cycles to failure were noted for each specimen.

Swelling experiments were carried out by immersing the specimens in reference oil IRM 903, at an elevated temperature of 100°C for a period of one hour. The specimens were removed from the hot oil and cooled in oil at ambient temperature for a short period, before being wiped dry and weighed. An average swelling ratio of 1.11 (11% increase in mass) was calculated for the samples. Following swelling calculations, the swollen test-pieces were inflated to failure under multi-axial fatigue loading, again using silicone fluid to inflate the test-pieces.

Results

The relationship between applied pressure and measured engineering stress was used to generate plots of stress-amplitude versus cycles to failure for both the swollen and unswollen test-pieces. The pressure-stress relationship for the swollen rubber is shown in Figure 2. The plot of stress amplitude versus cycles to failure is shown in Figure 3. Unsurprisingly, the unswollen specimens exhibited greater fatigue resistance by comparison with the swollen test-pieces. This can be partially attributed to the swollen test-pieces having a larger bubble radius and hence a higher engineering stress for a given applied pressure. It should be noted however, that the two curves began to converge at higher cycles, as the test progressed.

When considering stress-strain behaviour, the unswollen test-pieces exhibited higher stiffness than the swollen specimens over the stress ranges applied in the testing. This is shown in Figure 4, where the change in the deformation behaviour of the two sample types is shown for cycles 10 and 1000, for a maximum engineering stress of 0.6 MPa.

The change in complex modulus G* for these two specimens is shown in Figure 5. The initial modulus of the unswollen test-piece is greater than that of the swollen specimen. However, the rate of decrease in modulus is greater in the unswollen specimens than that of the swollen specimen with the accumulation of cycles.

Discussion

Results are presented showing the effect on mechanical properties of specimens exposed to oil for relatively short durations at temperatures comparable to those that a component may be subjected to in service. The fatigue life of an EPDM sample under dynamic multi-axial loads can be greatly reduced in the presence of the oil, even for relatively small amounts of swelling. The lower fatigue lives of the swollen specimens can be attributed to a number a factors, both physical and chemical in nature. Physical factors include higher tensile stresses for a given applied pressure and a lower initial complex modulus following swelling. Chemical factors include changes in the network structure due to swelling, where there is a reduction in the number of chains resisting the tensile force, while the reformation of polysulphidic linkages during a loading cycle can be inhibited in the presence of swelling fluid.

The change in complex modulus for each test-piece type at a given engineering stress was investigated and it was found that the rate of decrease of G* was greater in the unswollen specimens. This could be attributed to breakdown of filler-filler interactions in the unswollen specimens, which would have occurred prior to testing in the swollen specimens due to the swelling action of the oil. As previously stated, the results presented were obtained using a system which cycled the specimens using constant pressure control. While the specimens stay within acceptable constant engineering stress limits for a significant portion of the fatigue life of the sample, it has been shown (Murphy *et al.* (2007)) that there can be increases in the value of the engineering stress in later cycles in the test. Further results will be presented, where engineering stress limits are precisely maintained. This will allow more accurate assessments of the changes in complex modulus with cycles to specimen failure. Additionally the morphology of the failure surface of each specimen will be compared and analysed.

Acknowledgements

The authors would like to thank the Faculty of Engineering and the Directorate of Research and Enterprise in the Dublin Institute of Technology.

This work was made possible by funding from Enterprise Ireland under its 'Proof of Concept' programme.

References

1. Abhimanyu, P., Coolbaugh, T. Elastomers: A Literature Review With Emphasis on Oil Resistance. *Rubber Chemistry and Technology*. 2005; **78**: 516.
2. Beerbower, A., Pattison, D.A., Staffin, G.D. Predicting Elastomer-Fluid Compatibility For Hydraulic Systems, *Rubber Chemistry and Technology*. 1964; **37**: 246-260.
3. Gul, V., Fedyukin, D., Dogadkin, B.A. The Influence of Intermolecular Action on the Dynamic Fatigue of Rubbers. *Rubber Chemistry and Technology*. 1959; **32**: 454-462.

4. Cho, K., Wook, J.J., Daeho, L., Hyunaee, C., Young-Wook, C. Fatigue crack growth of elastomers in the swollen state. *Polymer*. 2000; **41**: 179-183.
5. Seldén, R. Fracture Mechanics Analysis of Fatigue of Rubber-A Review. *Progress in Rubber and Plastics Technology*. 1995; **11(1)**, The Institute of Materials/RAPRA.
6. Murphy, N., Hanley, J., Ali, H., Jerrams, S., "The Effect of Specimen Geometry on the Multiaxial Deformation of Elastomers", *5th European Conference on Constitutive Models for Rubber (ECCMR)*, Awaiting Publication.
7. D471-06. 2006. Standard Test Method for Rubber Property-Effect of Liquids, ASTM Book of Standards Volume: 09.01.
8. Murphy, N., Hanley, J., McCartin, J., Lanigan, B., McLoughlin, S., Jerrams, S., Clauss, G., Johannknecht, R. Determining multiaxial fatigue in elastomers using bubble inflation. *4th European Conference on Constitutive Models for Rubber (ECCMR)*. 2005; Stockholm.
9. Murphy, N. Spratt, C. Ronan, S. Jerrams, S. Johannknecht, R. A method for determining equi-biaxial fatigue in elastomers. *3rd European Conference on Constitutive Models for Rubber (ECCMR)*. 2003; London, England.
10. Johannknecht, R, Jerrams, S. Clauss, G. Determination of non-linear, large equal bi-axial stresses and strains in thin elastomeric sheets by bubble inflation. Proceedings of the Institute of Mechanical Engineers, *Journal of Materials, Design and Applications*. 2002; 216(Part L, No L4), (ISSN 1464-4207).
11. Mars, W. V., Fatemi, A. Factors that affect the Fatigue Life of Rubber: A Literature Survey. *Rubber Chemistry and Technology*. 2004; **77**: 391-412.
12. D412-06a. 2006. Standard Test Methods for Vulcanized Rubber and Thermoplastic Elastomers-Tension, ASTM Book of Standards Volume: 09.01.
13. Federal Motor Vehicle Safety Standards and Regulations No. 116 - Motor Vehicle Brake Fluids.

Tables and Illustrations

	IRM 903
Boiling Point	> 249°C
Vapour Pressure	<0.001 mm Hg @ 20°C
Specific Gravity	0.92 (Water = 1)
Molecular Weight	319
Viscosity	33.3 cST @ 99°C
Aniline Point	70.6°C

Table 1. Properties of reference oil used in tests.

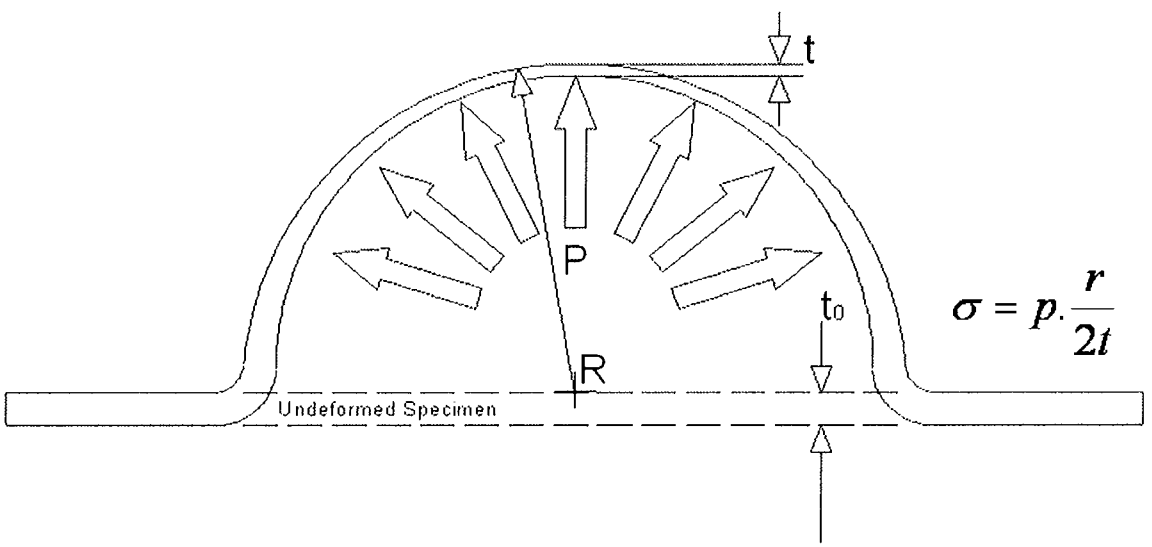

Figure 1. Geometric and physical relations for an inflated bubble.

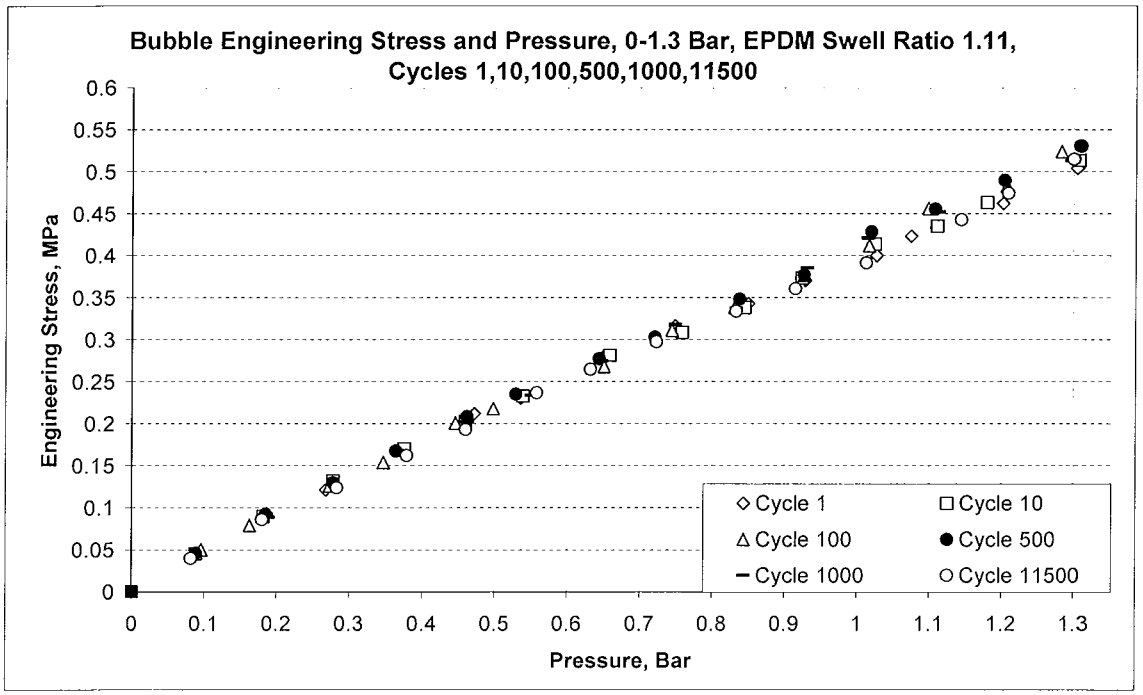

Figure 2. Pressure-Engineering Stress relationship for swollen rubber (0-0.6 MPa).

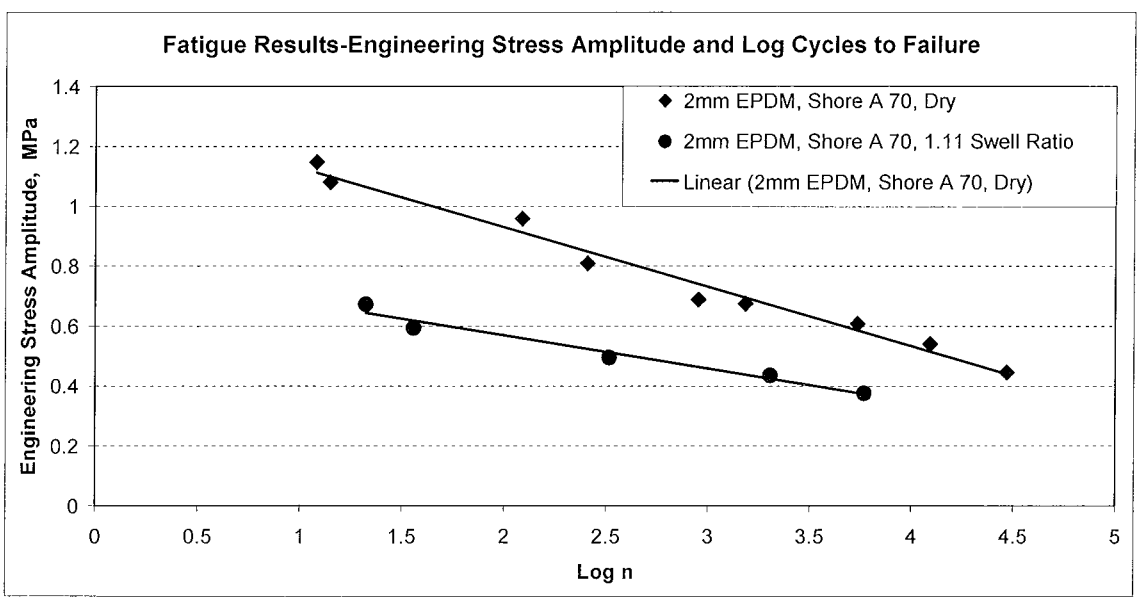

Figure 3. Stress amplitude versus cycles to failure, swollen/unswollen EPDM.

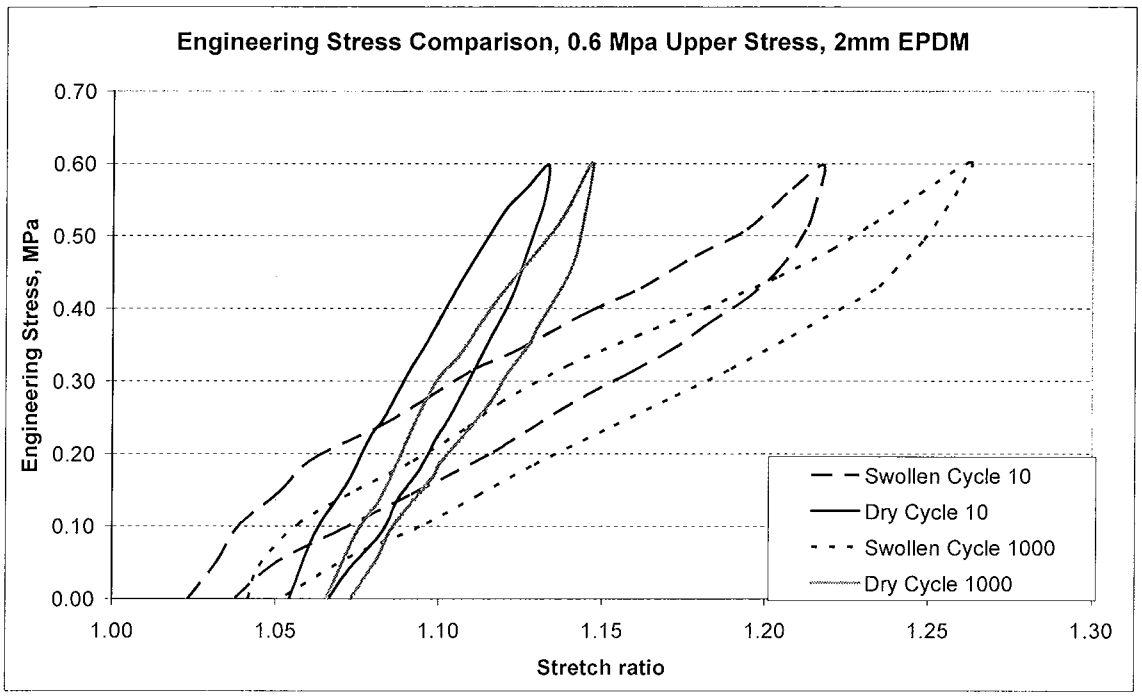

Figure 4. Stress-strain curves, swollen and unswollen EPDM, 0.6 MPa upper engineering stress, cycles 10 and 1000.

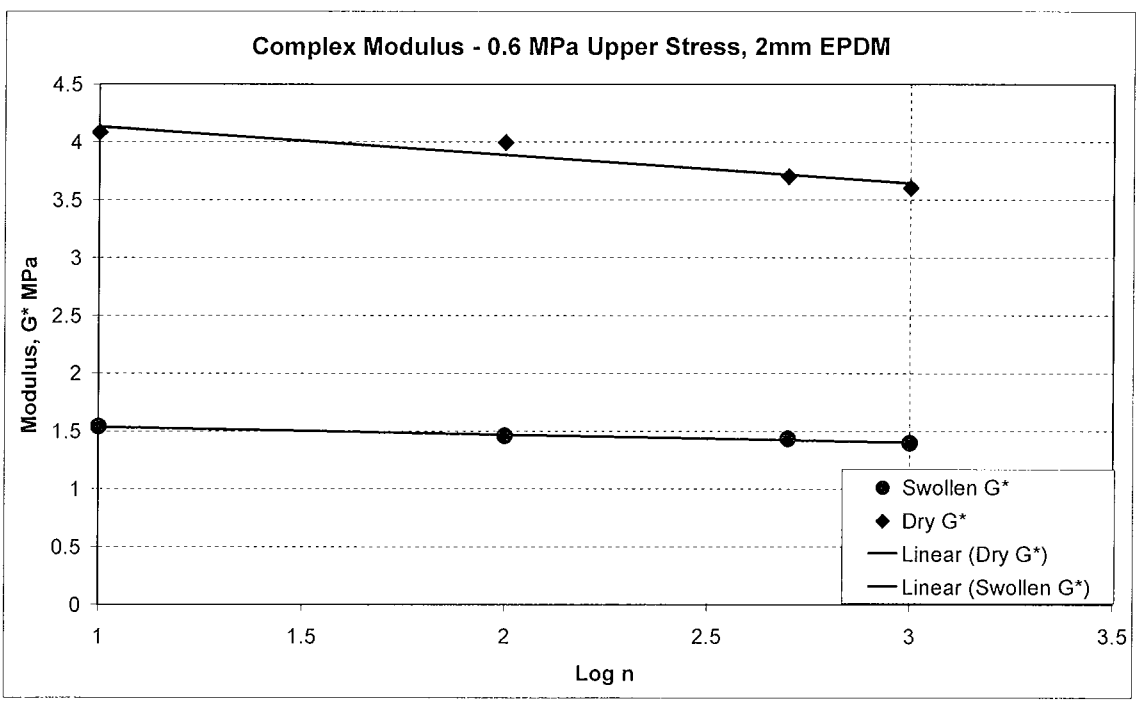

Figure 5. Changes in complex modulus, swollen and unswollen EPDM, 0.6 MPa upper engineering stress, selected cycles 1-1000.

6. J. Hanley, N. Murphy, H. Ali, S. Jerrams, "*The Effect of Oil Swelling on the Fatigue Life of Elastomers subjected to Multi-axial Fatigue using Bubble Inflation*", 11th International Seminar of Elastomers ISE 2007, Freiberg, Germany, September 2007 and awaiting publication in KGK Kautschuk Gummi Kunststoffe (In Press).

Elastomer · Swelling · Fatigue · Bubble inflation

This paper describes the behaviour of rubber in multi-axial fatigue, with respect to oil resistance. A series of tests were carried out on EPDM specimens subjected to varying degrees of swelling. The control methodology and the loading mechanism employed in the testing of elastomers using dynamic multi-axial bubble inflation are outlined. Swollen specimens were cycled to failure and the results were analysed. The number of cycles to failure for a given engineering stress amplitude was plotted for both unswollen and swollen specimens. Fracture surfaces for each set of specimens were analysed. The effect of swelling on the stress-strain behaviour and the change in complex modulus for each specimen set is discussed.

Der Einfluss der Ölquellung auf die Lebensdauer von Elastomeren im zyklischen Aufblasversuch

Elastomer · Quellung · Ermüdung · Aufblasversuch

In der Arbeit wird das Verhalten von Elastomeren im multilaxialen Ermüdungsversuch im Hinblick auf die Ölbeständigkeit eingehender beschrieben. Eine Reihe von Versuchen wurden mit unterschiedlich gequollenen EPDM Proben durchgeführt. Versuchsbedingungen und Auswertung wurden beschrieben. Gequollene Proben wurden bis zum Versagen zyklisch belastet. Die Anzahl der Zyklen bei konstanter Spannungsamplitude wurde für nichtgequollene wie für gequollene Proben aufgetragen. Die Bruchflächen wurden für jede Serie von Proben untersucht. Der Einfluss der Quellung auf das Zug-Dehnungsverhalten und die Änderungen des komplexen Moduls wird für jede Probe beschrieben.

The Effect of Oil Swelling on the Fatigue Life of Elastomers Subjected to Cyclic Bubble Inflation[1]

Most rubber components are subjected to fatigue conditions. In addition, there are cases where such components may be at risk from oil contamination. In such cases performance of the part in question may be severely compromised if the rubber and the fluid are compatible in terms of swelling potential. EPDM components are commonly used in automotive applications, where they have the advantage of having more functionality at higher temperatures than SBR or natural rubber. However, these advantages are offset by their poor resistance to numerous fluids used in vehicles. By using reference oils, their properties are comparable with such fluids and the parameters of the swelling liquid can be reported with the test results. While there have been previous studies into the fatigue behaviour of swollen rubber, none of these have considered repeated multi-axial loading. Few components are loaded uniaxially and rubbers are quite different materials when loaded multi-axially, due to the orientation of long chain molecules. The fundamental question this study addresses is whether altering the rubber filler matrix by the introduction of a swelling agent affects the multi-axial fatigue behaviour of the rubber. These tests allow quantification of the damage and the effect that swelling has on the fatigue life of EPDM. In order to fully evaluate the problems presented, parallel investigations were carried out to investigate the influence of swelling in multi-axial fatigue. Firstly, it was proposed to conduct fatigue tests on EPDM test-pieces, with one specimen set untreated and the other subjected to swelling before testing. These fatigue tests were carried out on both sets of test-pieces using equal pressure and subsequently equal stress amplitudes. Secondly, the structures of both sets of specimens at failure were studied to determine the effects of swelling on the fracture surfaces.

Theory

In terms of oil and rubber compatibility, it is important to consider that in any practical application both the oil and the rubber are made up of several different components. The compatibility can be made complex by such variables as fillers and plasticisers, rubber molecular structure, selective swelling action by fluid components, time-temperature effects on swelling rates and chemical degradation of the elastomer or fluid. All rubber will swell to some extent in oil [1], but the degree of swelling can be estimated for a particular oil-rubber combination, if the solubility parameters δ, for both substances are known. If the square root of the difference between the solubility parameters of the rubber and the oil is less than one, then the rubber will swell appreciably in the oil. It is clear that there can be difficulties in accurately determining the solubility parameter for a fluid when it consists of two or more fractions. Previous research [2] found that the solubility parameter for a hydraulic fluid may be estimated from known physical properties which are readily available. The experiments allowed the relationship between the solubility parameter and the ani-

[1] Presented at the ISE 2007, September 23.-27., Freiburg, Germany

Authors

J. Hanley, N. Murphy, H. Ali, S. Jerrams, Dublin (Ireland)

Corresponding author:
John Hanley
Dublin Institute of Technology
School of Manufacturing
and Design Engineering
Block E, Room 629
Bolton Street
Dublin 1
E-mail: john.hanley@dit.ie

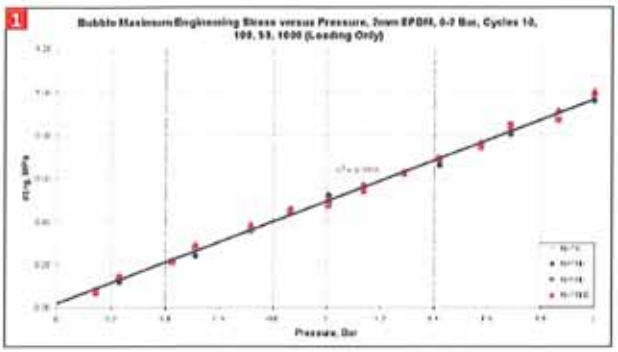

1 Plot of bubble pole stress versus inflation pressure for dry EPDM, selected cycles, 1-1000

line point of the oils being tested to be plotted as an empirical linear relationship. In order to best demonstrate the effects of swelling in typical hydraulic oils it is therefore necessary to use hydraulic fluids where the properties have been determined and can be used as a reference. From the ASTM standards for rubber liquid compatibility, the reference oil IRM 903 is the most appropriate choice for use as a high swelling oil for the physical testing of swollen rubbers. Its aniline point has been determined and can be compared with the solubility parameter for the test material to allow rubber-liquid compatibility to be gauged. Moreover, it is generally comparable with typical hydraulic oils in terms of liquid properties.

In terms of fatigue of swollen elastomers, previous research [3] investigated the phenomenon of fatigue resistance for constant 'stress-work' amplitudes with a range of degrees of swelling for a given rubber-solvent combination, using rubber plasticisers as the solvents. The results of these uniaxial tests showed that the relative fatigue resistance of the natural rubber decreased with an increase in the degree of swelling, regardless of the rubber-solvent combination used. Further work on fatigue of swollen rubber [4], investigated fatigue crack growth of elastomers on two types of SBR swollen in mineral oil and fatigue tested under conditions which replicated pure shear with sharp stress raisers (pre-cracks) and strains applied cyclically at magnitudes of 10-35 %. Tearing energy and crack growth rate were measured and compared against specimens that were not swollen. The study found that the fatigue resistance of the elastomers was decreased in the presence of low-viscosity fluid in proportion to the degree of swelling. This variation of the fatigue resistance of an elastomer in the swollen state was due to the reduction in viscoelastic energy loss and sharpening of the crack tip when the rubber was swollen. The tests presented in this work differ from those referenced in a number of respects. Firstly, test frequencies were maintained at 1 Hz, as opposed to frequencies in excess of 4 Hz, which would have led to heat build-up and consequent thermal degradation [5]. Secondly, virtually all components are complexly loaded in service, so constant stress-work or simulated pure shear do not give a complete picture of the fatigue behaviour of swollen elastomers.

Test procedure

Materials

EPDM rubber of 70 Shore A hardness, cross-linked with sulphur and containing low activity carbon black was first chosen for the investigation. Initially dry (unswollen) specimens were fatigued to failure with a zero minimum load. Dynamic multi-axial tests were carried out by clamping a circular specimen having a thickness of 2 mm and a clamped diameter of 35 mm around its edges and applying pressure to one face of the disc causing it to inflate in a balloon like manner.

Swelling tests

When inflating rubbers using liquids, the swelling potential of the inflation media must be taken into account. Silicone based fluids will not swell EPDM appreciably [6]. Following swelling tests to confirm this, such a fluid was chosen as the inflation medium and all fatigue tests were carried out at temperatures of 15 °C. Firstly, the unswollen test-pieces were fatigued to failure under multi-axial loading conditions. Stress-strain relations were recorded at different cycles and the cycles to failure were noted for each specimen.

Swelling experiments were carried out by immersing the specimens in reference oil IRM 903, at an elevated temperature of 100 °C for a period of one hour. The specimens were removed from the hot oil and cooled in oil at ambient temperature for a short period, before being wiped dry and weighed [7]. An average swelling ratio of 1.10 (10 % increase in mass) was calculated for the samples, where the swelling ratio Q can be expressed as,

$$Q = W_s / W_d, \quad (1)$$

where W_s is the weight of the swollen elastomer sample and W_d is the weight of dry elastomer before swelling. Following swelling calculations, the swollen test-pieces were inflated to failure under multi-axial fatigue loading, again using silicone fluid to inflate the test-pieces.

Multi-axial fatigue tests – Development of test procedure

Bubble inflation is considered to comply with theory for application of pressure to thin shell structures possessing negligible bending stiffness, alternatively described as membrane theory. Stresses at the bubble pole can be determined from the local radius and applied pressure using equation [2]:

$$\sigma = PR/2t \quad (2)$$

Where P is the pressure, R is the radius at the bubble pole and t is the original sheet thickness.

Local stretch ratios at the pole can be determined using equation [3]:

$$\lambda = ((x_{cir} - x_{orig})/x_{orig}) + 1 \quad (3)$$

Where λ is the principal stretch ratio, x_{cir} is the circumferential point spacing at the bubble pole and x_{orig} is the original point spacing.

Prior to fatigue testing, pre-defined pressure limits were selected. Thereafter, the specimen was inflated and deflated between these limits. During these deformations, the movements of markings on the surface of the sheet were recorded and stress and strain values were calculated from the applied pressure and measured bubble geometry. Initial tests were carried out using constant pressure as a control parameter for the fatigue tests. This was based on calculating the engineering stress from plots of pressure versus stress for selected loading cycles, where the relationship was found to be approximately linear up to 1000 cycles, as illustrated in Figure 1.

Subsequent analysis of the stress-strain behaviour of the fatigued samples showed that when constant pressure was used as a control mechanism during dynamic cycling of the EPDM test-pieces, engineering stress increased throughout the test for a given applied pressure. This is illustrated in Figure 2, where a sample loaded to an initial first cycle stress of 0.7 MPa showed a continued

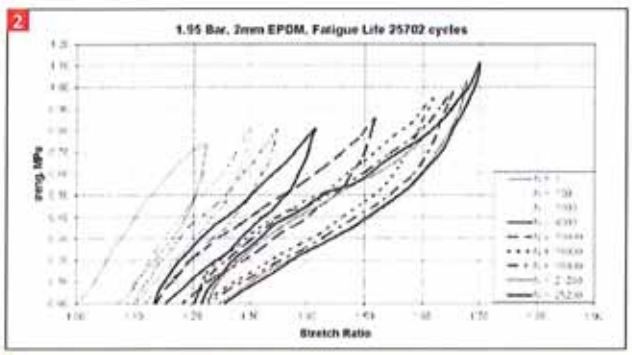

2 Stress-strain behaviour of EPDM for constant pressure controlled test, selected cycles, 1-25200

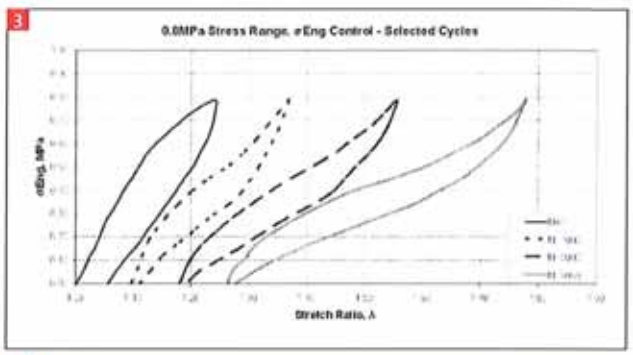

3 Stress-strain behaviour of EPDM for constant engineering stress controlled test, selected cycles, 1-9068

increase in maximum stress in subsequent cycles. The peak stress remained relatively constant between cycles 10-1000, but thereafter continued to increase until failure occurred. This was found to be the case for all the ranges tested.

To allow the peak engineering stress in a cycle to be maintained at the same value for each and every cycle throughout the test, the pressure set-point was adjusted continually throughout the test. By using this method of control, practical S-N curves could be obtained to compare the fatigue lives of the dry and swollen rubber. Figure 3 shows typical specimen stress-strain behaviour for selected cycles of an EPDM sample when the maximum engineering stress is controlled for a zero minimum stress and hence a constant stress range.

Results

Multi-axial fatigue tests – S-N curves

Plots were generated of stress-amplitude versus cycles to failure for both the swollen and unswollen test-pieces and these are shown in Figure 4.

Unsurprisingly, the unswollen specimens exhibited greater fatigue resistance than the swollen test-pieces. It can be seen that the S-N curve for the swollen material is shifted downwards from that of the unswollen material. In order to study this effect further, the complex modulus E* of both specimen sets was analysed for several stress ranges as shown in Figure 5.

E* was approximated by calculating the slope of the loading curve from zero stress and minimum strain to peak engineering stress and maximum strain for the cycle in question. It can be seen clearly that there is an offset in initial modulus for the swollen EPDM. The rate of decrease of E* in the dry rubber is more rapid E* values at failure appear to lie on a single line when plotted against the log of cycles to failure (Reference X-X on Fig. 5). The decrease in E* is less severe in the swollen specimens but the relationship between E* and the log of cycles to failure no longer appears to be linear (Reference Y-Y on Fig. 5).

Multi-axial fatigue tests - Sample fracture surfaces

The fracture surfaces of the dry samples were analysed using a digital imaging microscope. A magnification factor of X200 was used to view failure surfaces. For low cycle lives of less than 100 the type of failure is more akin to that of a single cycle test to destruction, with the surface morphology fibrous in nature and in some instances showing delamination at the failure surface. Failures at cycles greater than this show clear evidence of crack propagation and subsequent rupture. In most fatigue failures, the cracks appear on the surface of the bubble and continue to grow until failure. This behaviour was common to both the swollen and unswollen specimens. Surface morphologies for both dry and swollen fatigued specimens are shown in Figure 6. In the dry samples there is a coarser failure surface at lower cycles than for failures at higher cycles. The roughness of the failure surfaces of the swollen EPDM samples is much greater than that of the dry test-pieces for all stress ranges. These results correlate with those carried out by Cho *et al* [4] in shear tests on specimens which were fatigued to failure with a pre-crack. Their study reported that the smoother surface of the dry samples indicated blunt tearing, while the rough surfaces of the swollen test-pieces indicated sharp tearing.

Conclusions

The fatigue life of an EPDM sample under dynamic multi-axial loading can be greatly

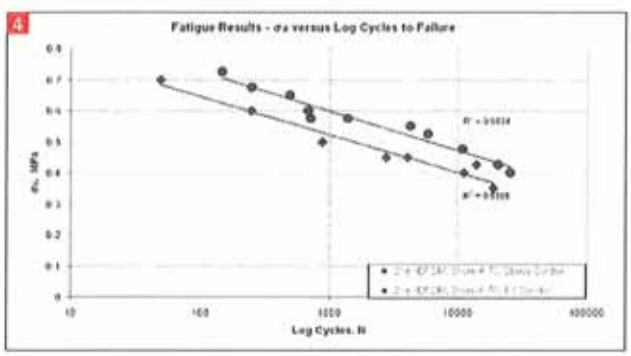

4 Plot of stress amplitude versus cycles to failure for the dry and swollen specimens

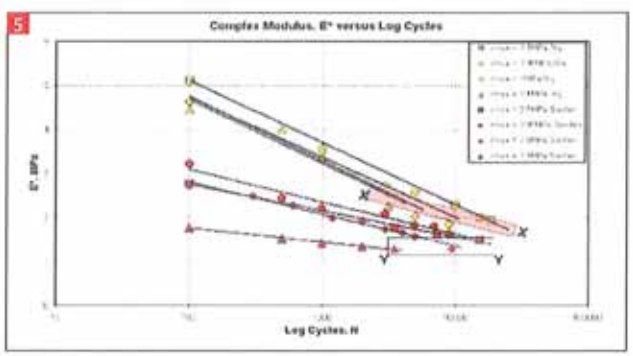

5 Log plot of complex modulus E* versus cycles for swollen and dry samples

reduced in the presence of the oil, even for relatively small amounts of swelling. The lower fatigue lives of the swollen specimens can be attributed to a number a factors, both physical and chemical in nature. Physical factors include a lower initial complex modulus following swelling, breakdown of filler-filler bonds and the presence of larger voids in the network due to the swelling action. Chemical factors include changes in the network structure due to swelling, where there is a reduction in the number of chains resisting the tensile force, while the reformation of polysulphidic linkages during a loading cycle can be inhibited in the presence of swelling fluid. The general fatigue behaviour of swollen elastomers loaded multi-axially is in close agreement with the experiments carried out in the uniaxial and shear loading cases.

Further testing is planned where longer fatigue tests will be performed on dry and swollen samples, with additional tests being carried out on EPDM swollen using a medium swelling reference oil (IRM 902). The stress-strain behaviour of each set of samples will be analysed in an attempt to determine if the stored energy in a cycle or a limiting value of E* can be used as a predictor of useful component life. Further imaging of the specimen fracture surfaces will also be carried out using scanning electron microscopy (SEM).

Acknowledgements

The authors would like to thank the Faculty of Engineering and the Directorate of Research and Enterprise in the Dublin Institute of Technology. This work was made possible by funding from Enterprise Ireland under its 'Proof of Concept' programme.

References

[1] P. Abhimanyu, T. Coolbaugh, Elastomers: A Literature Review With Emphasis on Oil Resistance. Rubber Chemistry and Technology **78** (2005) 516.

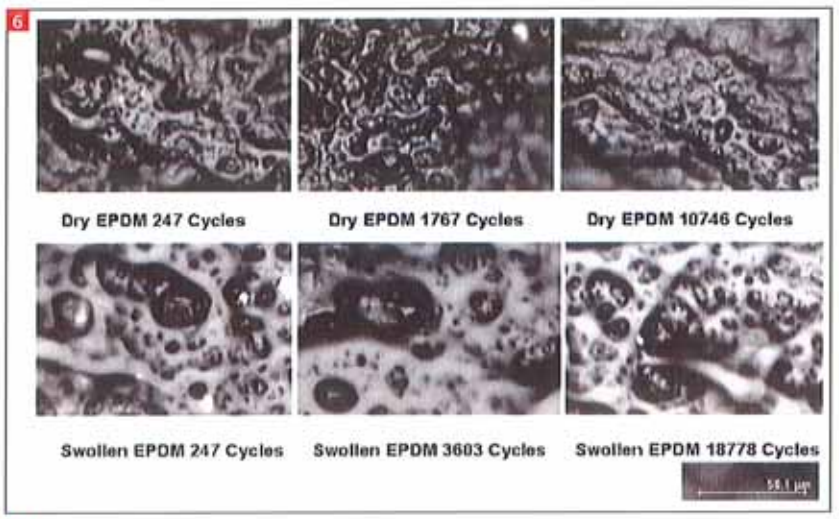

6 Fracture surface of dry and swollen specimens, magnification factor X200

[2] A. Beerbower, D.A. Pattison, G.D. Staffin, Predicting Elastomer-Fluid Compatibility For Hydraulic Systems, Rubber Chemistry and Technology **37** (1964) 246.

[3] Gul, V., Fedyukin, D., Dogadkin, B.A. The Influence of Intermolecular Action on the Dynamic Fatigue of Rubbers. Rubber Chemistry and Technology 32 (1959) 454.

[4] K. Cho, J.J. Wook, L. Daeho, C. Hyunaee, C. Young-Wook, Fatigue crack growth of elastomers in the swollen state. Polymer **41** (2000) 179.

[5] R. Seldén, Fracture Mechanics Analysis of Fatigue of Rubber-A Review. Progress in Rubber and Plastics Technology. 1995, 11(1) The Institute of Materials/RAPRA.

[6] Federal Motor Vehicle Safety Standards and Regulations No. 116 – Motor Vehicle Brake Fluids.

[7] D 471-06. 2006. Standard Test Method for Rubber Property-Effect of Liquids, ASTM Book of Standards Volume: 09.01.

[8] N. Murphy, J. Hanley, J. McCartin, B. Lanigan, S.D. McLoughlin, S. Jerrams, G. Clauss, R. Johannknecht "Determining multiaxial fatigue in elastomers using bubble inflation", 'Constitutive models for rubber IV' edited by P.-E. Austrell and L. Kari, pp 65-70, (Published by A.A. Balkema, ISBN 0415383463), 2005.

[9] N. Murphy, J. Hanley, H. Ali, S. Jerrams, "The Effect of Specimen Geometry on the Multiaxial Deformation of Elastomers", 'Constitutive models for rubber V' edited by A. Boukamel, L. Laiarinandrasana, S. Méo and E. Verron, pp61-65. (Published by Taylor & Francis, ISBN 0415454425), 2007.

[10] J. Hanley, N. Murphy, H. Ali, S. Jerrams, "Swelling Effects in Multiaxial Fatigue of Elastomers", Paper presented at Polymeric Materials in Automotive PMA 2007, Bratislava, May 2007.

[11] J. McCartin, N. Murphy, J. Hanley, S. Jerrams, B. Lanigan, "Determining levels of stress softening in multi-axial deformation", Poster for German Institute of Rubber Technology (DIK) 7th Fall Rubber Colloquium (KHK 2006), Hannover, November 2006.

[12] N. Murphy, S. Jerrams, C. Spratt, S. Ronan, R. Johannknecht, "Method for determining equi-biaxial fatigue in elastomers", 'Constitutive models for rubber III' edited by J. Busfield and A. Muhr, pp 21-26, (Published by A.A. Balkema, ISBN 9058095665), 2003.

7. J. Hanley, N. Murphy, H. Ali, S. Jerrams, "*The Effect of Oil Swelling on the Multi-Axial Fatigue Life of EPDM*", High Performance & Speciality Elastomers, 2007.

THE EFFECT OF OIL SWELLING ON THE MULTI-AXIAL FATIGUE LIFE OF EPDM

John Hanley[1*], Niall Murphy[1*], Hassan Ali[2] & Steve Jerrams[3*]

[1] School of Manufacturing and Design Engineering, Dublin Institute of Technology, Dublin, Ireland - john.hanley@dit.ie; [2] School of Chemical and Pharmaceutical Sciences, Dublin Institute of Technology, Dublin, Ireland - ali.hassan@dit.ie; [3] Directorate of Research and Enterprise, Dublin Institute of Technology, Dublin, Ireland - stephen.jerrams@dit.ie

*** - Corresponding authors**

BIOGRAPHICAL NOTE

John Hanley is currently employed as a research fellow on the Dynamet Project, which involves the development of testing equipment for the dynamic testing of non-linear materials, as part of Enterprise Ireland 'Proof of Concept' funding. In addition to 6 years research experience in the fields of polymer science, material testing and biomedical product design, he has 4 years industrial experience as a senior project/process engineer in hygienic manufacturing environments, including pharmaceutical, beverage, brewing & food processing facilities. He is currently studying for a PhD in Materials Science.

ABSTRACT

The effect of oil swelling on the fatigue life of EPDM has been studied in multi-axial fatigue using bubble inflation. Specimens were subjected to varying degrees of swelling in reference mineral oils at controlled temperatures and for fixed durations. The reference oils used for swelling the EPDM had known aniline points, allowing the rubber-oil compatibility to be determined. Following the swelling experiments, the swollen test-pieces were cycled to failure. The inflation fluid for fatigue testing was selected with a solubility parameter that would produce a desired level of incompatibility with the test specimens, thereby limiting the amount of additional swelling during cycling. Unswollen specimens were also cycled to failure in the same manner. Wöhler plots of stress amplitude versus cycles to failure were generated for both swollen and unswollen test-pieces and the changes in complex modulus and dynamic stored energy for each specimen type were compared. Specimen fractures were analysed using scanning electron microscopy.

Key words: Elastomer, Swelling, Fatigue, Bubble Inflation

INTRODUCTION

The effect of swelling on elastomers has been studied in detail under static loading, where the degree of cross-linking of the material and hence its modulus was found to be related to its swelling potential by the Flory-Rehner equation [1]. There have been fewer investigations of elastomeric dynamic behaviour, especially where oil swelling is concerned. Most rubber components fail in fatigue and consequently its determination has been of greater interest to materials researchers in recent years. The results of most fatigue tests are generated using testing equipment which loads the specimens in uniaxial tension, combined tension and torsion or in shear. While these methods provide much useful insight into the fatigue behaviour of elastomers, they do not describe the full spectrum of elastomeric material behaviour under cyclic loading. Dynamic bubble inflation, which is capable of loading test-pieces in multi-axial tension for multiple cycles, allows specimens to be fatigued to failure equi-biaxially and facilitates completion of the characterisation of fatigue life for all loading cases for a particular elastomer.

This study describes the fatigue properties and dynamic stress-strain behaviour of an EPDM elastomer which was swollen and cycled to failure and compares the results with those for dry specimens of the same material, tested in the same manner. Oil swelling causes modification in the mechanical properties of the EPDM and both the complex modulus and dynamic stored energy of each material is characterised and discussed. Thereafter, the failure modes of both specimen types are illustrated with a description of the surface morphologies at different stress amplitudes.

THEORY

A large amount of research has been carried out into the mechanical testing of swollen rubber, and the findings of this work are briefly reviewed here.

Early static testing of swollen rubbers in the 1930's and 1940's found that an increase in swelling caused a decrease in ultimate tensile strength, percentage elongation and modulus, [2][3][4]. More detailed research carried out in the 1940's and 1950's [5], quantified the effects of solvent swelling on the rubber network and found that with high solvent swelling, the bonds of the three dimensional network are destroyed. Analysis of swollen rubbers was relevant as the behaviour of swollen vulcanised rubber is close to that predicted by statistical theory [6]. The main findings of experimentation into the static strength of filled elastomers in the 1950's [7] found that the strength contributed by carbon black to the rubber network is diminished by swelling, leading to reduced hysteresis in the material.

In terms of dynamic testing of swollen rubbers, the first recorded studies were carried out by Gul et al [8] in the 1950's, where swollen rubbers were dynamically tested following swelling using rubber plasticisers as solvents. Specimens were cycled at constant load amplitude until the rubber samples reached 'dynamic equilibrium' and were then tested using a testing machine capable of 'constant swing', with test amplitudes measured in kg.m, and subsequently converted to Joules. In these tests the relative fatigue resistance of the rubber decreased with an increase in the degree of swelling.

In the last two decades research has concentrated on fatigue of swollen filled elastomers predominantly using strain control. Neogi et al [9] found in the 1990's that for NR and SBR, the hysteresis due to carbon black was reduced by swelling elastomers in a compatible solvent, where dynamic mechanical tests were carried out for small strains in simple tension. The most recent investigation took place in this decade where Cho et al [10] examined fatigue crack growth of swollen elastomers, using two types of SBR of different crosslink density swollen in mineral oil and fatigued in pure shear with a pre-crack at strain magnitudes of 10-35%. The tearing energy and crack growth rate were measured and compared against dry specimens. The study found that the fatigue resistance of the swollen elastomer was reduced in proportion to the degree of swelling. This was attributed to a reduction in internal friction between strands during deformation and less energy in the testpiece which could be dissipated by hysteresis.

This study differs from previous investigations in a number of respects. Firstly, test frequencies were maintained at 1Hz, instead of frequencies in excess of 4 Hz in the previous studies which would have led to heat build-up and consequent thermal degradation [11]. Secondly, previous fatigue tests were carried out using uniaxial and pure shear samples and test equipment. Dynamic bubble inflation, inducing multi-axial deformation allows a full range loading cases to be available for the investigation of fatigue in swollen elastomers. Thirdly, the properties of the swelling oil, in terms of aniline point and swelling potential is detailed in this study. Previous research [12] found by experiment that the solubility parameter for a hydraulic fluid may be estimated from known physical properties which are readily available. The experiments allowed the relationship between the solubility parameter and the aniline point of the oils being tested to be plotted as an empirical linear relationship. In order to best demonstrate the effects of swelling in typical hydraulic oils it is therefore necessary to use hydraulic fluids where the properties have been determined and can be used as a reference. From the ASTM standards for rubber liquid compatibility [13], the reference oil IRM 903 is the most appropriate choice for use as high swelling oil for the physical testing of swollen rubbers. Its aniline point has been determined and can be compared with the solubility parameter for the test material to allow rubber-liquid compatibility to be gauged. Moreover, it is generally comparable with typical hydraulic oils in terms of liquid properties.

TEST PROCEDURE

MATERIALS

EPDM rubber of 70 Shore A hardness, cross-linked with sulphur and containing low activity carbon black was first chosen for the investigation. Initially dry (unswollen) specimens were fatigued to failure with a zero minimum load.

TEST PREPARATION

When inflating rubbers using liquids, the properties of the liquid must be considered. If the square root of the difference between the solubility parameters of a rubber and fluid is less than 1, the rubber will swell appreciably in that fluid [14]. Therefore, it is important to select an inflation fluid which will not cause swelling of the test-piece with the accumulation of cycles. Furthermore, the swelling effects in elastomers in contact with most liquids are less pronounced at normal ambient temperatures. Silicone based fluids will not swell EPDM appreciably [15]. Following swelling tests to confirm this, such a fluid was chosen as the inflation medium and all fatigue tests were carried out at temperatures of 15°C. Oil swelling experiments were carried out using reference oil IRM 903. This oil has an aniline point of 70.6°C, which when matched against typical solubility parameter for EPDM of δ = 8-10, indicates high swelling potential for the oil elastomer mixture. The specimens were immersed in the reference oil at an elevated temperature of 100°C for a period of one hour. Following swelling, the test-pieces were removed from the hot oil and cooled in oil at ambient temperature for a short period, before being wiped dry and weighed. An average swelling ratio of 1.10 (10% increase in mass) was calculated for the samples, where the swelling ratio Q can be expressed as,

$$Q = W_s / W_d, \quad (1)$$

where W_s is the weight of the swollen elastomer sample and W_d is the weight of dry elastomer before swelling [13].

Dynamic multi-axial tests were carried out on the swollen and unswollen specimens by clamping a circular test-piece around its edges and applying pressure to one face of the disc causing it to inflate in a balloon like manner.

MULTI-AXIAL FATIGUE TESTS – DEVELOPMENT OF TEST PROCEDURE

The DYNAMET Dynamic Bubble Inflation Test System is shown in Figure 1. Detailed description of the dynamic bubble inflation method can be found elsewhere [16] [17] [18]. Specimens of 50mm diameter were clamped and dynamically inflated and deflated between pre-set engineering stress limits through a 35mm orifice. Prepared specimens had a pattern of dots applied to their surface. The deformation of this pattern during inflation and deflation is recorded by an optical system, with each image captured allowing correlation with a specific engineering stress value at the bubble pole.

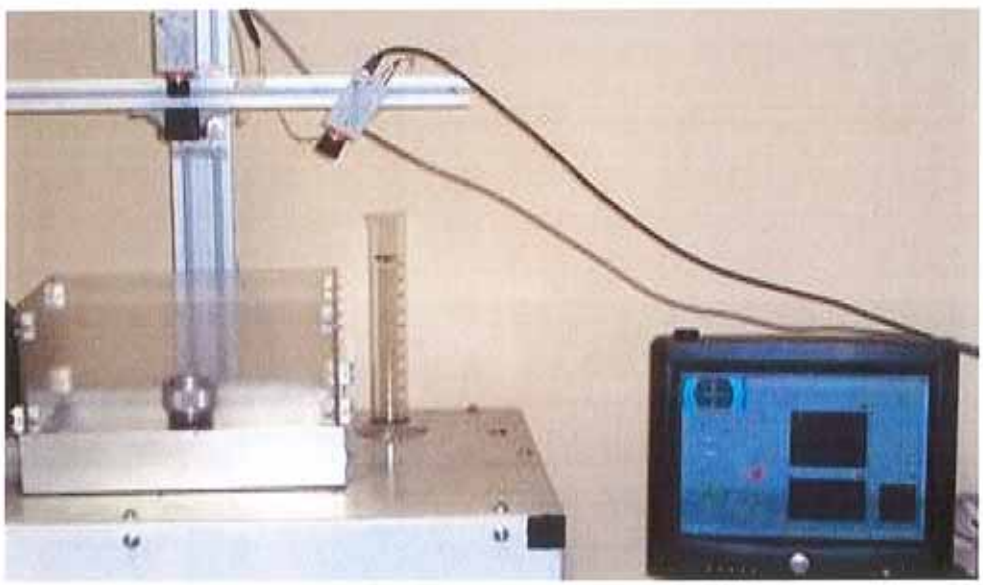

Figure 1 – DYNAMET Bubble Inflation Test Apparatus.

The stress-strain relation during bubble inflation is assumed to comply with membrane theory where, from the measurement of pressure P and the radius of curvature R, the equation for stress at the pole can be determined using Equation [2].

$$\sigma = PR/2t \qquad (2)$$

Where P is the pressure, R is the radius at the bubble pole and t is the original sheet thickness.

Local stretch ratios at the pole can be determined using Equation [3]:

$$\lambda = ((x_{cir} - x_{orig})/x_{orig}) + 1 \qquad (3)$$

Where λ is the principal stretch ratio, x_{cir} is the circumferential point spacing at the bubble pole and x_{orig} is the original point spacing.

RESULTS

It is crucial that maximum engineering stress limits are not exceeded throughout the test and the results of this control method are illustrated in Figure 2. Over stressing on any cycle during a multi-axial test will give an unrepresentative change in the viscoelastic trend of complex elastic modulus E* and will invalidate the results of any Wöhler (S-N) plots generated.

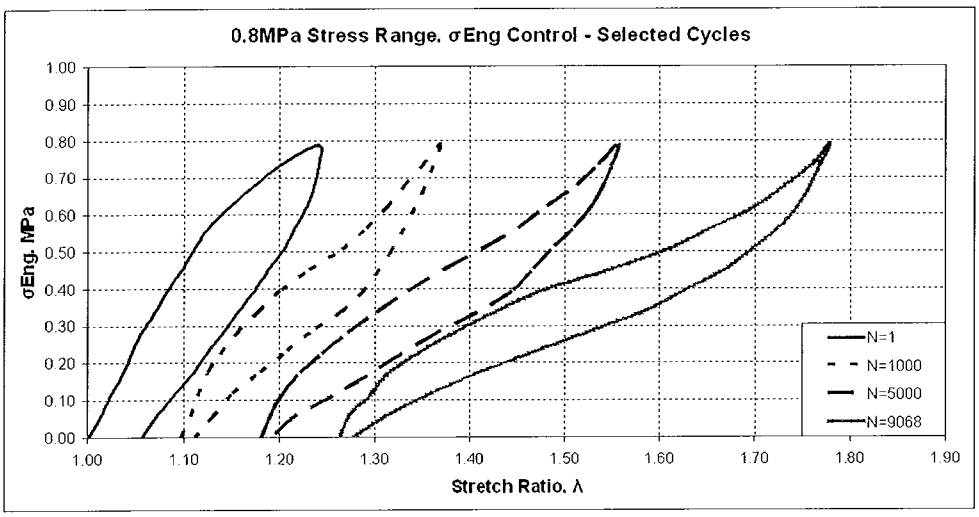

Figure 2 – Stress-strain behaviour of EPDM for constant engineering stress controlled test, selected cycles, 1-9068.

The amount of dissipated energy in the material (area bound by the hysteresis curve during the loading and unloading cycle) reduces significantly during the initial conditioning cycles and then begins to increase until failure occurs. This behaviour was common for both specimen sets, but the effect in the initial conditioning cycles was more pronounced for the dry specimens. This can be attributed to the swelling effect of the oil breaking some of the chemical bonds in the material prior to any mechanical loading.

MULTI-AXIAL FATIGUE TESTS – S-N CURVES

Plots were generated of stress-amplitude versus cycles to failure for both the swollen and unswollen test-pieces and these are shown in Figure 3.

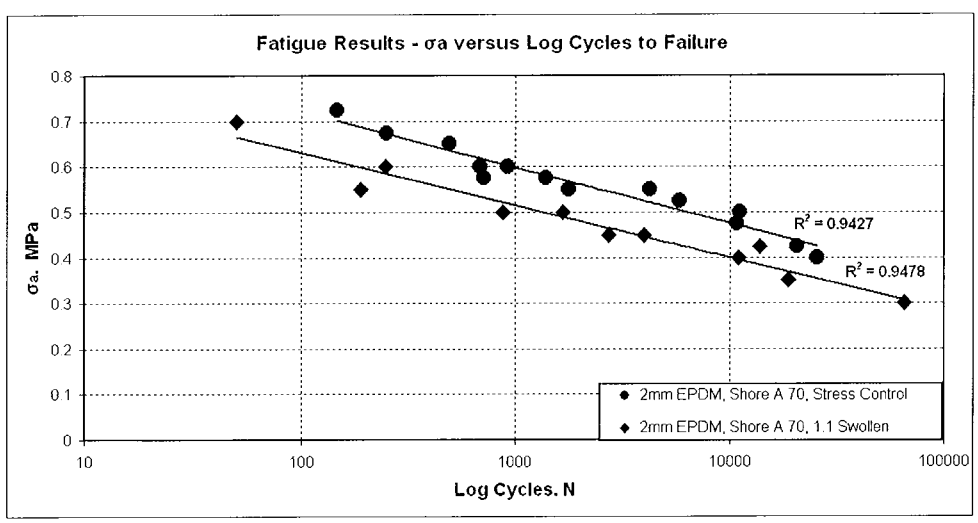

Figure 3 – Plot of stress amplitude versus cycles to failure for the dry and swollen specimens.

Unsurprisingly, the unswollen specimens exhibited greater fatigue resistance than the swollen test-pieces. In order to study this effect further, the reduction in complex modulus E* of both specimen sets was analysed for several stress ranges as shown in Figure 4.

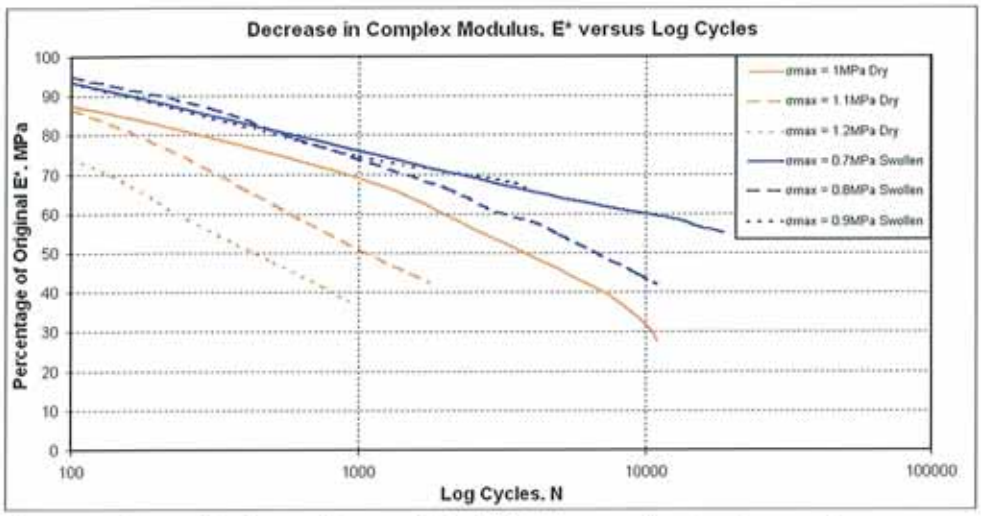

Figure 4 – Log plot of complex modulus E versus cycles for dry samples.*

E* was approximated by calculating the slope of the loading curve from zero stress and minimum strain to peak engineering stress and maximum strain for the cycle in question. The percentage drop in E* was calculated by comparing the E* values during cycling with the original E* value, with the original (100%) value based on the modulus after several conditioning cycles at the beginning of the test.

In the dry test-pieces, the effect of higher stress amplitudes on the rate of decrease in E* is noticeable, with a greater reduction in E* with cycles in specimens subjected to higher stress amplitudes. The rate of decrease in E* is less severe in the swollen specimens, with the rate for low and higher stress amplitudes being similar.

The effect of swelling on the dynamic stored energy was also studied. The dynamic stored energy is defined as the strain energy in the unloading cycle, or the area under the stress-strain curve for the unloading portion of the stress-strain curve. The dynamic stored energy in both specimen sets was found to continually increase throughout the fatigue testing. Plots of dynamic stored energy versus cycles to failure were generated for the dry and swollen rubber specimens. Figure 5 (a) and (b) illustrate that the estimated values of stored energy at failure approximately lie on a straight line, when plotted against the log of cycles, for both dry and swollen specimens. However, it should be noted that the curve of dynamic stored energy versus cycles for failure has a shallower gradient for the dry test-pieces than for the swollen specimens.

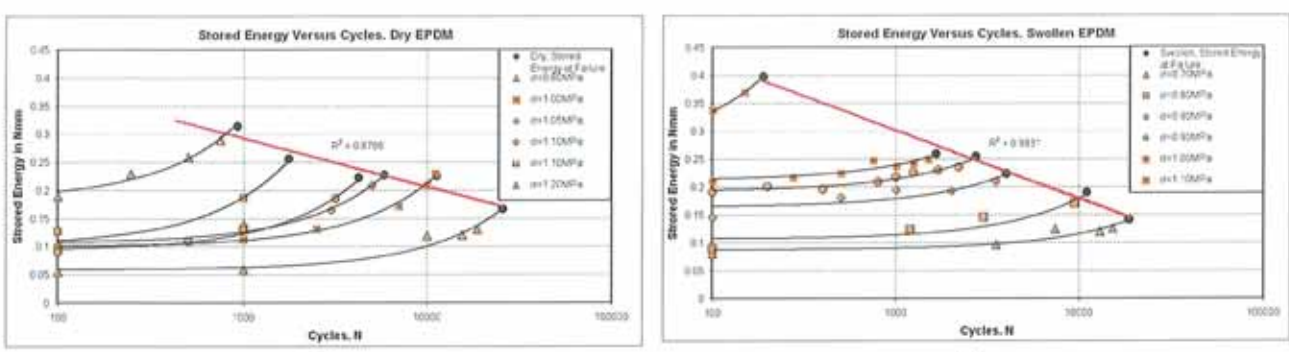

(a) (b)

Figure 5 – Log plot of stored strain energy versus cycles to failure for (a) dry rubber and (b) swollen rubber.

This is illustrated in Figure 6, where the linear plots of dynamic stored energy at failure versus cycles to failure are plotted for the dry and swollen specimens together. It can be seen that the swollen rubber specimens have higher values of dynamic stored energy for lower fatigue lives (less than approximately

5000 cycles). This is due to the rubber being softer due to the oil swelling, with more deformation for a given applied stress.

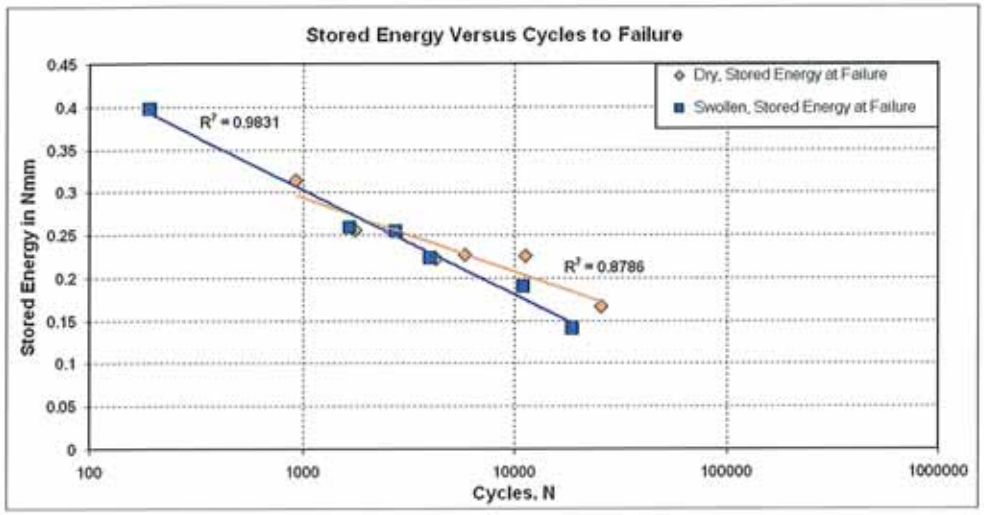

Figure 6 – Log plot of stored energy versus cycles to failure for dry and swollen samples.

Moreover, the material property of dynamic stored energy has been altered for the swollen material, when compared with that of the dry test-pieces. The slope of the curves of each specimen set are different, showing that while dynamic stored energy can be used as a fatigue life predictor, it's characteristic is changed once the rubber becomes swollen, meaning that different parameters for lifetime prediction have to be applied.

MULTI-AXIAL FATIGUE TESTS - SAMPLE FRACTURE SURFACES

For low cycle lives of less than 100 the type of failure is more akin to that of a single cycle test to destruction, with the surface morphology fibrous in nature and in some instances showing delamination at the failure surface. Failures at cycles greater than this show clear evidence of crack propagation and subsequent rupture. In the multi-axial tests presented, the crack is initiated at the bubble pole and propagates until failure. This behaviour was apparent in both the swollen and unswollen specimens. The fracture surfaces of both sets of samples were analysed using scanning electron microscopy (SEM). Figure 7 shows images of the swollen and dry specimen fractures at a magnification of X190.

The roughness of the failure surfaces of the swollen EPDM samples is greater than that of the dry test-pieces for all stress ranges. These results correlate with those carried out by Cho *et al* [4] in shear tests on specimens which were fatigued to failure with a pre-crack. Their study reported that the smoother surface of the dry samples indicated blunt (smooth) tearing, while the rough surfaces of the swollen test-pieces indicated sharp tearing. This is confirmed by the images shown in Figure 8, taken at a higher magnification factor of X400, where the smoother surface of the dry specimens can be contrasted with the rougher surface of the swollen test-pieces. This blunt tearing could be attributed to more polymer filler interaction in the dry material, with the material being tougher for a given applied stress.

It can be seen that there are more flaws in the swollen material, which can be attributed to the swelling effects of the oil breaking down filler-filler bonds. Due to the presence of these flaws the probability of crack growth being initiated from them would be expected to be high, with these areas potentially having localised low values of complex modulus than other points in the network.

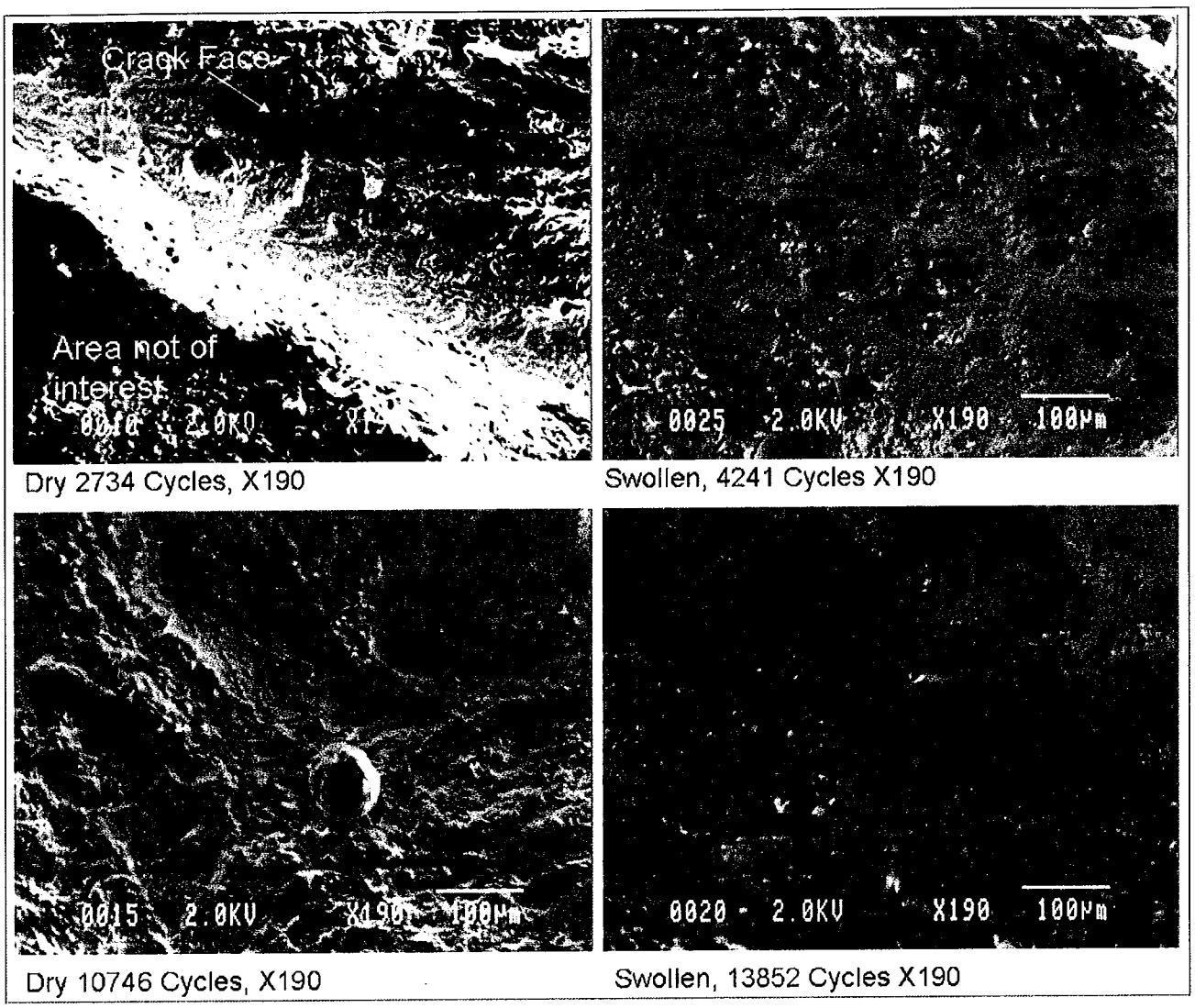

Figure 7 – SEM Imaging of fracture surface of dry and swollen specimens, magnification factor X190.

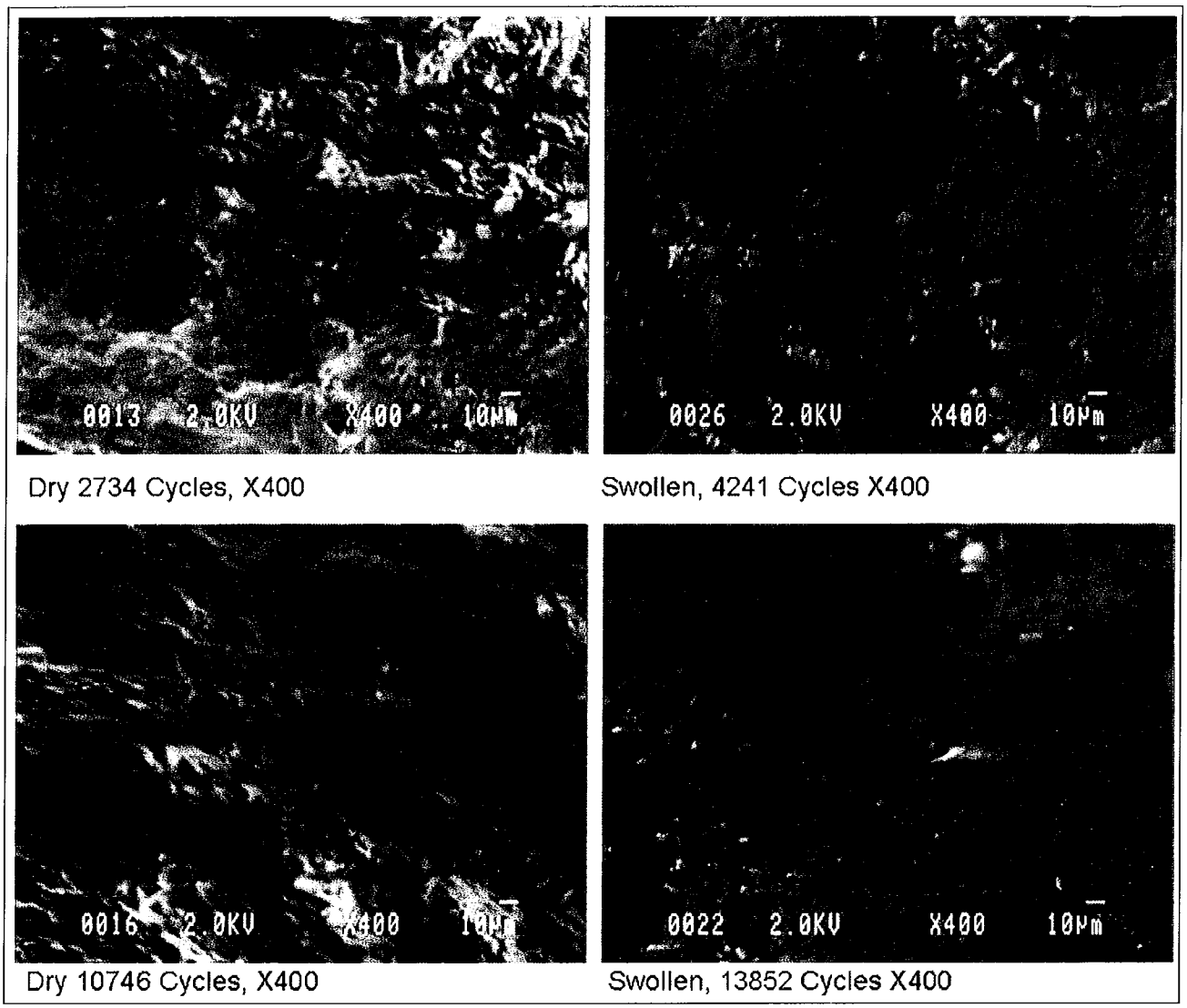

Figure 8 – SEM Imaging of fracture surface of dry and swollen specimens, magnification factor X400.

CONCLUSIONS

The fatigue life of an EPDM sample under dynamic multi-axial loading can be greatly reduced in the presence of the oil in the rubber network, even for relatively small amounts of swelling. Despite being in contact with the oil for only one hour at 100°C, the dynamic properties such as the complex modulus E* and the dynamic stored energy are fundamentally altered from that of the untreated EPDM. The changes in these properties and the lower fatigue lives of the swollen specimens can be attributed to a number a factors, both physical and chemical in nature.

Physical factors include the presence of larger voids in the network due to the swelling action which in turn leads to a lower initial complex modulus. The presence of these flaws in the elastomer network structure was confirmed by the SEM imaging, which showed that the failure surfaces for each set of test-pieces is markedly different in the dry and swollen cases.

Chemical factors which explain the difference in the dynamic mechanical properties of the unswollen specimens include changes in the network structure due to the oil swelling, where there is a reduction in the number of cross-links resisting the tensile force, while the reformation of polysulphidic linkages during a loading cycle can be inhibited in the presence of swelling fluid.

The general fatigue behaviour of swollen elastomers loaded multi-axially is in close agreement with the experiments carried out in the uniaxial and shear loading cases. Analysis of the stress-strain behaviour of each set of samples indicates that the stored energy in a cycle may be used as a predictor for the fatigue life

of the specimen. This is in agreement with findings for the dynamic uniaxial testing of non-strain crystallising elastomers [19]. However, while the stored energy in a cycle can be used to predict fatigue resilience for both the dry and swollen specimens, each specimen set exhibits different stored energy characteristics with the accumulation of cycles.

The practical significance of this study is to highlight the effect of contamination on the mechanical performance of non-strain crystallising elastomers. EPDM components are commonly used in automotive applications, where they have the advantage of having more functionality at higher temperatures than SBR or natural rubber. However, some of these advantages are offset by their poor resistance to the numerous fluids used in vehicles. The results presented here illustrate that if a risk of oil contamination is sufficiently high and the automotive design engineer has failed to fully take swelling into account, safety factors and life expectations may be unrealistically high and components will lack the residual mechanical strength to withstand levels of fatigue loading.

Further testing and analysis will determine if a limiting value of E* can be used as a predictor of useful component fatigue life. Fatigue tests will be performed on dry and swollen samples at lower stress amplitudes than those presented in this work, with additional tests being carried out on EPDM swollen using medium swelling reference oil (IRM 902). This will allow the effect of the swelling ratio on the stored energy characteristic curves to be more fully described.

ACKNOWLEDGEMENTS

The authors would like to thank the Faculty of Engineering and the Directorate of Research and Enterprise in the Dublin Institute of Technology. This work was made possible by funding from Enterprise Ireland under its 'Proof of Concept' programme.

REFERENCES

[1] Flory, P. J., Rehner, J., "Statistical Mechanics of Cross-Linked Polymer Networks II. Swelling", J. Chem. Phys. 11, 521 (1943).

[2] Tanaka, Y., Kambara, S., Noto, J., "The Oil Resistance of Rubber I. Study of the Swelling of Vulcanised Rubber", Rubber Chemistry and Technology, Volume 9, 70-73, (1936).

[3] Tiltman, H.A., Porritt, B.D., "The effect of solvents on the stress-strain curve of vulcanised rubber", India Rubber Journal, Vol.78, p345-346 (1929).

[4] Parris, R.W., Scott, J.R., "Properties of Hard Rubber, IX. Swelling in various liquids (Part XIII of Swelling of Rubber)", Rubber Chemistry and Technology, Vol 15, p.280-300, (1942).

[5] Dogadkin, B.A., Gul, V., "The Role of Intermolecular Forces in the Mechanism of High Elastic Deformation III. Effect of Swelling on the Mechanical Properties of Vulcanised Rubber", Rubber Chemistry and Technology, Volume 24, P.344-353, (1951).

[6] Treloar, L.R.G., "The Swelling of Cross-Linked Amorphous Polymers Under Strain", Rubber Chemistry and Technology, Vol 24, P.290-298, (1951).

[7] Zapp, R.L., Guth, E., "Elastic Modulus and Swelling of Butyl Vulcanizates", Rubber Chemistry and Technology, Vol 24, P.894-913 (1951)

[8] Gul, V., Fedyukin, D., Dogadkin, B.A. The Influence of Intermolecular Action on the Dynamic Fatigue of Rubbers. Rubber Chemistry and Technology. 1959; 32: 454-462.

[9] Neogi, C, Bhattacharya, A.K., Bhowmick, A.K., "Dynamic Mechanical Analysis of Carbon-Black-Filled Rubber Vulcanizates under Swollen Conditions", Rubber Chemistry and Technology, Volume 63, p651-659 (1990).

[10] Cho, K., Wook, J.J., Daeho, L., Hyunaee, C., Young-Wook, C. Fatigue crack growth of elastomers in the swollen state. Polymer. 2000; 41: 179-183.

[11] Seldén, R. Fracture Mechanics Analysis of Fatigue of Rubber-A Review. Progress in Rubber and Plastics Technology. 1995; 11(1), The Institute of Materials/RAPRA.

[12] Beerbower, A., Pattison, D.A., Staffin, G.D. Predicting Elastomer-Fluid Compatibility For Hydraulic Systems, Rubber Chemistry and Technology. 1964; 37: 246-260.

[13] D471-06. 2006. Standard Test Method for Rubber Property-Effect of Liquids, ASTM Book of Standards Volume: 09.01.

[14] Abhimanyu, P., Coolbaugh, T. Elastomers: A Literature Review With Emphasis on Oil Resistance. Rubber Chemistry and Technology. 2005; 78: 516.

[15] Federal Motor Vehicle Safety Standards and Regulations No. 116 - Motor Vehicle Brake Fluids.

[16] Murphy N, Hanley J, McCartin J, Lanigan B, McLoughlin S, Jerrams S, Clauss G, Johannknecht R, "Determining multiaxial fatigue in elastomers using bubble inflation", 'Constitutive models for rubber IV' edited by P.-E. Austrell and L. Kari, pp 65-70, (Published by A. A. Balkema, ISBN 0415383463), 2005.

[17] Murphy N, Hanley J, Ali H, Jerrams S, "The Effect of Specimen Geometry on the Multiaxial Deformation of Elastomers", 'Constitutive models for rubber V' edited by A.Boukamel, L.Laiarinandrasana, S.Méo and E.Verron, pp 61-65. (Published by Taylor & Francis, ISBN 0415454425), 2007.

[18] Murphy N, Jerrams S, Spratt C, Ronan S, Johannknecht R, "Method for determining equi-biaxial fatigue in elastomers", 'Constitutive models for rubber III' edited by J. Busfield and A. Muhr, pp 21-26, (Published by A. A. Balkema, ISBN 9058095665), 2003.

[19] Alshuth T, Abraham F, Jerrams S, "Parameter Dependence and Prediction of Fatigue Properties of Elastomer Products" Rubber Chemistry and Technology Journal, Vol 75, Issue 4, p 365, September/October 2002.

8. S. Jerrams, J. Hanley, N. Murphy, H. Ali, "Equi-Biaxial Fatigue of Elastomers – The Effect of Oil Swelling on Fatigue Life" Rubber Chemistry and Technology, Under Peer Review at Time of Writing, February 2008.

EQUI-BIAXIAL FATIGUE OF ELASTOMERS - THE EFFECT OF OIL SWELLING ON FATIGUE LIFE

STEVE JERRAMS*

DIRECTORATE OF RESEARCH AND ENTERPRISE, DUBLIN INSTITUTE OF TECHNOLOGY, 143-149 RATHMINES, DUBLIN 6, IRELAND

JOHN HANLEY, NIALL MURPHY

SCHOOL OF MANUFACTURING AND DESIGN ENGINEERING, DUBLIN INSTITUTE OF TECHNOLOGY, BOLTON STREET, DUBLIN 1, IRELAND

HASSAN ALI

SCHOOL OF CHEMICAL AND PHARMACEUTICAL SCIENCES, DUBLIN INSTITUTE OF TECHNOLOGY, KEVIN STREET, DUBLIN 2, IRELAND

ABSTRACT

The effect of oil swelling on the fatigue life of ethylene propylene diene monomer rubber (EPDM) has been studied under conditions of equi-biaxial cycling using dynamic bubble inflation. Specimens were subjected to varying degrees of swelling in reference mineral oils and fatigued at constant engineering stress amplitudes. The reference oils used for swelling the EPDM had known aniline points, allowing the rubber-oil compatibility to be determined. The inflation fluid for fatigue testing was selected with a solubility parameter that would produce a desired level of incompatibility with the test specimens, thereby limiting the amount of additional swelling during cycling. Wöhler (S-N) plots were generated for dry and swollen specimens and the changes in complex elastic modulus E* and dynamic stored energy were analysed. Specimen fractures were analysed using scanning electron microscopy. The fractures in the swollen samples show that the failure surfaces flowed more readily over each other than did those of the dryer specimens.

INTRODUCTION

Most rubber components fail in fatigue and consequently determining elastomeric component fatigue life has acquired greater interest to materials scientists in recent years. Fatigue testing to date has generated results using equipment which loaded the specimens in uniaxial tension, combined tension and torsion or in shear. While these methods provide much useful insight into the fatigue behaviour of elastomers, they do not describe the full spectrum of elastomeric material behaviour under cyclic loading[1].

Dynamic bubble inflation is capable of loading test-pieces in equi-biaxial tension for any stress or strain amplitude to record the total cycles to failure. This method allows specimens to be fatigued to failure equi-biaxially and facilitates completion of the characterisation of fatigue life for all loading cases for a particular elastomer. In this case, the characterisation of the dynamic properties of EPDM is further explored to establish the effect of swelling on the equi-biaxial properties of initially dry elastomers.

A fundamental question posed is whether oil swelling agents affect the fatigue behaviour of the rubber, where it is subjected to prior treatment before loading. The effect of swelling on elastomers has been studied comprehensively under static loading, where the degree of cross-linking of the material and hence its modulus was found to be related to swelling potential by the Flory-Rehner equation.[2]

* Corresponding author. Ph: +353 1 4027537; Fax: +353 1 4023393; email: stephen.jerrams@dit.ie

There have been fewer investigations of elastomeric dynamic behaviour, especially where oil swelling is considered.[3,4,5,6]

By undertaking these tests, it was anticipated that the resultant damage caused by swelling and the consequent influence that swelling has on fatigue resistance could be determined for the equi-biaxial load case.

OBJECTIVE

To investigate the influence of swelling in equi-biaxial fatigue, it was proposed to test three different EPDM specimen sets using dynamic bubble inflation between pre-set maximum and zero minimum engineering stress limits. The test specimens were prepared in the following manner:

- Dry specimens, fatigued to failure. Test-pieces were not pre-treated and silicone based oil was selected as the inflation fluid for the tests to minimise any swelling effects.
- Prior to fatigue testing, specimens were swollen in two different ASTM reference oils, IRM 902 and IRM 903. Test-pieces were not conditioned before fatigue testing. Following removal from the swelling medium, test-pieces were equi-biaxially tested to failure in fatigue, again using silicone based oil to minimise additional swelling effects during the dynamic tests.

Consequently, the aims of this investigation were as follows:

1) To determine if fatigue strength reductions due to swelling in rubber specimens loaded equi-biaxially were consistent with strength reductions in samples subjected to uniaxial tests to failure.
2) To establish equi-biaxial Wöhler (S-N) curves for a range of rubbers swollen in different media in tests conducted at constant stress amplitudes.
3) To establish relationships between cycles to failure and dynamic modulus and stored energy.
4) To offer predictors of fatigue life for dry/swollen specimens subjected to equi-biaxial fatigue.

TEST METHODOLOGY

MATERIALS AND SPECIMENS

EPDM rubber of 70 Shore A hardness, cross-linked with sulphur and containing low activity carbon black was chosen for this investigation. Specimens had a 50mm original diameter and 2mm original thickness. For the bubble inflation tests, these samples were clamped and dynamically inflated and deflated through a 35mm diameter orifice. Prepared specimens had a pattern of dots applied to their surface. The deformation of this pattern during inflation and deflation is recorded by an optical system, with each image captured allowing correlation to a specific engineering stress value at the bubble pole.

SWELLING EXPERIMENTS

All rubber will swell to some extent in oil, but the degree of swelling can be estimated for a particular oil-rubber combination if the solubility parameters δ for both components of the

mixture are known. If the square root of the difference between the solubility parameters of the rubber and the oil is less than 1, as shown in Equation (1), then the rubber will swell appreciably in that oil.[7]

$$(\delta_1 - \delta_2)^{\frac{1}{2}} < 1 \qquad (1)$$

There can be difficulties in accurately determining the solubility parameter for a fluid when it consists of two or more fractions. However, it has been found from experimentation that that the solubility parameter for a hydraulic fluid may be estimated from other known physical properties which are readily available, such as the aniline point of the oil. The relationship between the solubility parameter and the aniline point of the oils being tested can be plotted as an empirical linear relationship.[8]

To control the degree of oil swell in rubbers it is necessary to use hydraulic fluids where the properties have been determined and which can consequently be used as a reference. From the ASTM standards for rubber-liquid compatibility, the reference oil IRM 903 is the most appropriate choice of oil for high swelling of EPDM.[9] Its aniline point has been determined and can be compared with the solubility parameter for the test material to allow rubber-liquid compatibility to be gauged. Moreover, it is generally comparable with typical hydraulic oils in terms of liquid properties. By using reference oil, IRM 902, which imparts medium swell effects, the influence of variation of oil solubility on rubber properties may also be investigated. The properties of the liquids used are summarised in Table 1.

TABLE 1
REFERENCE OIL PROPERTIES

	IRM 902	**IRM 903**
Boiling Point	> 316°C	> 249°C
Vapour Pressure	<0.001 mm Hg @ 20°C	<0.001 mm Hg @ 20°C
Specific Gravity	0.93 (Water = 1)	0.92 (Water = 1)
Molecular Weight	460 $gmol^{-1}$	319 $gmol^{-1}$
Viscosity	20.48 cST @ 99°C	33.3 cST @ 99°C
Aniline Point	92.7°C	70.6°C

Swelling experiments were carried out by immersing the specimens in reference oil at 100°C for one hour. The specimens were removed from the hot oil and cooled in oil at ambient temperature for a short period, before being wiped dry and weighed. An average swelling ratio was calculated for the samples, where the swelling ratio Q was expressed as,

$$Q = \frac{W_s}{W_d} \qquad (2)$$

where W_s is the weight of the swollen elastomer sample and W_d is the weight of dry elastomer before swelling.[9] A swelling ratio of 1.10 (10% increase in mass) was calculated for the

EPDM swollen in IRM 903 and a ratio of 1.042 (4.2% increase in mass) for the EPDM swollen in IRM 902.

The three different EPDM specimen sets (Dry, 10% Swell, 4.2% Swell) were then tested in equi-biaxial fatigue, between pre-set maximum and zero minimum engineering stress limits. An inflation fluid (silicone based oil) was chosen that would minimise any additional swelling effects during dynamic loading.

TEST METHOD

The dynamic bubble inflation test rig (DYNAMET) provides a method of determining the mechanical properties of elastomers in equi-biaxial deformation under fatigue conditions.[10,11,12] The test apparatus consists of a hydraulic inflation/deflation system and a strain measurement system. The strain measurement is based on a stereo vision system, with two charge coupled device (CCD) cameras connected to a PC. The cameras are mounted over the specimen and the output from each camera is combined to allow 3-dimensional data to be determined. A calibration routine is required to ensure that the co-ordinates measured by each camera can be related to each other. The raw measured X,Y,Z data is output in pixel coordinates and this data must be combined for each camera and rotated, translated and scaled using constants generated as part of the calibration process. Once scaled into millimetres, the X, Y, Z data is used for two purposes. Firstly, the radius of the bubble is calculated using a least squares fit based on an elliptical contour function through the X, Z co-ordinates for a particular frame. Secondly the X data for a particular frame is combined with the corresponding radial data to calculate the circumferential spacing of the markings on the surface of the test-piece. Pressure readings are synchronised with the cameras during the image capture sequences, by taking a pressure measurement every time an image capturing trigger signal is output to the cameras.

The DYNAMET system is shown in Figure 1, where the displacement of specimen markings for a number of inflation/deflation cycles is shown.

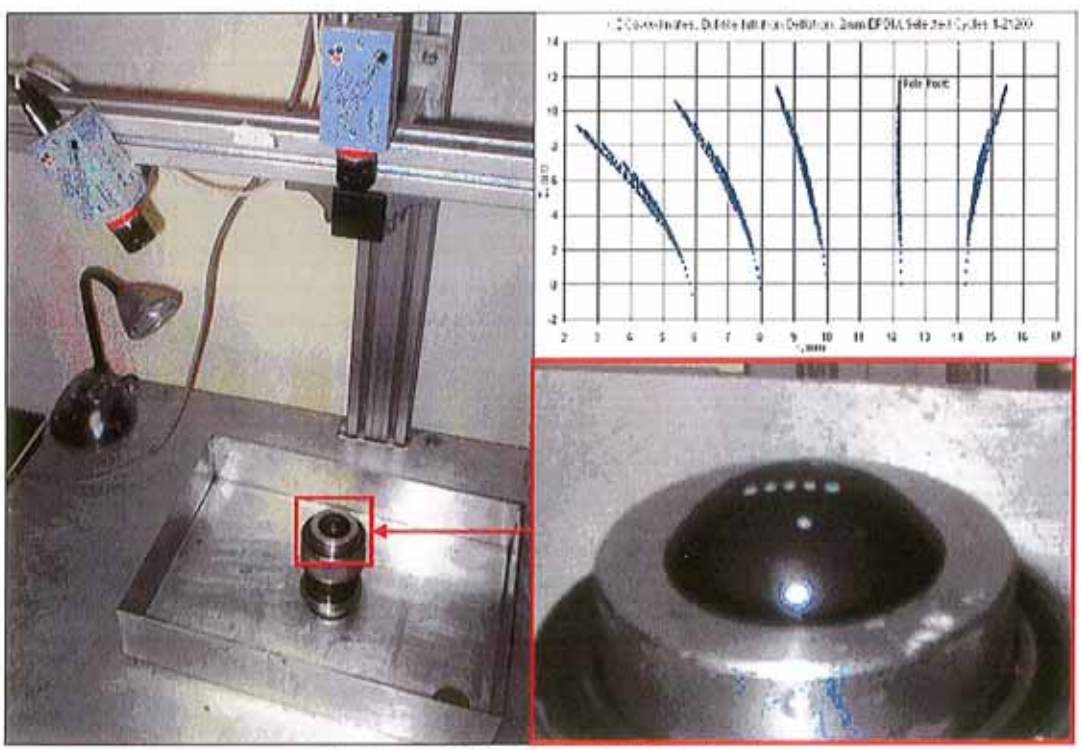

FIG. 1.— DYNAMET Bubble Inflation Tester.

The stress-strain relation during bubble inflation is assumed to comply with membrane theory where, from the measurement of pressure P and the radius of curvature R, the equation for stress at the pole can be determined using Equation (3).

$$\sigma = \frac{PR}{2t} \tag{3}$$

Local stretch ratios at the pole can be determined using Equation (4):

$$\lambda = ((x_{cir} - x_{orig})/x_{orig}) + 1 \tag{4}$$

Where λ is the principal stretch ratio, x_{cir} is the circumferential point spacing at the bubble pole and x_{orig} is the original point spacing.[13]

RESULTS

FATIGUE TESTS

All fatigue tests were carried out at frequencies of 1Hz. This minimised any potential sample degradation due to heat build-up during cyclic loading.[14] To maintain a constant peak engineering stress in a cycle for each and every cycle, the pressure set-point was adjusted continually throughout a test. By using this method of control, practical S-N curves could be obtained to compare the fatigue lives of the dry versus the swollen rubber. Figure 2 shows hysteresis curves for four cycles in a fatigue test where constant stress control is used.

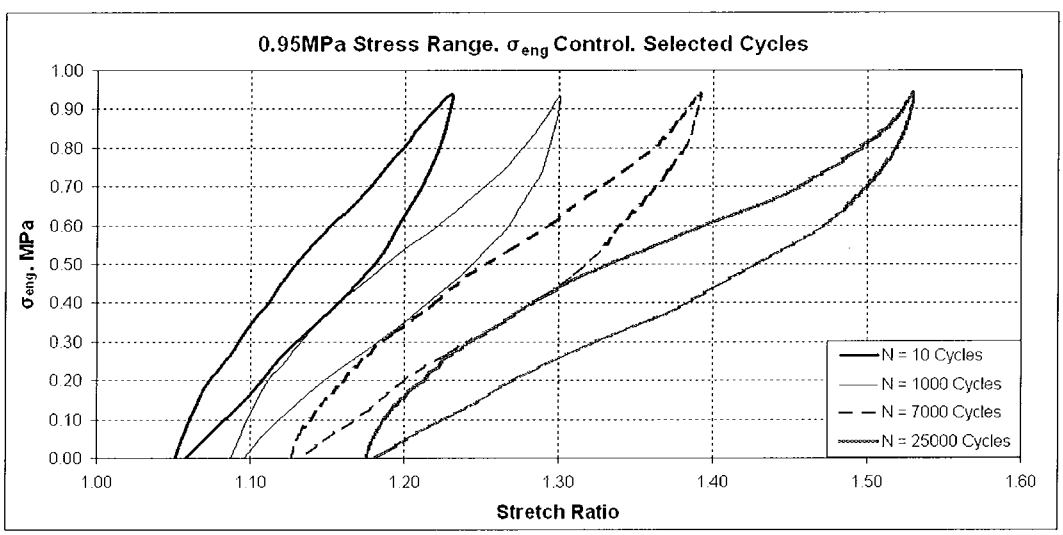

FIG. 2.— Hysteresis curves for cycles N= 10, 1000, 7000, 25000.

All fatigue tests were carried out with a zero minimum stress. The plot of stress amplitude versus cycles to failure for all three specimen sets is shown in Figure 3.

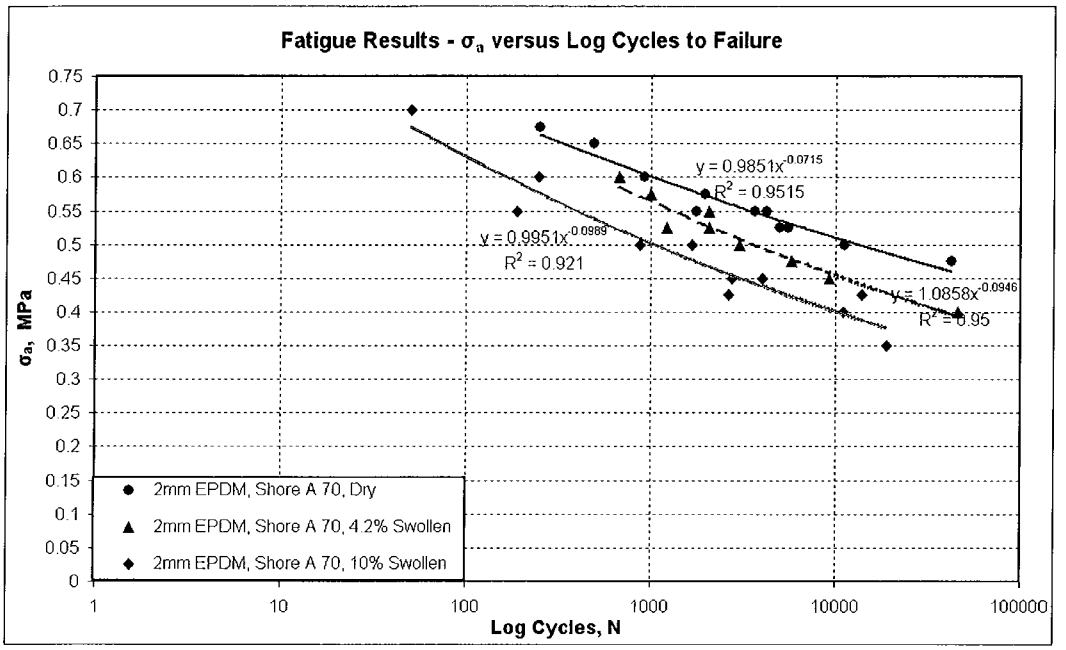

FIG. 3.— Plot of stress amplitude and cycles to failure for the dry and swollen specimens.

Unsurprisingly, the unswollen specimens exhibited greater fatigue resistance by comparison with the swollen test-pieces. It was clear that the fatigue life of the EPDM was reduced in proportion to the degree of swelling.

CHANGES IN COMPLEX ELASTIC MODULUS, E*

The fatigue behaviour of the three specimen sets was subsequently analysed with respect to the complex elastic modulus, E*, where E* was determined from the slope of the loading curve from zero stress and minimum strain to peak engineering stress and maximum strain for the cycle in question. Plots of the decrease in modulus E* with cycling of the test-piece for a stress amplitude of σ_a = 1MPa for the three sample sets are shown in Figure 4.

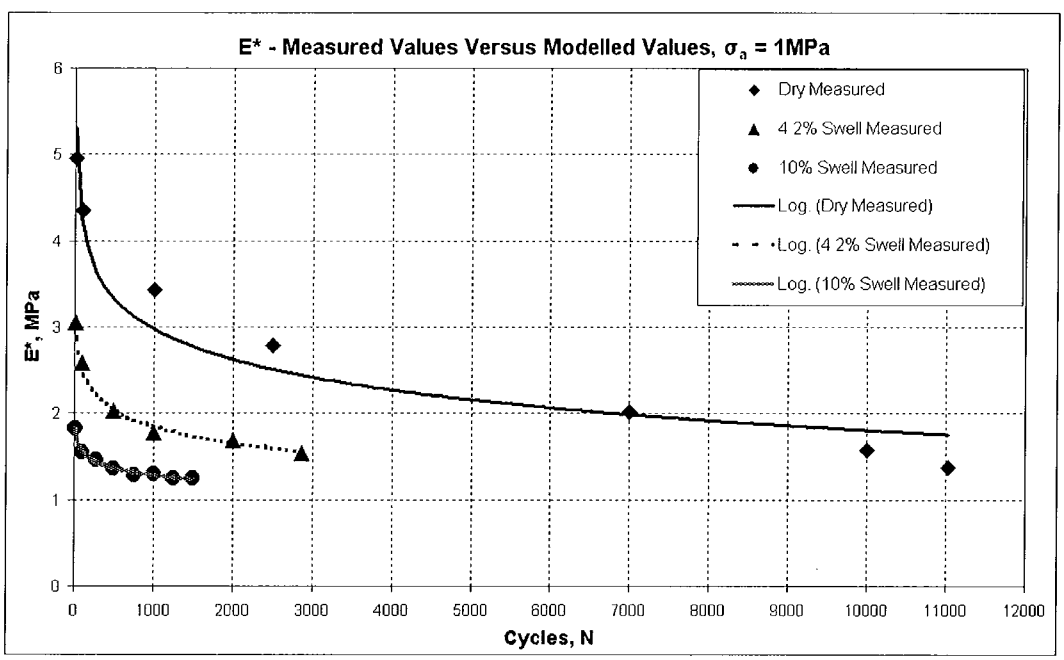

FIG. 4.— E* versus cycles N for dry, 4.2% and 10% swollen specimens at σ_a = 1MPa.

In tests carried out by Abraham[15], it was found that for a given material, failure consistently occurred after a specific loss in complex modulus E*. This predictor, termed $E^*_{residual}$ can be represented as:

$$E^*_{residual} = \frac{E^*}{E^*_{conditioning}}.100\% \qquad (4)$$

This value of $E^*_{residual}$ is quoted as a percentage and appeared to be independent of the applied loading. The dry and swollen specimens were analysed using this approach, where the % value of $E^*_{residual}$ versus cycles was plotted up to 95 % of the fatigue life of the specimen. $E^*_{conditioning}$ was defined as the modulus of the material after ten conditioning cycles. The plot of decrease in $E^*_{residual}$ is shown for the dry EPDM in Figure 5. $E^*_{residual}$ was found to have an average value of 33% ±10% of its original value at 95% of the fatigue life of each dry specimen. The 4.2% and 10% swollen specimens had values of $E^*_{residual}$ of 50.5%±10% and 60.1%±5% at 95% of specimen life respectively.

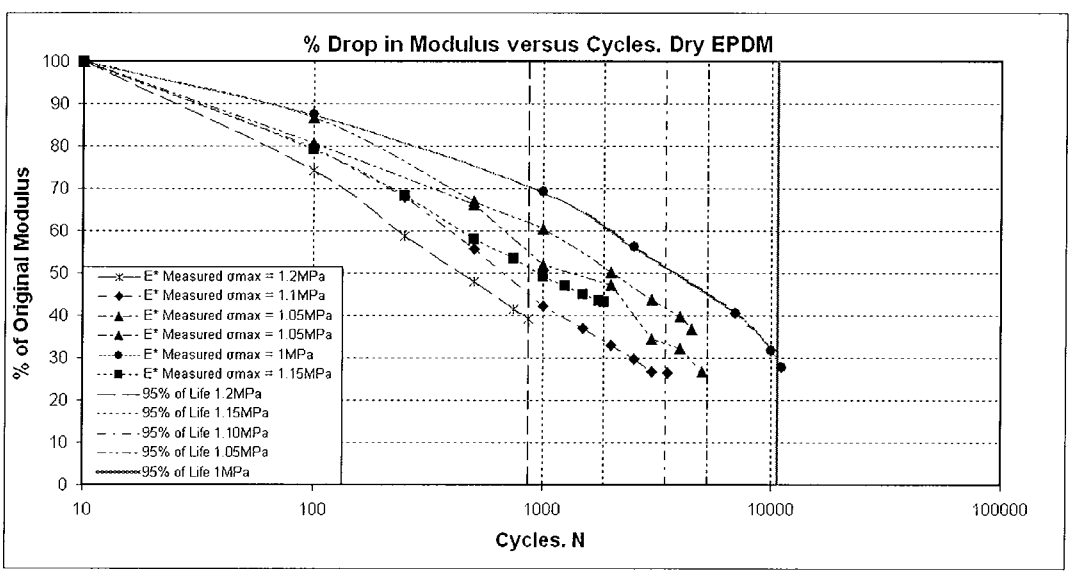

FIG. 5.— $E^*_{residual}$ versus log cycles, N for dry EPDM at five different stress amplitudes.

TABLE 2
$E^*_{RESIDUAL}$ AT 95% OF SPECIMEN LIFE

Degree of Swell	$E^*_{Residual}$ at 95% of specimen Life
Dry	33%±10%
4.2% Swell	50.5%±10%
10% Swell	60.1%±5%

CORRELATION BETWEEN DRY AND SWOLLEN MODULI

The dry and 4.2% swell specimen sets were compared at similar stress amplitudes, where the 100% initial modulus value ($E^*_{conditioning}$) for both sets of specimens was taken as the value at ten conditioning cycles in the dry specimens, for each respective stress amplitude. The trends for each specimen set are shown for five stress amplitudes in Figure 6.

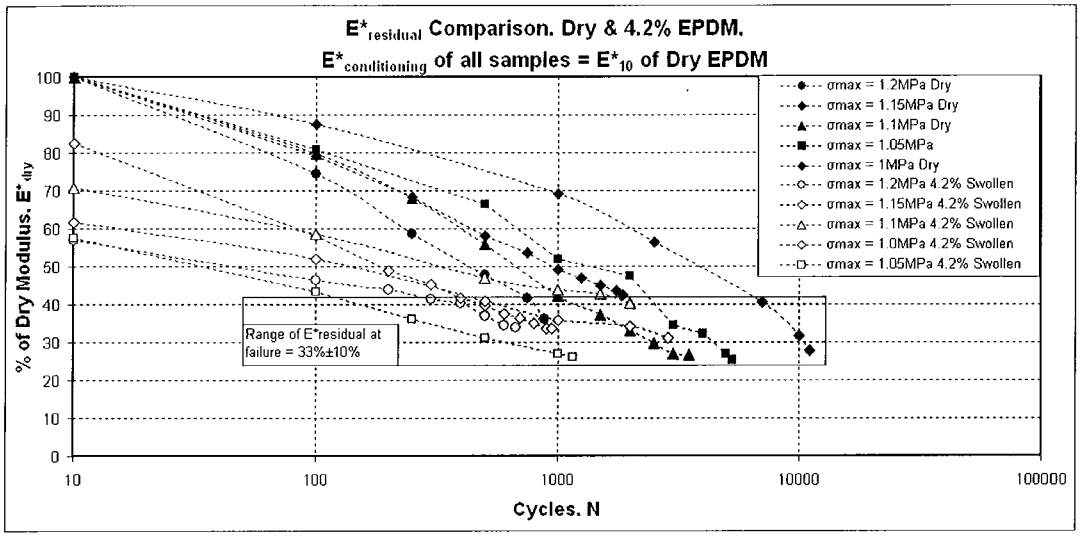

FIG. 6.— $E^*_{residual}$ versus log cycles, N for dry and 4.2% swollen EPDM at five different stress amplitudes.

There is an average $E^*_{residual}$ at failure of 33% ±10% for these sets of specimens, at the four different stress ranges. By knowing the initial modulus ($E^*_{conditioning}$) for the dry specimens, an approximation of the failure modulus for the swollen test-pieces can be determined.

When comparing the three specimen sets at similar stress amplitudes, the number of samples which could be analysed was limited, due to the 10% swollen specimens having short lives at higher stress amplitudes and the dry specimens having extremely long fatigue lives at lower stress amplitudes, with many of these tests typically ending with failures at the clamp edge. However, for a stress amplitude of 1MPa, comparison can be made between all three sample sets in terms of the decrease in specific modulus. Analysis of the value to which $E^*_{residual}$ decreases for each sample type at a stress amplitude of σ_a = 1MPa, with $E^*_{conditioning}$ taken as the modulus of the dry EPDM after ten conditioning cycles, suggested that $E^*_{residual}$ fell within the 33% ±10% range at failure for each of the three specimens.

CHANGES IN DYNAMIC STORED ENERGY

Previous analysis of uniaxial test data on EPDM found good correlation between the dynamic stored energy in the specimen versus the cycles at failure and proposed its use as a plausible fatigue life predictor.[15, 16] The dynamic stored energy is defined as the area bounded by the unloading portion of the stress-strain curve during a measurement cycle, where the energy was quoted in units of Nmm. Figure 7 shows how the dynamic stored energy was calculated from the stress-strain data.

The results for the fatigued specimens presented in this work were also analysed with respect to the dynamic stored energy.

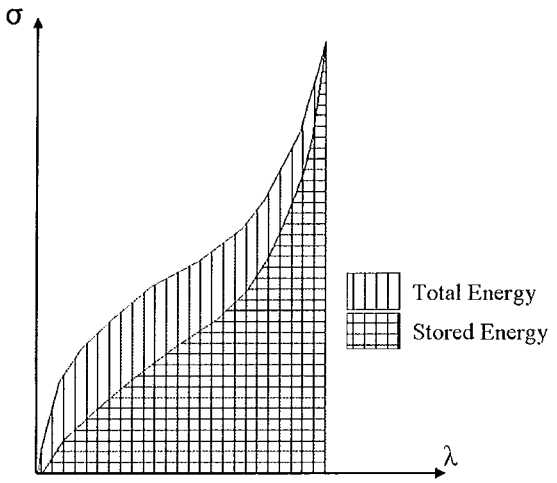

FIG. 7.— Calculation of total and stored energy for a cyclic stress-strain curve.

During equi-biaxial fatigue testing, a number of stress-strain measurements were made at intervals throughout the test. The dynamic stored energy in a cycle was subsequently calculated for these measured cycles. When plotted against the cycles to failure, the dynamic stored energy was found to increase linearly following conditioning of the test-piece. Figure 8 shows the plot of dynamic stored energy for the dry EPDM specimens. Similar plots were generated for the 4.2% and 10% swollen EPDM. The three plots are shown together in Figure 9.

At similar stress amplitudes, the dry EPDM samples had higher dynamic stored energy at failure than the swollen specimens, with the 10% swollen rubber having the lowest dynamic stored energy for a given stress amplitude. This result is due to the stiffness of the specimen decreasing with greater swelling. This is accompanied by a consequent increase in stored energy in a sample for a constant magnitude of stress amplitude. This is consistent with the simple relationship between energy and stiffness given by Equation (5):

$$W = \frac{1}{2}\frac{F^2}{k} \qquad (5)$$

Where W is strain energy, F is the applied load and k is the stiffness of the material.

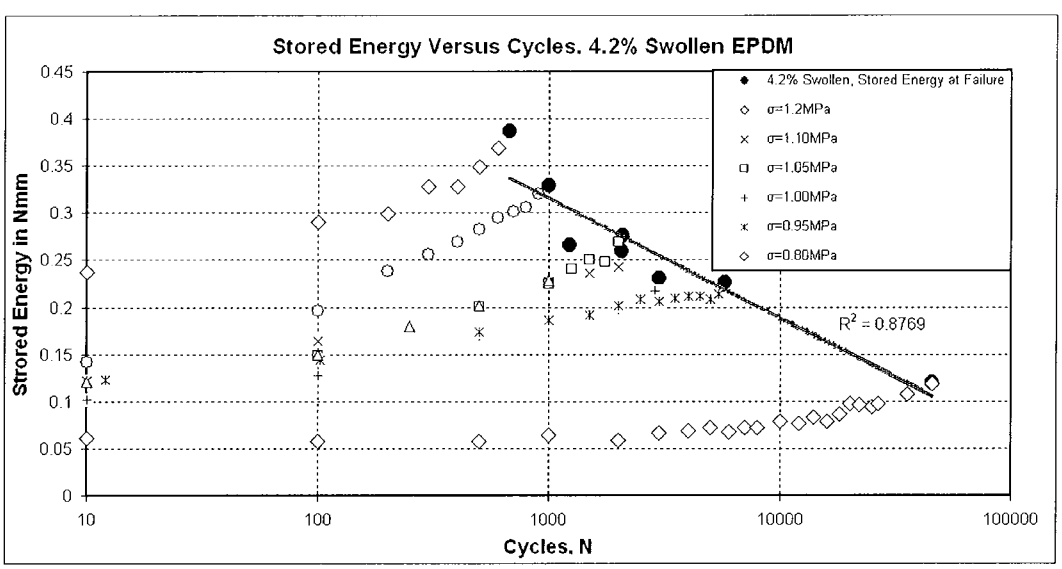

FIG. 8.— Plot of Dynamic Stored Energy for the 4.2% Swollen EPDM at several stress amplitudes.

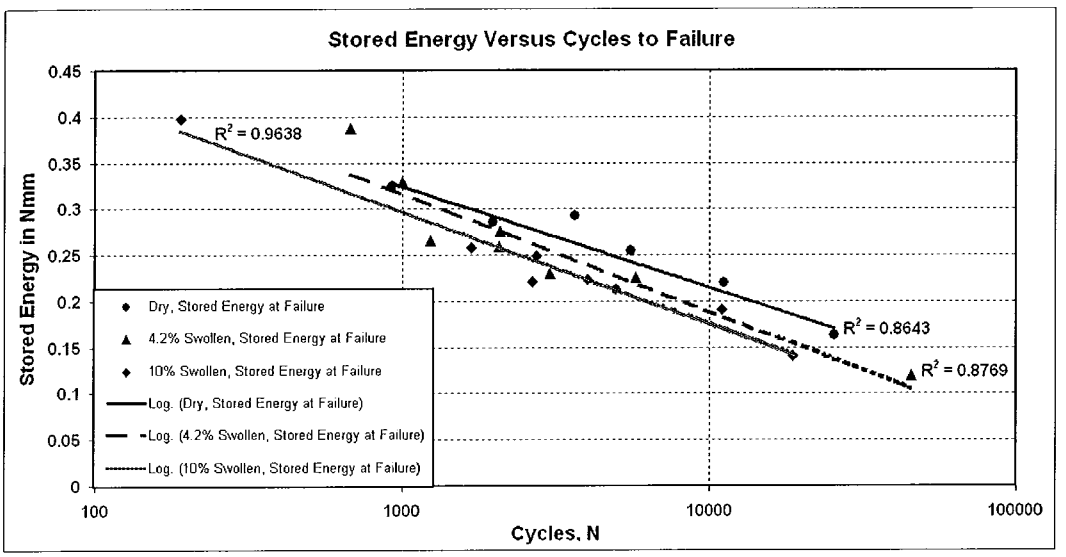

FIG. 9.— Plot of Dynamic Stored Energy versus log cycles to failure for the three specimen sets.

SURFACE MORPHOLOGY AT FAILURE

The fracture surfaces of the dry samples were analysed using a scanning electron microscope. A magnification factor of X400 at 2.0kV was used to view failure surfaces. For low cycle lives of less than one hundred, the type of failure is more akin to that of a single cycle test to destruction, with the surface morphology fibrous in nature and in some instances showing de-lamination at the failure surface. Failures at cycles greater than this show clear evidence of crack propagation and subsequent rupture. In most fatigue failures, cracks predominately propagated in the bubble pole region. Failure was deemed to have occurred when rupture took place at these crack sites. This behaviour was common to both the dry and swollen specimens. SEM images of the surface morphologies of the specimens at a similar stress amplitude of 1 MPa are shown in Figure 10. In the dry samples there is a coarser failure surface at lower cycles than for failures at higher cycles. Fatigue tests carried out elsewhere reported that the surface of the dry samples indicated blunt tearing, while the surfaces of the swollen test-pieces indicated sharp tearing.[2]

This was confirmed by the SEM images taken in this study, where the blunter surface of the dry specimens can be contrasted with the smoother surface of the swollen test-pieces. This blunt tearing could be attributed to more polymer filler interaction in the dry material, with the material being tougher for a given applied stress. The SEM imaging suggests that the swollen failure surfaces 'flow' more easily over one another than those of the dryer specimens.

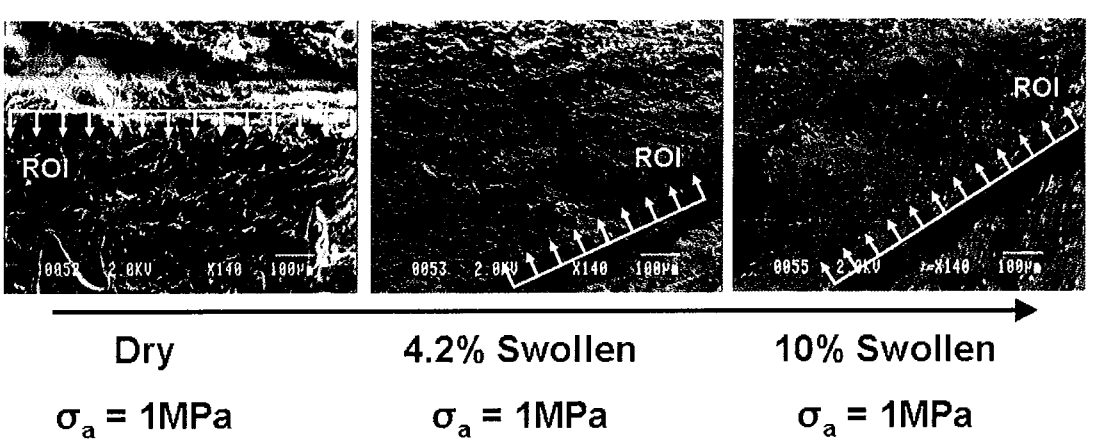

FIG. 10.— SEM Imaging of specimen fracture surfaces, σ_{eng} = 1 MPa (ROI = Region of interest).

It can be seen that flaws are more abundant in the swollen material, which can be attributed to the swelling effects of the oil. Due to the presence of these flaws the probability of crack growth being initiated at these flaws would be expected to be high, as the areas around the flaws would potentially have a lower complex modulus than other points in the network.

DISCUSSION

It was found that the fatigue life results produced in the equi-biaxial tests agreed with those for the dynamic uniaxial load case; that is, the fatigue life of the specimens was reduced in proportion to the amount of swelling.

The relationship between dynamic stored energy and cycles to failure is influenced by the degree of swelling of the test-pieces, with the energy at failure reducing for increases in swelling levels. It may be possible to relate the swollen predictor curve to the dry predictor curve by using some offsetting factor similar to those determined by Ronan *et al* to predict long-term stress relaxation in elastomers.[17]

A more practical approach to predicting realistic fatigue lives in rubber compounds may be to use the limiting value of the residual modulus $E^*_{residual}$. When the residual modulus for swollen specimens is based on a calculation using the initial conditioned modulus of the dry rubber at a similar stress amplitude, $E^*_{residual}$ values exhibited reasonable correlation, with a limiting value of 33%±10% for both the dry and swollen specimens. By knowing the limiting value of $E^*_{residual}$, the effect of swelling on fatigue life can be calculated, if the value of $E^*_{conditioning}$ is known at a particular stress amplitude.

This approach could have practical significance in the design of elastomeric components subjected to fatigue loading conditions. Consider a component manufactured from a similar compound to that used in these tests. If the part was loaded within a constant engineering stress range and the value of $E^*_{conditioning}$ at that stress range known, it could be proposed that once the value of $E^*_{residual}$ fell below a material specific value of 43% then replacement of the part should be considered.

CONCLUSION

In summary, the fatigue life of an EPDM sample under dynamic equi-biaxial loading can be greatly reduced in the presence of an oil in the rubber network, even for relatively small amounts of swelling. Despite being in contact with the oil for only one hour at 100°C, the dynamic properties such as the complex modulus E* and the dynamic stored energy are fundamentally altered from those of untreated EPDM. The changes in these properties and the lower fatigue lives of the swollen specimens can be attributed to a number of factors, both physical and chemical in nature.

Physical factors include the presence of larger voids in the network and a lower initial complex modulus due to the swelling action. The presence of these flaws in the elastomer network structure was confirmed by SEM imaging, which showed that the failure surfaces for each set of test-pieces is markedly different in the dry and swollen cases.

Chemical factors which may explain the difference in the dynamic mechanical properties of the unswollen specimens include changes in the network structure due to oil swelling, where there may be a reduction in the number of cross-links resisting the tensile force or where the swelling may lead to differences in the equilibrium length of individual chains. Also, it has been reported elsewhere that the reformation of polysulphidic linkages during a loading cycle can be inhibited in the presence of oil.[3]

The practical significance of this study is to highlight the effect of contamination on the mechanical performance of non-strain crystallising elastomers subjected to realistic loading conditions. EPDM components are commonly used in automotive applications, where they provide the advantage of having more functionality at higher temperatures than SBR or natural rubber. However, some of these advantages are offset by their poor resistance to the numerous fluids used in vehicles. The results presented here illustrate that if a risk of oil contamination is sufficiently high and the automotive design engineer has failed to fully take swelling into account, safety factors and life expectations may be unrealistically high and components will lack the residual mechanical strength to withstand levels of fatigue loading.

ACKNOWLEDGEMENT

The authors would like to thank the Faculty of Engineering and the Directorate of Research and Enterprise in the Dublin Institute of Technology. This work was made possible by funding from Enterprise Ireland under its 'Proof of Concept' programme.

REFERENCES

1 Mars, W., Fatemi, A., RUBBER CHEM. TECHNOL. **77**, 391 (2004).

2 Flory, P. J., Rehner, J., *J. Chem. Phys.* **11**, 521 (1943).

3 Cho, K., Wook, J.J., Daeho, L., Hyunaee, C., Young-Wook, C., *Polymer*. **41**, 179 (2000).

4 Gul, V., Fedyukin, D., Dogadkin, B.A., RUBBER CHEM. TECHNOL. **32**, 454 (1959).

5 Dogadkin, B.A., Gul, V., RUBBER CHEM. TECHNOL. **24**, 344 (1951).

6 Neogi, C, Bhattacharya, A.K., Bhowmick, A.K., RUBBER CHEM. TECHNOL. **63**, 651 (1990).

7 Abhimanyu, P., Coolbaugh, T., RUBBER CHEM. TECHNOL. **78**, 516 (2005).

8 Beerbower, A., Pattison, D.A., Staffin, G.D., RUBBER CHEM. TECHNOL. **37**, 246 (1964).

9 ASTM Standard D471-95, "Standard Test Method for Rubber Property-Effect of Liquids", *Annu. Book ASTM Stand.* **08.01**, 86 (1995).

10 Murphy N, Hanley J, McCartin J, Lanigan B, McLoughlin S, Jerrams S, Clauss G, Johannknecht R. Determining multiaxial fatigue in elastomers using bubble inflation. In *Constitutive Models for Rubber*; Austrell, P.E., Kari, L., Ed.; Balkema, 2005; Vol. 4; p 65.

11 Murphy N, Hanley J, Ali H, Jerrams S,. The Effect of Specimen Geometry on the Multiaxial Deformation of Elastomers. In *Constitutive Models for Rubber*; Boukamel, A., Laiarinandrasana, L., Méo, S., Verron, E., Taylor & Francis, 2007; Vol. 5; p 61.

12 Hanley, J. Ph.D. thesis, Dublin Institute of Technology, Dublin, Ireland, 2008.

13 Johannknecht, R, Jerrams, S. Clauss, G., *Journal of Materials, Design and Applications,* **216** Part L, No L4 (2002).

14 R. Seldén "Fracture mechanics analysis of fatigue of rubber - a review" *Progress in Rubber and Plastics Technology Vol 11, No 1* The Institute of Materials/RAPRA (1995).

15 Abraham, F. Ph.D. thesis, Coventry University, Coventry, United Kingdom, 2002.

16 Alshuth T., Abraham F., Jerrams S., RUBBER CHEM. TECHNOL. **75**, 365 (2002).

17 Ronan, S., Alshuth T., Jerrams, S., Murphy, N., *Journal of Materials and Design*, **28**, 1513 (2007).

Appendix 2 – Control Program Process Description

Appendix 2.1 System Hardware

At the time of the testing presented in this work, the system control and GUI was carried out using Labview 7.1, with hardware interfacing via an M-6251NI-DAQ.

The system consists of the following input/outputs:

- *Digital Out*: Hardware Trigger Signal for CCD cameras.
- *Analog In*: Feedback from Pressure Transmitter, Feedback from Linear Variable Differential Transducer.
- *Analog Out*: Activation signal to proportional control valve.

There are three programs, which exist as 3 different Labview files. The fourth program, the vision acquisition program is integrated into the other three programs as a sub-program.

- Program 1: Pressure Controlled Test Program
- Program 2: Volume Controlled Test Program
- Program 3: Engineering Stress Controlled Test Program
- Program 4: Digital Camera Image Acquisition Program

Program 1 – Pressure Controlled Test Program

The test rig inflates and deflates a soft material test-piece between 2 pressure limits.

The pressure limits are set by the user at the start of the program in the GUI, along with the specimen thickness and the zero LVDT value (this allows the test to be started with the cylinder in different initial positions without affecting the control). Pressure feedback during the testing is from a pressure transmitter, which sends an analog voltage signal to the DAQ.

The inflations and deflations are carried out hydraulically, via a proportional control valve, where valve actuation is through solenoids. These solenoids are activated by a single analog voltage signal from the DAQ. The test-piece will be cycled between the preset limits until failure of the test-piece occurs. The control program also counts the cycles and calculates the cycle rate of the test in Hz throughout the duration of the test. The inflation will continue until the real pressure signal is >= the upper pressure setpoint, then deflation will take place until real pressure is <= the lower pressure limit. The cycling between limits continues until the test-piece fails, or the target cycle's value is reached, or the user stops the program.

Program 2– Volume Controlled Test Program

The system is also capable of volume control. The test rig inflates and deflates the test-piece between 2 volume limits. The volume limits are set by the user at the start of the program in the GUI in a similar manner to the pressure program.

Volume feedback during the testing is from a Linear Variable Differential Transducer (LVDT), which sends an analog voltage signal to the DAQ.

The proportional control valve again controls the hydraulic inflation and deflation.

The control program counts the cycles and calculates the cycle rate of the test in Hz throughout the duration of the test. The inflation will continue until the real volume signal is >= the upper volume setpoint, then deflation will take place until real volume is <= the lower volume limit. The cycling between limits continues until the test-piece fails, or the target cycle's value is reached, or the user stops the program.

Program 3– Engineering Stress Controlled Test Program

For stress control, the program operates in the following manner. The test rig inflates and deflates the test-piece between 2 stress limits. The values of stress are calculated using a sub-routine, which reads the LVDT volume voltage and converts it to a radius value, the relationship between volume and radius existing in the program as a 4th order polynomial function which Labview can use to generate the radius value. The pressure transducer voltage is also read at the same time as the LVDT voltage and is converted from voltage in Pascal's by applying a straight line calibration equation to the voltage. The calculated radius and pressure and then multiplied together and divided by twice the specimen thickness value to give the stress. The stress limits are set by the user at the start of the program in the GUI in a similar manner to programs 2 and 3 and hydraulic inflation and deflation is initiated by the proportional valve. The cycling between limits continues until the test-piece fails, or the target cycle's value is reached, or the user stops the program.

Program 4– Digital Camera Image Acquisition Program

A separate software application is used to run two digital cameras. They require a hardware trigger signal to allow frames to be taken by each camera. This hardware trigger is provided by LabView.

The number of triggers to be sent by LabView is pre-selected in the GUI. The pressure (or volume, or stress) are then selected.

When running, the program inflates and deflates between the two preset limits. The trigger to the cameras is sent out at increments of the inflation parameter (e.g. 20 frames at 0-2 bar, pressure frame capture every 0.2 Bar).

The incremented pressure/volume values are written to a .dat file as part of the program.

The program runs for one inflation/deflation cycles, then waits for user intervention for a restart etc.

Appendix 2.2 Labview Program Overview

Whether constant pressure, LVDT (Volume) or stress control, the program operates as follows:

There are 2 selections, 'Fatigue' or 'Vision'. Fatigue cycles the test-piece between limits until failure, or if the user intervenes, while Vision measures the pressure and LVDT values during a single inflation and deflation.

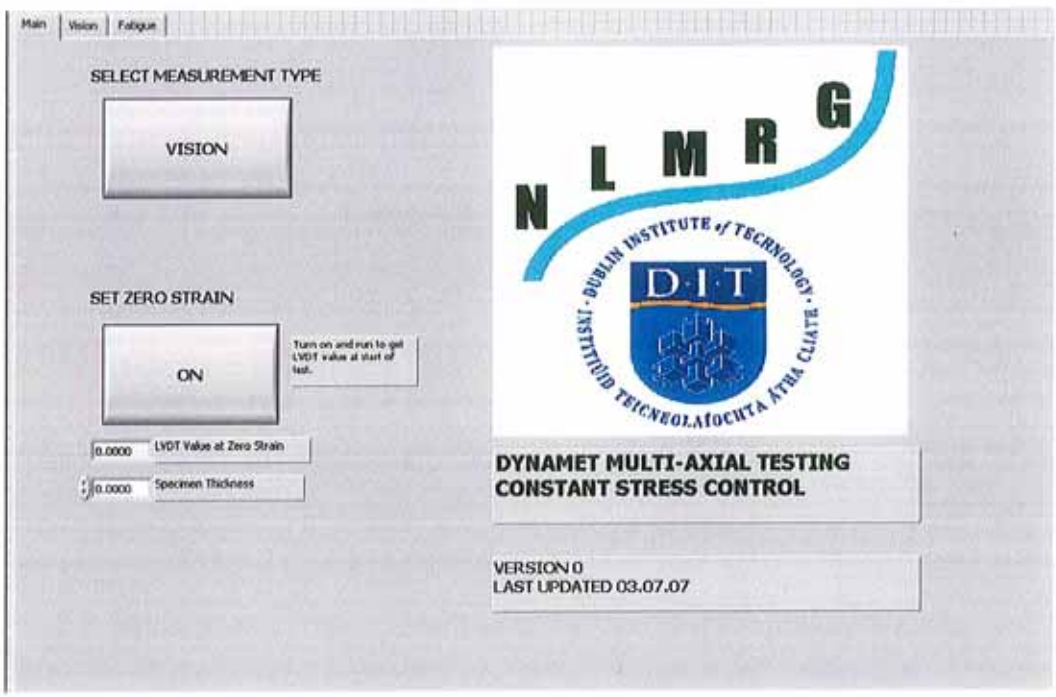

Figure Appendix 2.1 Main User Screen.

Set Zero Strain

If this is selected and the program started, the LVDT value is stored. This value is then subtracted from the measured LVDT value in subsequent measurement. In effect, it 'zeroes' the LVDT, meaning a test can be started without the cylinder being fully retracted. It also allows the LVDT value to be related to the radius measurement.

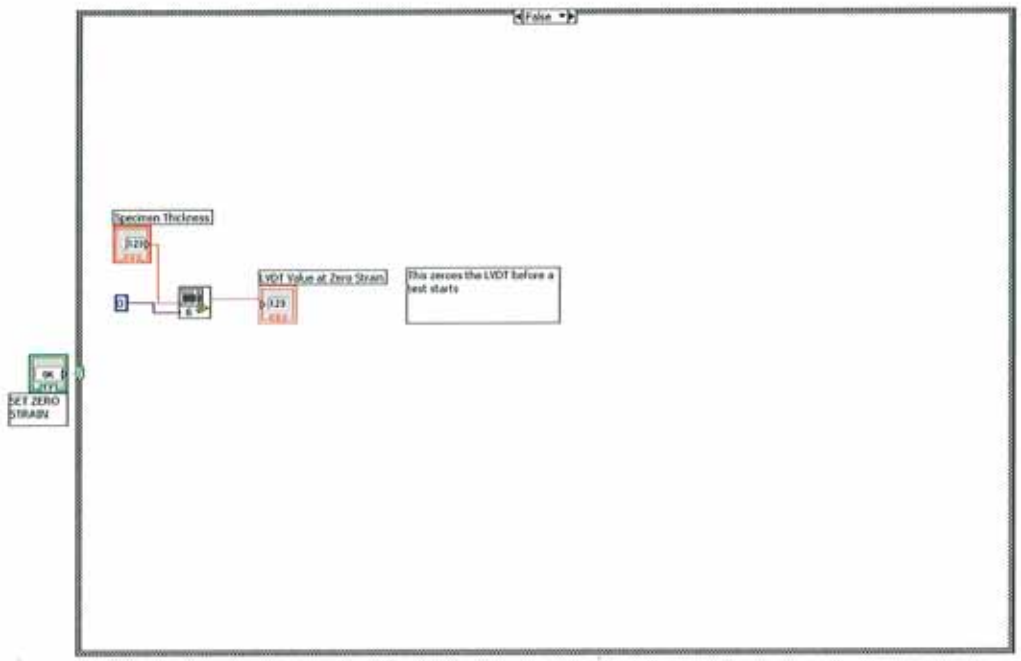

Figure Appendix 2.2 Interlocks and Zero LVDT Setting

General Interlocks

The 'Vision' program cannot be run while 'Fatigue' is selected and vice versa. Neither 'Fatigue' nor 'Vision' selections can be made if the 'Set Zero Strain' button is selected.

Appendix 2.2.1 Fatigue Program

There are a number of preset values for this program:

- High Limit
- Low Limit
- Inflation Rate Up

- Inflation Rate Down
- Stop at Cycle Value

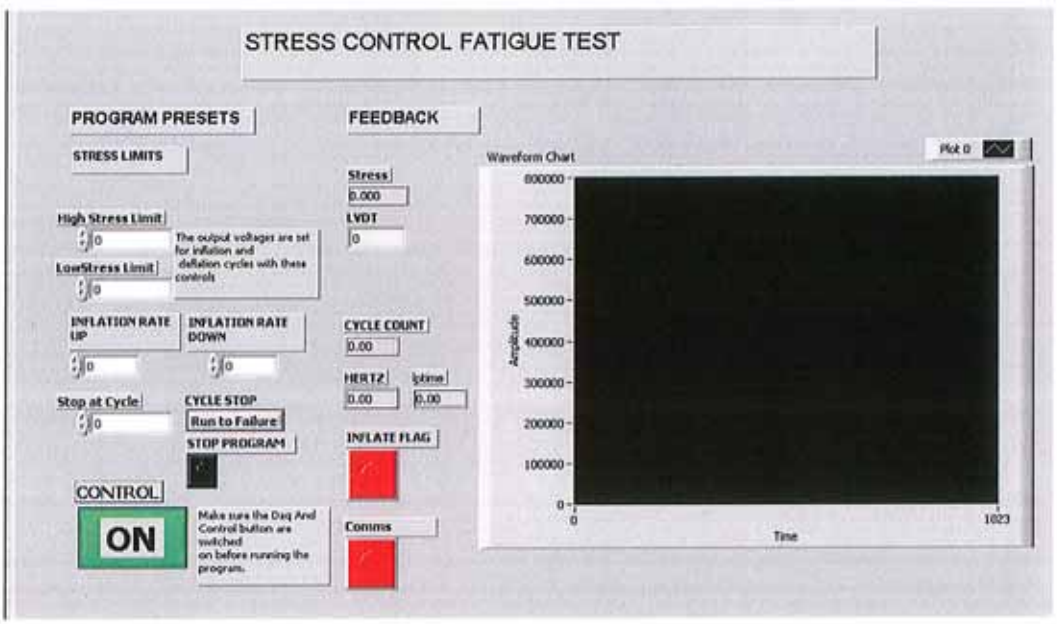

Figure Appendix 2.3 Fatigue Program User Interface.

This program consists of the following steps:

Step 1

The rate out to the valve is set at 50%.

Step transition

When the program scan time for has elapsed.

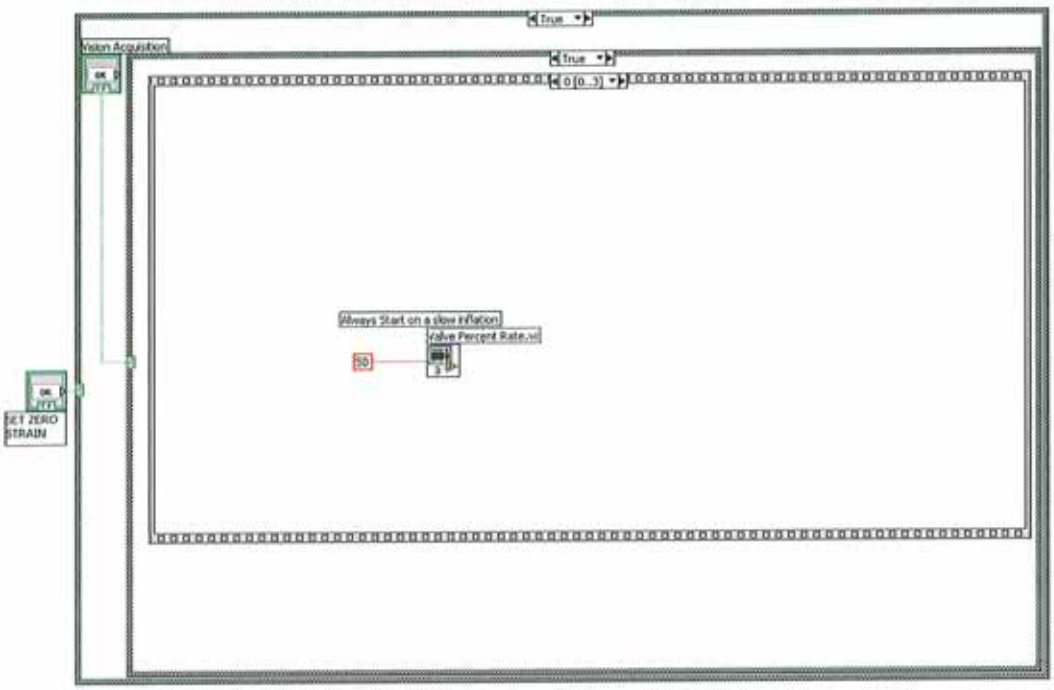

Figure Appendix 2.4 Fatigue Program Step 1.

Step 2

A 'While' Loop is started

This loop reads the following values continuously:

- Inflation Rate Up
- Inflation Rate Down
- Inflate Flag
- Cycle Count

A subroutine is also executed during this step.

Step Transition

This loop will stop when either of the following conditions is met:

'Stop at Cycle Value' is equal to the cycle count. This means if the user wants the test to run to 1000 cycles, once the cycle count reaches 1000 the loop will stop.

LVDT Value is greater than a user defined value. This means if the test-piece bursts and the cylinder moves beyond an upper limit, the loop will stop.

Subroutine

Read in analog values. This can be pressure, LVDT and stress.

If the process variable (PV) is greater than the high setpoint, then the inflation rate down is multiplied by -1 and this value is output to the valve.

The time that this part of the program executed at is stored (Deflate time).

If the inflate flag is low, then 1 is added to the value of Cycle Count.

If the PV is less than or equal to the low setpoint, then the inflation up value is output to the valve.

The time required to execute this part of the program is stored (Inflate time).

The deflate time is subtracted from the time value at this stage in the loop and divided by -500 to get the Hertz value.

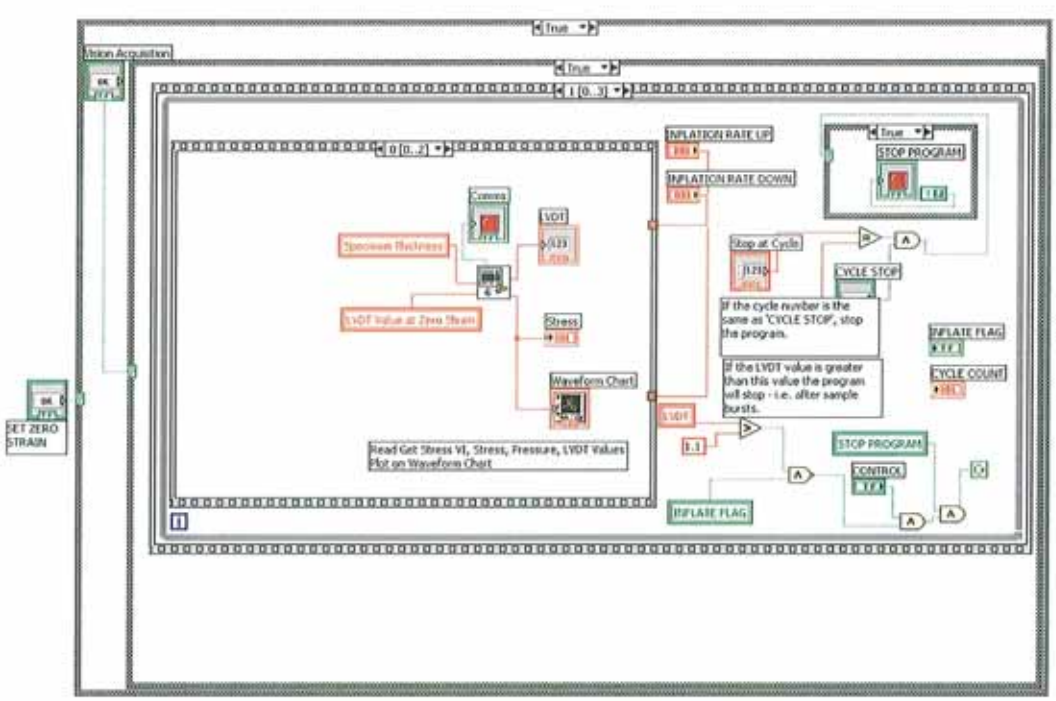

Figure Appendix 2.5 Fatigue Program Step 2, Subroutine Step 1.

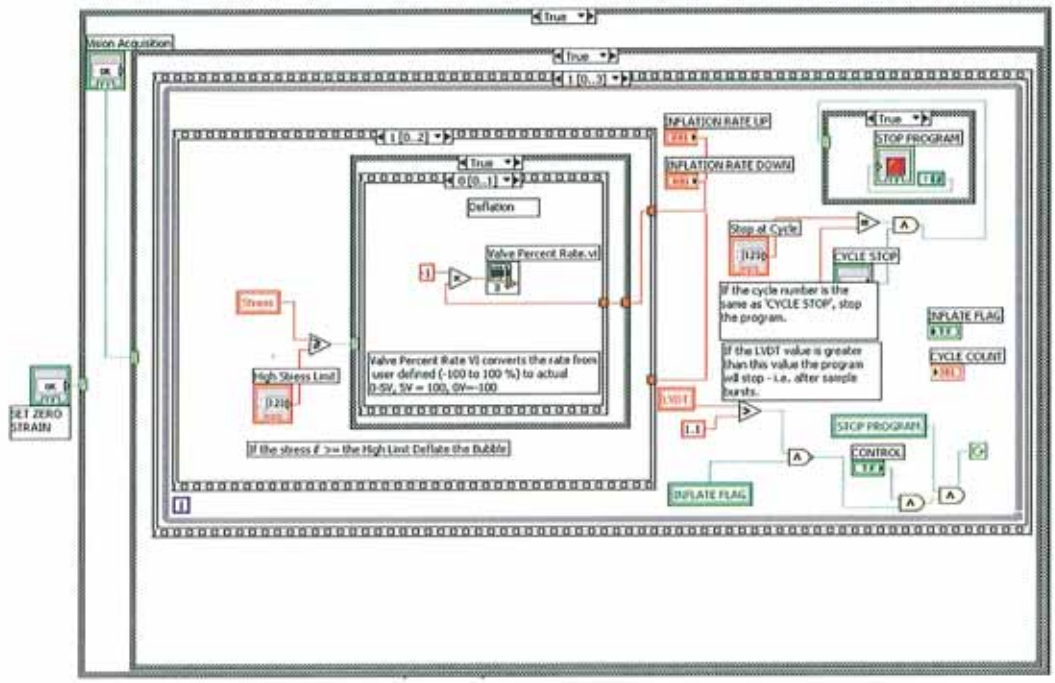

Figure Appendix 2.6 Fatigue Program Step 2, Subroutine Step 2a.

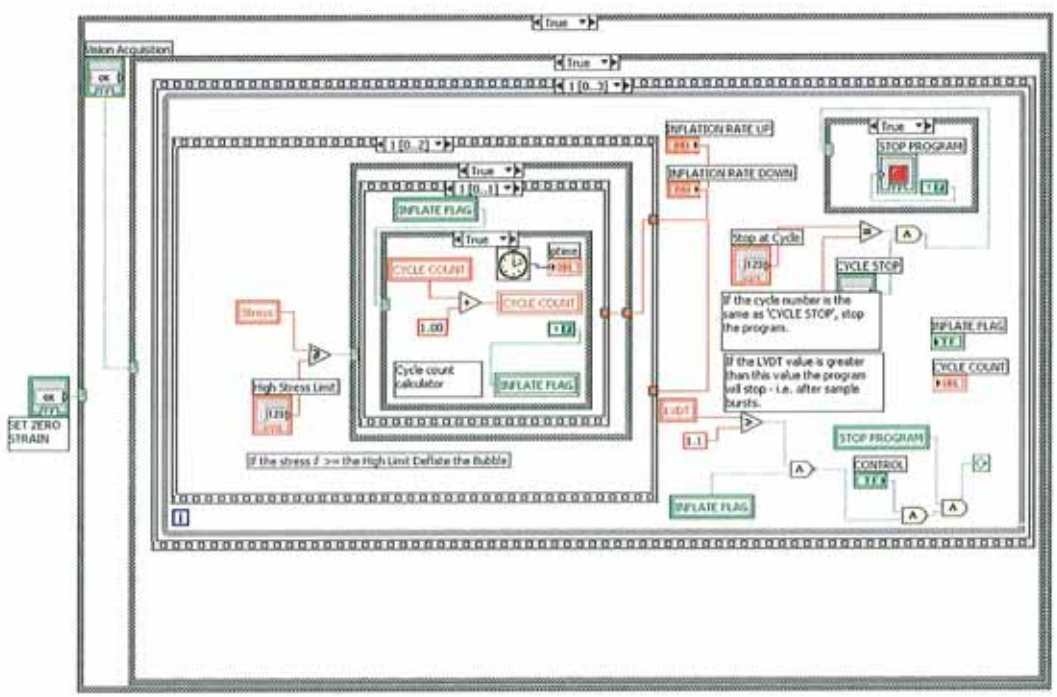

Figure Appendix 2.7 Fatigue Program Step 2, Subroutine Step 2b.

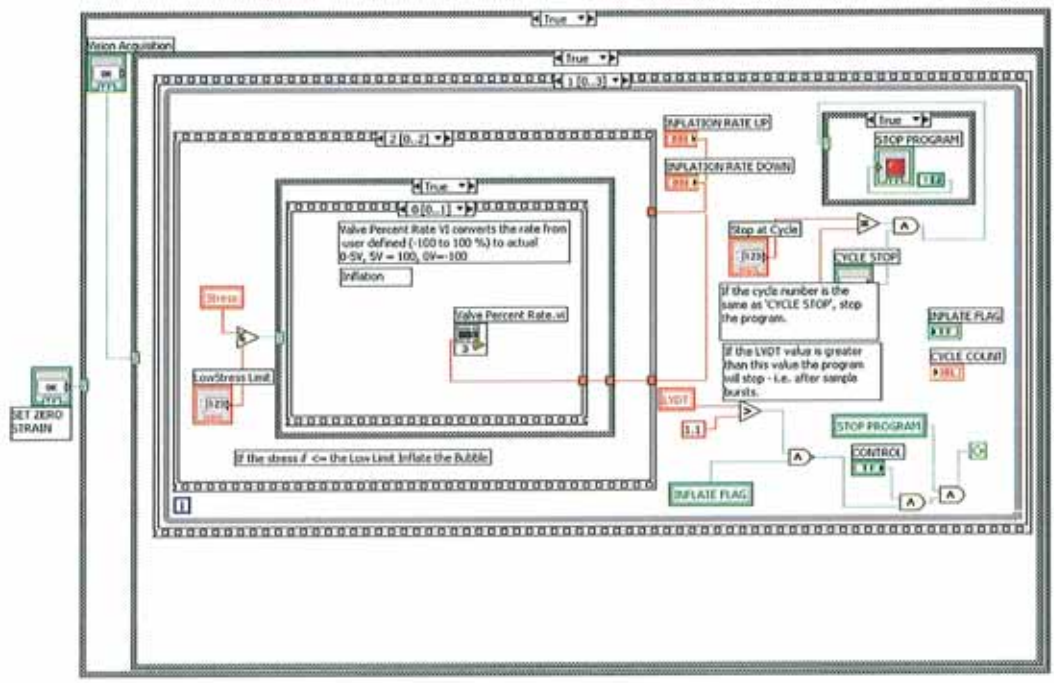

Figure Appendix 2.8 Fatigue Program Step 2, Subroutine Step 3a.

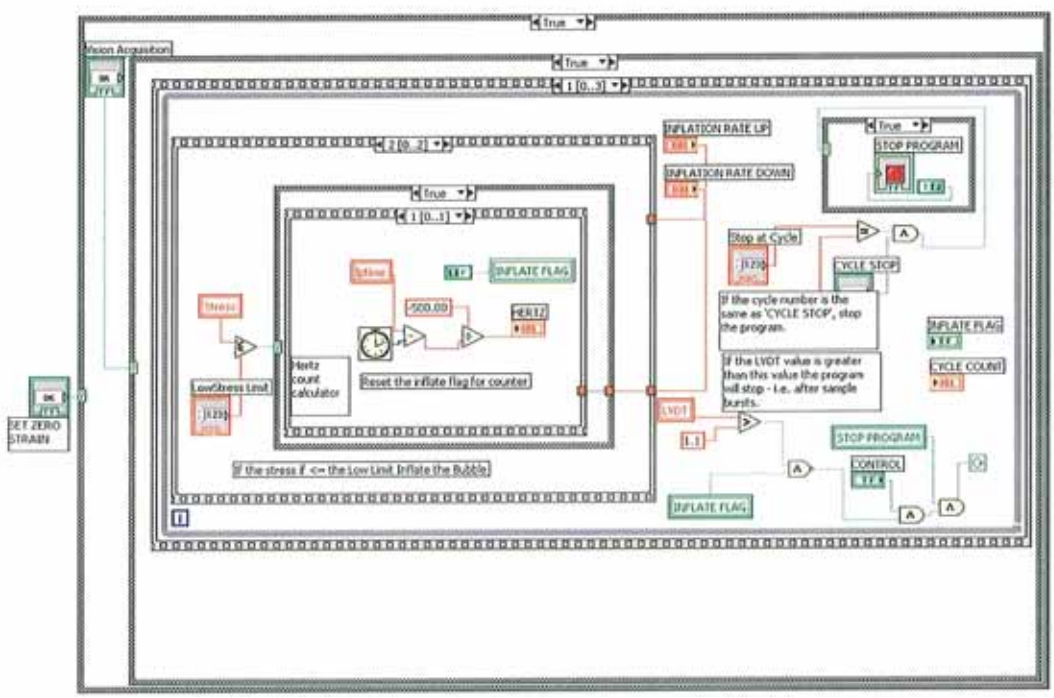

Figure Appendix 2.9 Fatigue Program Step 2, Subroutine Step 3b.

Step 3

When the 'While' Loop in Step 2 completes, another 'While' loop is started in this step. While the PV is greater than or equal to the low limit, the inflation rate down is multiplied by -1 and this value is sent to the valve.

Step Transition

The loop will stop when the PV is less than or equal to the low limit.

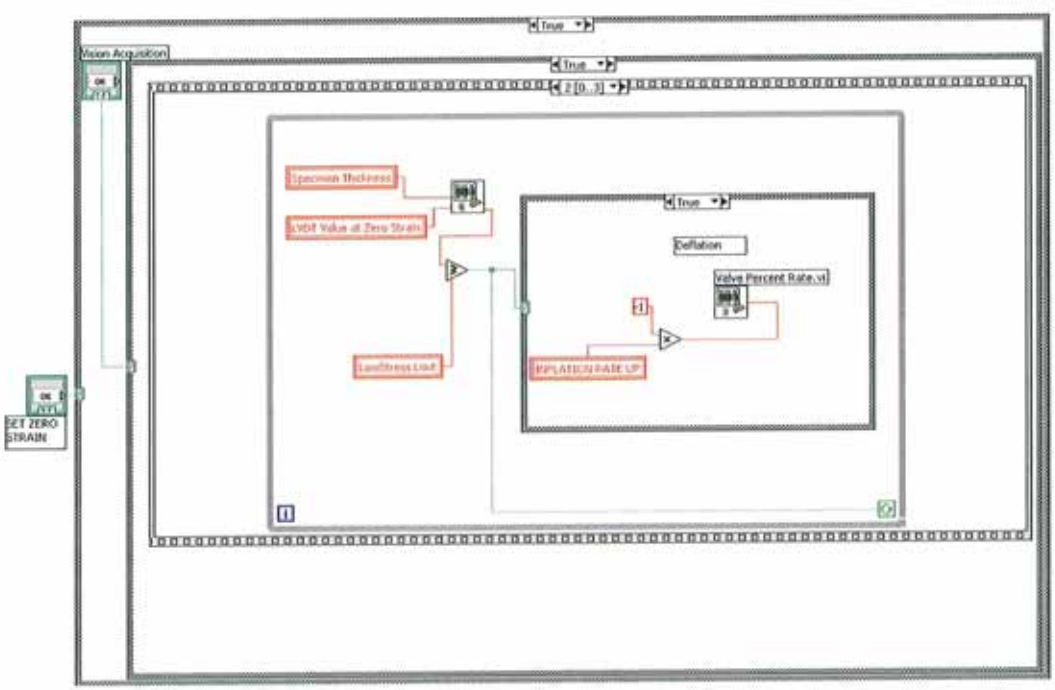

Figure Appendix 2.10 Fatigue Program Step 3.

Step 4

When the 'While' Loop in Step 3 completes, a value of zero is sent to the valve and the program waits for user input.

Step Transition

When the program scan time for has elapsed.

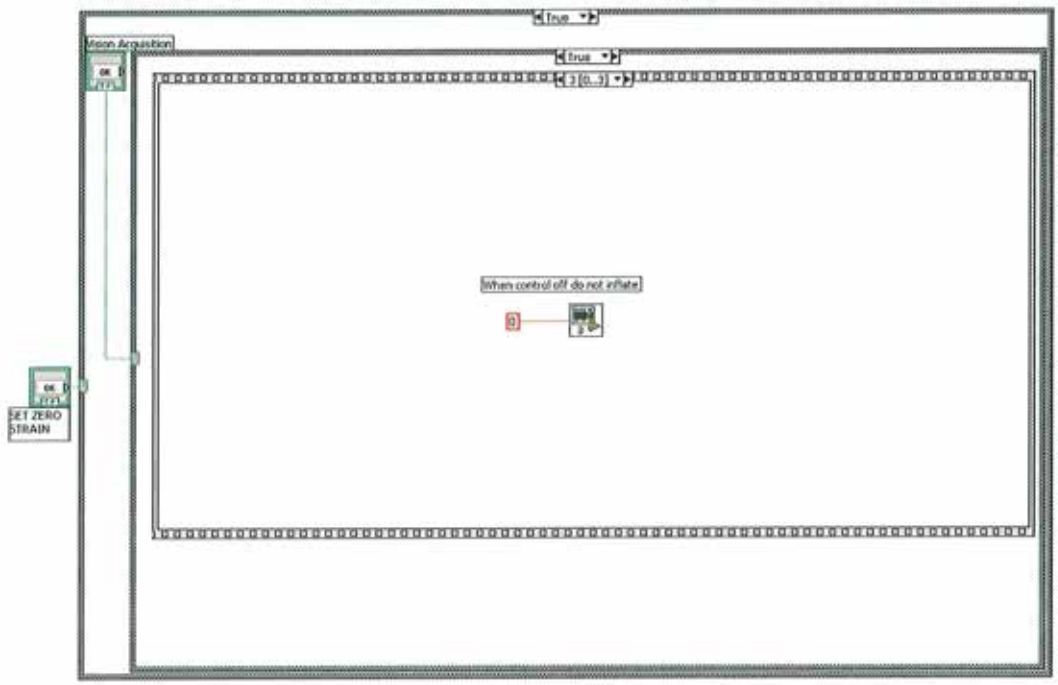

Figure Appendix 2.11 Fatigue Program Step 4.

Appendix 2.2.2 Vision Program

There are a number of preset values for this program:

- High Limit
- Low Limit
- Number of Frames to Max PV
- Inflation Rate Up
- Inflation Rate Down

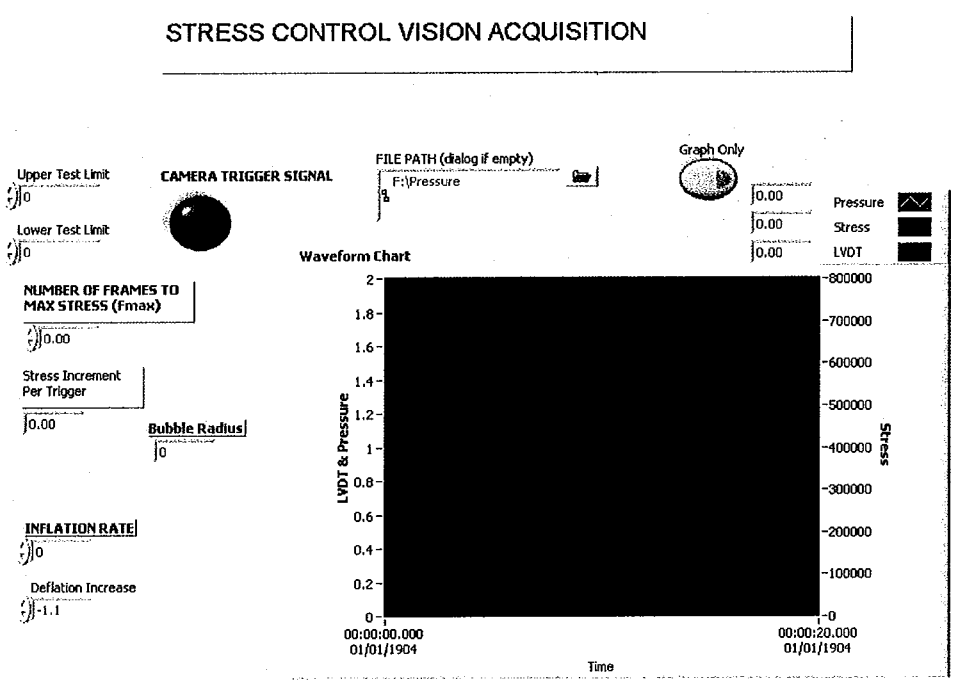

Figure Appendix 2.12 Vision Program User Interface.

A 'While' loop executes in parallel with every step in the program. This reads in the analog inputs (pressure, LVDT, stress) and plots them on a graph, so the user can monitor what is happening.

This program consists of the following steps:

Step 1

The rate out to the valve is set at 0%.

The PV is measured.

The inflation rates are measured.

Step transition

When the program scan time for has elapsed.

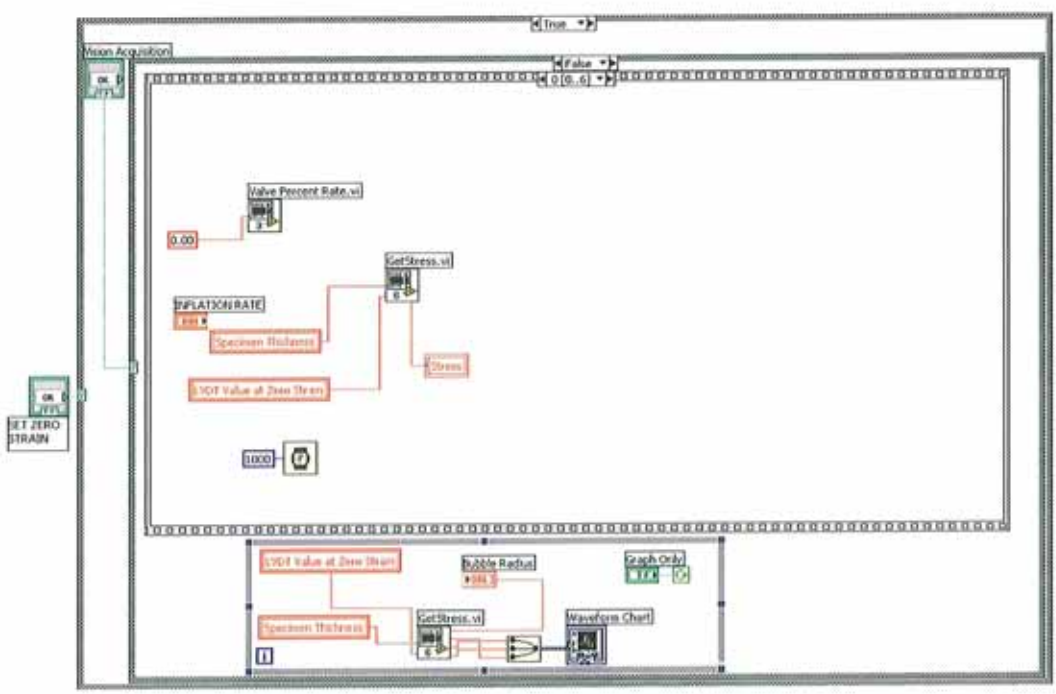

Figure Appendix 2.13 Vision Program Step 1.

Step 2

The following calculations are carried out:

PV Increment Per Trigger = (High Limit – Low Limit)/(Number of Frames to Max PV-1))

2% of Range = (High Limit – Low Limit)/ 50

Step transition

When the program scan time for has elapsed.

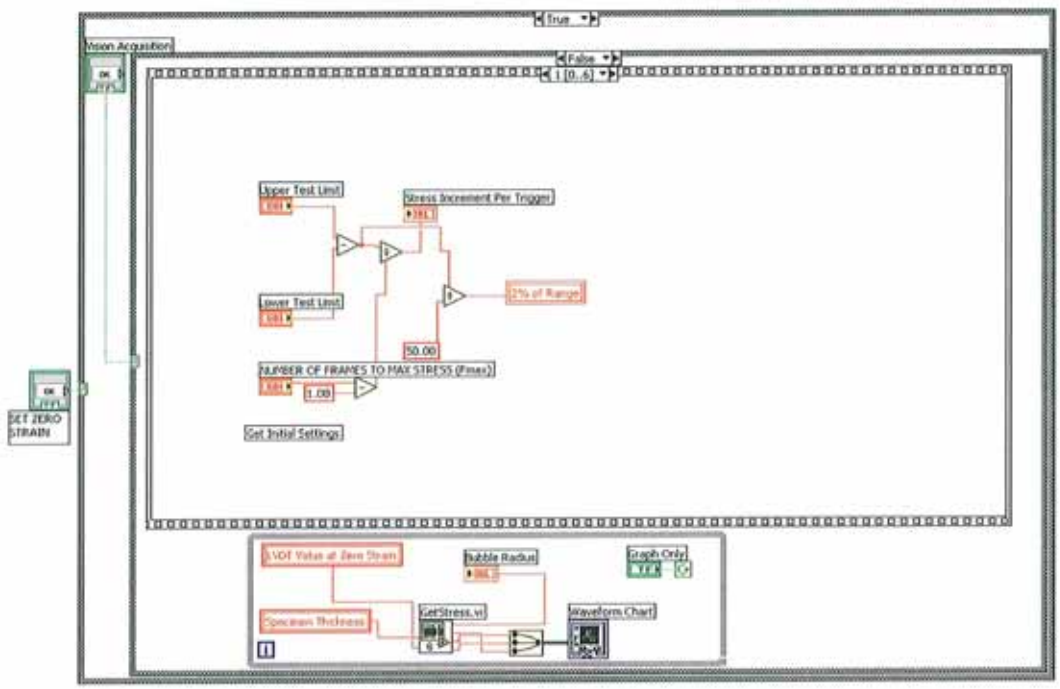

Figure Appendix 2.14 Vision Program Step 2.

Step 3

If the PV is greater than the Low Limit, multiply the Inflation Rate Down by -1.

This deflates the test-piece to the lower limit before measurement begins.

Step transition

When the PV is less than (Low Limit – 2% of Range).

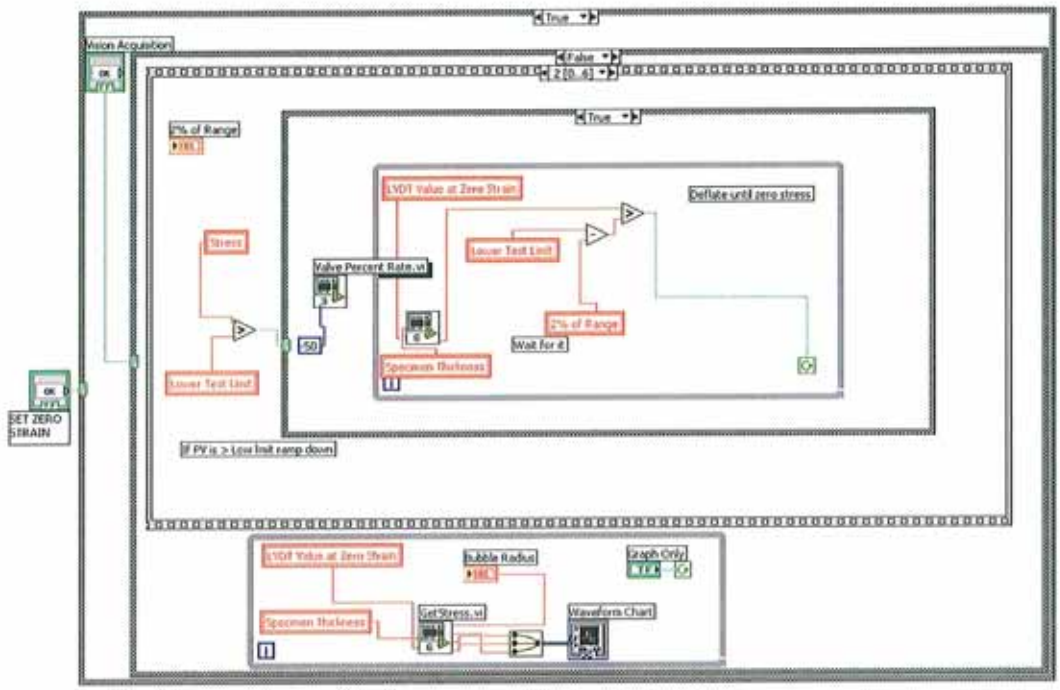

Figure Appendix 2.15 Vision Program Step 3.

Step 4

Stop the deflation by sending a value of zero to the valve.

Step transition

When the program scan time for has elapsed.

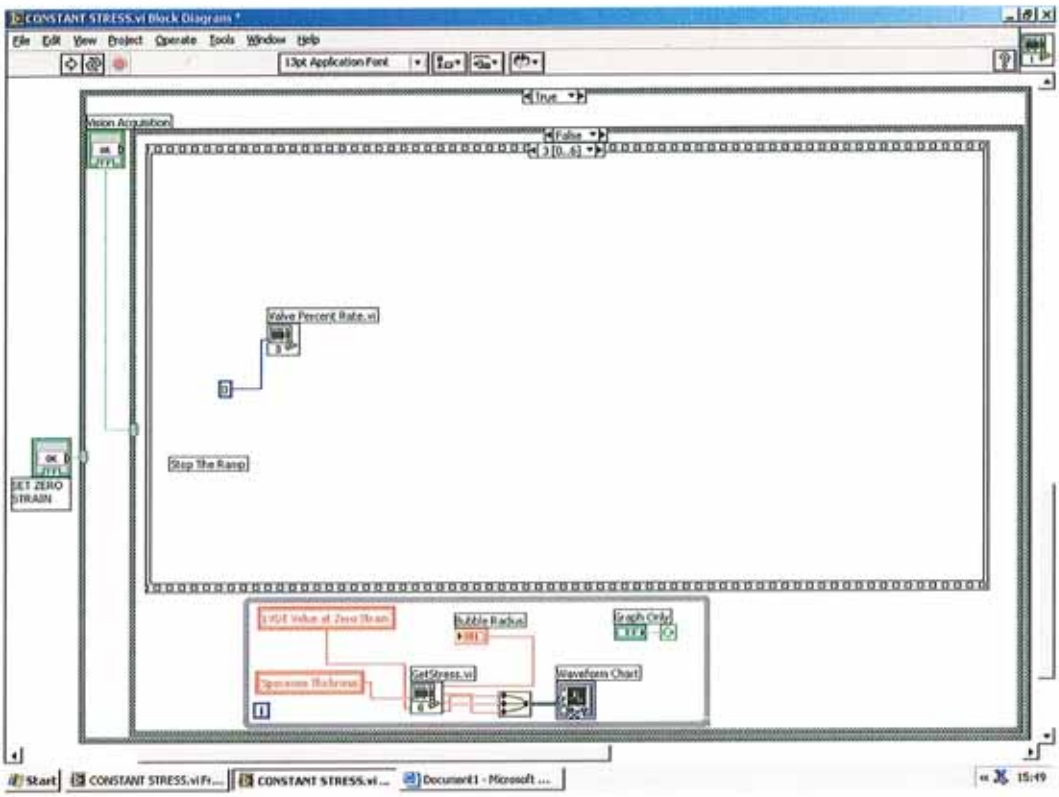

Figure Appendix 2.16 Vision Program Step 4.

Step 5

The Inflation Rate Up is output to the valve.

At the same time in this step, a 'For' Loop is started.

The number of iterations in the loop is equal to the 'Number of Frames to Max PV'.

Substep 1

While Loop which waits until the target PV is reached:

For the iteration number, wait while PV is less than

(Low Limit) + (PV Increment per Trigger X Iteration Number)

Substep Transition

For the iteration number, PV is greater than

(PV Increment per Trigger X Iteration Number) + Low Limit

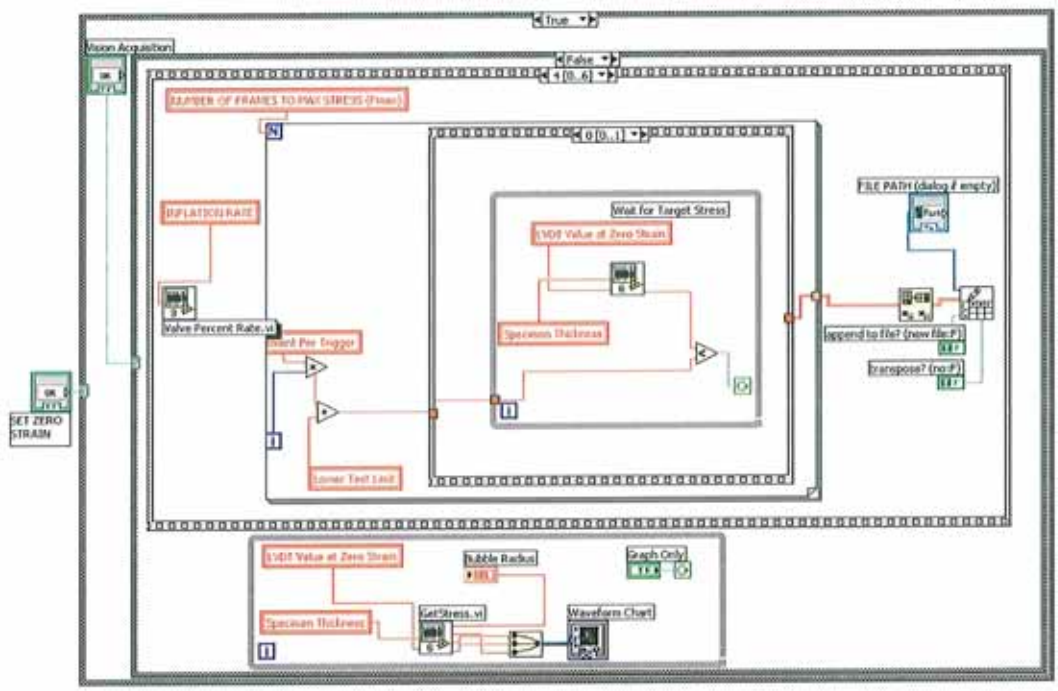

Figure Appendix 2.17 Vision Program Step 5, Substep 1.

Substep 2

For the iteration number, write the pressure and LVDT values to file.

Then send digital output to the CCD Cameras.

Then wait 60mS.

Then stop digital output to the CCD Cameras.

Substep Transition

When the program scan time for has elapsed.

Step transition

When 'For' Loop reaches the required number of iterations.

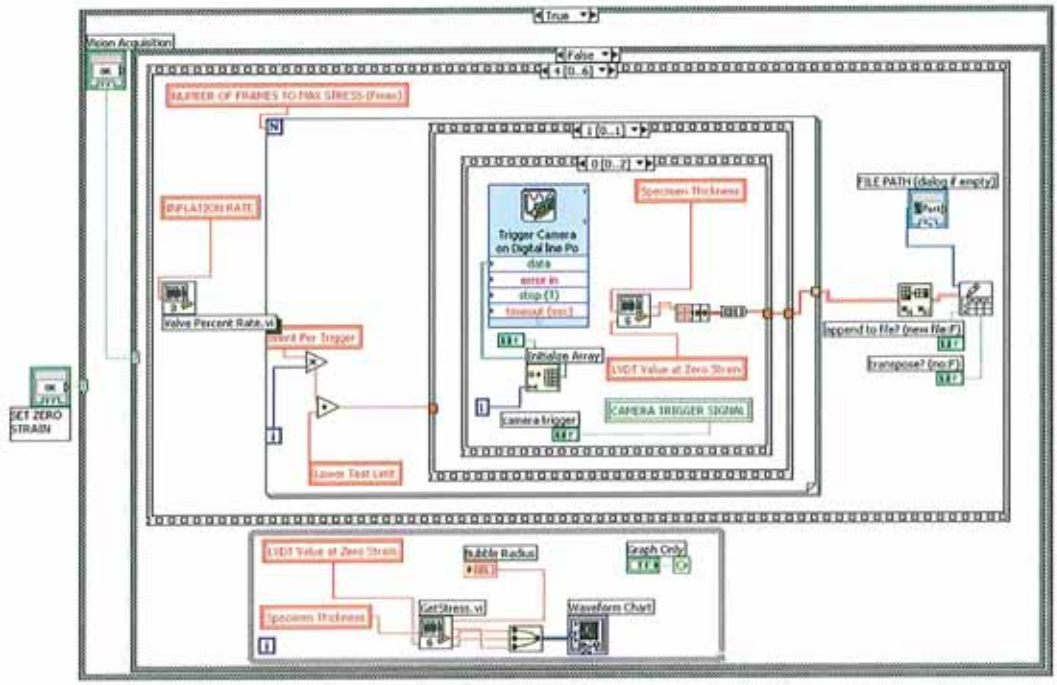

Figure Appendix 2.18 Vision Program Step 5, Substep 2a.

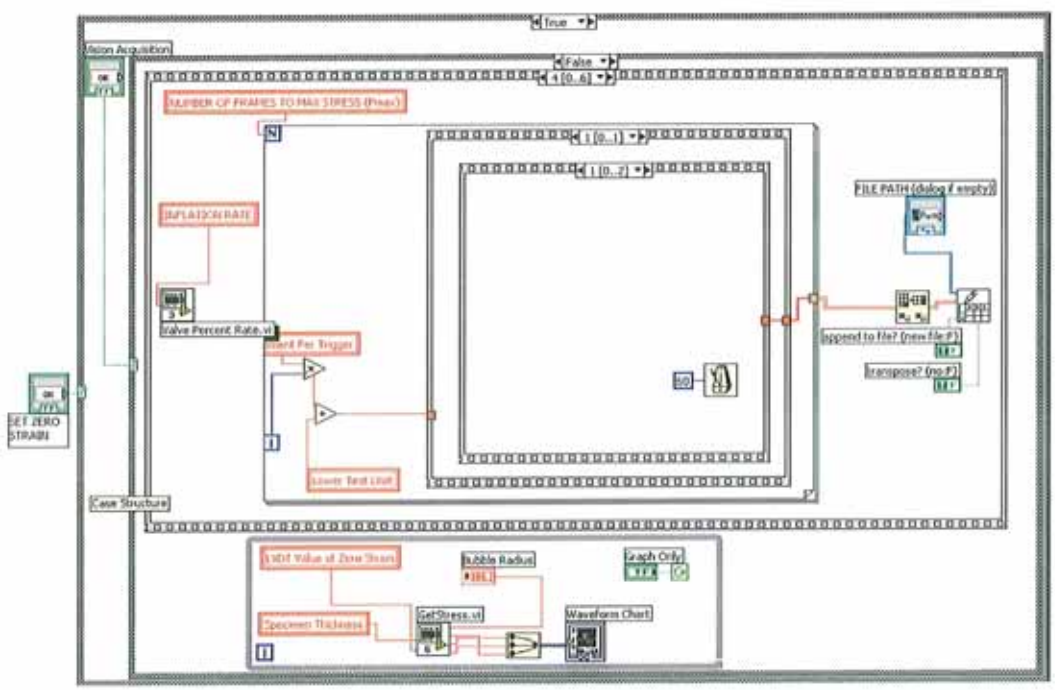

Figure Appendix 2.19 Vision Program Step 5, Substep 2b.

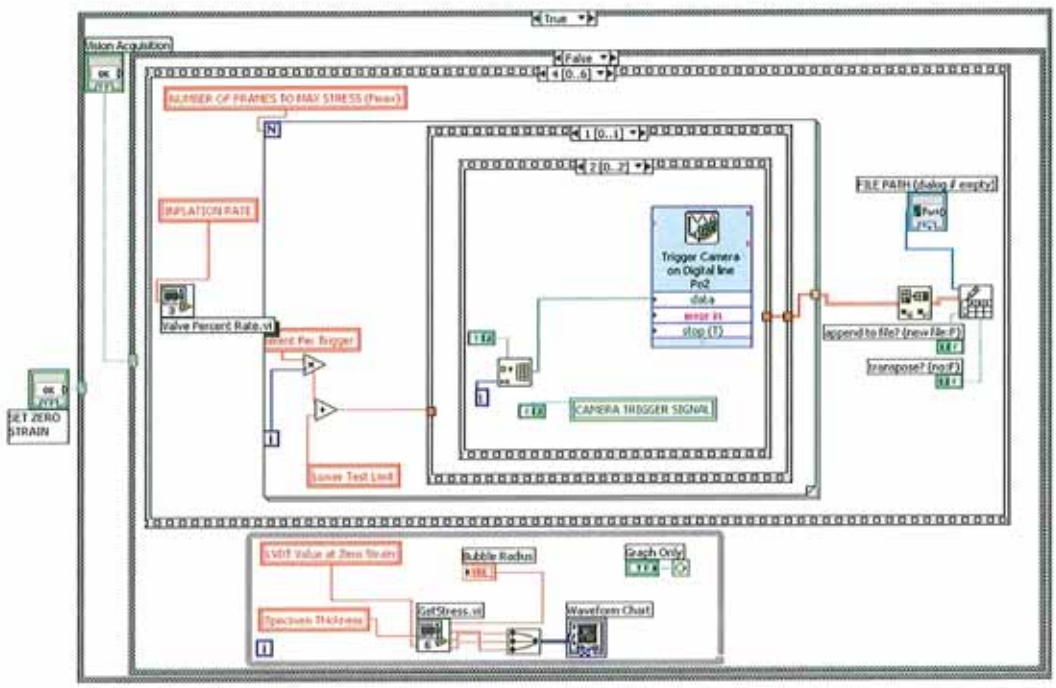

Figure Appendix 2.20 Vision Program Step 5, Substep 2c.

Step 6

The Inflation Rate Down is multiplied by -1 and is output to the valve.

At the same time in this step, a 'For' Loop is started.

The number of iterations in the loop is equal to the ('Number of Frames to Max PV' – 1).

Substep 1

While Loop which waits until the target PV is reached:

For the iteration number, wait while PV is greater than

(Upper Limit – PV Increment per Trigger) - (PV Increment per Trigger X Iteration Number)

Substep Transition

For the iteration number, PV is less than

(Upper Limit – PV Increment) - (PV Increment per Trigger X Iteration Number)

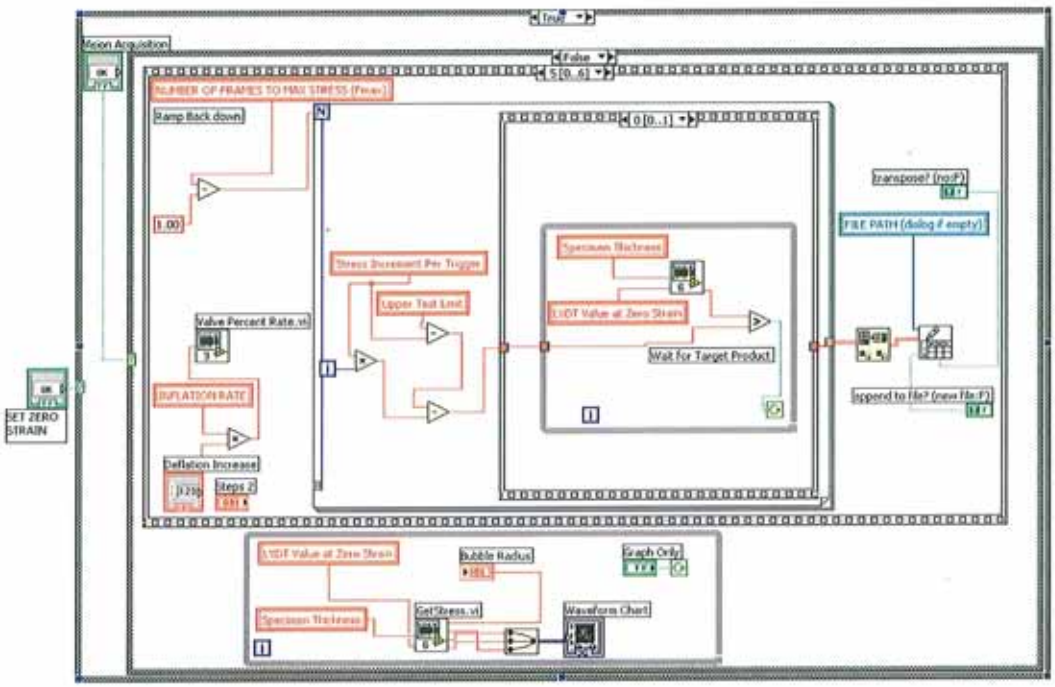

Figure Appendix 2.21 Vision Program Step 6, Substep 1.

Substep 2

For the iteration number, write the pressure and LVDT values to file.

Then send digital output to the CCD Cameras.

Then wait 60mS.

Then stop digital output to the CCD Cameras.

Substep Transition

When the program scan time for has elapsed.

Step transition

When 'For' Loop reaches the required number of iterations and the output file has been written.

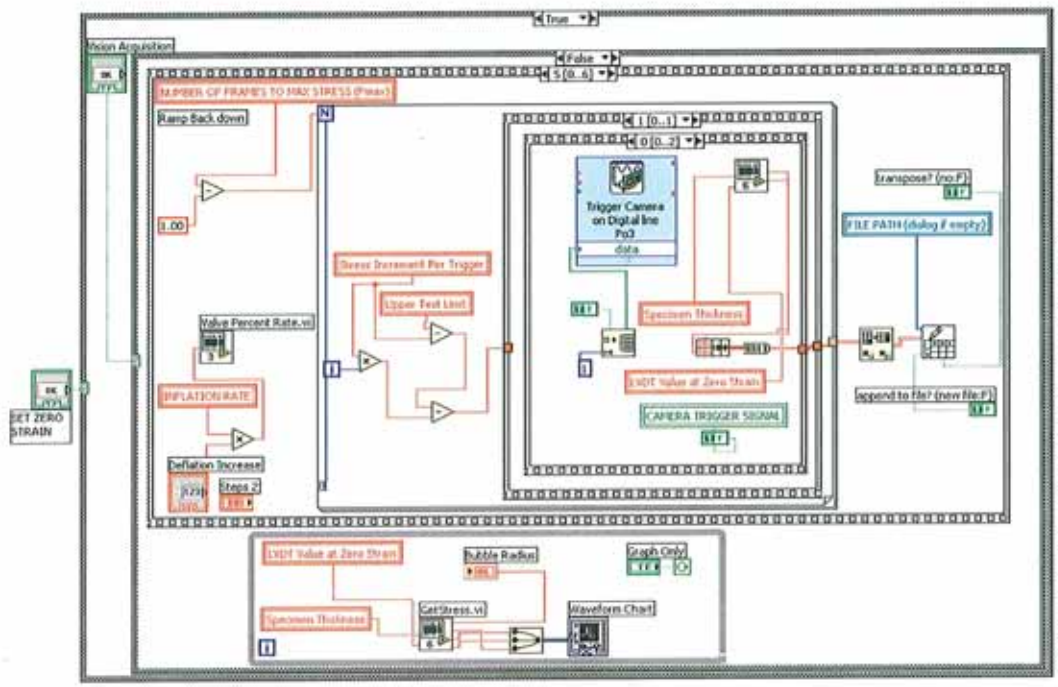

Figure Appendix 2.22 Vision Program Step 6, Substep 2a.

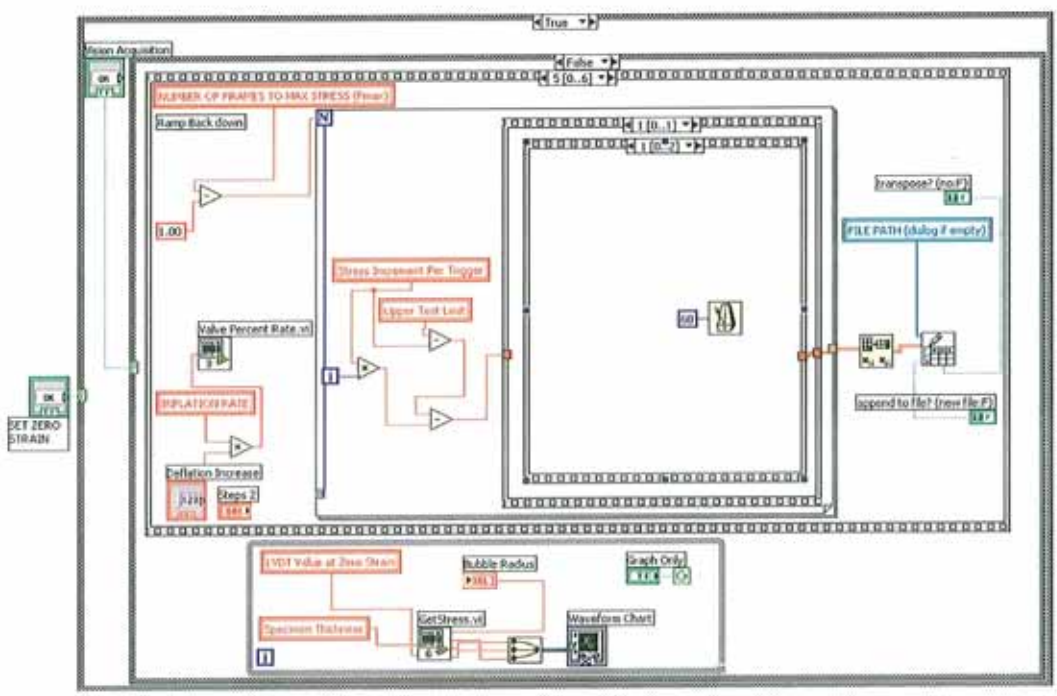

Figure Appendix 2.23 Vision Program Step 6, Substep 2b.

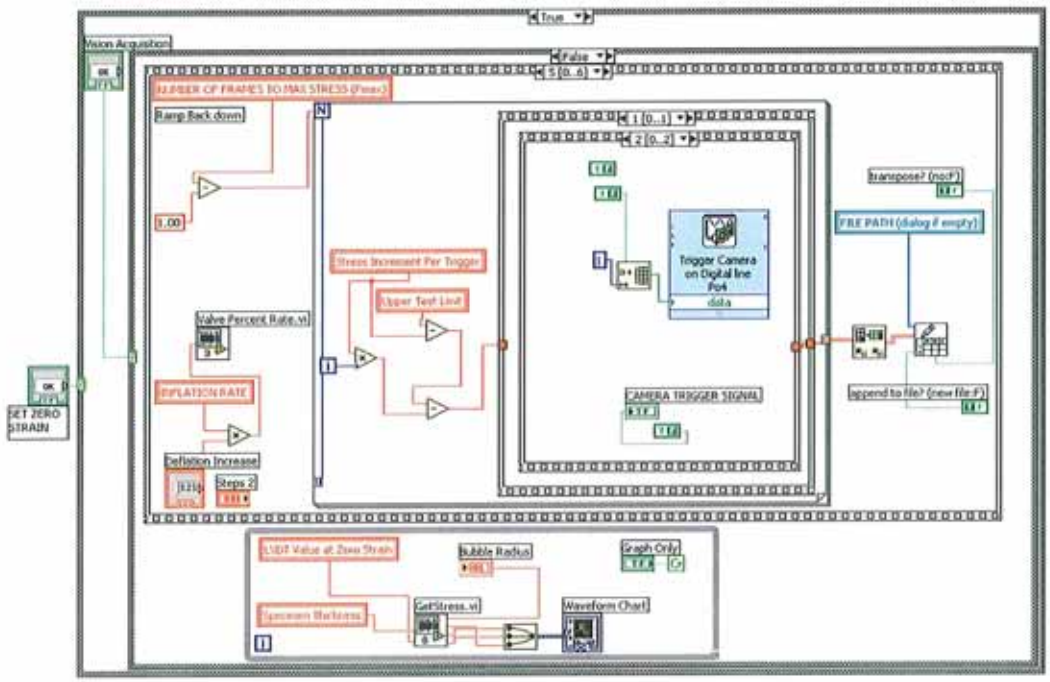

Figure Appendix 2.24 Vision Program Step 6, Substep 2c.

Step 7

The rate out to the valve is set at 0%.

Step transition

When the program scan time for has elapsed.

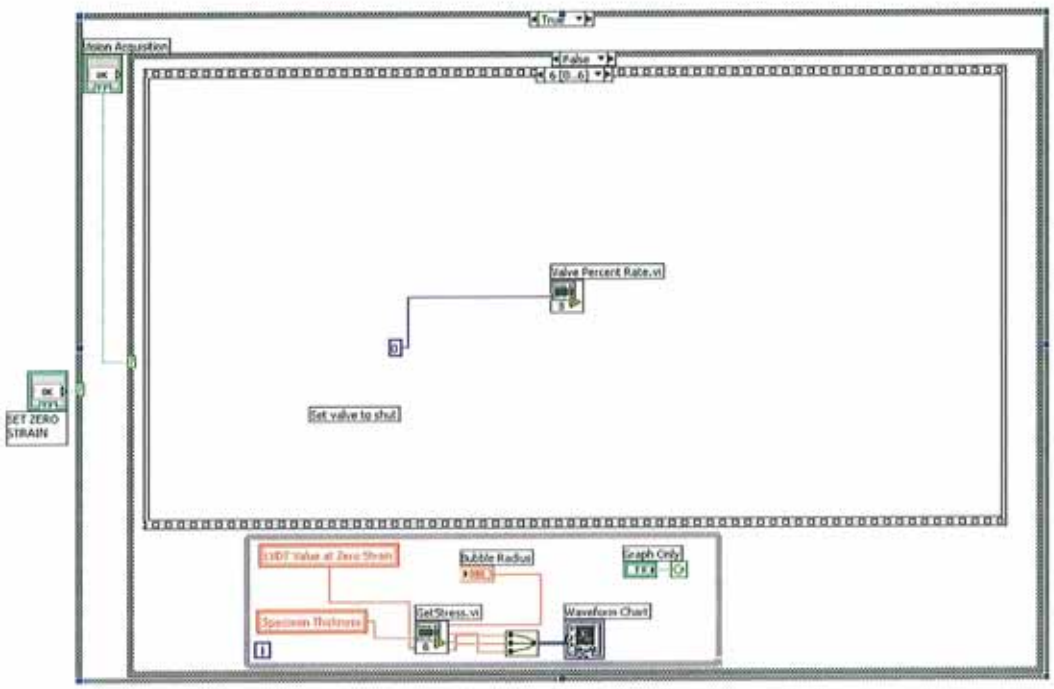

Figure Appendix 2.25 Vision Program Step 7.

Appendix 2.2.3 Stress and Valve Rate Sub-Programs

Two sub programs are also used in both the Fatigue and Vision programs. The first of these is the 'Get Stress' program. This program reads the analog in values and converts the LVDT and pressure values to an engineering stress in four steps.

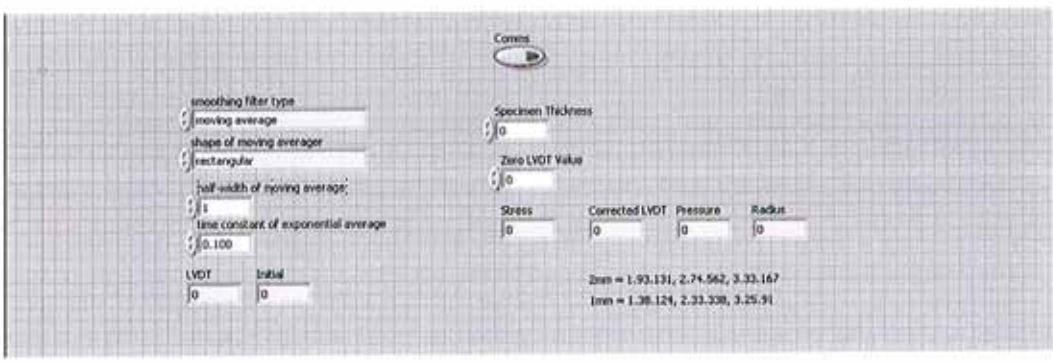

Figure Appendix 2.26 Get Stress Sub Program User Interface.

The first step in the Get Stress program is to read in the raw voltage values from the pressure and LVDT instruments. The pressure values are then scaled into engineering units of bar.

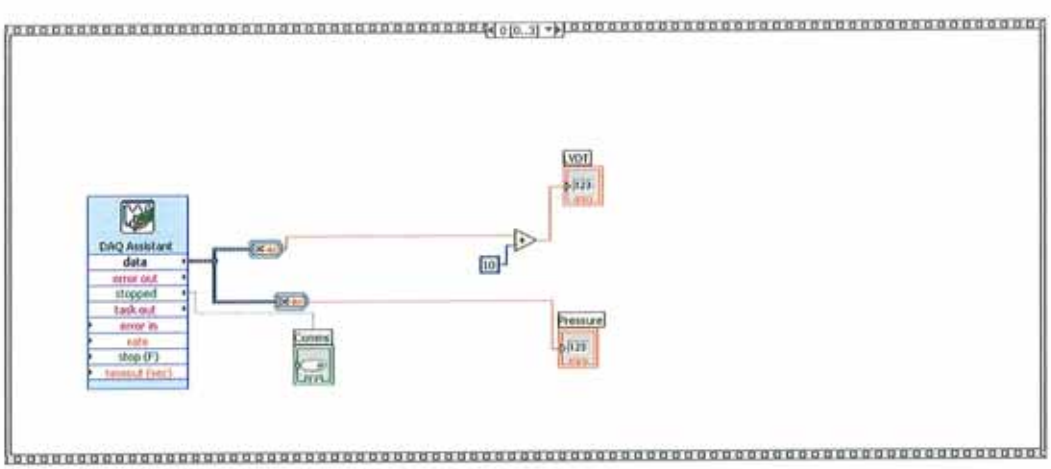

Figure Appendix 2.27 Get Stress Sub Program Step 1.

The second step in the program applies the zero LVDT value to establish what the volume is with respect to the starting position of the cylinder. This value is then multiplied by a fourth order polynomial function to convert the voltage to a bubble radius.

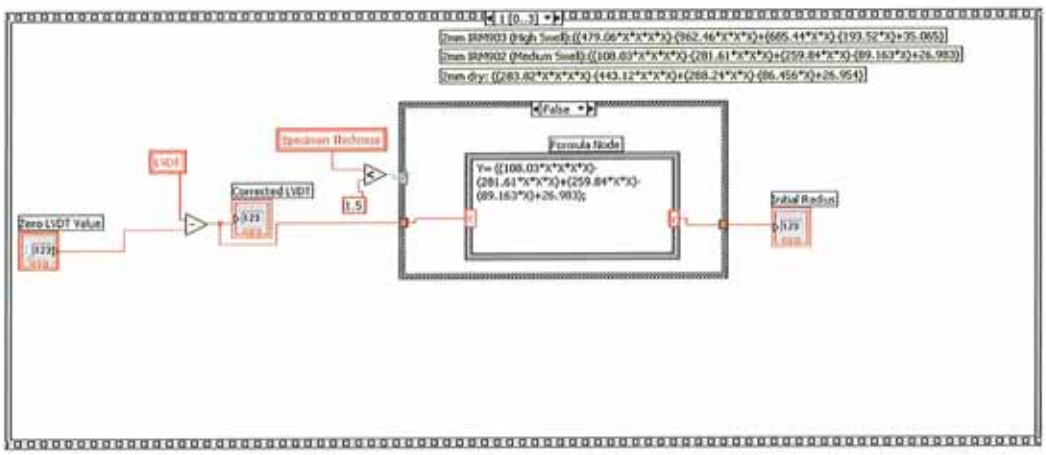

Figure Appendix 2.28 Get Stress Sub Program Step 2.

The third step in the program ensures that whatever value of radius generated by the function is sensible, i.e. it should be greater than zero and less than 40 (this upper value of 40 was found by experiment for the material tested and will vary for different materials).

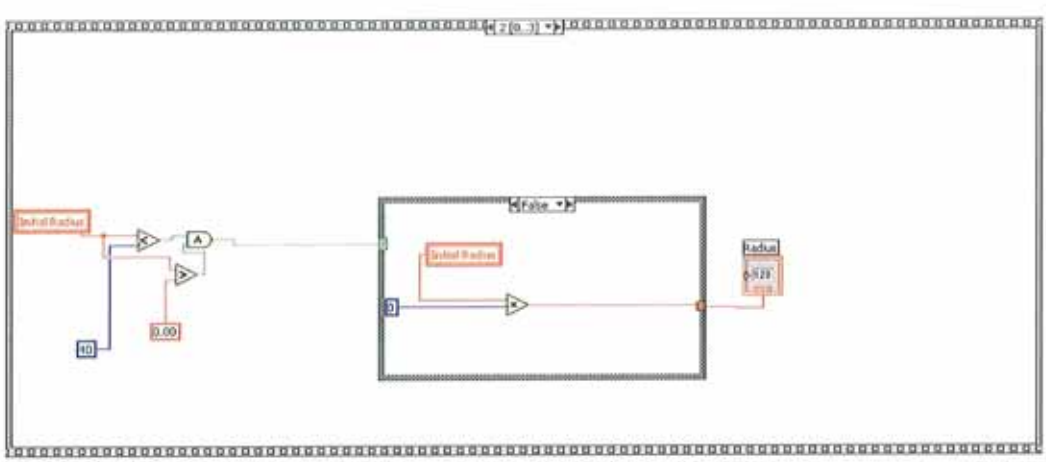

Figure Appendix 2.29 Get Stress Sub Program Step 3.

The fourth step in the program converts the pressure and radius values to engineering stress, in units of Pascals. Finally the output signal is conditioned through a smoothing filter.

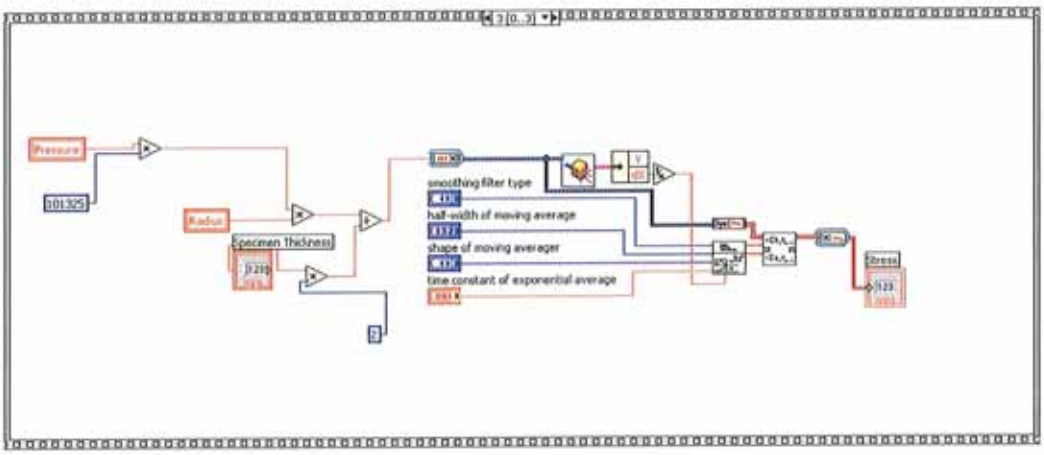

Figure Appendix 2.30 Get Stress Sub Program Step 4.

The Valve Rate sub-program converts the percentage output from the Labview program into voltage values. The valve has a 0-5V range, corresponding to 0V = -100%, 2.5V = 0% and 5V = 100%. The sub-program scales these values accordingly.

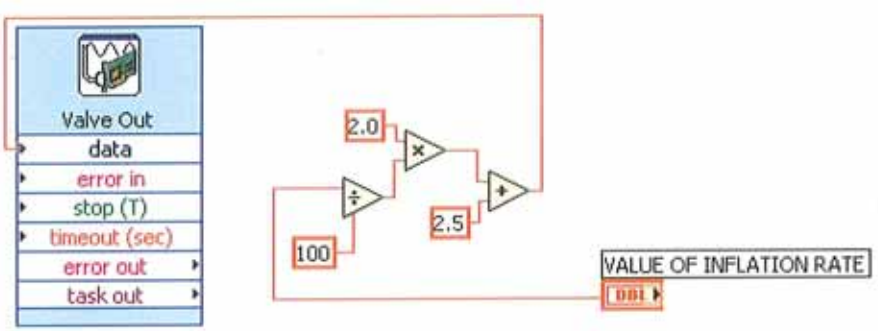

Figure Appendix 2.31 Valve Rate Sub Program.

Appendix 3 – Vision System Details and Stress-Strain Calculations

Appendix 3 Contents

1 CCD Camera Specifications

2 Camera Calibration Spreadsheets

3 Conversion of Camera Measurements from Pixels to Millimetres

4 Radius Calculation Method

5 Stress and Stretch Ratio Calculations

Appendix 3.1 CCD Camera Specifications

PL-A782 MV Camera Features

Sensor

- 1" CMOS 2208 x 3000 resolution (7.73 mm x 10.50 mm - 13.1 mm diagonal)
- 3.5 µm square pixels
- Rolling Shutter

Frame Rate – frames per second

ROI Size	Max Frame Rate
1584 x 1200	5
648 x 480	25
2208 x 3000	17
1272 x 1008	88

Performance

- Spectral Range 400 – 1000 nm
- FPN – TBD
- PRNU – TBD
- Dynamic Range – 56 dB linear (TBD)

Triggering / Strobe / Flash

- S/W or H/W (external) trigger (TTL to 12V).
- Two user-programmable outputs that can be used.
- Stand-alone or synchronized to trigger.

Controls

- Exposure (0.063 ms to 2 seconds)
- White balance and colour gains
- Brightness (black level adjust)
- Gamma
- Frame Rate (2 fps to max)
- Trigger & Strobe Modes
- Region of Interest & Decimation
- Pixel format 8-bit or 10-bit

Other Features

- Programmable LUT
- On-camera configuration memory
- FPN and PRNU correction (gain/offset correction,
- flat field correction – per pixel)

Compatibility

- IIDC 1.31
    - Format 0, Modes 1, 3, 5 and 6
    - Format 7

Computer Interface

- Two FireWire (IEEE 1394) connectors allow daisy chaining of the camera.

Optical Interface

- Standard C-mount 1" optics (Compatible with most 2/3" optics)
- IR cut-off protective filter

Mechanical Interface

- M3 threaded holes – 4 in front plate around C-mount and 4 in camera base.

Trigger Interface

- Pin Hirose connector

Power Requirements

- Power supplied over the FireWire bus
- Max consumption – 5 W

Size and Weight

- Standard Configuration (PL-A782)
    - H x W x L: 1.65" x 1.97" x 4.02" (41 mm x 50mm x 102mm)
    - Weight (without lens): 200g

Environmental

- FCC Class B & CE
- Shock – 50 G
- Vibration – 10 G (20 to 200 Hz)
- Temperature – 0° C to 50° C (non-condensing)

Status LED

- Flashing red and green
- Signals indicate idle, operating, warning and
- failed status

Appendix 3.2 Camera Calibration Spreadsheets

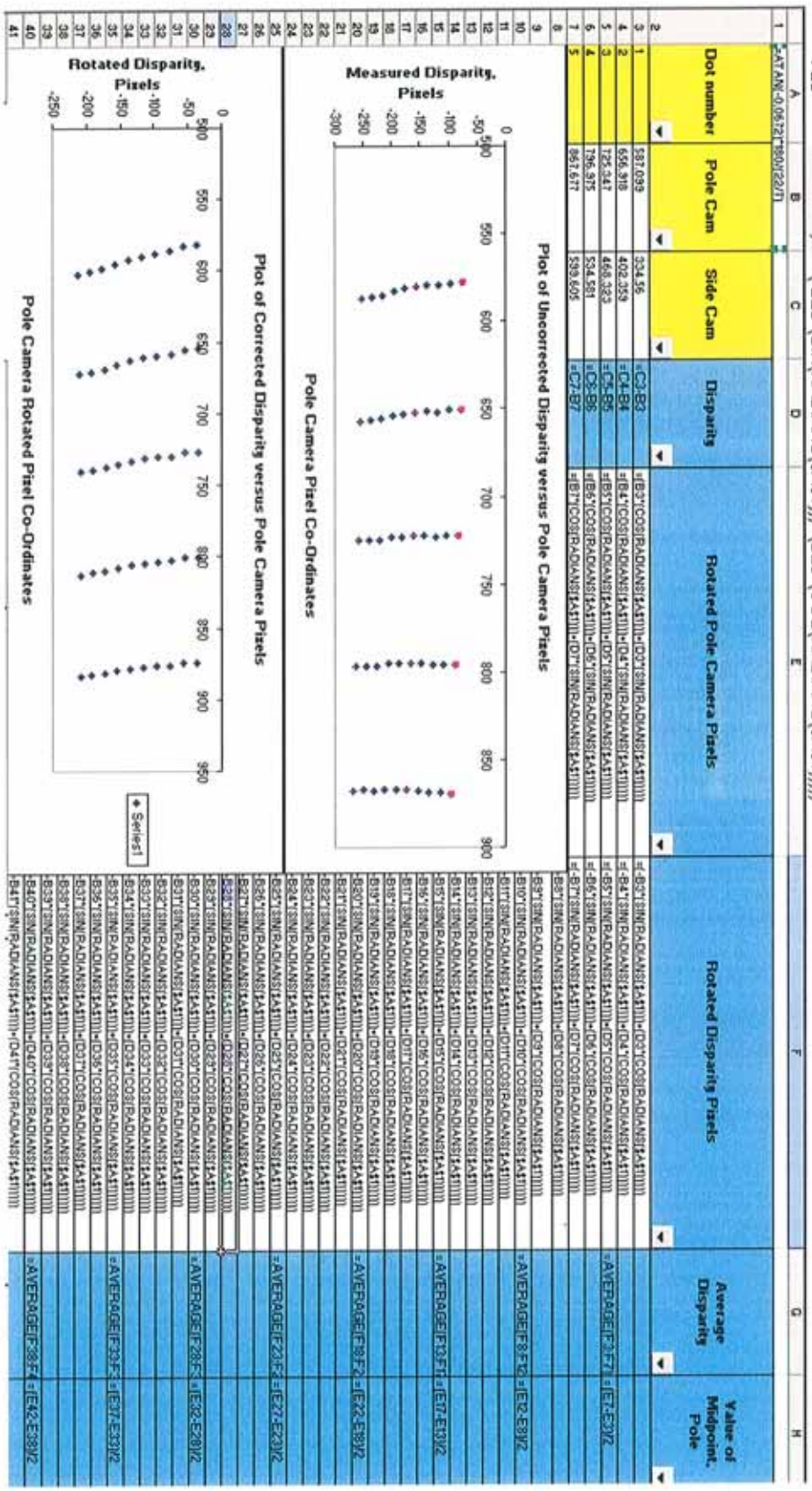

Figure Appendix 3.1 Rotation Calibration Procedure

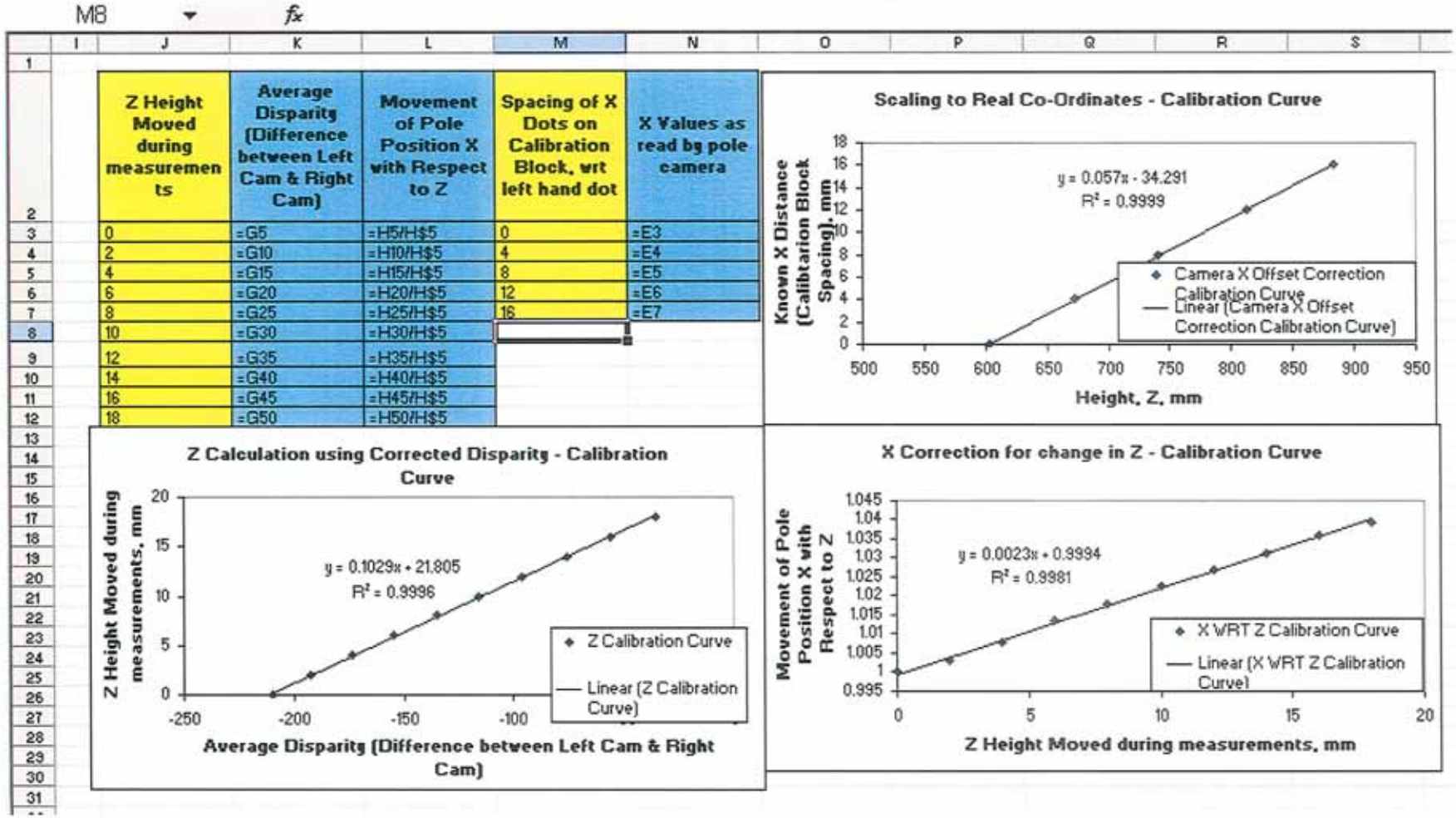

Figure Appendix 3.2 Translation and Scaling Calibration Procedure

Appendix 3.3. Conversion of Camera Measurements from Pixels to Millimetres

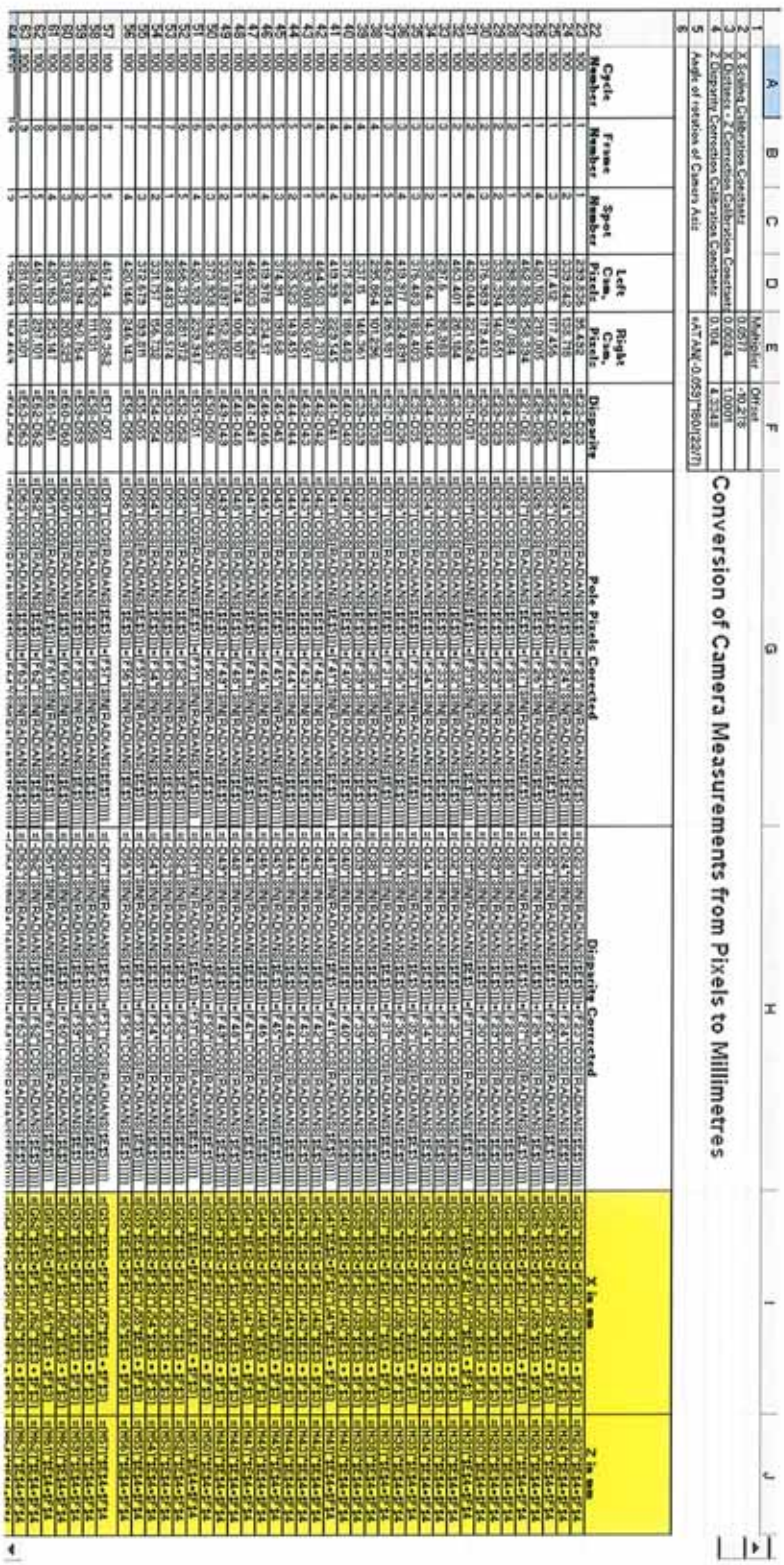

Figure Appendix 3.3 Calculations for converting pixels to millimetres.

Appendix 3.4. Method of calculating the radius of the ellipse

When the vision data has been post-processed, the following data is available for the curve fit for each measured frame:

1. Major Axis, a
2. Minor Axis, b
3. Centre of Ellipse, x_0, z_0

This will be an equation of the form:

$$\frac{(x-x_0)^2}{a^2}+\frac{(z-z_0)^2}{b^2}=1 \qquad \text{(A.3.1)}$$

The centre of the ellipse may not be at (0, 0). For ease of computation in subsequent steps, it is translated to (0, 0) to get equation (A.3.1) in the form:

$$\frac{x}{a^2}+\frac{z}{b^2}=1 \qquad \text{(A.3.2)}$$

At the pole the radius can be simply calculated from

$$R=\frac{a^2}{b} \qquad \text{(A.3.3)}$$

However, the average radius of curvature is required. This average value is defined by the user and is dependant on the material being tested. In the test-pieces used in the tests presented, this average is based on radius measurements at x = 0mm, x = 2mm and x = 4mm.

The radius of curvature on any point on the ellipse can be determined once the major and minor axes and the centre of curvature (different from the centre of the ellipse) are known. All the points corresponding to centres of curvature lie on a closed curve, known as the evolute of the ellipse. A typical ellipse and its evolute are shown in Figure Appendix 3.4.

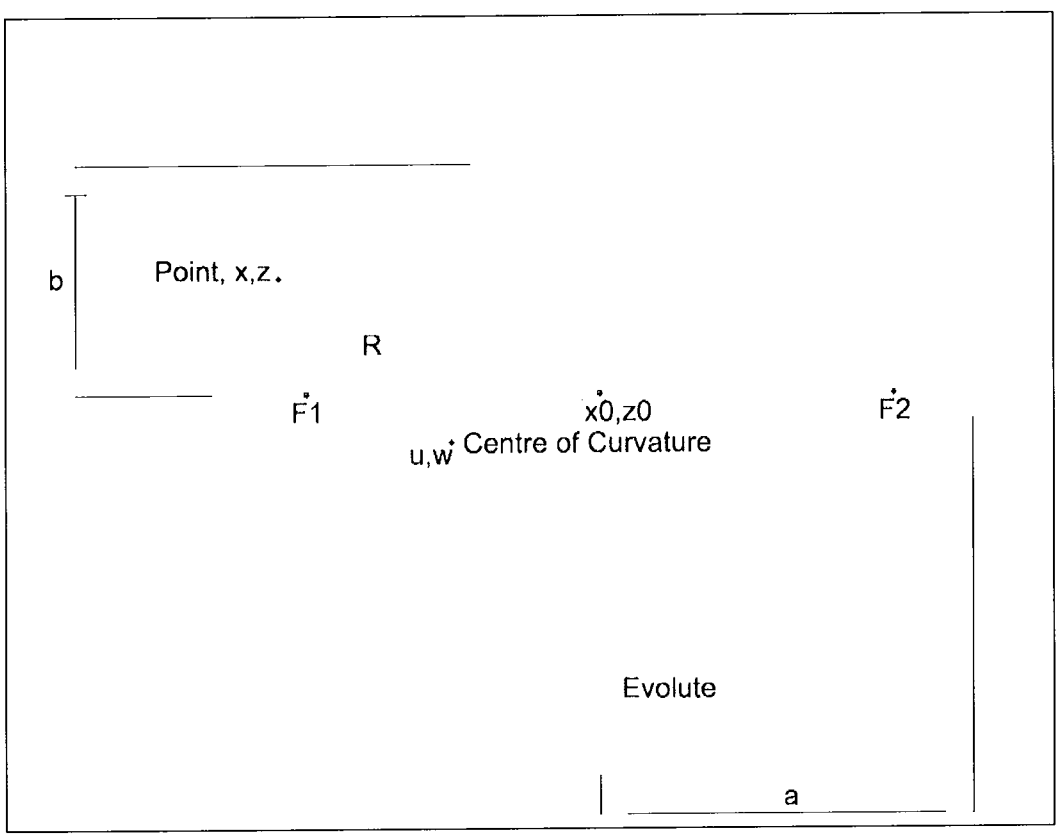

Figure Appendix 3.4. Ellipse parameters and evolute curve.

If the coordinates on the ellipse are denoted x and z, then for clarity the corresponding co-ordinates on the evolute curve (in the same Cartesian system)

can be designated u and w. For any point x on the ellipse, the centre of curvature (u, w) can be calculated from the following equations:

$$u = \frac{a^2 - b^2}{a} \cos^3 t \tag{A.3.4}$$

$$w = \frac{a^2 - b^2}{b} \sin^3 t \tag{A.3.5}$$

where t is calculated from:

$$t = \cos^{-1} \frac{x}{a} \tag{A.3.6}$$

and t has units of radians.

The distance from the centre of curvature (u, w) to the point x is the radius of curvature R, which can be calculated simply from:

$$R = \sqrt{|u - x|^2 + |w - z|^2} \tag{A.3.7}$$

To summarise, the radius fit is carried out as follows:

1. Read in x,z data for the measured frame.
2. Use least squares fit to get ellipse parameters a, b, x_0, z_0.
3. Translate (if required) the ellipse to origin (0, 0).

4. At x = 0, compute R_1, using equation (3).
5. At x = 2, compute u and w, using equations (4), (5) and (6).
6. At x = 2, compute R_2, using equation (7).
7. At x = 4, compute u and w, using equations (4), (5) and (6).
8. At x = 4, compute R_3, using equation (7).
9. Get average of R_1, R_2 and R_3.
10. Output $R_{average}$.

Appendix 3.5. Stress and Stretch Ratio Calculations

	A	B	C	F	G	I	J	K	L	S	T	U	V
1													
2	Original Sheet Thickness 2												
3	Original Point Spacing	=[Visiondata#Id-Visiondata#Id]^2											
4	Orifice Radius	=25/2											
5													
6										This data is referenced from the pixels readings converted to millimetres (Figure Appendix 3.3)			
8	Pressure, Bar	LVDT, Volts	Bubble Radius	Tree Stress	Engineering Stress	Thickness at pole	Point Spacing	Circumferential Spacing	Stretch Ratio (lambda L2)	x1	Z1	x2	Z2
9	-0.0002	0.078	=[E9]	=[A9*0.1]*[C9]*(2*[I9])	=[F9]/(L$1*L9)	=[I9]*3^2)*[C12]	=ABS([U9-S9]*2)	=[2*ASIN(J9/2/C9)]*C9	=([K9-$C$3]/$C$3)+1	=Visiondata!I26	=Visiondata!J26	=Visiondata!K26	=Visiondata!L26
10	0.105	0.085	=[E10]	=[A10*0.1]*[C10]*(2*[I10])	=[F10]/(L$1*L10)	=[I10]*3^2)*[C12]	=ABS([U10-S10]*2)	=[2*ASIN(J10/2/C10)]*C10	=([K10-$C$3]/$C$3)+1	=Visiondata!I31	=Visiondata!J31	=Visiondata!K30	=Visiondata!L30
11	0.28	0.095	=[E11]	=[A11*0.1]*[C11]*(2*[I11])	=[F11]/(L$1*L11)	=[I11]*3^2)*[C12]	=ABS([U11-S11]*2)	=[2*ASIN(J11/2/C11)]*C11	=([K11-$C$3]/$C$3)+1	=Visiondata!I36	=Visiondata!J36	=Visiondata!K35	=Visiondata!L35
12	0.438	0.107	=[E12]	=[A12*0.1]*[C12]*(2*[I12])	=[F12]/(L$1*L12)	=[I12]*3^2)*[C12]	=ABS([U12-S12]*2)	=[2*ASIN(J12/2/C12)]*C12	=([K12-$C$3]/$C$3)+1	=Visiondata!I41	=Visiondata!J41	=Visiondata!K40	=Visiondata!L40
13	0.602	0.118	=[E13]	=[A13*0.1]*[C13]*(2*[I13])	=[F13]/(L$1*L13)	=[I13]*3^2)*[C12]	=ABS([U13-S13]*2)	=[2*ASIN(J13/2/C13)]*C13	=([K13-$C$3]/$C$3)+1	=Visiondata!I46	=Visiondata!J46	=Visiondata!K45	=Visiondata!L45
14	0.77	0.132	=[E14]	=[A14*0.1]*[C14]*(2*[I14])	=[F14]/(L$1*L14)	=[I14]*3^2)*[C12]	=ABS([U14-S14]*2)	=[2*ASIN(J14/2/C14)]*C14	=([K14-$C$3]/$C$3)+1	=Visiondata!I51	=Visiondata!J51	=Visiondata!K50	=Visiondata!L50
15	0.957	0.147	=[E15]	=[A15*0.1]*[C15]*(2*[I15])	=[F15]/(L$1*L15)	=[I15]*3^2)*[C12]	=ABS([U15-S15]*2)	=[2*ASIN(J15/2/C15)]*C15	=([K15-$C$3]/$C$3)+1	=Visiondata!I56	=Visiondata!J56	=Visiondata!K55	=Visiondata!L55
16	1.143	0.164	=[E16]	=[A16*0.1]*[C16]*(2*[I16])	=[F16]/(L$1*L16)	=[I16]*3^2)*[C12]	=ABS([U16-S16]*2)	=[2*ASIN(J16/2/C16)]*C16	=([K16-$C$3]/$C$3)+1	=Visiondata!I61	=Visiondata!J61	=Visiondata!K60	=Visiondata!L60
17	1.34	0.184	=[E17]	=[A17*0.1]*[C17]*(2*[I17])	=[F17]/(L$1*L17)	=[I17]*3^2)*[C12]	=ABS([U17-S17]*2)	=[2*ASIN(J17/2/C17)]*C17	=([K17-$C$3]/$C$3)+1	=Visiondata!I66	=Visiondata!J66	=Visiondata!K65	=Visiondata!L65
18	1.525	0.201	=[E18]	=[A18*0.1]*[C18]*(2*[I18])	=[F18]/(L$1*L18)	=[I18]*3^2)*[C12]	=ABS([U18-S18]*2)	=[2*ASIN(J18/2/C18)]*C18	=([K18-$C$3]/$C$3)+1	=Visiondata!I71	=Visiondata!J71	=Visiondata!K70	=Visiondata!L70
19	1.723	0.218	=[E19]	=[A19*0.1]*[C19]*(2*[I19])	=[F19]/(L$1*L19)	=[I19]*3^2)*[C12]	=ABS([U19-S19]*2)	=[2*ASIN(J19/2/C19)]*C19	=([K19-$C$3]/$C$3)+1	=Visiondata!I76	=Visiondata!J76	=Visiondata!K75	=Visiondata!L75
20	1.901	0.231	=[E20]	=[A20*0.1]*[C20]*(2*[I20])	=[F20]/(L$1*L20)	=[I20]*3^2)*[C12]	=ABS([U20-S20]*2)	=[2*ASIN(J20/2/C20)]*C20	=([K20-$C$3]/$C$3)+1	=Visiondata!I81	=Visiondata!J81	=Visiondata!K80	=Visiondata!L80
21	2.093	0.243	=[E21]	=[A21*0.1]*[C21]*(2*[I21])	=[F21]/(L$1*L21)	=[I21]*3^2)*[C12]	=ABS([U21-S21]*2)	=[2*ASIN(J21/2/C21)]*C21	=([K21-$C$3]/$C$3)+1	=Visiondata!I86	=Visiondata!J86	=Visiondata!K85	=Visiondata!L85
22	2.272	0.253	=[E22]	=[A22*0.1]*[C22]*(2*[I22])	=[F22]/(L$1*L22)	=[I22]*3^2)*[C12]	=ABS([U22-S22]*2)	=[2*ASIN(J22/2/C22)]*C22	=([K22-$C$3]/$C$3)+1	=Visiondata!I91	=Visiondata!J91	=Visiondata!K90	=Visiondata!L90
23	2.461	0.264	=[E23]	=[A23*0.1]*[C23]*(2*[I23])	=[F23]/(L$1*L23)	=[I23]*3^2)*[C12]	=ABS([U23-S23]*2)	=[2*ASIN(J23/2/C23)]*C23	=([K23-$C$3]/$C$3)+1	=Visiondata!I96	=Visiondata!J96	=Visiondata!K95	=Visiondata!L95
24	2.643	0.26	=[E24]	=[A24*0.1]*[C24]*(2*[I24])	=[F24]/(L$1*L24)	=[I24]*3^2)*[C12]	=ABS([U24-S24]*2)	=[2*ASIN(J24/2/C24)]*C24	=([K24-$C$3]/$C$3)+1	=Visiondata!I101	=Visiondata!J101	=Visiondata!K100	=Visiondata!L100
25	2.09	0.256	=[E25]	=[A25*0.1]*[C25]*(2*[I25])	=[F25]/(L$1*L25)	=[I25]*3^2)*[C12]	=ABS([U25-S25]*2)	=[2*ASIN(J25/2/C25)]*C25	=([K25-$C$3]/$C$3)+1	=Visiondata!I106	=Visiondata!J106	=Visiondata!K105	=Visiondata!L105
26	1.914	0.251	=[E26]	=[A26*0.1]*[C26]*(2*[I26])	=[F26]/(L$1*L26)	=[I26]*3^2)*[C12]	=ABS([U26-S26]*2)	=[2*ASIN(J26/2/C26)]*C26	=([K26-$C$3]/$C$3)+1	=Visiondata!I111	=Visiondata!J111	=Visiondata!K110	=Visiondata!L110
27	1.741	0.243	=[E27]	=[A27*0.1]*[C27]*(2*[I27])	=[F27]/(L$1*L27)	=[I27]*3^2)*[C12]	=ABS([U27-S27]*2)	=[2*ASIN(J27/2/C27)]*C27	=([K27-$C$3]/$C$3)+1	=Visiondata!I116	=Visiondata!J116	=Visiondata!K115	=Visiondata!L115
28	1.554	0.234	=[E28]	=[A28*0.1]*[C28]*(2*[I28])	=[F28]/(L$1*L28)	=[I28]*3^2)*[C12]	=ABS([U28-S28]*2)	=[2*ASIN(J28/2/C28)]*C28	=([K28-$C$3]/$C$3)+1	=Visiondata!I121	=Visiondata!J121	=Visiondata!K120	=Visiondata!L120
29	1.378	0.224	=[E29]	=[A29*0.1]*[C29]*(2*[I29])	=[F29]/(L$1*L29)	=[I29]*3^2)*[C12]	=ABS([U29-S29]*2)	=[2*ASIN(J29/2/C29)]*C29	=([K29-$C$3]/$C$3)+1	=Visiondata!I126	=Visiondata!J126	=Visiondata!K125	=Visiondata!L125
30	1.198	0.209	=[E30]	=[A30*0.1]*[C30]*(2*[I30])	=[F30]/(L$1*L30)	=[I30]*3^2)*[C12]	=ABS([U30-S30]*2)	=[2*ASIN(J30/2/C30)]*C30	=([K30-$C$3]/$C$3)+1	=Visiondata!I131	=Visiondata!J131	=Visiondata!K130	=Visiondata!L130
31	1.014	0.193	=[E31]	=[A31*0.1]*[C31]*(2*[I31])	=[F31]/(L$1*L31)	=[I31]*3^2)*[C12]	=ABS([U31-S31]*2)	=[2*ASIN(J31/2/C31)]*C31	=([K31-$C$3]/$C$3)+1	=Visiondata!I136	=Visiondata!J136	=Visiondata!K135	=Visiondata!L135
32	0.836	0.176	=[E32]	=[A32*0.1]*[C32]*(2*[I32])	=[F32]/(L$1*L32)	=[I32]*3^2)*[C12]	=ABS([U32-S32]*2)	=[2*ASIN(J32/2/C32)]*C32	=([K32-$C$3]/$C$3)+1	=Visiondata!I141	=Visiondata!J141	=Visiondata!K140	=Visiondata!L140
33	0.645	0.155	=[E33]	=[A33*0.1]*[C33]*(2*[I33])	=[F33]/(L$1*L33)	=[I33]*3^2)*[C12]	=ABS([U33-S33]*2)	=[2*ASIN(J33/2/C33)]*C33	=([K33-$C$3]/$C$3)+1	=Visiondata!I146	=Visiondata!J146	=Visiondata!K145	=Visiondata!L145
34	0.471	0.138	=[E34]	=[A34*0.1]*[C34]*(2*[I34])	=[F34]/(L$1*L34)	=[I34]*3^2)*[C12]	=ABS([U34-S34]*2)	=[2*ASIN(J34/2/C34)]*C34	=([K34-$C$3]/$C$3)+1	=Visiondata!I151	=Visiondata!J151	=Visiondata!K150	=Visiondata!L150
35	0.301	0.122	=[E35]	=[A35*0.1]*[C35]*(2*[I35])	=[F35]/(L$1*L35)	=[I35]*3^2)*[C12]	=ABS([U35-S35]*2)	=[2*ASIN(J35/2/C35)]*C35	=([K35-$C$3]/$C$3)+1	=Visiondata!I156	=Visiondata!J156	=Visiondata!K155	=Visiondata!L155
36	0.142	0.104	=[E36]	=[A36*0.1]*[C36]*(2*[I36])	=[F36]/(L$1*L36)	=[I36]*3^2)*[C12]	=ABS([U36-S36]*2)	=[2*ASIN(J36/2/C36)]*C36	=([K36-$C$3]/$C$3)+1	=Visiondata!I161	=Visiondata!J161	=Visiondata!K160	=Visiondata!L160
37	0.001	0.086	=[E37]	=[A37*0.1]*[C37]*(2*[I37])	=[F37]/(L$1*L37)	=[I37]*3^2)*[C12]	=ABS([U37-S37]*2)	=[2*ASIN(J37/2/C37)]*C37	=([K37-$C$3]/$C$3)+1	=Visiondata!I166	=Visiondata!J166	=Visiondata!K165	=Visiondata!L165

Figure Appendix 3.5 Calculations of σ_t, σ_e and $\lambda_{1,2}$ (stretch ratio).

Appendix 4 – Supplemental Literature Review

The following topics are contained in this appendix and are intended to give further background into some of the topics covered in Chapter 2 of this thesis, namely:

1 Hyperelastic and Viscoelastic Properties of Rubber

2 Development of Phenomenological Theories

3 Thermodynamics of Swelling and Cohesive Energy Densities

4 Fatigue of Elastomers

Appendix 4.1. Hyperelastic and Viscoelastic Properties of Rubber

Hyperelasticity

Rubbers exhibit the unique property of being able to withstand high levels of reversible strain without suffering permanent deformation or fracture. Figure Appendix 4.1 shows a typical uniaxial tensile stress-strain curve for a filled rubber. The property of hyperelasticity makes elastomers fundamentally different from most other solid materials.

Much research has been devoted to describing mathematically how these high levels of reversible strains are achieved and several theories have been formulated for the purpose of describing the hyperelastic properties and non-linear behaviour of rubber-like materials. In order to understand how a complex material like rubber behaves when deformed, early research into its behaviour concentrated on the material at the molecular level.

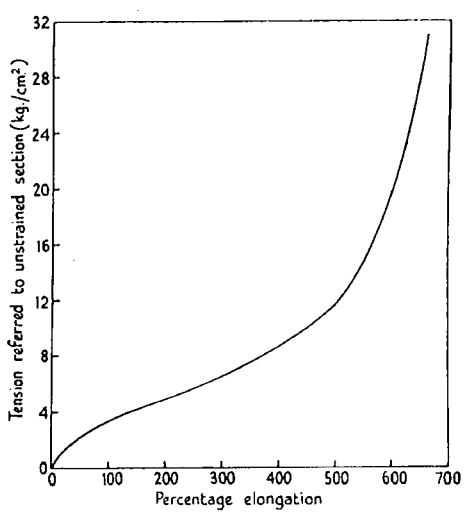

Figure Appendix 4.1. A typical uniaxial stress/strain curve for a filled rubber

Figure Appendix 4.2 (a) shows in two dimensions the ordering of long chain molecules of rubber in the unstrained and strained state. In reality the chain segments lie in a disordered state in a three dimensional matrix. When a specimen of rubber is in its unloaded state, it is made up of a tangled mass of long chain molecules, free to rotate around crosslinks that join them together. As there are small intermolecular attractions (van der Waals forces) between the long chain molecules they can slide readily past one another. Due to thermal vibrations, the atoms in the long chain molecules are in constant motion, causing individual molecules to assume irregular sinuous shapes. If loaded in any way the molecules will become approximately aligned with the loading (Figure Appendix 4.2 (b)). The rubber resists this alignment and when the load is removed, returns to its more natural random state (Figure Appendix 4.2 (a)). This is the state of maximum entropy of the rubber and always tends to its original shape when unconstrained.

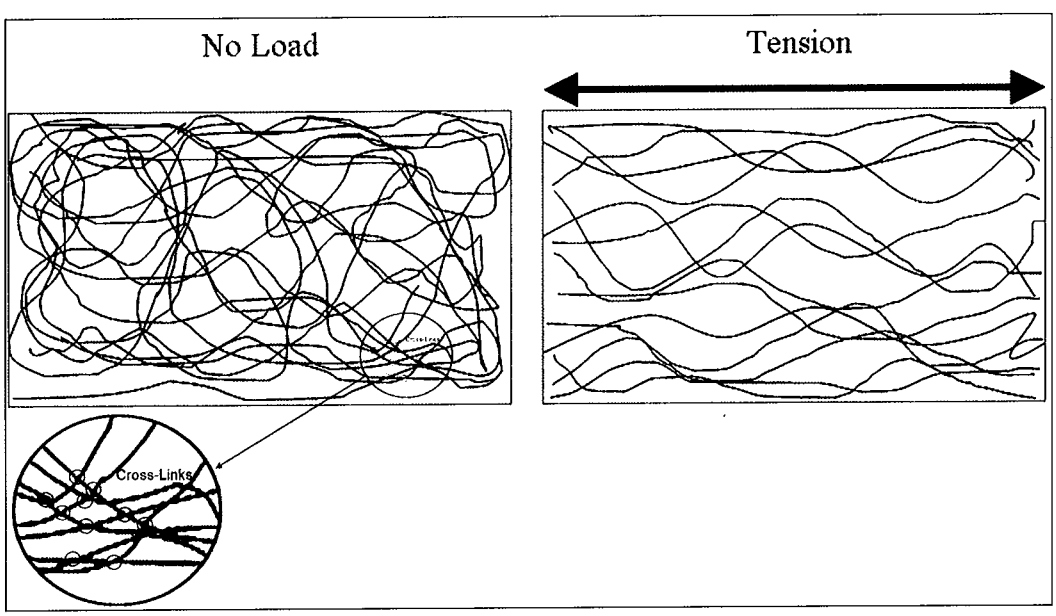

(a) **(b)**

Figure Appendix 4.2. Rubber in the strained and unstrained state

Viscoelasticity

The viscoelastic properties of rubber make it inevitable that the deformation of a component will vary when repeatedly loaded, even if it is loaded in the same manner and with the same magnitude of force. These time dependent properties can be diverse and dissimilar for different compounds. In service, rubber can experience some or all of the following effects:-

creep - strain increases at a constant force,

stress relaxation - stress changes over time when a component is subject to constant strain,

set - the component fails to recover its initial shape when an applied load is removed,

stress softening (Mullins' effect) - the component softens with subsequent loading cycles,

and adhesion which is a thermally activated stick-slip process that causes local bonding between rubber and rigid contact surfaces.

These phenomena can be influenced by both physical and chemical change and are exhibited in rubbers that have aged.

Creep

All rubbers creep. For an instantaneously applied stress, a slow continual deformation occurs after the initial large deformation that takes place. Deformation due to creep is not entirely recoverable and unlike in metals is not just confined to high strains and high temperatures but occurs for any form of loading. Creep in elastomers will display linearity if plotted against time on a logarithmic scale. However if a stress is maintained for a very long time the rate

of creep will eventually rise sharply which is associated with oxidative breakdown of crosslinks. The amount of creep varies greatly in rubbers, dependent on a number of factors, but some observations are: -

i) vulcanised synthetic rubbers tend to creep more than vulcanised natural rubbers,

ii) increases in filler content in a compound lead to higher levels of creep,

iii) hard rubbers creep more than soft rubbers

and iv) rubbers containing more crosslinks creep less than less well vulcanised rubbers.

Two simultaneously occurring phenomena which may in fact be a single phenomenon are work softening and fatigue. Work softening is a reduction in shear modulus resulting from cyclical loading. It can be unnoticed because no permanent deformation occurs and, on the removal of a load, a work softened rubber will revert to its original state. Also, if work softening and set are present in the same component, their effects often cancel each other out. If a cyclic stress is applied to a rubber the modulus (or stiffness) gradually reduces. This process is indicative of fatigue and can be considered a form of stress relaxation that mirrors an increase of strain at constant stress, or creep. Plotted against log time, the modulus gives a straight line similar to that of creep. Some interesting work on reduction in complex modulus (E*) in fatigue of non-strain crystallising elastomers, EPDM and SBR, has been carried out by Abraham *et al.* [3].

Stress relaxation

Stress relaxation and creep are initially physical changes resulting from the same viscoelastic phenomenon. Whereas an ideal elastic solid subjected to a fixed strain for a time period will record a constant stress, a viscoelastic material having a nominally instantaneous strain applied to it will suffer a reduction in the initial stress with time.

Set

A component made from a conventional solid, will normally be assumed to fail when it fractures or reaches a level of wear that impairs its function. A rubber component can fail for several reasons. Creep, work softening or set all cause elastomeric components to lose functionality. Set is an important parameter when maintaining component function, for instance when needing an efficient seal. The rubber industry has tended to place a large emphasis on measuring recovery. The notion of 'permanent set' in respect of rubbers has less meaning since an infinite recovery time would be required to measure it. Hence, set is normally expressed as a percentage of the applied deformation for a particular recovery time as shown below.

$$\text{Set} = \frac{t_0 - t_r}{t_0 - t_s} \times 100\% \text{ (Compression set)} \qquad \text{(A.4.1)}$$

where: - t_0 = initial thickness, t_r = recovered thickness and t_s = compressed thickness.

Stress softening

When subjected to cyclic loading, energy is dissipated in rubber as a result of hysteresis. Filled rubbers stress soften and elastomeric components will have 'steady state' responses very different from initial responses. Carbon black is added to rubber for economy and to increase stiffness and toughness. Strain-induced stress softening in filled rubbers results from a break down of crosslinks and a gradual detachment of reinforcing fillers from long chain molecules. This phenomenon is known as the Mullins effect after the researcher who conducted the first experiments into history dependant stiffness [102].

Appendix 4.2. Development of Phenomenological Theories

Theories to describe hyperelastic material behaviour

Since understanding of the deformation of rubber (Section 2.2) has been based on statistics and probability, the term statistical theory was applied to its early development. The development of statistical theory was advanced markedly by Treloar [9].

The statistical theory is also known as the 'kinetic theory' since deformations were related to thermal motions of molecules and analogous to kinetic theories of gases. For long chain molecules, the probability that the distance between their ends has a specific value was thought to comply with a Gaussian error function. This assumption is central to the statistical theory. However, it ceases to be valid at higher strains and subsequent (phenomenological) theories attempted to more accurately represent elastomer behaviour over large strain ranges. The statistical theory assumes that

$$G = NkT = \rho RT / M_c \qquad \text{(A.4.2)}$$

Where,

G = Shear (rigidity) modulus,

N = the number of chains per unit volume,

k = Boltzmann's constant,

T = absolute temperature,

ρ = density,

R = the gas constant and

M_c = the mean 'chain molecular weight'

The development of the statistical theory and it application to swelling phenomenon is discussed in section 2.2.2.

Determining principal stresses using statistical/kinetic theory

Figure Appendix 4.3 shows a triaxial stress system applied to a unit cuboid of elastomeric material. The three principal stretch ratios are denoted by λ_1 λ_2 and λ_3. When a hyperelastic material undergoes strain, there are large changes in cross-section. Consequently, the Cauchy stresses (forces per unit strained area), or true stresses, are denoted by t_1, t_2 and t_3, while the engineering stresses (forces per unit unstrained area) are denoted by σ_1 σ_2 and σ_3.

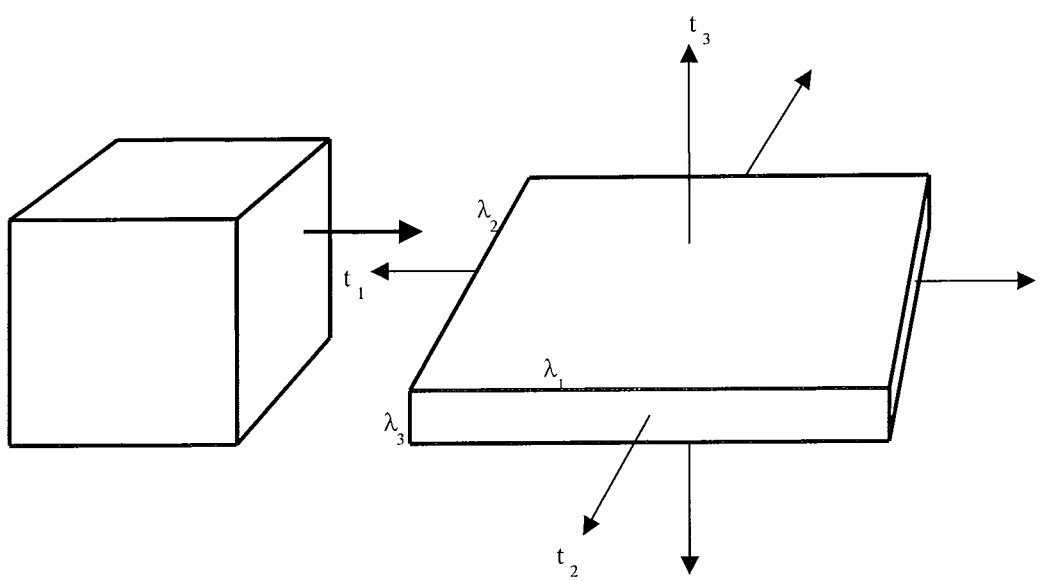

Figure Appendix 4.3 Tri-axial stress system applied to a cuboid of elastomeric material

For incompressibility, $\lambda_1\lambda_2\lambda_3=1$ and

$$t_1 = \sigma_1 / \lambda_2 \lambda_3 = \lambda_1 \sigma_1 \qquad \text{(A.4.3)}$$

If a hydrostatic stress was added to this loading system, the state of strain is not changed due to the assumed incompressibility of the material though stresses would decrease or increase by the amount of the compressive or tensile hydrostatic stress.

Two equivalent expressions can be written for the other two principal stresses. Constant volume means that λ_1, λ_2 and λ_3 cannot be varied independently of each other, so that if λ_1 and λ_2 are independent variables then

$$\lambda_3 = \frac{1}{\lambda_1 \lambda_2} \qquad \text{(A.4.4)}$$

The work of deformation or the elastically stored free energy per unit volume is given by the expression [103].

$$W = \frac{1}{2} G(\lambda_1^2 + \lambda_2^2 + \lambda_3^2 - 3) \qquad \text{(A.4.5)}$$

An important point to note with regard to the above equation is that for no work to be present at zero values of strain i.e. when $\lambda_1 = \lambda_2 = \lambda_3 = 1$, the last term in the bracket must have a value of –3.

If, for simplicity, only two forces/unit area (t_1 and t_2) are applied and λ_1 is increased whilst λ_2 is held constant, considering work done, gives a value for stress normal to λ_1 of

$$\sigma_1 = G(\lambda_1 - 1/\lambda_1^3\lambda_2^2) \qquad \text{(A.4.6)}$$

From (A.4.3) the corresponding principal stress is

$$t_1 = G(\lambda_1^2 - \lambda_3^2) \text{ and } t_2 = G(\lambda_2^2 - \lambda_3^2), \text{ while, } t_3 = 0 \qquad \text{(A.4.7)}$$

The kinetic theory applied to simple extension

For simple extension ($t_2 = t_3 = 0$) we find that

$$t_1 = G(\lambda_1^2 - \frac{1}{\lambda_1}) \text{ and } \sigma_1 = G(\lambda_1^2 - \frac{1}{\lambda_1^2}) \qquad \text{(A.4.8)}$$

Treloar carried out tests on a vulcanised natural rubber with an 8% sulphur content ($G = 0.39$ N mm^{-2}), which was chosen for its low levels of hysteresis. Results compared poorly with those predicted by the kinetic theory. For moderate strains, between stretch ratios of about 1.5 and 4, the theory over-predicts stress levels. For high strains, ($\lambda > 4$) the values of stress predicted by theory are higher than the experimental results. This shows that the Gaussian statistical theory is invalid for large extensions, since the material will have a finite extensibility and crosslinks will begin to break down. The inconsistency

between theory and experiment for moderate strains is less easily understood and a number of competing explanations remain unresolved. Two possible explanations of why this happens occur at the molecular level. Firstly, chain entanglements may act as partial crosslinks and secondly, non random packing of chains may have the effect of modifying the expressions for the entropy of deformation [9]. The second explanation forms the basis for equations (A.4.5) and (A.4.6).

Applying the kinetic theory to a simple shear problem

Study of simple shear shows clearly the limitations of the statistical theory. In Figure Appendix 4.4 a unit cuboid is deformed in simple shear. It is observed that regardless of whether the material is incompressible or not, a constant volume deformation takes place.

As the volume is constant the three principal stretch ratios will be λ_1 $\lambda_2 = 1$ and $\lambda_3 = 1/\lambda_1$. The shear strain is given by:

$$\gamma = \tan\phi = \lambda_1 - 1/\lambda_1 \qquad \text{(A.4.9)}$$

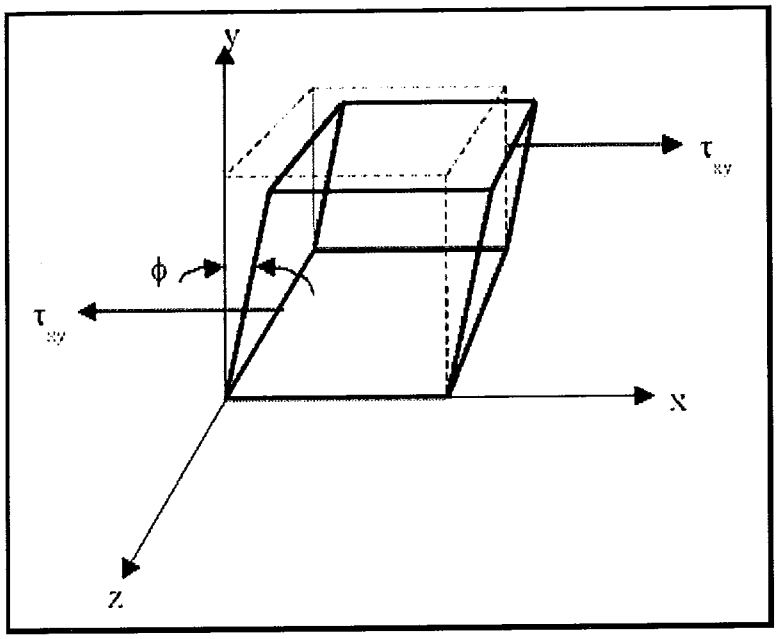

Figure Appendix 4.4. Unit cuboid in simple shear

and so the shear strain energy is

$$W = \frac{1}{2}G\left(\lambda_1^2 + {}^{1}\!/\!_{\lambda_1^2} - 2\right) = \frac{1}{2}G\gamma^2 \qquad \text{(A.4.10)}$$

and since this work done is due to the shear stress τ_{xy}, then

$$\tau_{xy} = dW/d\gamma = G\gamma \qquad \text{(A.4.11)}$$

This suggests that shear stress is proportional to shear strain or that the material complies with linear Hookean behaviour in shear. This is not so for most rubbers and a finite element analysis based on strain energy density functions which

assume a constant rigidity modulus fails to accurately model even the simplest load cases [104].

Phenomenological theories

The phenomenological theories used to describe large elastic deformations do not investigate behaviour at the molecular level. These phenomenological theories seek to describe in formulae how large elastic deformations occur in hyperelastic materials as classical theory of linear elasticity sought to explain small deformations. The mechanical properties of a perfectly elastic material can be determined if the elastically stored energy (strain energy) is calculated in terms of the variation in strain. Mooney [103] originated this approach and Rivlin [105] developed it further. The derivation of these theories is contained in the appendix. Early phenomenological theories used terms for strain invariants to represent stress-strain relations (strain energy) in rubber. Later theories, most notably that of Ogden [106], dispensed with this approach and characterised physical behaviour using stretch ratios.

The Mooney equation

Mooney proposed a semi-empirical formula that sought to resolve inadequacies of the statistical theory:-

$$\sigma = 2(\lambda - \frac{1}{\lambda^2})(C_1 + \frac{C_2}{\lambda}) \qquad \text{(A.4.12)}$$

C_1 and C_2 are empirical constants and formula (8) represents the particular case when $C_2 = 0$ and hence G (Rigidity Modulus) = $2C_1$.

Rearranging (A.4.11) gives

$$\frac{\sigma}{2(\lambda - \frac{1}{\lambda^2})} = (C_1 + \frac{C_2}{\lambda}) \qquad \text{(A.4.13)}$$

and a plot of $\frac{\sigma}{2(\lambda - 1/\lambda^2)}$ against $1/\lambda$ produces a straight line graph over a large range in which C_2 is the slope and $C_1 + C_2$ is the intercept at $1/\lambda = 1$. Figure Appendix 4.5 shows typical Mooney plots.

Mooney's theory assumes that i) for low strains, rubber is incompressible and isotropic and ii) that Hooke's law is obeyed in simple shear. The formula for stress σ (11) is obtained by differentiating, with respect to λ, an expression suggested by Mooney for strain energy in simple extension or uniaxial compression (A.4.14).

$$W = C_1(\lambda^2 + 2/\lambda - 3) + C_2(1/\lambda^2 + 2\lambda - 3) \qquad \text{(A.4.14)}$$

Without revision, the Mooney equation gives no improvement on the statistical theory. Experimental data for uniaxial tension correlates reasonably well with formula (A.4.11), but data for equi-biaxial extension, which is kinematically identical to uniaxial compression, highlights the inadequacy of the theory. Tests

suggest that in compression C_2 is approximately equal to zero, but if the data for uniaxial tension is extrapolated into the compression region the predicted forces for high values of $1/\lambda$ are too large. This inconsistency is more pronounced for more complex loading situations.

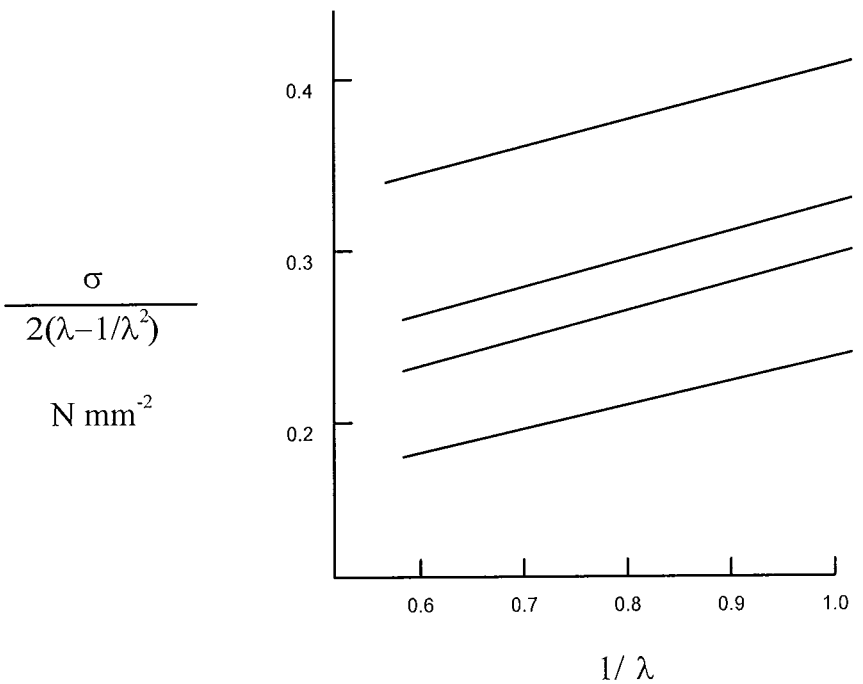

Figure Appendix 4.5. Typical Mooney plots

Rivlin's development of the Mooney theory

Rivlin [105] considered the most general form of strain energy density for rubber. He derived an expression for strain energy W assuming pure homogeneous strain. He also assumed the material to be incompressible and isotropic in the unstrained state. Isotropy requires that W will be symmetrical with respect to the three principal stretch ratios (λ_1, λ_2 and λ_3). Rivlin wrongly argued that the strain energy function must depend only on even powers of the stretch ratios and the three simplest even powered expressions were:-

$$I_1 = \lambda_1^2 + \lambda_2^2 + \lambda_3^2$$
$$I_2 = \lambda_1^2\lambda_2^2 + \lambda_2^2\lambda_3^2 + \lambda_2^2\lambda_3^2 \qquad \text{(A.4.15)}$$
$$I_3 = \lambda_1^2\lambda_2^2\lambda_3^2$$

For the strain system described by (A.4.15) the values of I_1, I_2 and I_3 will be unaltered by changing from one Cartesian co-ordinate system to another, so are termed 'strain invariants' and it follows for an isochoric material that

$$I_3 = \lambda_1^2\lambda_2^2\lambda_3^2 = 1 \qquad \text{(A.4.16)}$$

So I_1 and I_2 can be expressed thus

$$I_1 = \lambda_1^2 + \lambda_2^2 + \lambda_3^2$$
$$I_2 = \frac{1}{\lambda_1^2} + \frac{1}{\lambda_2^2} + \frac{1}{\lambda_3^2} \qquad \text{(A.4.17)}$$

Hence I_1 and I_2 are two independent variables derived from the three extension ratios, two of which are independent if the material is assumed to be isochoric. A strain energy function can be written for an isochoric, isotropic elastic solid as the sum of a series of terms:-

$$W = \sum_{i=0,j=0}^{\infty} C_{ij} (I_1 - 3)^i (I_2 - 3)^j \qquad \text{(A.4.18)}$$

As in the statistical theory W will be zero for no strain, necessitating the use of $(I_1 - 3)$ and $(I_2 - 3)$, so for $\varepsilon = 0$, $I_1 = I_2 = 3$ and $C_{00} = 0$. For mathematical simplicity, a few terms complying with the lowest members of the series have most influence and combining expressions for i = 1, j = 0 and i = 0, j = 1 gives

$$W = C_{10}(I_1 - 3) + C_{01}(I_2 - 3) \qquad \text{(A4.19)}$$

which is of the same form as (A.4.14) and shows that the Mooney equation is the most general first order relationship using I_1 and I_2. The general strain energy function (W, I_1, I_2) can be thought of as a curved surface in space relative to the three mutually perpendicular axes W, I_1 - 3 and I_2 - 3. This leads to the conclusion that the relationship between I_1 and I_2 varies greatly for different load cases and questions the ability of the strain energy function to be used for modelling complex strain cases [9].

Expressions for true stress in simple load cases are simply derived from the Mooney-Rivlin function and those for uniaxial extension and simple shear are shown below.

Uniaxial Extension:- $\lambda_2^2 = \lambda_3^2 = \lambda^{-1}$, $t_2 = t_3 = 0$ (A.4.20)

Simple shear :- $\lambda_3 = 1/\lambda_1$, $\lambda_2 = 1$, $\gamma = \lambda_1 - 1/\lambda_1$

$$t_\gamma = 2\left(\frac{\partial W}{\partial I_1} + \frac{\partial W}{\partial I_2}\right)\gamma \qquad \text{(A.4.21)}$$

Biaxial tests by Rivlin and Saunders [107], where I_1 was kept constant and I_2 varied, suggested that the strain energy function should have the form

$$W = C_1(I_1 - 3) + \Phi(I_2 - 3) \qquad \text{(A.4.22)}$$

where Φ is a function whose slope diminishes as I_2 increases.

Multi-term Rivlin functions

Following Mooney and Rivlin, many researchers worked on expanding the Rivlin formulation (A.4.18) to include higher-order terms, with the intention of modelling non-Gaussian behaviour for higher extensions [108-110]. Each of the different strain energy (density) functions can accurately represent certain rubbers in certain load cases, but relying on increased elaboration provided by the functions is problematic. This is because I_1 and I_2 are theoretically not independent variables, but are each functions of λ for a uniaxial test and most of the higher-order functions are based on data from uniaxial testing. Two of these formulae postulated by Tschoegl [109] are an indication of the limited use of any function based on strain invariants.

$$W = C_{10}(I_1 - 3) + C_{01}(I_2 - 3) + C_{11}(I_1 - 3)(I_2 - 3) \qquad \text{(A.4.23)}$$

This function will represent the full extension curve for a carbon-reinforced, vulcanised natural rubber in simple extension to acceptable accuracy, whilst (A.4.24) provides a good fit for a butadiene-styrene 'pure gum'.

$$W = C_{10}(I_1 - 3) + C_{01}(I_2 - 3) + C_{22}(I_1 - 3)^2(I_2 - 3)^2 \qquad \text{(A.4.24)}$$

It is evident that curve-fitting procedures can be applied to any particular case without allowing a function for all rubbers and all load cases to be derived.

Strain energy functions based on stretch ratios

Functions based on polynomial functions of strain invariants are found to be inaccurate. Consideration of two alternatives where the strain energy density is a separable function of the three principal stretch ratios is given.

Ogden's Theory

Ogden [106] argued that the use of strain invariants was unnecessary and that a formula based on stretch ratios would be mathematically simpler. He derived a strain energy function for an incompressible rubber in series form shown in (A.4.25).

$$W = \sum_n \frac{\mu_n}{\alpha_n}(\lambda_1^{\alpha_n} + \lambda_2^{\alpha_n} + \lambda_3^{\alpha_n} - 3) \qquad \text{(A.4.25)}$$

The α_n terms can have any values and be positive or negative. The μ_n terms are constants and can also be positive or negative. Pairs should possess the same sign as the initial rigidity modulus, which must have a positive value and is given by the equation

$$G_0 = \frac{1}{2}\sum_{n=1}^{N} \mu_n \alpha_n \qquad \text{(A.4.26)}$$

Previous research [111][112] has provided instances where Ogden has rendered superior results for modelling of complex components based on uniaxial test data.

Determination of expressions from the Ogden equation

The expressions for simple stress cases can be determined from the Ogden equation: -

Simple extension.

$$t_1 = \sum_n \mu_n (\lambda_1^{\alpha_n} - \lambda_1^{-\alpha_n/2}) \qquad \text{(A.4.27)}$$

$$\sigma_1 = \sum_n \mu_n (\lambda_1^{\alpha_n - 1} - \lambda_1^{(-\alpha_n/2)-1}) \qquad \text{(A.4.28)}$$

$$\lambda_2 = \lambda_3 = \lambda_1^{-\frac{1}{2}} \qquad \text{(A.4.29)}$$

Equi-biaxial extension (t1 = 0, t2 = t3)

$$t_2 = \sum_n \mu_n (\lambda_2^{\alpha_n} - \lambda_2^{-\alpha_n/2}) \qquad \text{(A.4.30)}$$

$$\sigma_2 = \sum_n \mu_n (\lambda_2^{\alpha_n - 1} - \lambda_2^{-2\alpha_n - 1}) \qquad \text{(A.4.31)}$$

$$\lambda_1 = \lambda_2^{-2} = \lambda_3^{-2} \qquad \text{(A.4.32)}$$

(Assuming stretches in the '2' and '3' direction)

Appendix 4.3. Thermodynamics of Swelling and Cohesive Energy Densities

When investigating the mixing of two liquids, consider that at the molecular level the molecules of a liquid are close together and therefore exert strong forces on one another. This is the origin of the latent heat of evaporation, which represents the work done in overcoming the cohesive energy of the molecules. As different liquids do not have the same molar latent heats, it must be concluded that their molecules cohere with different energies. This difference depends partly on the chemical nature of the molecules and partly on the way they pack together.

Imagine that a typical molecule in the liquid is surrounded by Z number of similar molecules each of which exerts an attractive force on it. This force is equivalent to a bond, whose energy depends on the nature of the molecules and on their distance apart. If two liquids, 1 and 2, are mixed together it is necessary to break some of the 1-1 and 2-2 bonds, at the same time producing 1-2 bonds. A typical molecule 1 will still be surrounded by other Z molecules, but these will not all be 1 molecules but on average will consist of $\upsilon_1 Z1$ molecules and $\upsilon_2 Z2$ molecules where υ_1 and υ_2 are the volume fractions of 1 and 2 in the mixture. Now the cohesive energy of 1 cc of liquid is made up of the sum of the energies of all the bonds between the molecules in the liquid. The cohesive energy of a mixture will not in general be equal to the sum of the cohesive energies of its separated components. It would be easy to calculate on this basis what the cohesive energy would be if how the energy e_{12} of a 1-2 bond was related to the energies e_{11} and e_{22} of 1-1 and 2-2 bonds was known. Hildebrand [83], suggested that $e_{12} = \sqrt{e_{11}e_{22}}$ and showed that, on this basis the increase of energy ΔL on mixing is given by:

$$\Delta L = \upsilon_1 \upsilon_2 \left(\sqrt{\frac{L_1}{V_1}} - \sqrt{\frac{L_2}{V_2}} \right)^2 \text{ cals. per cc of mixture} \qquad \text{(A.4.33)}$$

where E is the latent heat of evaporation at constant volume in calories per mol, V is molar volume in cc's and $\sqrt{\frac{L_1}{V_1}}$ and $\sqrt{\frac{L_2}{V_2}}$ are the cohesive energy densities (C.E.D) of the two liquids.

Development of the thermodynamics of swelling using C.E.D.

Gee developed the thermodynamic theory of swelling further by calculating the entropy of a rubber benzene system as follows:

The mixing of liquids is accompanied in general by two changes, firstly an increase of entropy which tends to make them mix and secondly an absorption of heat, which represents energy which has to be supplied before mixing is possible. These factors are in opposition and to discover their joint effect it is necessary to introduce the concept of free energy, which can be regarded in its simplest terms as a chemical potential. In the same way as the temperatures of two bodies determine the direction of heat flow, so the free energies of two systems determine the direction of chemical reaction or mixing. Two liquids will mix only as long as the process involves a decrease of free energy.

Writing ΔH as the increase in energy, ΔG as the increase in free energy and T as the absolute temperature, it can be shown that

$$\Delta G = \Delta H - T\Delta S \qquad \text{(A.4.34)}$$

Hence, liquids will mix as long as ΔG is negative, i.e., $T\Delta S > \Delta H$. Thus liquids which are only partially miscible are in general those which have different C.E.D.'s, while liquids of similar C.E.D values are miscible in all proportions.

In terms of solubility, Gee treated rubber as a liquid. The justification for this is that the rubber molecules have a good deal of freedom to slip past one another, which is a similar characteristic to that associated with liquids. From experiments carried out on a rubber-benzene system, Gee calculated the entropy of the system, as shown in Figure Appendix 4.6.

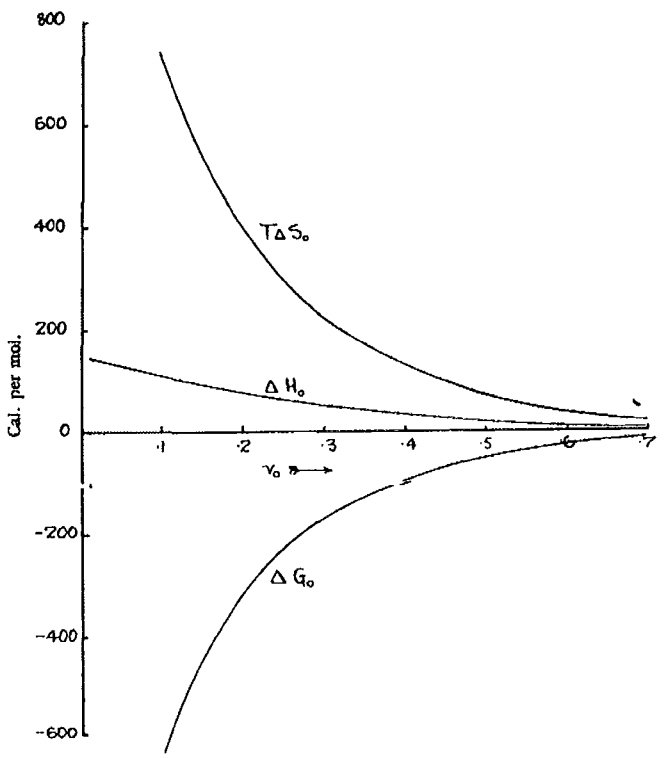

Figure Appendix 4.6. Thermodynamic representation of a rubber benzene system.

Figure Appendix 4.6 can be explained if one imagines a piece of rubber swollen to a certain extent by a liquid, then immersed in more of the same liquid. Absorption of more liquid would be assisted by the entropy increase ΔS_0, but

resisted by the heat absorption ΔH_0. If ΔG_0 is negative, i.e., $\Delta TS_0 > \Delta H_0$, more liquid will be absorbed and the process will continue either until the rubber is dissolved or until a point is reached at which $\Delta G_0 = 0$.

The heat of dilution ΔH_0 is approximately proportional to the square of the rubber concentration C, so that $\Delta H_0 / C_2$ is independent of the degree of swelling Q (cc of liquid per gram of rubber). This is represented in Figure Appendix 4.7 by a series of horizontal lines, each characteristic of one liquid. As ΔS_0 is independent of the nature of the liquid, a single curve of $\frac{T\Delta S_0}{C_2}$ against Q can be drawn, as the Figure shows. The curve drawn is for a vulcanised rubber. When this curve cuts the $\Delta H_0 / C_2$ line for a given liquid, $T\Delta S_0 = \Delta H_0$ and $\Delta G_0 = 0$ for that liquid; the corresponding value of Q is the equilibrium degree of swelling of the rubber in that liquid.

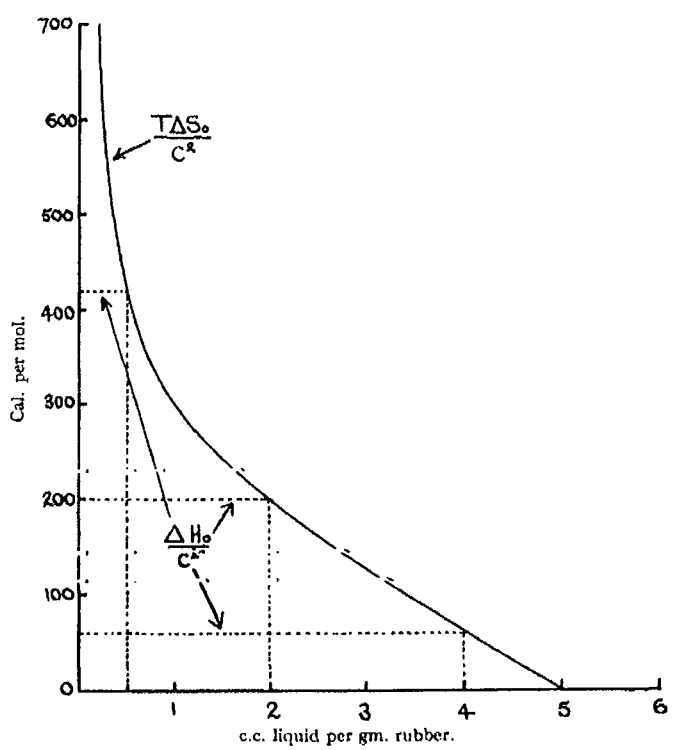

Figure Appendix 4.7. $\frac{T\Delta S_0}{C_2}$ against degree of swelling Q.

The description given of the mixing of simple liquids relates ΔH_0 to the difference between the C.E.D.'s of the liquids. Hence vulcanised rubber should swell to its greatest extent in a liquid having the same C.E.D. as itself and a plot of Q in a series of liquids against the C.E.D.'s of the liquids should give a curve with a maximum. There are some individual discrepancies to this statement, but it remains broadly correct.

Gee developed his theories further to show that the molecular volume of the liquid was also important and that the swelling Q should be a function of $\sqrt{V_0}\left(\sqrt{\frac{L_0}{V_0}} - \sqrt{\frac{L_r}{V_r}}\right)$, where the suffix r applies to rubber. The C.E.D. of a liquid can be easily found from its latent heat of evaporation, but this method cannot be applied to rubber. It is possible however, to estimate $\frac{L_r}{V_r}$ for a sample of rubber from its swelling in a series of liquids of known C.E.D. If the swelling of a vulcanised rubber is measured in a series of liquids, covering as continuously as possible, a range of C.E.D., the C.E.D. of the liquid in which the swelling is a maximum will be approximately equal to that of the rubber. This principle can be refined by using a mathematical method to locate the exact position of the swelling vs. C.E.D. curve.

Estimation of C.E.D. of Rubber from Swelling Data

The swelling Q is a function of $\sqrt{V_0}\left(\sqrt{\frac{L_0}{V_0}} - \sqrt{\frac{L_r}{V_r}}\right)$. Therefore, $\sqrt{V_0}\left(\sqrt{\frac{L_0}{V_0}} - \sqrt{\frac{L_r}{V_r}}\right)$ can be denoted by x.

Q has its maximum value Q_{max} when $\sqrt{\frac{L_0}{V_0}} = \sqrt{\frac{L_r}{V_r}}$ or x = 0. The Q vs. x curve is roughly of the form of the error function, so that we may write:

$$Q = Q_{\max} e^{-\beta x^2} \qquad \text{(A.4.35)}$$

where β will in general not be a constant (as in the error function) but will be a function of x. This may be rearranged to:

$$x = \pm\sqrt{\frac{1}{\beta}} \log_e \frac{Q_{\max}}{Q} \qquad \text{(A.4.36)}$$

Substituting for x, gives:

$$\sqrt{\frac{L_0}{V_0}} = \sqrt{\frac{L_r}{V_r}} \pm \sqrt{\frac{1}{\beta V_0}} \log_e \frac{Q_{\max}}{Q} \qquad \text{(A.4.37)}$$

Hence if Q_{max} is estimated by a rough plot of Q against $\sqrt{\frac{L_0}{V_0}}$ and $\sqrt{\frac{L_0}{V_0}}$ plotted as a function of $\sqrt{\frac{1}{V_0}} \log_e \frac{Q_{\max}}{Q}$, the resulting curve will have a slope $\sqrt{\frac{1}{\beta}}$ and an intercept of $\sqrt{\frac{L_r}{V_r}}$. This procedure is illustrated by Figure Appendix 4.8, drawn from the data used for a natural rubber.

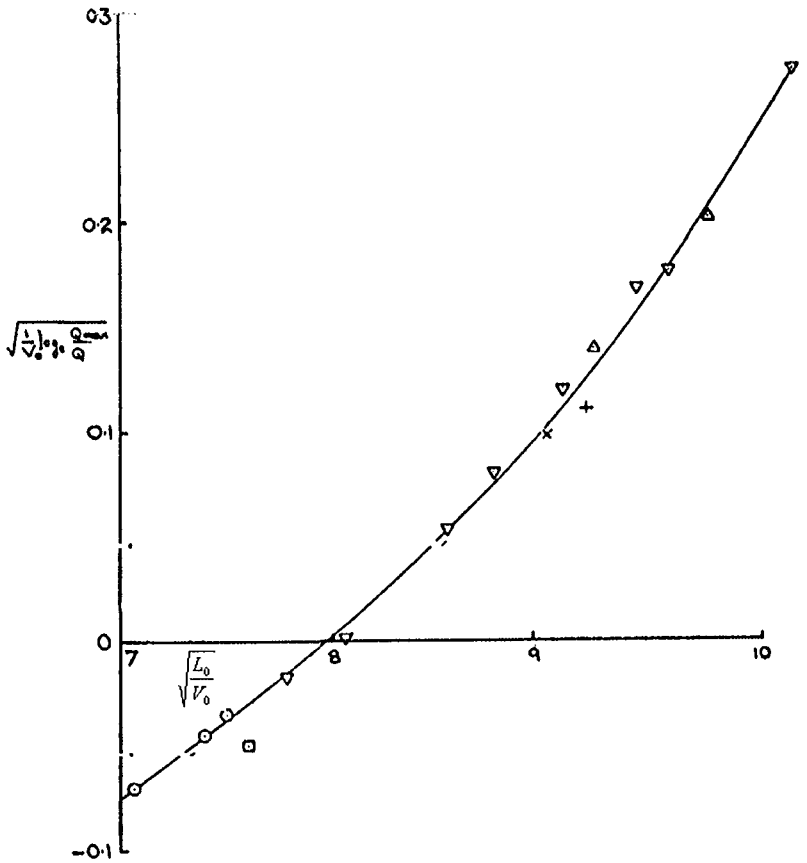

Figure Appendix 4.8. Plot of Q against $\sqrt{\frac{L_0}{V_0}}$

Using this principle to estimate the C.E.D. of natural rubber swollen in 20 different aliphatic liquids with values ranging from 50 calories per cc (n-pentane) to 141 calories per cc (acetonitrile), Gee generated a plot of the swelling Q as a function of $\sqrt{V_0}\left(\sqrt{\frac{L_0}{V_0}}-\sqrt{\frac{L_r}{V_r}}\right)$, shown in Figure Appendix 4.9. The C.E.D. of the rubber was found to be unaffected by compounding, while the absolute swelling of a rubber in a good swelling agent is reduced by a reinforcing filler. The effect of the filler is to link the rubber chains together and restrict their maximum distension.

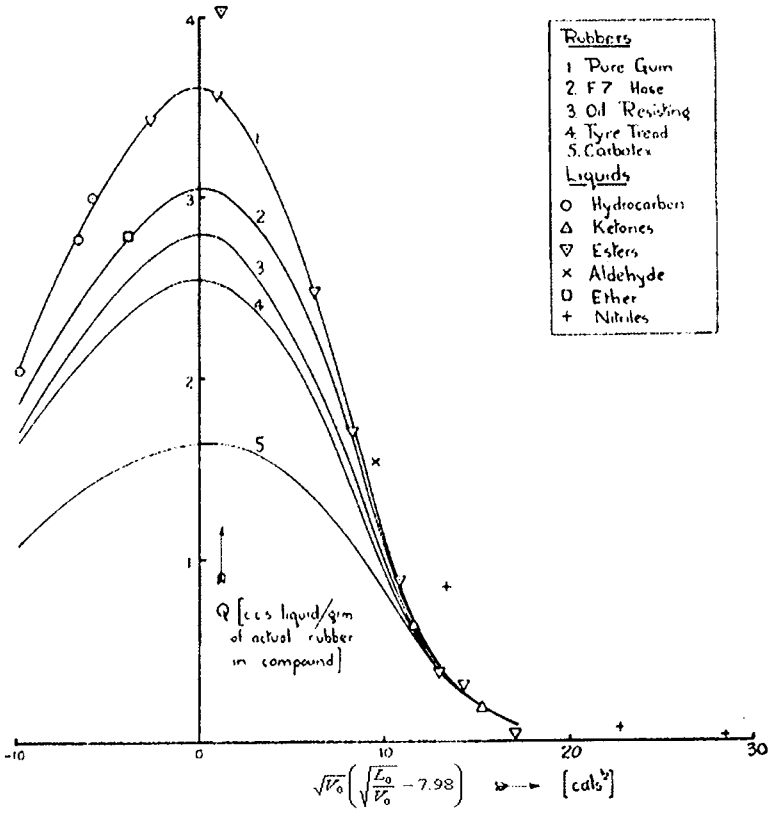

Figure Appendix 4.9. Q as a function of $\sqrt{V_0}\left(\sqrt{\frac{L_0}{V_0}}-\sqrt{\frac{L_r}{V_r}}\right)$.

Using the same technique on synthetic rubbers, Gee also found agreement with theory, but this was less so than with natural rubber. This is explained by considering that equation (A.4.33) can only be true if there are no specific interactions between the two components of the mixture. When both rubber and swelling agents possess polar groups, such interactions must be general and will lead to deviations from the simple theory.

Appendix 4.4. Fatigue of Elastomers

For a clearer understanding of fracture mechanics and crack propagation theory, consider the changes in stored elastic energy as a crack grows. Imagine a strip constraining an edge crack of length 'a' under uniaxial tension, as shown in Figure Appendix 4.10. If a load W is applied gradually, the load points will move a distance x and the strain energy U stored in the body will be given by:

$$U = \frac{1}{2} Wx \qquad \text{(A.4.38)}$$

For purely elastic deformation, the load and displacement are related by the 'compliance *c*,

$$x = cW \qquad \text{(A.4.39)}$$

Which is a function of the crack length, but varies with the geometry of the cracked body.

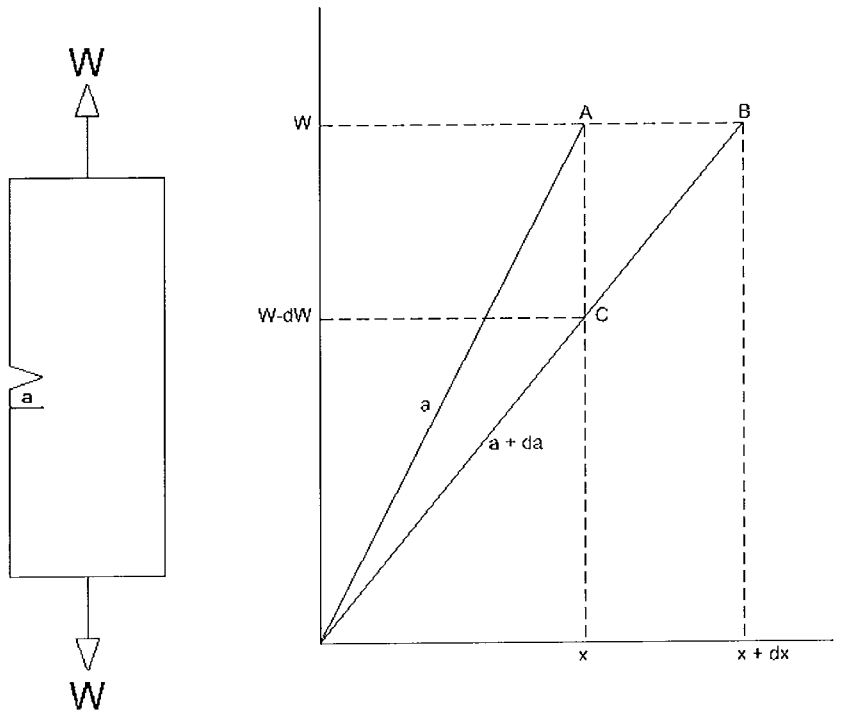

(a) **(b)**

Figure Appendix 4.10. (a) Cracked body under tensile load and (b) associated force displacement curves for changes in crack length a, due to constant displacement and load.

It can be shown [48], that the change in stored energy due to an increase in crack length from 'a' to a+δa is:

$$\delta U_x = -\frac{1}{2} W \delta x \qquad \text{(A.4.40)}$$

This is regardless of the loading conditions, for small increases in crack length. In the case of an increase in crack length for a constant displacement loading condition the load moves from A to C in Figure Appendix 4.10. This will result in a reduction in W.

In the case of an increase in crack length for a constant load, the displacement moves from A to B in Figure Appendix 4.10. This will result in a reduction in the potential energy of the system, because the work required to extend the crack from A to C has come from external sources. There is no such equality for large increases, but this is not of major significance, as it is the onset of crack growth which is of interest, with failure in fatigue normally following crack initiation.

In summary, if there is a decrease in potential energy when there is an increase in crack growth, then there is an energy requirement for the production of a crack. As shown in Figure Appendix 4.11 for an infinite sheet with an applied uniaxial stress σ and with a central crack of length 2a, there is a decrease in potential energy when a crack grows.

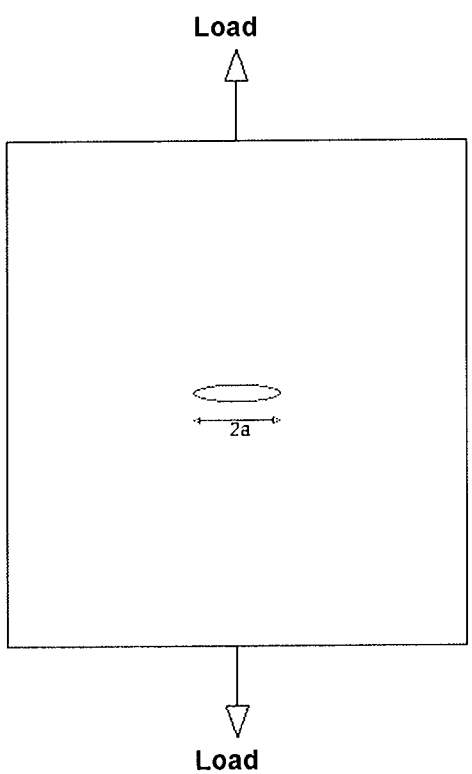

Figure Appendix 4.11. Physical model for Griffith's analysis.

For an increase in crack length of δa,

$$\delta U_x = 2\gamma b \delta a \tag{A.4.41}$$

Where

γ = Surface energy of the crack faces.

b = thickness of the sheet.

At the onset of crack growth, δa is small and we have,

$$\frac{dU}{da} = 2b\gamma \tag{A.4.42}$$

$\frac{dU}{da}$ is termed the 'critical strain energy release' and is denoted as G_c, giving

$$G_c = \frac{\delta U}{\delta a} = 2b\gamma \tag{A.4.43}$$

This is known as the Griffith criterion for fracture.

In general,

$$G_c = \frac{\sigma_f^2 \pi a}{E} \text{ under plane stress conditions.} \tag{A.4.44}$$

$$G_c = \frac{\sigma_f^2 \pi a}{E}(1-\nu^2) \text{ under plane strain conditions.} \tag{A.4.45}$$

Specimen types used in crack propagation tests on elastomers

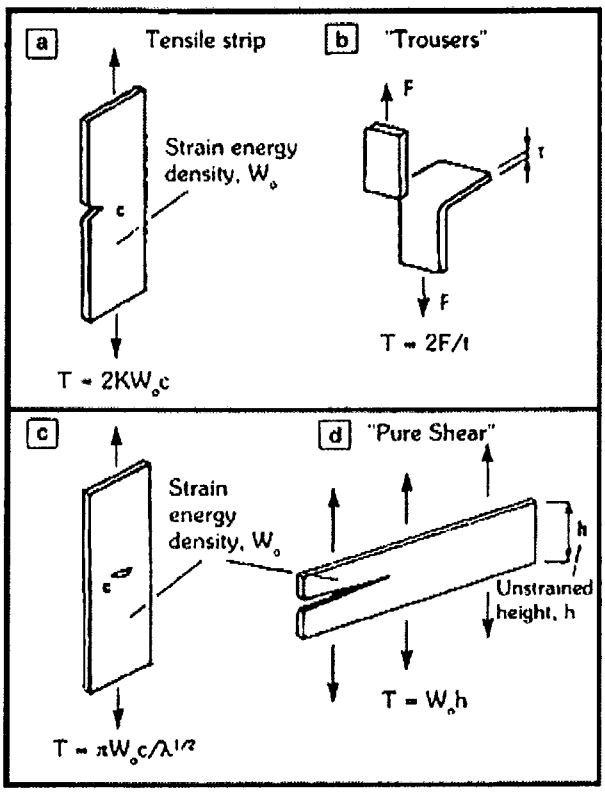

Figure Appendix 4.12. Typical specimen types used in crack propagation tests on elastomers, (a) Tensile strip, (b) Trousers test-piece, (c), Specimen with central crack, (d), Pure shear specimen [49].

a) – Tensile strip,

$$T = 2KW_0c \qquad \text{(A.4.46)}$$

Where,

c = crack length

W = Strain energy density at a strain, e.

K = Strain dependant parameter.

b) – Trousers test-piece.

$$T = \frac{2F}{t} \qquad \text{(A.4.47)}$$

Where,

F = Applied force.

t = Specimen thickness.

c) – Specimen with central crack

$$T = \frac{\pi W_0 c}{\lambda^{\frac{1}{2}}} \qquad \text{(A.4.48)}$$

Where,

c = crack length

W = Strain energy density at a strain, e.

λ = Stretch ratio.

d) – Pure shear specimen

$$T = W_0 h \qquad \text{(A.4.49)}$$

Where,

W = Strain energy density at a strain, e.

h = Specimen unstrained height.

Appendix 5 – Plots of E* Models

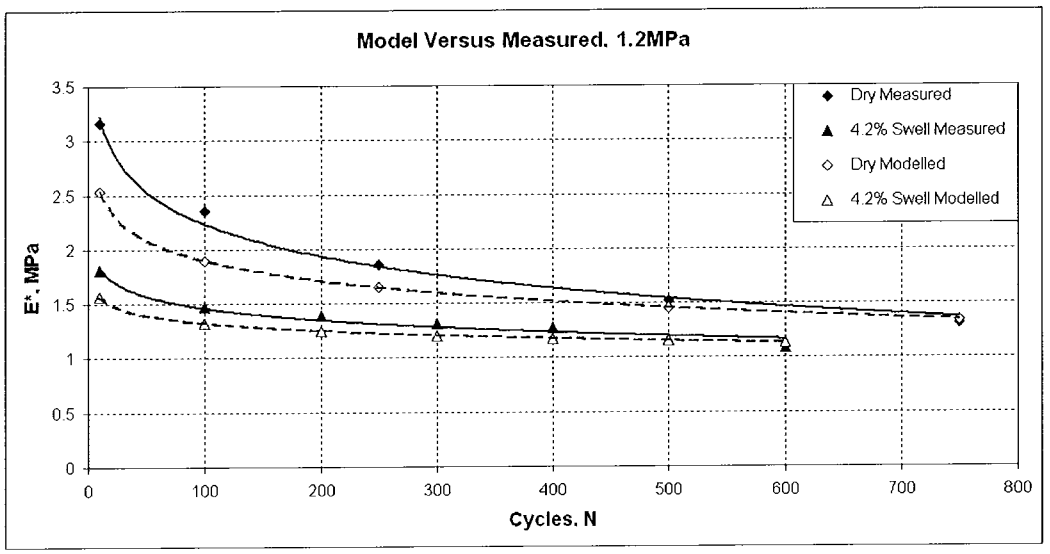

Figure Appendix 5.1 E* Measured versus E* modelled, σ_a = 1.2MPa

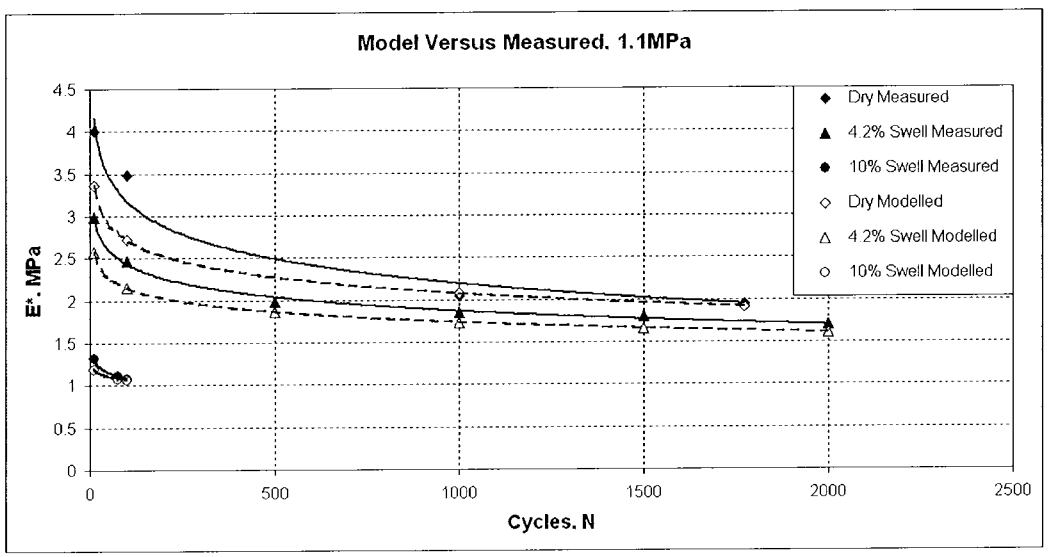

Figure Appendix 5.2 E* Measured versus E* modelled, σ_a = 1.1MPa

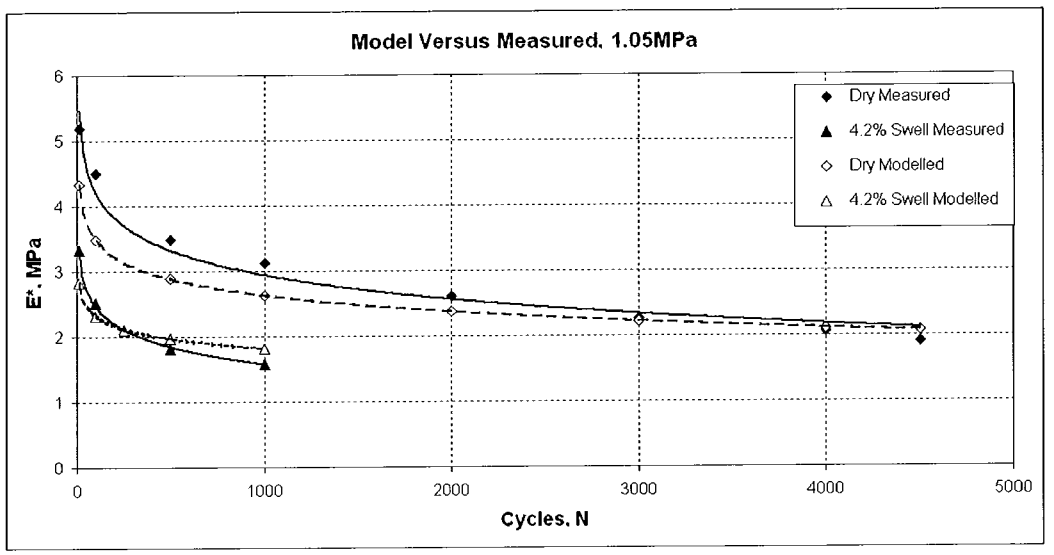

Figure Appendix 5.3 E* Measured versus E* modelled, σ_a = 1.05MPa

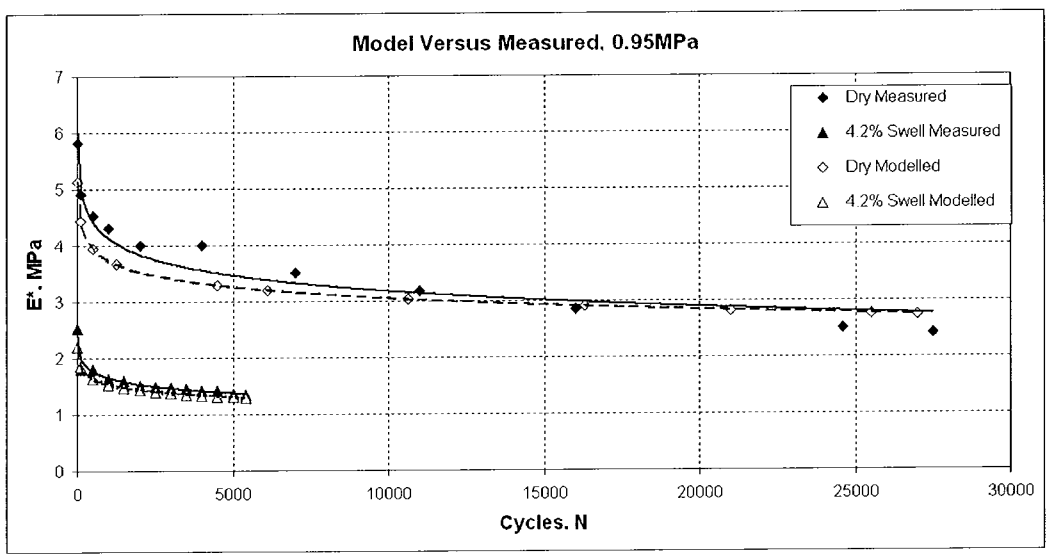

Figure Appendix 5.4 E* Measured versus E* modelled, σ_a = 0.95MPa

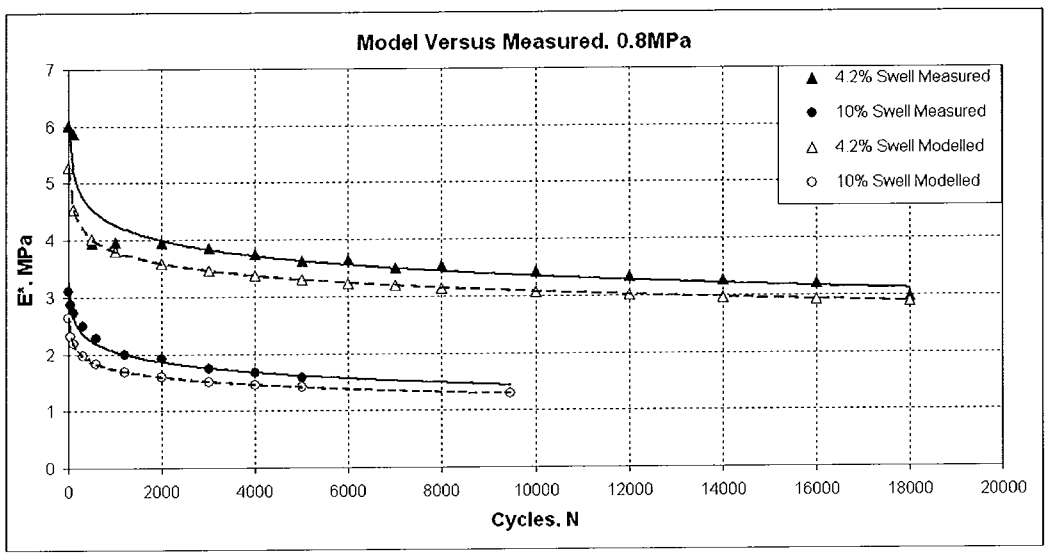

Figure Appendix 5.5 E* Measured versus E* modelled, σ_a = 0.8MPa

Appendix 6 – Test Materials Specifications

E1M Material – data from Deutsches Institut für Kautschuktechnologie (DIK)

Component	*pphr*
KELTAN 7631 A	140.0
Carbon N550	50.0
ZnO RS	4.0
Stearic Acid	2.0
Sulphur	0.7
TBBS	1.0
TBzTD	3.5

C-14 Material - data from Deutsches Institut für Kautschuktechnologie (DIK)

Component	*pphr*
EPDM	110.0
Carbon N550	70.0
Carbon N772	40.0
Stearic Acid	1.0
ZnO RS	5.0
Oil Sunpar 2280	70.0
Sulphur	1.5
Accelerator CZ (CBS)	1.0
Accelerator Thiuram (TMTD)	0.8

EPDM Shore A 70 Material – data from http://www.semperflex.com

EPDM	Semperit E9566
Filler	Carbon Black
Crosslinking agent	Sulphur
Tensile Strength	7 N/mm^2
Elongation at break	250%
Density	1.32 g/cm^3
Temperature Range	-40/+100°C

Compression Set DIN ISO 815

Duration	*pphm Ozone*	*Temperature*
35%	70 °C	22 hours

Ageing DIN 53508

Conditions	*Hardness*	*Strength*	*Elongation*
70 h/100 °C	+10 Shore A	-10 %	-25 %

Ozone Resistance

Duration	*pphm Ozone*	*Temperature*	*Crack Level*
48 h	200 pphm	40 °C	0